Summary of the Bulletin of the International Seismological Centre

2012

January – June

Volume 49 Issue 1-6

www.isc.ac.uk

isc-mirror.iris.washington.edu

ISSN 2309-236X

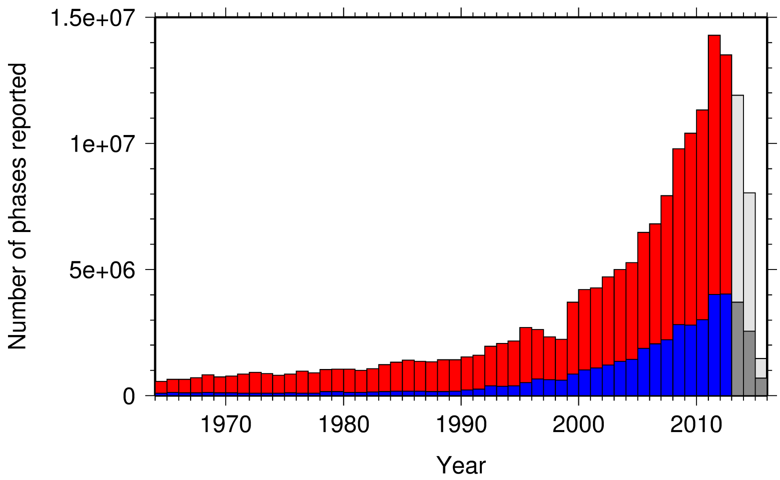

The number of phases (red) and number of amplitudes (blue) collected by the ISC for events each year since 1964. The data in grey covers the current period where data are still being collected before the ISC review takes place and are accurate at the time of publication. See Section 9.3.

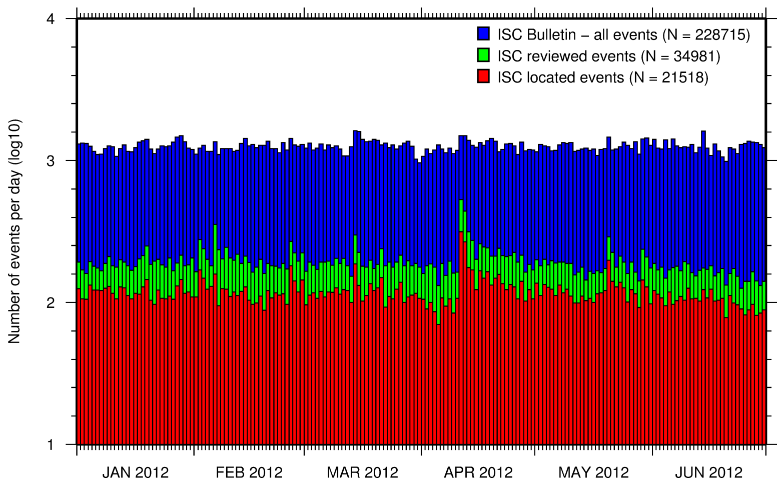

The number of events within the Bulletin for the current summary period. The vertical scale is logarithmic. See Section 10.1.

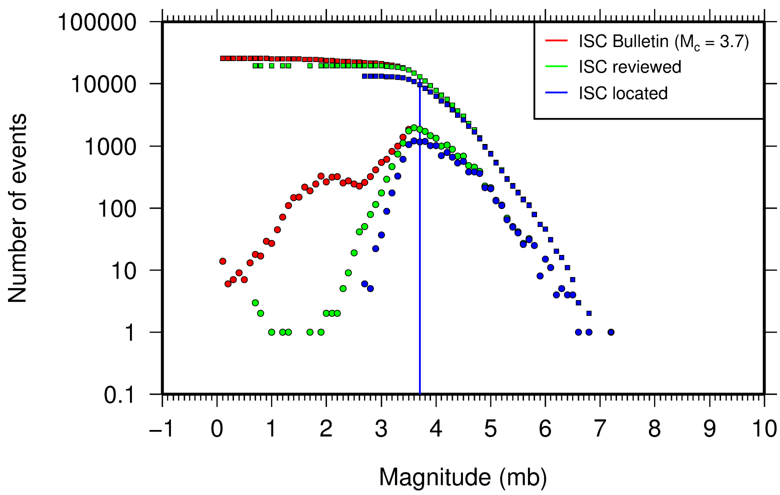

Frequency and cumulative frequency magnitude distribution for all events in the ISC Bulletin, ISC reviewed events and events located by the ISC. The magnitude of completeness (M_C) is shown for the ISC Bulletin. Note: only events with values of m_b are represented in the figure. See Section 10.4.

Contents

1

Preface

Dear Colleague,

This is the first 2012 issue of the Summary of the ISC Bulletin which remains the most fundamental reason for the ISC continued operations. This issue covers seismic events that occurred during the period of January to June 2012.

This publication presents a description of the ISC data available on the attached DVD-ROM and from the ISC website. It contains information on the ISC, its Members, Sponsors and Data providers. This issue also includes important seismological standards and procedures used by the ISC in its operations. It offers analysis of the data contributed to the ISC by many seismological agencies worldwide as well as analysis of the data in the ISC Bulletin itself.

We continue publishing invited articles describing the history, current status and operational procedures at those networks that contribute data to the ISC. This time it is the turn for the Brazilian Seismographic Network to be described.

We hope that you find this relatively new publication useful in your work. If your home-institution or company is unable, for one reason or another, to support the long-term international operations of the ISC in full by becoming a Member, then, please, consider subscribing to this publication by contacting us at admin@isc.ac.uk.

With kind regards to our Data Contributors, Members, Sponsors and users,

Dr Dmitry A. Storchak
Director
International Seismological Centre (ISC)

2

The International Seismological Centre

2.1 The ISC Mandate

The International Seismological Centre (ISC) was set up in 1964 with the assistance of UNESCO as a successor to the International Seismological Summary (ISS) to carry forward the pioneering work of Prof. John Milne, Sir Harold Jeffreys and other British scientists in collecting, archiving and processing seismic station and network bulletins and preparing and distributing the definitive summary of world seismicity.

Under the umbrella of the International Association of Seismology and Physics of the Earth Interior (IASPEI/IUGG), the ISC has played an important role in setting international standards such as the International Seismic Bulletin Format (ISF), the IASPEI Standard Seismic Phase List (SSPL) and both the old and New IASPEI Manual of the Seismological Observatory Practice (NMSOP-2) (www.iaspei.org/projects/NMSOP.html).

The ISC has contributed to scientific research and prominent scientists such as John Hodgson, Eugine Herrin, Hal Thirlaway, Jack Oliver, Anton Hales, Ola Dahlman, Shigeji Suehiro, Nadia Kondorskaya, Vit Karnik, Stephan Müller, David Denham, Bob Engdahl, Adam Dziewonski, John Woodhouse and Guy Masters all considered it an important duty to serve on the ISC Executive Committee and the Governing Council.

The current mission of the ISC is to maintain:

- the ISC **Bulletin** – the longest continuous definitive summary of World seismicity (collaborating with 130 seismic networks and data centres around the world). (www.isc.ac.uk/iscbulletin/)
- the **International** Seismographic Station Registry (**IR**, jointly with the World Data Center for Seismology, Denver). (www.isc.ac.uk/registries/)
- the IASPEI Reference Event List (Ground Truth, **GT**, jointly with IASPEI). (www.isc.ac.uk/gtevents/)

These are fundamentally important tasks. Bulletin data produced, archived and distributed by the ISC for almost 50 years are the definitive source of such information and are used by thousands of seismologists worldwide for seismic hazard estimation, for tectonic studies and for regional and global imaging of the Earth's structure. Key information in global tomographic imaging is derived from the analysis of ISC data. The ISC Bulletin served as a major source of data for such well known products as the ak135 global 1-D velocity model and the EHB (*Engdahl et al.*, 1998) and Centennial (*Engdahl and Villaseñor*, 2002) catalogues. It presents an important quality-control benchmark for the Comprehensive Nuclear-Test-Ban Treaty Organization (CTBTO). Hypocentre parameters from the ISC Bulletin are used by the Data Management Center of the Incorporated Research Institutions for Seismology (IRIS DMC) to serve event-oriented user-requests for waveform data. The ISC-GEM Bulletin is a cornerstone of the ISC-GEM Global Instrumental Reference Earthquake Catalogue for Global Earthquake risk Model (GEM).

The ISC relational database currently holds approximately 90 Gb of unique data. The ISC Bulletin contains over 5 million seismic events: earthquakes, chemical and nuclear explosions, mine blasts and mining induced events. At least 1.5 million of them are regional and teleseismically recorded events that have been reviewed by the ISC analysts. The ISC Bulletin contains approximately 150 million individual seismic station readings of arrival times, amplitudes, periods, SNR, slowness and azimuth, reported by approximately 17,000 seismic stations currently registered in the IR. Over 6,000 stations have contributed to the ISC Bulletin in recent years. This number includes the numerous sites of the USArray. The IASPEI GT List currently contains 7802 events for which latitude, longitude and depth of origin are known with high confidence (to 5 km or better) and seismic signals were recorded at regional and/or teleseismic distances.

2.2 Brief History of the ISC

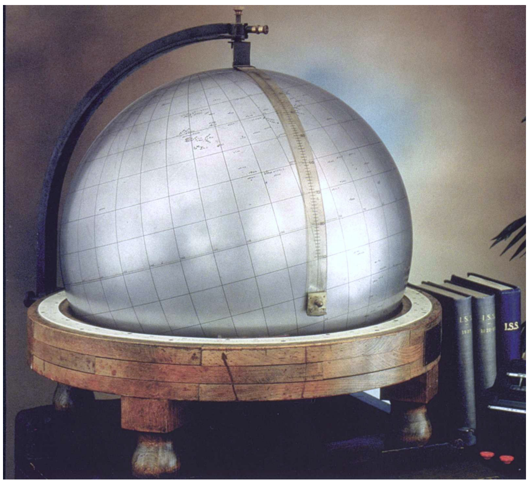

Figure 2.1: *The steel globe bearing positions of early seismic stations was used for locating positions of earthquakes for the International Seismological Summaries.*

Earthquake effects have been noted and documented from the earliest times, but it is only since the development of earthquake recording instruments in the latter half of the 19th century that a proper study of their occurrence has been possible. After the first teleseismic observation of an earthquake in 1889, the need for international exchange of readings was recognised in 1895 by Prof. John Milne and by Ernst von Rebeur Paschwitz together with Georg Gerland, resulting in the publication of the first international seismic bulletins. Milne's "Shide Circulars" were issued under the auspices of the Seismological Committee of the British Association for the Advancement of Science (BAAS), while co-workers of Gerland at the Central Bureau of the International Association of Seismology worked independently in Strasbourg (BCIS).

Following Milne's death in 1913, Seismological Bulletins of the BAAS were continued under Prof. H.H. Turner, later based at Oxford University. Upon formal post-war dissolution of the International Association of Seismology in 1922 the newly founded Seismological Section of the International Union of Geodesy and Geophysics (IUGG) set up the International Seismological Summary (ISS) to continue at Oxford under Turner, to produce the definitive global catalogues from the 1918 data-year onwards, under the auspices of IUGG and with the support of the BAAS.

ISS production, led by several professors at Oxford University, and Sir Harold Jeffreys at Cambridge University, continued until it was superseded by the ISC Bulletin, after the ISC was formed in Edinburgh in 1964 with Dr P.L. Willmore as its first director.

During the period 1964 to 1970, with the help of UNESCO and other international scientific bodies, the ISC was reconstituted as an international non-governmental body, funded by interested institutions from various countries. Initially there were supporting members from seven countries, now there are almost 60, and member institutions include national academies, research foundations, government departments and research institutes, national observatories and universities. Each member, contributing a minimum unit of subscription or more, appoints a representative to the ISC's Governing Council, which meets every two years to decide the ISC's policy and operational programme. Representatives from the International Association of Seismology and Physics of the Earth's Interior also attend these meetings. The Governing Council appoints the Director and a small Executive Committee to oversee the ISC's operations.

Figure 2.2: *ISC building in Thatcham, Berkshire, UK.*

In 1975, the ISC moved to Newbury in southern England to make use of better computing facilities there. The ISC subsequently acquired its own computer and in 1986 moved to its own building at Pipers Lane, Thatcham, near Newbury. The internal layout of the new premises was designed for the ISC and includes not only office space but provision for the storage of extensive stocks of ISS and ISC publications and a library of seismological observatory bulletins, journals and books collected over many tens of years.

In 1997 the first set of the ISC Bulletin CD-ROMs was produced (not counting an earlier effort at USGS). The first ISC website appeared in 1998 and the first ISC database was put in day-to-day operations from 2001.

Throughout 2009-2011 a major internal reconstruction of the ISC building was undertaken to allow for more members of staff working in mainstream ISC operations as well as major development projects such as the CTBTO Link, ISC-GEM Catalogue and the ISC Bulletin Rebuild.

2.3 Former Directors of the ISC and its U.K. Predecessors

John Milne
Publisher of the Shide Cicular Reports on Earthquakes
1899-1913

Herbert Hall Turner

Seismological Bulletins of the BAAS

1913-1922
Director of the ISS
1922-1930

Harry Hemley Plaskett
Director of the ISS
1931-1946

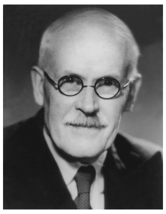

Harold Jeffreys
Director of the ISS
1946-1957

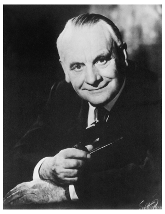

Robert Stoneley
Director of the ISS
1957-1963

P.L. (Pat) Willmore
Director of the ISS
1963-1970
Director of the ISC
1964-1970

Edouard P. Arnold
Director of the ISC
1970-1977

Anthony A. Hughes
Director of the ISC
1977-1997

Raymond J. Willemann
Director of the ISC
1998-2003

Avi Shapira
Director of the ISC
2004-2007

2.4 Member Institutions of the ISC

Article IV(a-b) of the ISC Working Statutes stipulates that any national academy, agency, scientific institution or other non-profit organisation may become a Member of the ISC on payment to the ISC of a sum equal to at least one unit of subscription and the nomination of a voting representative to serve on the ISC's governing body. Membership shall be effective for one year from the date of receipt at the ISC of the annual contribution of the Member and is thereafter renewable for periods of one year.

The ISC is currently supported with funding from its 62 Member Institutions and a four-year Grant Award EAR-1417970 from the US National Science Foundation.

Figures 2.3 and 2.4 show major sectors to which the ISC Member Institutions belong and proportional financial contributions that each of these sectors make towards the ISC's annual budget.

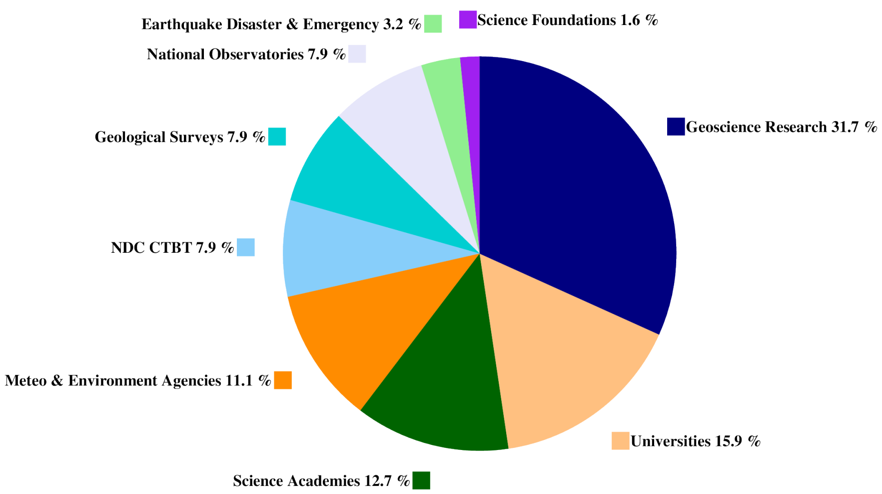

Figure 2.3: *Distribution of the ISC Member Institutions by sector in year 2014 as a percentage of total number of Members.*

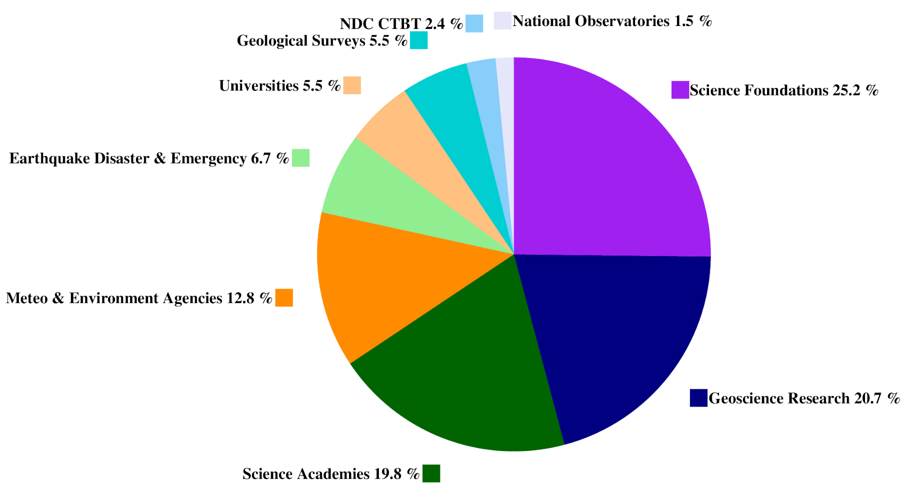

Figure 2.4: *Distribution of Member's financial contributions to the ISC by sector in year 2013 as a percentage of total annual Member contributions.*

There follows a list of all current Member Institutions with a category (1 through 9) assigned according to the ISC Working Statutes. Each category relates to the number of membership units contributed.

Centre de Recherche en Astronomie, Astrophysique et Géophysique (CRAAG)
Algeria
www.craag.dz
Category: 1

Instituto Nacional de Prevención Sísmica (INPRES)
Argentina
www.inpres.gov.ar
Category: 1

Geoscience Australia
Australia
www.ga.gov.au
Category: 3

The University of Melbourne
Australia
www.unimelb.edu.au
Category: 1

Seismology Research Centre
Australia
www.seis.com.au
Category: 1

Bundesministerium für Wissenschaft und Forschung
Austria
www.bmbwk.gv.at
Category: 2

Centre of Geophysical Monitoring (CGM) of the National Academy of Sciences of Belarus
Belarus
www.cgm.org.by
Category: 1

Observatoire Royal de Belgique
Belgium
www.astro.oma.be
Category: 1

Universidade de São Paulo, Centro de Sismologia
Brazil
www.sismo.iag.usp.br
Category: 1

The Geological Survey of Canada
Canada
gsc.nrcan.gc.ca
Category: 4

Department of Geophysics, University of Chile
Chile
ingenieria.uchile.cl
Category: 1

China Earthquake Administration
China
www.gov.cn
Category: 5

Institute of Earth Sciences, Academia Sinica
Chinese Taipei
www.earth.sinica.edu.tw
Category: 1

Geological Survey Department
Cyprus
www.moa.gov.cy
Category: 1

Academy of Sciences of the Czech Republic
Czech Republic
www.cas.cz
Category: 2

Geological Survey of Denmark and Greenland - GEUS
Denmark
www.geus.dk
Category: 2

National Research Institute for Astronomy and Geophysics (NRIAG), Cairo
Egypt
www.nriag.sci.eg
Category: 1

The University of Helsinki
Finland
www.helsinki.fi
Category: 2

Institute National des Sciences de l'Univers
France
www.insu.cnrs.fr
Category: 4

Laboratoire de Détection et de Géophysique/CEA
France
www-dase.cea.fr
Category: 2

Bundesanstalt für Geowissenschaften und Rohstoffe
Germany
www.bgr.bund.de
Category: 4

GeoForschungsZentrum Potsdam
Germany
www.gfz-potsdam.de
Category: 2

The Seismological Institute, National Observatory of Athens
Greece
www.noa.gr
Category: 1

The Hungarian Academy of Sciences
Hungary
www.mta.hu
Category: 1

The Icelandic Meteorological Office
Iceland
www.vedur.is
Category: 1

India Meteorological Department
India
www.imd.ernet.in
Category: 4

Iraqi Seismic Network
Iraq
www.imos-tm.com
Category: 1

Dublin Institute for Advanced Studies
Ireland
www.dias.ie
Category: 1

The Geophysical Institute of Israel
Israel
www.gii.co.il
Category: 1

Soreq Nuclear Research Centre (SNRC)
Israel
www.soreq.gov.il
Category: 1

Istituto Nazionale di Oceanografia e di Geofisica Sperimentale
Italy
www.ogs.trieste.it
Category: 1

Istituto Nazionale di Geofisica e Vulcanologia
Italy
www.ingv.it
Category: 3

University of the West Indies
Jamaica
www.mona.uwi.edu
Category: 1

Japan Agency for Marine-Earth Science and Technology (JAMSTEC)
Japan
www.jamstec.go.jp
Category: 3

The Japan Meteorological Agency (JMA)
Japan
www.jma.go.jp
Category: 5

Earthquake Research Institute, University of Tokyo
Japan
www.eri.u-tokyo.ac.jp
Category: 3

National Institute of Polar Research (NIPR)
Japan
www.nipr.ac.jp
Category: 1

Natural Resources Authority, Amman
Jordan
www.nra.gov.jo
Category: 1

Institute of Geophysics, National University of Mexico
Mexico
www.igeofcu.unam.mx
Category: 1

The Royal Netherlands Meteorological Institute
Netherlands
www.knmi.nl
Category: 2

Institute of Geological and Nuclear Sciences
New Zealand
www.gns.cri.nz
Category: 3

The University of Bergen
Norway
www.uib.no
Category: 2

Stiftelsen NORSAR
Norway
www.norsar.no
Category: 2

Institute of Geophysics, Polish Academy of Sciences
Poland
www.igf.edu.pl
Category: 1

Instituto Português do Mar e da Atmosfera
Portugal
www.ipma.pt
Category: 2

Red Sísmica de Puerto Rico
Puerto Rico
redsismica.uprm.edu
Category: 1

Korean Meterological Administration
Republic of Korea
www.kma.go.kr
Category: 1

National Institute for Earth Physics
Romania
www.infp.ro
Category: 1

Russian Academy of Sciences
Russia
www.ras.ru
Category: 5

Council for Geoscience
South Africa
www.geoscience.org.za
Category: 1

Uppsala Universitet
Sweden
www.uu.se
Category: 2

The Swiss Academy of Sciences
Switzerland
www.scnat.ch
Category: 2

Disaster and Emergency Management Presidency
Turkey
www.deprem.gov.tr
Category: 2

The Royal Society of London
United Kingdom
www.royalsociety.org
Category: 6

British Geological Survey
United Kingdom
www.bgs.ac.uk
Category: 2

Incorporated Research Institutions for Seismology
U.S.A.
www.iris.edu
Category: 1

Environmental Agency of Slovenia
Slovenia
www.arso.gov.si
Category: 1

Institut Cartogràfic i Geològic de Catalunya (ICGC)
Spain
www.igc.cat
Category: 1

National Defence Research Establishment
Sweden
www.foi.se
Category: 1

University of the West Indies
Trinidad and Tobago
sta.uwi.edu
Category: 1

Kandilli Observatory and Earthquake Research Institute
Turkey
www.koeri.boun.edu.tr
Category: 1

AWE Blacknest
United Kingdom
www.blacknest.gov.uk
Category: 1

University of Texas at Austin
U.S.A.
www.utexas.edu
Category: 1

The National Science Foundation of the United States. (Grant No. EAR-1417970)
U.S.A.
www.nsf.gov
Category: 9

National Earthquake Information Center, U.S. Geological Survey
U.S.A.
www.neic.usgs.gov
Category: 2

In addition the ISC is currently in receipt of grants from the International Data Centre (IDC) of the Preparatory Commission of the Comprehensive Nuclear-Test-Ban Treaty Organization (CTBTO), the Global Earthquake risk Model Foundation (GEM), FM Global, Lighthill risk Network, OYO and USGS (Award G14AC00149).

2.5 Sponsoring Organisations

Article IV(c) of the ISC Working Statutes stipulates any commercial organisation with an interest in the objectives and/or output of the ISC may become an Associate Member of the ISC on payment of an Associate membership fee, but without entitlement to representation with a vote on the ISC's governing body.

www.reftek.com

REF TEK designs and manufactures application specific, high-performance, battery-operated, field-portable geophysical data acquisition devices for the global market. With over 35 years of experience, REF TEK provides customers with complete turnkey solutions that include high resolution recorders, broadband sensors, state-of-the-art communications (V-SAT, GPRS, etc), installation, training, and continued customer support. Over 7,000 REF TEK instruments are currently being used globally for multiple applications. From portable earthquake monitoring to telemetry earthquake monitoring, earthquake aftershock recording to structural monitoring and more, REF TEK equipment is suitable for a wide variety of application needs.

2.6 Data Contributing Agencies

In addition to its Members and Sponsors, the ISC owes its existence and successful long-term operations to its 137 seismic bulletin data contributors. These include government agencies responsible for national seismic networks, geoscience research institutions, geological surveys, meteorological agencies, universities, national data centres for monitoring the CTBT and individual observatories. There would be no ISC Bulletin available without the regular stream of data that are unselfishly and generously contributed to the ISC on a free basis.

The Institute of Seismology, Academy of Sciences of Albania
Albania
TIR

Centre de Recherche en Astronomie, Astrophysique et Géophysique
Algeria
CRAAG

Instituto Nacional de Prevención Sísmica
Argentina
SJA

Universidad Nacional de La Plata
Argentina
LPA

National Survey of Seismic Protection
Armenia
NSSP

Geoscience Australia
Australia
AUST

Österreichischer Geophysikalischer Dienst
Austria
VIE

International Data Centre, CTBTO
Austria
IDC

Republic Center of Seismic Survey
Azerbaijan
AZER

Centre of Geophysical Monitoring
Belarus
BELR

Royal Observatory of Belgium
Belgium
UCC

Observatorio San Calixto
Bolivia
SCB

Instituto Astronomico e Geofísico
Brazil
VAO

Geophysical Institute, Bulgarian Academy of Sciences
Bulgaria
SOF

Canadian Hazards Information Service, Natural Resources Canada
Canada
OTT

Departamento de Geofísica, Universidad de Chile
Chile
GUC

China Earthquake Networks Center
China
BJI

Institute of Earth Sciences, Academia Sinica
Chinese Taipei
ASIES

Red Sismológica Nacional de Colombia
Colombia
RSNC

Sección de Sismología, Vulcanología y Exploración Geofísica
Costa Rica
UCR

Seismological Survey of the Republic of Croatia
Croatia
ZAG

Cyprus Geological Survey Department
Cyprus
NIC

Geophysical Institute, Academy of Sciences of the Czech Republic
Czech Republic
PRU

West Bohemia Seismic Network
Czech Republic
WBNET

The Institute of Physics of the Earth (IPEC)
Czech Republic
IPEC

Observatoire Volcanologique de Goma
Democratic Republic of the Congo
GOM

Geological Survey of Denmark and Greenland
Denmark
DNK

Observatoire Géophysique d'Arta
Djibouti
ARO

Servicio Nacional de Sismología y Vulcanología
Ecuador
IGQ

National Research Institute of Astronomy and Geophysics
Egypt
HLW

University of Addis Ababa
Ethiopia
AAE

Institute of Seismology, University of Helsinki
Finland
HEL

Institut de Physique du Globe
France
STR

Laboratoire de Détection et de Géophysique/CEA
France
LDG

Centre Sismologique Euro-Méditerranéen (CSEM/EMSC)
France
CSEM

Laboratoire de Géophysique/CEA
French Polynesia
PPT

Seismological Observatory Skopje
FYR Macedonia
SKO

Seismic Monitoring Centre of Georgia
Georgia
TIF

Alfred Wegener Institute for Polar and Marine Research
Germany
AWI

Bundesanstalt für Geowissenschaften und Rohstoffe
Germany
BGR

Seismological Observatory Berggießhübel, TU Bergakademie Freiberg
Germany
BRG

Geophysikalisches Observatorium Collm
Germany
CLL

Department of Geophysics, Aristotle University of Thessaloniki
Greece
THE

National Observatory of Athens
Greece
ATH

Hong Kong Observatory
Hong Kong
HKC

Geodetic and Geophysical Research Institute
Hungary
BUD

Icelandic Meteorological Office
Iceland
REY

India Meteorological Department
India
NDI

National Geophysical Research Institute
India
HYB

Badan Meteorologi, Klimatologi dan Geofisika
Indonesia
DJA

International Institute of Earthquake Engineering and Seismology (IIEES)
Iran
THR

Tehran University
Iran
TEH

Iraqi Meteorological and Seismology Organisation
Iraq
ISN

Dublin Institute for Advanced Studies
Ireland
DIAS

The Geophysical Institute of Israel
Israel
GII

MedNet Regional Centroid - Moment Tensors
Italy
MED_RCMT

Istituto Nazionale di Geofisica e Vulcanologia
Italy
ROM

Istituto Nazionale di Oceanografia e di Geofisica Sperimentale (OGS)
Italy
TRI

Station Géophysique de Lamto
Ivory Coast
LIC

Jamaica Seismic Network
Jamaica
JSN

National Institute of Polar Research
Japan
SYO

National Research Institute for Earth Science and Disaster Prevention
Japan
NIED

Japan Meteorological Agency
Japan
JMA

The Matsushiro Seismological Observatory
Japan
MAT

Jordan Seismological Observatory
Jordan
JSO

National Nuclear Center
Kazakhstan
NNC

Seismological Experimental Methodological Expedition
Kazakhstan
SOME

Kyrgyz Seismic Network
Kyrgyzstan
KNET

Institute of Seismology, Academy of Sciences of Kyrgyz Republic
Kyrgyzstan
KRNET

National Council for Scientific Research
Lebanon
GRAL

Geological Survey of Lithuania
Lithuania
LIT

Macao Meteorological and Geophysical Bureau
Macao, China
MCO

Geological Survey Department Malawi
Malawi
GSDM

Malaysian Meteorological Service
Malaysia
KLM

Red Sismica del Noroeste de Mexico (RESOM)
Mexico
ECX

Instituto de Geofísica de la UNAM
Mexico
MEX

Institute of Geophysics and Geology
Moldova
MOLD

Research Centre of Astronomy and Geophysics
Mongolia
OBM

Seismological Institute of Montenegro
Montenegro
PDG

The Geological Survey of Namibia
Namibia
NAM

Department of Mines and Geology, Ministry of Industry of Nepal
Nepal
DMN

Koninklijk Nederlands Meteorologisch Instituut
Netherlands
DBN

Institute of Geological and Nuclear Sciences
New Zealand
WEL

Stiftelsen NORSAR
Norway
NAO

University of Bergen
Norway
BER

Sultan Qaboos University
Oman
OMAN

Micro Seismic Studies Programme, PINSTECH
Pakistan
MSSP

Manila Observatory
Philippines
QCP

Philippine Institute of Volcanology and Seismology
Philippines
MAN

Institute of Geophysics, Polish Academy of Sciences
Poland
WAR

Instituto Português do Mar e da Atmosfera, I.P.
Portugal
INMG

Sistema de Vigilância Sismológica dos Açores
Portugal
SVSA

Instituto Geofisico do Infante Dom Luiz
Portugal
IGIL

Korea Meteorological Administration
Republic of Korea
KMA

National Institute for Earth Physics
Romania
BUC

Mining Institute of the Ural Branch of the Russian Academy of Sciences
Russia
MIRAS

Kamchatkan Experimental and Methodical Seismological Department, GS RAS
Russia
KRSC

Kola Regional Seismic Centre, GS RAS
Russia
KOLA

Altai-Sayan Seismological Centre, GS SB RAS
Russia
ASRS

Baykal Regional Seismological Centre, GS SB RAS
Russia
BYKL

Geophysical Survey of Russian Academy of Sciences
Russia
MOS

North Eastern Regional Seismological Centre, GS RAS
Russia
NERS

Yakutiya Regional Seismological Center, GS SB RAS
Russia
YARS

Sakhalin Experimental and Methodological Seismological Expedition, GS RAS
Russia
SKHL

Institute of Environmental Problems of the North, Russian Academy of Sciences
Russia
IEPN

Saudi Geological Survey
Saudi Arabia
SGS

Seismological Survey of Serbia
Serbia
BEO

Geophysical Institute, Slovak Academy of Sciences
Slovakia
BRA

Environmental Agency of the Republic of Slovenia
Slovenia
LJU

Ministry of Mines, Energy and Rural Electrification
Solomon Islands
HNR

Council for Geoscience
South Africa
PRE

Institut Cartogràfic de Catalunya
Spain
MRB

Instituto Geográfico Nacional
Spain
MDD

University of Uppsala
Sweden
UPP

Swiss Seismological Sevice (SED)
Switzerland
ZUR

National Syrian Seismological Center
Syria
NSSC

Thai Meteorological Department
Thailand
BKK

University of the West Indies
Trinidad and Tobago
TRN

Kandilli Observatory and Research Institute
Turkey
ISK

The Earthquake Research Center Ataturk University
Turkey
ATA

Disaster and Emergency Management Presidency
Turkey
DDA

Subbotin Institute of Geophysics, National Academy of Sciences
Ukraine
SIGU

Dubai Seismic Network
United Arab Emirates
DSN

British Geological Survey
United Kingdom
BGS

National Earthquake Information Center
U.S.A.
NEIC

The Global CMT Project
U.S.A.
GCMT

IRIS Data Management Center
U.S.A.
IRIS

Pacific Northwest Seismic Network
U.S.A.
PNSN

Red Sísmica de Puerto Rico
U.S.A.
RSPR

IASPEI Working Group on Reference Events
U.S.A.
IASPEI

United States Geological Survey
U.S.A.
USGS

National Center for Scientific Research
Vietnam
PLV

Yemen National Seismological Center
Yemen
DHMR

Geological Survey Department of Zambia
Zambia
LSZ

Goetz Observatory
Zimbabwe
BUL

East African Network

EAF

CWB
Chinese Taipei
TAP

2.7 ISC Staff

Listed below are the staff (and their country of origin) who were employed at the ISC at the time of this ISC Bulletin Summary.

- Dmitry Storchak
- Director
- Russia/United Kingdom

- Maureen Aspinwall
- Administration Officer
- United Kingdom

- James Harris
- System and Database Administrator
- United Kingdom

- John Eve
- Data Collection Officer
- United Kingdom

- Emily Delahaye
- Seismologist/Lead Analyst
- Canada

- Blessing Shumba
- Seismologist/Analyst
- Zimbabwe

- Rosemary Wylie
- Analyst
- United Kingdom

- Rebecca Verney
- Analyst
- United Kingdom

- Wayne Richardson
- Senior Seismologist
- New Zealand

- Domenico Di Giacomo
- Seismologist
- Italy

- Konstantinos Lentas
- Seismologist/Developer
- Greece

- Przemek Ozgo
- System Administrator
- Poland

- Natalia Safronova
- Historical Data Entry Officer
- Russia

- Elizabeth Ball
- Historical Data Entry Officer
- United Kingdom

- Daniela Catanescu
- Historical Data Entry Officer
- Romania

3

ISC Operational Procedures

3.1 Introduction

The relational database at the ISC is the primary source for the ISC Bulletin. This database is also the source for the ISC web-based search, the ISC CD-ROMs and this printed Summary. The ISC database is also mirrored at several institutions such as the Data Management Center of the Incorporated Research Institutions for Seismology (IRIS DMC), Earthquake Research Institute (ERI) of the University of Tokyo and a few others.

The database holds information about ISC events, both natural and anthropogenic. Information on each event may include hypocentre estimates, moment tensors, event type, felt and damaging reports and associated station observations reported by different agencies and grouped together per physical event.

The majority of the ISC events (∼80%) are small and are not reviewed by the ISC analysts. Those that are reviewed (∼20%, usually magnitude greater than 3.5) may or may not include an ISC hypocentre solution and magnitude estimates. The decision depends on whether the wealth of combined information from several agencies as compared to the data of each single agency alone warrants the ISC location. The events are called ISC events regardless of whether they have been reviewed or located by the ISC or not.

All events located by the ISC are reviewed by the ISC analysts but not the other way round. Analyst review involves an examination of the integrity of all reported parametric information. It does not involve review of waveforms. Even if waveforms from all of the ∼6,000 stations included in a typical recent month of the ISC Bulletin were freely available, it would be an unmanageable task to inspect them all.

We shall now describe briefly current processes and procedures involved in producing the Bulletin of the International Seismological Centre. These have been developed from former practices described in the Introduction to earlier issues of the ISC Bulletin to account for modern methods and technologies of data collection and analysis.

3.2 Data Collection

Parametric data, mainly comprising seismic event hypocentre solutions, phase arrival observations and associated magnitude data, are now mostly emailed to the ISC (seismo@isc.ac.uk) by agencies around the world. Other macroseismic and source information associated with seismic events may also be incorporated in accordance with modern standards. The process of data collection at the ISC involves the automatic parsing of these data into the ISC relational database. The ISC now has over 200 individual parsers to account for legacy and current bulletin data formats used by data reporters.

Figure 3.1 shows the 313 agencies that have reported bulletin data to the ISC, directly or via regional data centres, during the entire period of the ISC existence: these agencies are also listed in Table 12.1 of the Appendix. In Figure 3.1, corresponding countries are shown shaded in red. Please note that the continent of Antarctica appears white on the map despite a steady stream of bulletin data from Antarctic stations: the agencies that run these stations are based elsewhere.

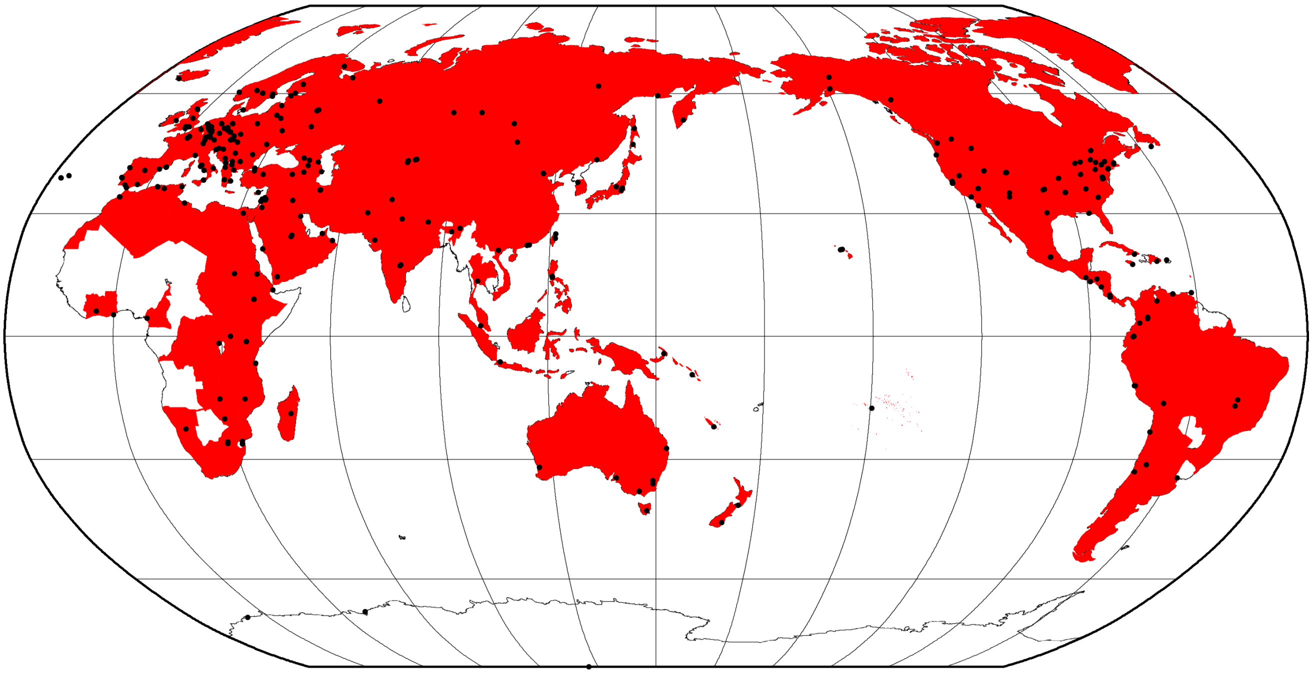

Figure 3.1: *Map of 313 agencies and corresponding countries that have reported seismic bulletin data to the ISC at least once during the entire period of the ISC operations, either directly or via regional data centres. Corresponding countries are shaded in red.*

3.3 ISC Automatic Procedures

3.3.1 Grouping

Grouping is the automatic process by which the many hypocentre solutions sent by the agencies reporting to the ISC for the same physical event are merged together into a single ISC event. This process possibly begins with an alert message and ends before a final review by ISC analysts. The process periodically runs through a set time interval of the input data stream, typically one day, looking for hypocentres in newly received data that are not yet grouped into an ISC event. Thus it considers only data more recent than the last data month reviewed by the ISC analysts. Immediately after grouping the seismic arrival associator is run on the same time interval, dealing with new phase arrival data not associated with any hypocentre.

The first stage of grouping gets a score where possible for each hypocentre to determine whether the reported hypocentre will be considered to be the primary estimate, or prime, for an ISC event. This score is based on the station arrival times reported in association with the hypocentre in four epicentral distance zones that characterise the networks of stations reporting:

1. Whole network
2. Local, 0 - 150 km
3. Near-regional, 3° - 10°
4. Teleseismic, 28° - 180°

For each distance zone, the azimuthal gap, the secondary azimuthal gap (the largest azimuthal gap filled by a single station), the minimum and maximum epicentral distance and number of stations are all used to calculate the value of dU, the normalised absolute deviation from best fitting uniformly distributed stations (*Bondár and McLaughlin*, 2009a). Clearly, this procedure can only use:

1. Bulletin data with hypocentres and sufficient associated seismic arrivals
2. Data for stations that are in the International Registry (IR)
3. Station data that are actually reported to ISC: CENC (China), for example, reports at most 24 stations, whilst many more may have been used to determine the hypocentre.

The hypocentres are then each considered in turn for grouping using one of two methods, the first by searching for a similar hypocentre, and the second by searching for the best fit of the reported phase arrival data that are associated with the candidate hypocentre. The method chosen for a reporter is based on feedback gained from ISC analysts.

For finding similar hypocentres, three sets of limits for origin-time difference and epicentral separation are used according to the type of bulletin data, be it alert, provisional or final: these limits are, respectively:

- ± 2 minutes and 10°
- ± 2 minutes and 4°
- ± 1 minutes and 2°

If there is no overlap with the hypocentre of an existing ISC event, a new event is formed. For each candidate hypocentre, a proximity score is otherwise calculated based on differences in time, t, and distance, s, between the candidate hypocentre and a hypocentre in an event with which it could potentially be grouped.

Proximity score $= 2 - (dt/dt_{max}) - (ds/ds_{max})$

where ds_{max} is the maximum distance between hypocentres and dt_{max} the maximum difference in origin time.

As long as there is no duplication of hypocentre (with the same author, origin time and location within tight limits) the candidate hypocentre together with the associated phase data is grouped with the prime hypocentre of the event and the initial dU score is used to reassess the prime hypocentre designation. Apparent duplicated hypocentre estimations, including preliminary solutions relayed by other agencies, need to be assessed to determine whether they should really be split between different events. Should there be two or more equally valid events, these can be assessed in turn and may eventually be merged together.

Grouping by fit of the associated phase arrival data is simpler. The residuals of the arrival data are calculated using ak135 travel times for all suitable prime hypocentres within the widest proximity limits given above for similar hypocentres. The hypocentre and associated phase arrival data is then grouped with the event with the best fitting prime hypocentre, which may similarly be re-designated according to the dU scores. Associations of phase arrival data are updated to be with the prime hypocentre estimate of each ISC event.

It follows that a hypocentre and associated phase arrival data submitted by a reporter will have the reported hypocentre set as the prime hypocentre in the ISC event if no other submitted hypocentre estimate is a closer match. It follows also that a hypocentre submitted without phase data can only be grouped with a similar hypocentre. Generally, early arriving data may be superseded by later arriving data: the data will still be in the ISC database but be deprecated, that is, marked as being no longer useful for further processes.

3.3.2 Association

Association is the automatic procedure, run routinely after grouping, that links reported phase arrivals at IR stations with the prime hypocentres of ISC events. As grouping took care of those phases associated with reported hypocentres, by associating the phases to the respective prime hypocentres of the ISC events without further checks, this procedure is only required for phase arrival observations that were sent without any association of event made for them by the reporter. Currently only 5% of arrival data is sent unassociated compared with 25% ten years ago.

If a phase arrival is found to be very similar to another already reported, it is placed in the same event, otherwise the procedure below is followed.

For associating a phase arrival, suitable events are sought with prime hypocentre origin-times in the window 40 minutes before and 100 s after the arrival time. For each phase arrival and prime hypocentre an ak135 travel-time residual is calculated for either the reported arrival phase name or an alternative from a default list if appropriate. Possible timing errors that are multiples of 60 s (a minute) are considered if the phase arrival is at a station not known to be digitally recording. A reporting likelihood is then determined based on the reported event magnitude: a magnitude default of 3.0 is used if no magnitude is given.

A final score is calculated from the residuals, from the likelihood of the phase observations for the magnitude of the event and from the S-P misfit. A phase arrival along with all other phase arrivals in that reading for the station is then associated with the prime hypocentre with the best score. If no suitable match is found, the reading remains unassociated but may be used at some later stage.

3.3.3 Thresholding

Thresholding is the process determining which events are to be reviewed by the ISC analysts. In former times, before email transmission of data was convenient, all events were reviewed, with magnitudes nearly always 3.5 or above. Nowadays, data contributors are encouraged to send all their data, which are stored in the ISC database. The overwhelming amount of data, including that for many more smaller events and from many more seismograph stations, led to the advent of ISC Comprehensive Bulletin, for all events, and the ISC Reviewed Bulletin, for selected events reviewed by ISC analysts. Thresholding has been under constant review since the start of the 1999 data year.

Several criteria are considered to decide which events merit review. Once a decision is made, whether or not an event is to be reviewed, further criteria are not considered.

In this section, M is the maximum magnitude reported by any agency for the event. The sequence of tests in the automatic decision process for reviewing events is currently:

- All events reported by the International Data Centre (IDC) of the Comprehensive Nuclear-Test-Ban Treaty Organization (CTBTO) are reviewed.
- If M is greater than or equal to 3.5, the event is reviewed.
- If M is less than 2.5, the event is not reviewed.
- If M is unknown, the number of data sources of hypocentres and phase arrivals is used. Care is taken here to avoid counting indirect reports arriving via agencies such as NEIC, CSEM and CASC, which compile regional and global data:
  - If the number of hypocentre authors is greater than two and the maximum epicentral distance of arrival data is greater than 10°, the event is reviewed.
  - If the number of arrival authors is greater than two and the maximum epicentral distance of arrival data is greater than 10°, the event is reviewed.
  - Otherwise the event is not reviewed.
- If M is between 2.5 and 3.5:
  - If the number of hypocentre and seismic arrival authors is less than two, the event is not reviewed.
  - If any bulletin contributing to the event has at least ten stations within 3° and the secondary azimuthal gap (the largest azimuthal gap filled by a single station) is less than 135°, the event is not reviewed.

3.3.4 Location by the ISC

The automatic processes group and associate incoming data into ISC events as indicated above. These data are available to users before review by the ISC analysts but there will be no ISC hypocentre solutions for any of the events. The candidate events due for review by the ISC analysts are determined by the thresholding process, which is why many smaller events remain without an ISC hypocentre solution even after the analyst review.

Several further checks of the data are made in preparation for the analyst review, and initial trial estimates for ISC hypocentres are then generated using the accumulated data. If sufficiently robust, the ISC hypocentre estimation will be retained and be made the prime solution for the event, but this, of course, will itself be subject to the analyst review.

It is important to note that not all reviewed events will have an ISC hypocentre. For the reviewed events certain criteria must be met for an initial ISC location of an event to be made. These criteria are shown below:

- All events with an IDC hypocentre, unless IDC is the only hypocentre author and there are less than six associated phases.
- Two or more reporters of data
- Phase data at epicentral distance $\geq 20°$

The ISC locator also needs an intial seed location; in all events except those with eight or more reporters of data where the existing prime is used, this is calculated using a Neighbourhood Algorithm (NA) (*Sambridge*, 1999; *Sambridge and Kennett*, 2001). More information about the ISC location algorithm and initial seed is given in the next section.

3.4 ISC Location Algorithm

The new ISC location algorithm is described in detail in *Bondár and Storchak* (2011) (doi: 10.1111/j.1365-246X.2011.05107.x, Manual www.isc.ac.uk/iscbulletin/iscloc/); here we give a short summary of the major features. Ever since the ISC came into existence in 1964, it has been committed to providing a homogeneous bulletin that benefits scientific research. Hence the location algorithm used by the ISC, except for some minor modifications, has remained largely unchanged for the past 40 years (*Adams et al.*, 1982; *Bolt*, 1960). While the ISC location procedures have served the scientific community well in the past, they can certainly be improved.

Linearised location algorithms are very sensitive to the initial starting point for the location. The old procedures made the assumption that a good initial hypocentre is available among the reported hypocentres. However, there is no guarantee that any of the reported hypocentres are close to the global minimum in the search space. Furthermore, attempting to find a free-depth solution was futile when the data had no resolving power for depth (e.g. when the first arrival is not within the inflection point of the P travel-time curve). When there was no depth resolution, the algorithm would simply pick a point on the origin time – depth trade-off curve. The old ISC locator assumed that the observational errors are independent. The recent years have seen a phenomenal growth both in the number of reported events and phases, owing to the ever-increasing number of stations worldwide. Similar ray paths will produce correlated travel-time prediction errors due to unmodelled heterogeneities in the Earth, resulting in underestimated location uncertainties and for unfavourable network geometries, location bias. Hence, accounting for correlated travel-time prediction errors becomes imperative if we want to improve (or simply maintain) location accuracy as station networks become progressively denser. Finally, publishing network magnitudes that may have been derived from a single station measurement was rather prone to producing erroneous event magnitude estimates.

To meet the challenge imposed by the ever-increasing data volume from heavily unbalanced networks we introduced a new ISC location algorithm to ensure the efficient handling of data and to further improve the location accuracy of events reviewed by the ISC. The new ISC location algorithm

- Uses all ak135 (*Kennett et al.*, 1995) predicted phases (including depth phases) in the location;
- Obtains the initial hypocentre guess via the Neighbourhood Algorithm (NA) (*Sambridge*, 1999; *Sambridge and Kennett*, 2001);
- Performs iterative linearised inversion using an *a priori* estimate of the full data covariance matrix to account for correlated model errors (*Bondár and McLaughlin*, 2009b);
- Attempts a free-depth solution if and only if there is depth resolution, otherwise it fixes the depth to a region-dependent default depth;
- Scales uncertainties to 90% confidence level and calculates location quality metrics for various distance ranges;
- Obtains a depth-phase depth estimate based on reported surface reflections via depth-phase stacking (*Murphy and Barker*, 2006);
- Provides robust network magnitude estimates with uncertainties.

3.4.1 Seismic Phases

One of the major advantages of using the ak135 travel-time predictions (*Kennett et al.*, 1995) is that they do not suffer from the baseline difference between P, S and PKP phases compared with the Jeffreys-Bullen tables (*Jeffreys and Bullen*, 1940). Furthermore, ak135 offers an abundance of phases from the IASPEI Standard Seismic List (*Storchak et al.*, 2003; 2011) that can be used in the location, most notably the PKP branches and depth-sensitive phases. Elevation and ellipticity corrections (*Dziewonski and Gilbert*, 1976; *Engdahl et al.*, 1998; *Kennett et al.*, 1996), using the WG84 ellipsoid parameters, are added to the ak135 predictions. For depth phases, bounce point (elevation correction at the surface reflection point) and water depth (for pwP) corrections are calculated using the algorithm of *Engdahl et al.* (1998). We use the ETOPO1 global relief model (*Amante and Eakins*, 2009) to obtain the elevation or the water depth at the bounce point.

Phase picking errors are described by *a priori* measurement error estimates derived from the inspection of the distribution of ground truth residuals (residuals calculated with respect to the ground truth location) from the IASPEI Reference Event List (*Bondár and McLaughlin*, 2009a). For phases that do not have a sufficient number of observations in the ground truth database we establish *a priori* measurement errors so that the consistency of the relative weighting schema is maintained. First-arriving P-type phases (P, Pn, Pb, Pg) are picked more accurately than later phases, so their measurement error estimates are the smallest, 0.8 s. The measurement error for first-arriving S-phases (S, Sn, Sb, Sg) is set to 1.5 s. Phases traversing through or reflecting from the inner/outer core of the Earth have somewhat larger (1.3 s for PKP, PKS, PKKP, PKKS and P'P' branches as well as PKiKP, PcP and PcS, and 1.8 s for SKP, SKS, SKKP, SKKS and S'S' branches as well as SKiKP, ScP and ScS) measurement error estimates to account for possible identification errors among the various branches. Free-surface reflections and conversions (PnPn, PbPb, PgPg, PS, PnS, PgS and SnSn, SbSb, SgSg, SP, SPn, SPg) are observed less frequently and with larger uncertainty, and therefore suffer from large, 2.5 s, measurement errors. Similarly, a measurement error of 2.8 s is assigned to the longer period and typically emergent diffracted phases (Pdif, Sdif, PKPdif). The *a priori* measurement error for the commonly observed depth phases (pP, sP, pS, sS and pwP) is set to 1.3 s, while the remaining depth phases (pPKP, sPKP, pSKS, sSKS branches and pPb, sPb, sSb, pPn, sPn, sSn) have the measurement error estimate set to 1.8 s. We set the measurement error estimate to 2.5 s for the less reliable depth phases (pPg, sPg, sSg, pPdif, pSdif, sPdif and sSdif). Note that we also allow for distance-dependent measurement errors. For instance, to account for possible phase identification errors at far-regional distances the *a priori* measurement error for Pn and P is increased from 0.8 s to 1.2 s and for Sn and S from 1.5 s to 1.8 s between 15° and 28°. The measurement errors between 40° and 180° are set to 1.3 s and 1.8 s for the prominent PP and SS arrivals respectively, but they are increased to 1.8 s and 2.5 s between 25° and 40°.

The relative weighting scheme (Figure 3.2) described above ensures that arrivals picked less reliably or prone to phase identification errors are down-weighted in the location algorithm. Since the ISC works with reported parametric data with wildly varying quality, we opted for a rather conservative set of *a priori* measurement error estimates.

3.4.2 Correlated Travel-Time Prediction Error Structure

Most location algorithms, either linearised or non-linear, assume that all observational errors are independent. This assumption is violated when the separation between stations is less than the scale length of local velocity heterogeneities. When correlated travel-time prediction errors are present, the data covariance matrix is no longer diagonal, and the redundancy in the observations reduces the effective number of degrees of freedom. Thus, ignoring the correlated error structure inevitably results in underestimated location uncertainty estimates. For events located by an unbalanced seismic network this may also lead to a biased location estimate. *Chang et al.* (1983) demonstrated that accounting for correlated error structure in a linearised location algorithm is relatively straightforward once an estimate of the non-diagonal data covariance matrix is available. To determine the data covariance matrix we follow the approach described by *Bondár and McLaughlin* (2009b). They assume that the similarity between ray paths is well approximated by the station separation. This simplifying assumption allows for the estimation of covariances between station pairs from a generic P variogram model derived from ground truth residuals. Because the overwhelming number of phases in the ISC Bulletin is teleseismic P, we expect that the generic variogram model will perform reasonably well anywhere on the globe.

Since in this representation the covariances depend only on station separations, the covariance matrix (and its inverse) needs to be calculated only once. We assume that different phases owing to the different ray paths they travel along as well as station pairs with a separation larger than 1000 km are uncorrelated. Hence, the data covariance matrix is a sparse, block-diagonal matrix. Furthermore, if the stations in

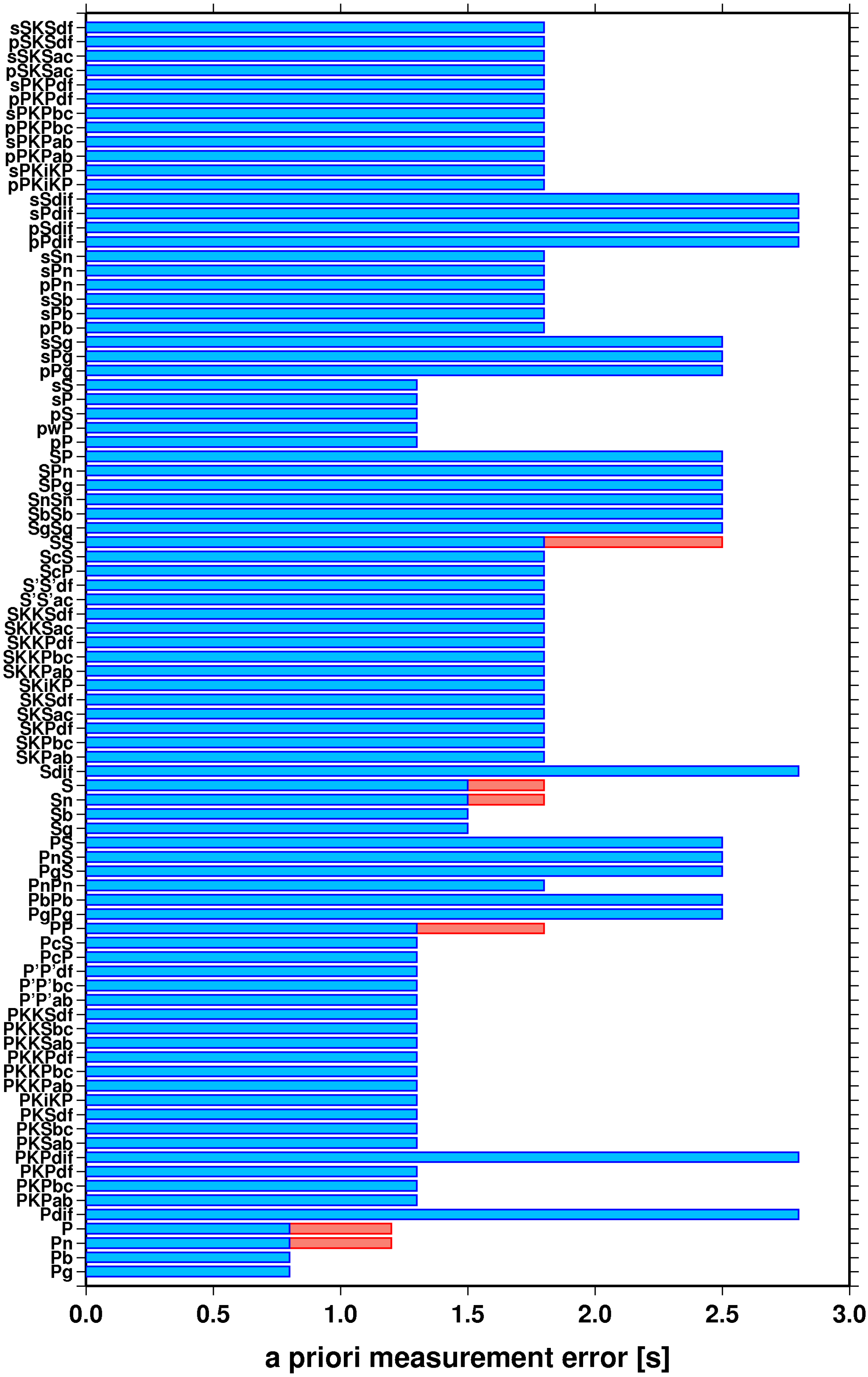

Figure 3.2: A priori *measurement error estimates for phases used in the location algorithm. The red coloured errors are distance-dependent, which are applied for distances when phase identification errors may occur (see text).*

each phase block are ordered by their nearest neighbour distance, the phase blocks themselves become block-diagonal. To reduce the computational time of inverting large matrices we exploit the inherent block-diagonal structure by inverting the covariance matrix block-by-block. The *a priori* measurement error variances are added to the diagonal of the data covariance matrix.

3.4.3 Depth Resolution

In principle, depth can be resolved if there is a mixture of upgoing and downgoing waves emanating from the source, that is, if there are stations covering the distance range where the vertical partial derivative of the travel-time of the first-arriving phase changes sign (local networks), or if there are phases with vertical slowness of opposite sign (depth phases). Core reflections, such as PcP, and to a lesser extent, secondary phases (S in particular) could also help in resolving the depth.

We developed a number of criteria to test whether the reported data for an event have sufficient depth resolution:

- local network: one or more stations within 0.2° with time-defining phases
- depth phases: five or more time-defining depth phases reported by at least two agencies (to reduce a chance of misinterpretation by a single inexperienced analyst)
- core reflections: five or more time-defining core reflections (PcP, ScS) reported by at least two agencies
- local/near regional S: five or more time-defining S and P pairs within 3°

We attempt a free-depth solution if any of the above criteria are satisfied; otherwise we fix the depth to a default depth dependent on the epicentre location. The default depth grid was derived from the EHB (*Engdahl et al.*, 1998) free-depth solutions, including the fixed-depth EHB earthquakes that were flagged as having reliable depth estimate (personal communication with Bob Engdahl), as well as from free-depth solutions obtained by the new locator when locating the entire ISC Bulletin data-set. As Figure 3.3 indicates, the default depth grid provides a reasonable depth estimate where seismicity is well established. Note that the depths of known anthropogenic events and landslides are fixed to the surface.

3.4.4 Depth-Phase Stack

While we use depth phases directly in the location, the depth-phase stacking method (*Murphy and Barker*, 2006) provides an independent means to obtain robust depth estimates. Because the depth obtained from the depth-phase stacking method implicitly depends on the epicentre itself, we perform the depth-phase stack only twice: first, with respect to the initial location in order to obtain a reasonable starting point for the depth in the grid search described in the following section; second, with respect to the final location to obtain the final estimate for the depth-phase constrained depth.

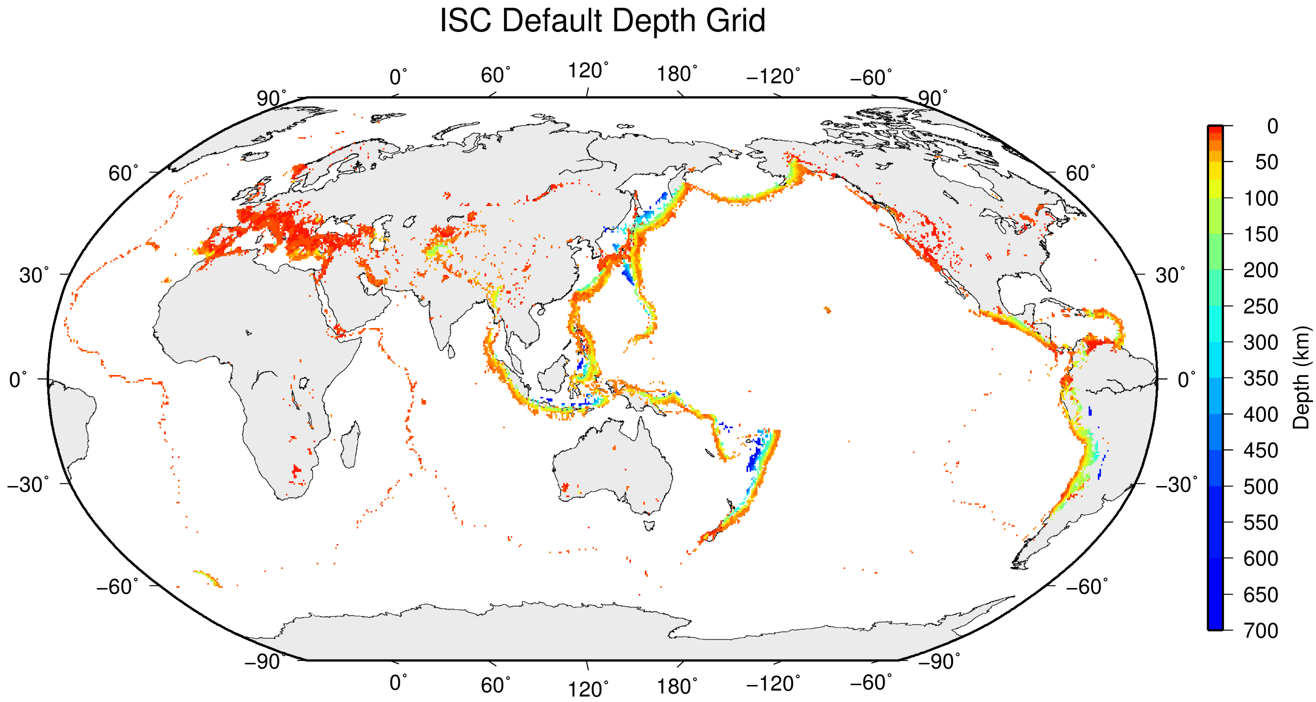

Figure 3.3: *Default depths on a 0.5×0.5 degree grid derived from EHB free-depth solutions and EHB events flagged as reliable depth, as well as free-depth solutions from the entire ISC Bulletin located with the new locator.*

3.4.5 Initial Hypocentre

For poorly recorded events the reported hypocentres may exhibit a large scatter and they could suffer from large location errors, especially if they are only recorded teleseismically. In order to obtain a good initial hypocentre guess for the linearised location algorithm we employ the Neighbourhood Algorithm (NA) (*Sambridge*, 1999; *Sambridge and Kennett*, 2001). NA is a nonlinear grid search method capable of exploring a large search space and rapidly closing in on the global optimum. *Kennett* (2006) discusses in detail the NA algorithm and its use for locating earthquakes.

We perform a search around the median of reported hypocentre parameters with a generously defined search region – within a 2° radius circle around the median epicentre, 10 s around the median origin time and 150 km around the median reported depth. These default search parameters were obtained by trial-and-error runs to achieve a compromise between execution time and allowance for gross errors in the median reported hypocentre parameters. Note that if our test for depth resolution fails, we fix the depth to the region-dependent default depth. The initial hypocentre estimate will be the one with the smallest L1-norm misfit among the NA trial hypocentres. Once close to the global optimum, we proceed with the linearised location algorithm to obtain the final solution and corresponding formal uncertainties.

3.4.6 Iterative Linearised Location Algorithm

We adopt the location algorithm described in detail in *Bondár and McLaughlin* (2009b). Recall that in the presence of correlated travel-time prediction errors the data covariance matrix is no longer diagonal. Using the singular value decomposition of the data covariance matrix we construct a projection matrix that orthogonalises the data set and projects redundant observations into the null space. In other words, we solve the inversion problem in the eigen coordinate system in which the transformed observations are independent.

The model covariance matrix yields the four-dimensional error ellipsoid whose projections provide the two-dimensional error ellipse and one-dimensional errors for depth and origin time. These uncertainties are scaled to the 90% confidence level. Note that since we projected the system of equations into the eigen coordinate system, the number of independent observations is less than the total number of observations. Hence, the estimated location error ellipses necessarily become larger, providing a more realistic representation of the location uncertainties. The major advantage of this approach is that the projection matrix is calculated only once for each event location.

3.4.7 Validation Tests

To demonstrate improvements due to the new location procedures, we located some 7,200 GT0-5 events in the IASPEI Reference Event List (*Bondár and McLaughlin*, 2009a) both with the old ISC locator (which constitutes the baseline) and with the new location algorithm. We also located the entire (1960-2010) ISC Bulletin, including four years of the International Seismological Summary (ISS, the predecessor of the ISC) catalogue (*Villaseñor and Engdahl*, 2005; 2007).

The location of GT events demonstrated that the new ISC location algorithm provides small but consistent location improvements, considerable improvements in depth determination and significantly more accurate formal uncertainty estimates. Even using a 1-D model and a variogram model that fits teleseismic observations we could achieve realistic uncertainty estimates, as the 90% confidence error ellipses cover the true locations 80-85% of the time. The default depth grid provides reasonable depth estimates where there is seismicity. We have shown that the location and depth accuracy obtained by the new algorithm matches or surpasses the EHB accuracy.

We noted above that the location improvements for the ground truth events are consistent, but minor. This is not surprising as most of the events in the IASPEI Reference Event List are very well-recorded with a small azimuthal gap and dominated by P-type phases. In these circumstances we could expect significant location improvements only for heavily unbalanced networks where large numbers of correlated ray paths conspire to introduce location bias. On the other hand, the ISC Bulletin represents a plethora of station configurations ranging from reasonable to the most unfavourable network geometries. Hence, we could expect more dramatic location improvements when locating the entire ISC Bulletin. Although in this case we cannot measure the improvement in location accuracy due to the lack of ground truth information, we show that with the new locator we obtain significantly better clustering of event locations (Figure 3.4), thus providing an improved view of the seismicity of the Earth.

3.4.8 Magnitude Calculation

Currently the ISC locator calculates body and surface wave magnitudes. MS is calculated for shallow events (depth $<$ 60 km) only. At least three station magnitudes are required for a network (mb or MS) magnitude. The network magnitude is defined as the median of the station magnitudes, and its

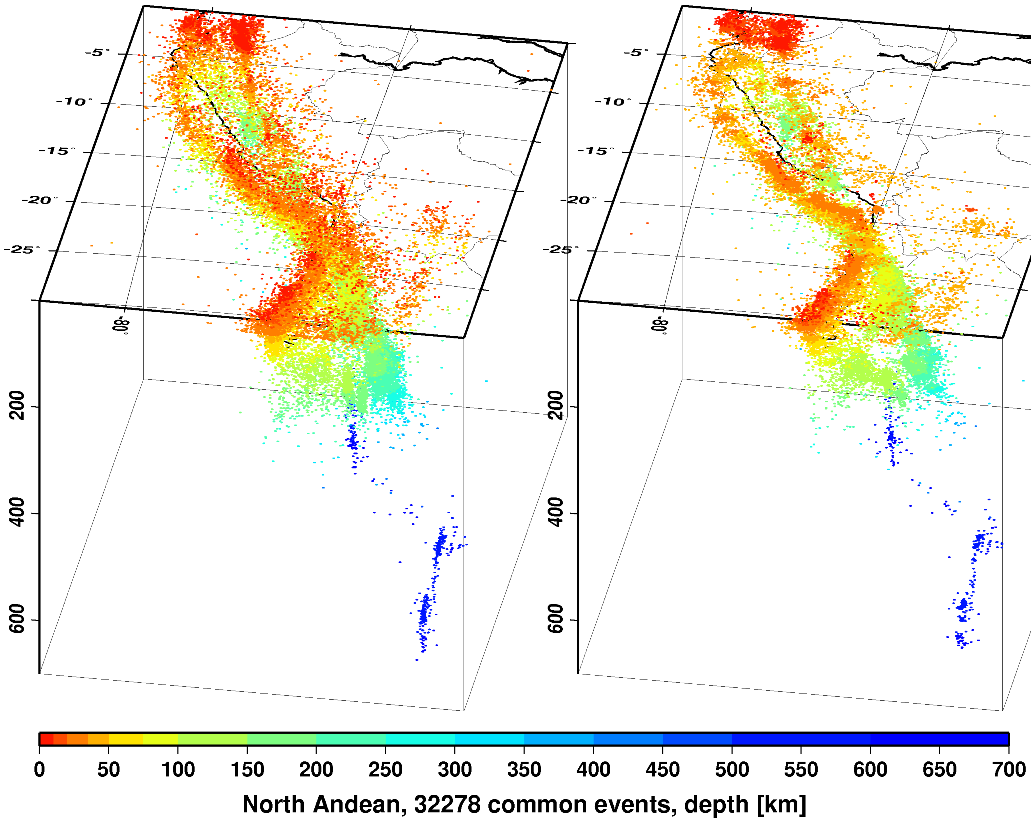

(a)

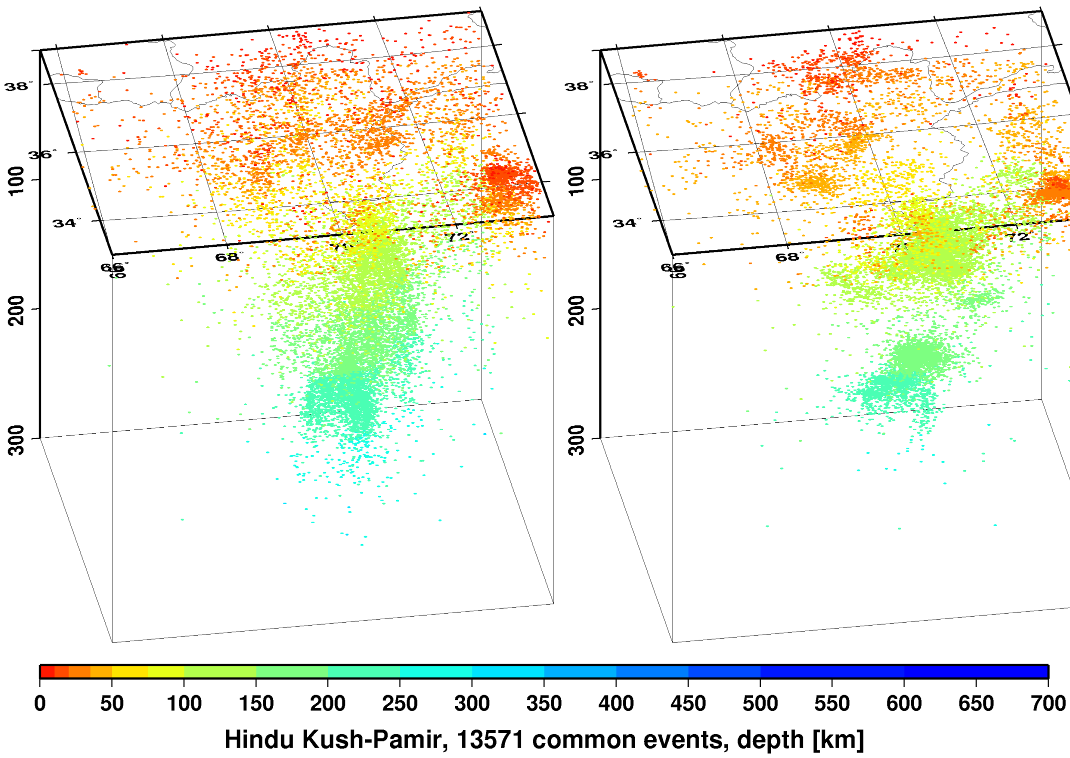

(b)

Figure 3.4: *Comparison of seismicity maps for common events in the reviewed ISC Bulletin (old locator, left) and the located ISC Bulletin (new locator, right) for the North Andean (a) and Hindu Kush - Pamir regions (b). The events are better clustered when located with the new locator.*

uncertainty is defined as the standard median absolute deviation (SMAD) of the alpha-trimmed (*alpha* = 20%) station magnitudes.

The station magnitude is defined as the median of reading magnitudes for a station. The reading magnitude is defined as the magnitude computed from the maximal log(A/T) in a reading. Amplitude magnitudes are calculated for each reported amplitude-period pair.

3.4.9 Body-Wave Magnitudes

Body-wave magnitudes are calculated for each reported amplitude-period pair, provided that the phase is in the list of phases that can contribute to *mb* (P, pP, sP, AMB, IAmb, pmax), the station is between the epicentral distances 21 – 100° and the period is less than 3 s.

A reading contains all parametric data reported by a single agency for an event at a station, and it may have several reported amplitude and periods. The amplitudes are measured as zero-to-peak values in nanometres. For each pair an amplitude *mb* is calculated.

$$mb_{amp} = log(A/T) + Q(\Delta, h) - 3 \tag{3.1}$$

If no amplitude-period pairs are reported for a reading, the body-wave magnitude is calculated using the reported logat values for $log(A/T)$.

$$mb_{amp} = logat + Q(\Delta, h) - 3 \tag{3.2}$$

where the magnitude attenuation $Q(\Delta, h)$ value is calculated using the Gutenberg-Richter tables (*Gutenberg and Richter*, 1956).

For each reading the ISC locator finds the reported amplitude-period pair for which A/T is maximal:

$$mb_{rd} = log(max(A/T)) + Q(\Delta, h) - 3 \tag{3.3}$$

Or, if no amplitude-period pairs were reported for the reading:

$$mb_{rd} = max(logat) + Q(\Delta, h) - 3 \tag{3.4}$$

Several agencies may report data from the same station. The station magnitude is defined as the median of the reading magnitudes for a station.

$$mb_{sta} = median(mb_{rd}) \tag{3.5}$$

Once all station *mb* values are determined, the station magnitudes are sorted and the lower and upper alpha percentiles are made non-defining. The network *mb* and its uncertainty are then calculated as the median and the standard median absolute deviation (SMAD) of the alpha-trimmed station magnitudes, respectively.

3.4.10 Surface-Wave Magnitudes

Surface-wave magnitudes are calculated for each reported amplitude-period pair, provided that the phase is in the list of phases that can contribute to MS (*AMS, IAMs_20, LR, MLR, M, L*), the station is between the epicentral distances 20 – 160° and the period is between 10 – 60 s.

For each reported amplitude-period pair MS is calculated using the Prague formula (*Vaněk et al.*, 1962). Amplitude MS is calculated for each component (Z, E, N) separately.

$$MS_{amp} = log(A/T) + 1.66 * log(\Delta) + 0.3 \tag{3.6}$$

To calculate the reading MS, the ISC locator first finds the reported amplitude-period pair for which A/T is maximal on the vertical component.

$$MS_Z = log(max(A_Z/T_Z)) + 1.66 * log(\Delta) + 0.3 \tag{3.7}$$

Then it finds the max(A/T) for the E and N components for which the period measured on the horizontal components is within ±5s from the period measured on the vertical component.

$$MS_E = log(max(A_E/T_E)) + 1.66 * log(\Delta) + 0.3 \tag{3.8}$$

$$MS_N = log(max(A_N/T_N)) + 1.66 * log(\Delta) + 0.3 \tag{3.9}$$

The horizontal MS is calculated as

$$max(A/T)h = \begin{cases} \sqrt{2(max(A_E/T_E))^2} & \text{if } MS_N \text{ does not exist} \\ \sqrt{(max(A_E/T_E))^2 + (max(A_N/T_N))^2} & \text{if } MS_E \text{ and } MS_N \text{ exist} \\ \sqrt{2(max(A_N/T_N))^2} & \text{if } MS_E \text{ does not exist} \end{cases} \tag{3.10}$$

$$MS_H = log(max(A/T)_H) + 1.66 * log(\Delta) + 0.3 \tag{3.11}$$

The reading MS is defined as

$$MS = \begin{cases} (MS_Z + MS_H)/2 & \text{if } MS_Z \text{ and } MS_H \text{ exist} \\ MS_H & \text{if } MS_Z \text{ does not exist} \\ MS_Z & \text{if } MS_H \text{ does not exist} \end{cases} \tag{3.12}$$

Several agencies may report data from the same station. The station magnitude is defined as the median of the reading magnitudes for a station.

$$MS_{sta} = median(MS_{rd}) \tag{3.13}$$

Once all station MS values are determined, the station magnitudes are sorted and the lower and upper alpha percentiles are made non-defining. The network MS and its uncertainty are calculated as the median and the standard median absolute deviation (SMAD) of the alpha-trimmed station magnitudes, respectively.

3.5 Review Process

Typically, for each month, the ISC analysts now review approximately 20% of the events in the ISC database, currently 3,500-5,000 per data month. This review is done about 24 months behind real time to allow for the comprehensive collection of data from networks and data centres worldwide.

Users of the ISC Bulletin can be assured that all ISC Bulletin events with an ISC hypocentre solution have been reviewed by the ISC analysts. Not all reviewed events will end up having an ISC hypocentre solution, but events that have not been reviewed are flagged accordingly.

An automatic process creates a monthly listing of the events for the analysts to review. The analysis is performed in batches: thus, events are generally not finalised one at a time, and a completed month of events is published after all the analysis is finished.

The first batch of editing involves careful examination of all events selected for review for the month. The entire month is then reprocessed incorporating the editing changes deemed necessary by the analysts. The analysts next review the same events again in a second pass through the data, checking for each event where there is a change that the result was as could be expected by comparing the revised solution against the initial solution. When the analysts are satisfied with an event, it is no longer revised in a subsequent pass but analysis continues in several passes until all events are considered satisfactory.

The analysts initially print the entire monthly listing, which is split into sections each with about 150 events. Each event, uniquely identified in the monthly printout, shows the reported hypocentres, magnitudes and phase arrivals grouped and associated for the event, as well as an ISC solution of hypocentre, if there is one, along with quality metrics, error estimates, redetermined magnitudes and phase arrival-time residuals. Ancillary information including the geographic region and reported macroseismic observations is also present in the listing for each pass.

The analysts have the capability to execute a variety of commands that can be used to merge or split events, to move phase arrivals or hypocentres from one event to another or to modify the reported phase names. Each of these changes initiates a new revision of the relevant events and ISC hypocentre solutions. There are also several commands to change the starting depth or location in the location algorithm.

The main tasks in reviewing the ISC Bulletin are to:

1. Check that the grouping of hypocentres and association of phase arrivals is appropriate.
2. Check that the depth and location is appropriate for the region and reported phase arrivals.
3. Check that no data are missing for an event, given the region and magnitude, and that included data are appropriate.

4. Examine the phase arrival-time residuals to check that the ISC hypocentre solution is appropriate.

5. Look for outliers in the observations and for misassociated phases.

As well as examining each event closely, it is also important to scan the hypocentres and phase arrivals of adjacent events, close in time and space, to ensure that there is uniformity in the composition of the events. In some cases, two events should be merged into one event, as apparent in some other case. In other cases, one apparent event needs to be split into two events, when the automatic grouping has erroneously created one event with more than one reported hypocentre out of the observations for two real events that are distinct but closely occurring.

Misassociated phase arrivals are returned to the unassociated data stream, if not immediately placed by the analyst in another event where they belong, These unassociated phases are then available to be associated with some other event if the time and location is appropriate. The analysts also check that no phase is associated to more than one event.

Towards the end of the monthly analysis, the ISC 'Search' procedure runs, attempting to build events from the remaining set of unassociated phase arrivals. The algorithm is based on the methodology of *Engdahl and Gunst* (1966). Candidate events are validated or rejected by attempting to find ISC hypocentres for them using the ISC locator. The surviving events are then reviewed. Those events with phase arrival observations reported by stations from at least two networks are added to the ISC Bulletin if the solutions meet the standards set by the ISC analysts. These events have only an ISC determination of hypocentre.

At the end of analysis for a data month, a set of final checks is run for quality control, with the results reviewed by an analyst and the defects rectified. These are checks for inconsistencies and errors to ensure the general integrity of the ISC Bulletin.

3.6 History of Operational Changes

- From data-month January 2001 onwards, both P and S groups of arrival times are used in location.
- From data-month September 2002 onwards, the printed ISC Bulletins have been generated directly from the ISC Relational Database.
- From data-month October 2002, a new location program ISCloc has been used in operations. Also, the IASPEI standard phase list has now been adopted by the ISC. Please see Section 6.1 for details.
- From data-month January 2003 onwards, an updated regionalisation scheme has been adopted (*Young et al.*, 1996).
- From data-month January 2006 the ISC hypocentres are computed using the *ak135* earth velocity model (*Kennett et al.*, 1995) and then reviewed by ISC seismologists. The ISC still produces the hypocentre solutions based on Jeffreys-Bullen travel time tables (agency code ISCJB), yet these solutions are no longer reviewed.

  The ISC is planning to re-compute the entire ISC dataset using *ak135* once new procedures for the rebuild are designed, tested, discussed and approved by the ISC Governing Council. Until that time the automatic ISCJB locations will continue to be produced alongside the *ak135* solutions to maintain the long-time continuity of the ISC Bulletin.

- From data-month January 2009, a new location program (*Bondár and Storchak*, 2011) has been used in operations. The new program uses all predicted *ak135* phases and accounts for correlated model errors. An overview of the location algorithm is provided in this volume (Section 3.4).

4

Availability of the ISC Bulletin

The ISC Bulletin is available from the following sources:

- Web searches
  The entire ISC Bulletin is available directly from the ISC website via tailored searches.
  (www.isc.ac.uk/iscbulletin/search)
  (isc-mirror.iris.washington.edu/iscbulletin/search)
  - Bulletin search - provides the most verbose output of the ISC Bulletin in ISF or QuakeML.
  - Event catalogue - only outputs the prime hypocentre for each event, producing a simple list of events, locations and magnitudes.
  - Arrivals - search for arrivals in the ISC Bulletin. Users can search for specific phases for selected stations and events.
- CD-ROMs/DVD-ROMs

  CDs/DVDs can be ordered from the ISC for any published volume (one per year), or for all back issues of the Bulletin (not including the latest volume). The data discs contain the Bulletin as a PDF, in IASPEI Seismic Format (ISF), and in Fixed Format Bulletin (FFB) format. An event catalogue is also included, together with the International Registry of seismic station codes.
- FTP site

  The ISC Bulletin is also available to download from the ISC ftp site, which contains the Bulletin in PDF, ISF and FFB formats. (ftp://www.isc.ac.uk)
  (ftp://isc-mirror.iris.washington.edu)

Mirror service

A mirror of the ISC database, website and ftp site is available at IRIS DMC (isc-mirror.iris.washington.edu), which benefits from their high-speed internet connection, providing an alternative method of accessing the ISC Bulletin.

5

Citing the International Seismological Centre

Data from the ISC should always be cited. This includes use by academic or commercial organisations, as well as individuals. A citation should show how the data were retrieved and may be in one of these suggested forms:

Data retrieved from the ISC web site:

- International Seismological Centre, On-line Bulletin, http://www.isc.ac.uk, Internatl. Seis. Cent., Thatcham, United Kingdom, 2015.

Data transcribed from the IASPEI reference event bulletin:

- International Seismological Centre, Reference Event Bulletin, http://www.isc.ac.uk, Internatl. Seis. Cent., Thatcham, United Kingdom, 2015.

Data transcribed from the EHB bulletin:

- International Seismological Centre, EHB Bulletin, http://www.isc.ac.uk, Internatl. Seis. Cent., Thatcham, United Kingdom, 2015.

Data copied from ISC CD-ROMs/DVD-ROMs:

- International Seismological Centre, Bulletin Disks 1-2012 [CD-ROM], Internatl. Seis. Cent., Thatcham, United Kingdom, 2015.

Data transcribed from the printed Bulletin:

- International Seismological Centre, Bull. Internatl. Seis. Cent., 2015(1), Thatcham, United Kingdom, 2015.

The ISC is named as a valid data centre for citations within American Geophysical Union (AGU) publications. As such, please follow the AGU guidelines when referencing ISC data in one of their journals. The ISC may be cited as both the institutional author of the Bulletin and the source from which the data were retrieved.

BibTex entry example:

@manual{ISCcitation2015,
author = "International Seismological Centre",

title = "On-line Bulletin",
organization = "Int. Seis. Cent.",
note = "http://www.isc.ac.uk",
address = "Thatcham, United Kingdom",
year = "2015"
}

6

IASPEI Standards

6.1 Standard Nomenclature of Seismic Phases

The following list of seismic phases was approved by the IASPEI Commission on Seismological Observation and Interpretation (CoSOI) and adopted by IASPEI on 9th July 2003. More details can be found in *Storchak et al.* (2003) and *Storchak et al.* (2011). Ray paths for some of these phases are shown in Figures 6.1–6.6.

Crustal Phases

Pg	At short distances, either an upgoing P wave from a source in the upper crust or a P wave bottoming in the upper crust. At larger distances also, arrivals caused by multiple P-wave reverberations inside the whole crust with a group velocity around 5.8 km/s.
Pb	Either an upgoing P wave from a source in the lower crust or a P wave bottoming in the lower crust (alt: P*)
Pn	Any P wave bottoming in the uppermost mantle or an upgoing P wave from a source in the uppermost mantle
PnPn	Pn free-surface reflection
PgPg	Pg free-surface reflection
PmP	P reflection from the outer side of the Moho
PmPN	PmP multiple free surface reflection; N is a positive integer. For example, PmP2 is PmPPmP.
PmS	P to S reflection/conversion from the outer side of the Moho
Sg	At short distances, either an upgoing S wave from a source in the upper crust or an S wave bottoming in the upper crust. At larger distances also, arrivals caused by superposition of multiple S-wave reverberations and SV to P and/or P to SV conversions inside the whole crust.
Sb	Either an upgoing S wave from a source in the lower crust or an S wave bottoming in the lower crust (alt: S*)
Sn	Any S wave bottoming in the uppermost mantle or an upgoing S wave from a source in the uppermost mantle
SnSn	Sn free-surface reflection
SgSg	Sg free-surface reflection
SmS	S reflection from the outer side of the Moho
SmSN	SmS multiple free-surface reflection; N is a positive integer. For example, SmS2 is SmSSmS.
SmP	S to P reflection/conversion from the outer side of the Moho
Lg	A wave group observed at larger regional distances and caused by superposition of multiple S-wave reverberations and SV to P and/or P to SV conversions inside the whole crust. The maximum energy travels with a group velocity of approximately 3.5 km/s
Rg	Short-period crustal Rayleigh wave

Mantle Phases

P	A longitudinal wave, bottoming below the uppermost mantle; also an upgoing longitudinal wave from a source below the uppermost mantle
PP	Free-surface reflection of P wave leaving a source downward
PS	P, leaving a source downward, reflected as an S at the free surface. At shorter distances the first leg is represented by a crustal P wave.
PPP	Analogous to PP
PPS	PP which is converted to S at the second reflection point on the free surface; travel time matches that of PSP
PSS	PS reflected at the free surface
PcP	P reflection from the core-mantle boundary (CMB)
PcS	P converted to S when reflected from the CMB
PcPN	PcP reflected from the free surface N - 1 times; N is a positive integer. For example PcP2 is PcPPcP.
Pz+P	(alt: PzP) P reflection from outer side of a discontinuity at depth z; z may be a positive numerical value in km. For example, P660+P is a P reflection from the top of the 660 km discontinuity.
Pz-P	P reflection from inner side of a discontinuity at depth z. For example, P660-P is a P reflection from below the 660 km discontinuity, which means it is precursory to PP.
Pz+S	(alt:PzS) P converted to S when reflected from outer side of discontinuity at depth z
Pz-S	P converted to S when reflected from inner side of discontinuity at depth z
PScS	P (leaving a source downward) to ScS reflection at the free surface
Pdif	P diffracted along the CMB in the mantle (old: Pdiff)
S	Shear wave, bottoming below the uppermost mantle; also an upgoing shear wave from a source below the uppermost mantle
SS	Free-surface reflection of an S wave leaving a source downward
SP	S, leaving a source downward, reflected as P at the free surface. At shorter distances the second leg is represented by a crustal P wave.
SSS	Analogous to SS
SSP	SS converted to P when reflected from the free surface; travel time matches that of SPS
SPP	SP reflected at the free surface
ScS	S reflection from the CMB
ScP	S converted to P when reflected from the CMB
ScSN	ScS multiple free-surface reflection; N is a positive integer. For example ScS2 is ScSScS.
Sz+S	S reflection from outer side of a discontinuity at depth z; z may be a positive numerical value in km. For example S660+S is an S reflection from the top of the 660 km discontinuity. (alt: SzS)
Sz-S	S reflection from inner side of discontinuity at depth z. For example, S660-S is an S reflection from below the 660 km discontinuity, which means it is precursory to SS.
Sz+P	(alt: SzP) S converted to P when reflected from outer side of discontinuity at depth z
Sz-P	S converted to P when reflected from inner side of discontinuity at depth z
ScSP	ScS to P reflection at the free surface
Sdif	S diffracted along the CMB in the mantle (old: Sdiff)

Core Phases

PKP	Unspecified P wave bottoming in the core (alt: P')
PKPab	P wave bottoming in the upper outer core; ab indicates the retrograde branch of the PKP caustic (old: PKP2)
PKPbc	P wave bottoming in the lower outer core; bc indicates the prograde branch of the PKP caustic (old: PKP1)
PKPdf	P wave bottoming in the inner core (alt: PKIKP)

PKPpre	A precursor to PKPdf due to scattering near or at the CMB (old: PKhKP)
PKPdif	P wave diffracted at the inner core boundary (ICB) in the outer core
PKS	Unspecified P wave bottoming in the core and converting to S at the CMB
PKSab	PKS bottoming in the upper outer core
PKSbc	PKS bottoming in the lower outer core
PKSdf	PKS bottoming in the inner core
P'P'	Free-surface reflection of PKP (alt: PKPPKP)
P'N	PKP reflected at the free surface N - 1 times; N is a positive integer. For example, P'3 is P'P'P'. (alt: PKPN)
P'z-P'	PKP reflected from inner side of a discontinuity at depth z outside the core, which means it is precursory to P'P'; z may be a positive numerical value in km
P'S'	(alt: PKPSKS) PKP converted to SKS when reflected from the free surface; other examples are P'PKS, P'SKP
PS'	P (leaving a source downward) to SKS reflection at the free surface (alt: PSKS)
PKKP	Unspecified P wave reflected once from the inner side of the CMB
PKKPab	PKKP bottoming in the upper outer core
PKKPbc	PKKP bottoming in the lower outer core
PKKPdf	PKKP bottoming in the inner core
PNKP	P wave reflected N - 1 times from inner side of the CMB; N is a positive integer.
PKKPpre	A precursor to PKKP due to scattering near the CMB
PKiKP	P wave reflected from the inner core boundary (ICB)
PKNIKP	P wave reflected N - 1 times from the inner side of the ICB
PKJKP	P wave traversing the outer core as P and the inner core as S
PKKS	P wave reflected once from inner side of the CMB and converted to S at the CMB
PKKSab	PKKS bottoming in the upper outer core
PKKSbc	PKKS bottoming in the lower outer core
PKKSdf	PKKS bottoming in the inner core
PcPP'	PcP to PKP reflection at the free surface; other examples are PcPS', PcSP', PcSS', PcPSKP, PcSSKP. (alt: PcPPKP)
SKS	unspecified S wave traversing the core as P (alt: S')
SKSac	SKS bottoming in the outer core
SKSdf	SKS bottoming in the inner core (alt: SKIKS)
SPdifKS	SKS wave with a segment of mantleside Pdif at the source and/or the receiver side of the ray path (alt: SKPdifS)
SKP	Unspecified S wave traversing the core and then the mantle as P
SKPab	SKP bottoming in the upper outer core
SKPbc	SKP bottoming in the lower outer core
SKPdf	SKP bottoming in the inner core
S'S'	Free-surface reflection of SKS (alt: SKSSKS)
S'N	SKS reflected at the free surface N - 1 times; N is a positive integer
S'z-S'	SKS reflected from inner side of discontinuity at depth z outside the core, which means it is precursory to S'S'; z may be a positive numerical value in km.
S'P'	(alt: SKSPKP) SKS converted to PKP when reflected from the free surface; other examples are S'SKP, S'PKS.
S'P	(alt: SKSP) SKS to P reflection at the free surface
SKKS	Unspecified S wave reflected once from inner side of the CMB
SKKSac	SKKS bottoming in the outer core
SKKSdf	SKKS bottoming in the inner core
SNKS	S wave reflected N - 1 times from inner side of the CMB; N is a positive integer.
SKiKS	S wave traversing the outer core as P and reflected from the ICB
SKJKS	S wave traversing the outer core as P and the inner core as S
SKKP	S wave traversing the core as P with one reflection from the inner side of the CMB and then continuing as P in the mantle

SKKPab	SKKP bottoming in the upper outer core
SKKPbc	SKKP bottoming in the lower outer core
SKKPdf	SKKP bottoming in the inner core
ScSS’	ScS to SKS reflection at the free surface; other examples are ScPS’, ScSP’, ScPP’, ScSSKP, ScPSKP. (alt: ScSSKS)

Near-source Surface reflections (Depth Phases)

pP*y*	All P-type onsets (P*y*), as defined above, which resulted from reflection of an upgoing P wave at the free surface or an ocean bottom. WARNING: The character *y* is only a wild card for any seismic phase, which could be generated at the free surface. Examples are pP, pPKP, pPP, pPcP, etc.
sP*y*	All P*y* resulting from reflection of an upgoing S wave at the free surface or an ocean bottom; for example, sP, sPKP, sPP, sPcP, etc.
pS*y*	All S-type onsets (S*y*), as defined above, which resulted from reflection of an upgoing P wave at the free surface or an ocean bottom; for example, pS, pSKS, pSS, pScP, etc.
sS*y*	All S*y* resulting from reflection of an upgoing S wave at the free surface or an ocean bottom; for example, sSn, sSS, sScS, sSdif, etc.
pwP*y*	All P*y* resulting from reflection of an upgoing P wave at the ocean’s free surface
pmP*y*	All P*y* resulting from reflection of an upgoing P wave from the inner side of the Moho

Surface Waves

L	Unspecified long-period surface wave
LQ	Love wave
LR	Rayleigh wave
G	Mantle wave of Love type
G*N*	Mantle wave of Love type; *N* is integer and indicates wave packets traveling along the minor arcs (odd numbers) or major arc (even numbers) of the great circle
R	Mantle wave of Rayleigh type
R*N*	Mantle wave of Rayleigh type; *N* is integer and indicates wave packets traveling along the minor arcs (odd numbers) or major arc (even numbers) of the great circle
PL	Fundamental leaking mode following P onsets generated by coupling of P energy into the waveguide formed by the crust and upper mantle SPL S wave coupling into the PL waveguide; other examples are SSPL, SSSPL.

Acoustic Phases

H	A hydroacoustic wave from a source in the water, which couples in the ground
HPg	H phase converted to Pg at the receiver side
HSg	H phase converted to Sg at the receiver side
HRg	H phase converted to Rg at the receiver side
I	An atmospheric sound arrival which couples in the ground
IPg	I phase converted to Pg at the receiver side
ISg	I phase converted to Sg at the receiver side
IRg	I phase converted to Rg at the receiver side
T	A tertiary wave. This is an acoustic wave from a source in the solid earth, usually trapped in a low-velocity oceanic water layer called the SOFAR channel (SOund Fixing And Ranging).
TPg	T phase converted to Pg at the receiver side
TSg	T phase converted to Sg at the receiver side
TRg	T phase converted to Rg at the receiver side

Amplitude Measurement Phases

The following set of amplitude measurement names refers to the IASPEI Magnitude Standard (see www.iaspei.org/commissions/CSOI/Summary_of_WG_recommendations.pdf) compliance to which is indicated by the presence of leading letter I. The absence of leading letter I indicates that a measurement is non-standard. Letter A indicates a measurement in nm made on a displacement seismogram, whereas letter V indicates a measurement in nm/s made on a velocity seismogram.

IAML	Displacement amplitude measured according to the IASPEI standard for local magnitude ML
IAMs_20	Displacement amplitude measured according to IASPEI standard for surface-wave magnitude $MS(20)$
IVMs_BB	Velocity amplitude measured according to IASPEI standard for broadband surface-wave magnitude $MS(BB)$
IAmb	Displacement amplitude measured according to IASPEI standard for short-period teleseismic body-wave magnitude mb
IVmB_BB	Velocity amplitude measured according to IASPEI standard for broadband teleseismic body-wave magnitude $mB(BB)$
AX_IN	Displacement amplitude of phase of type X (e.g., PP, S, etc), measured on an instrument of type IN (e.g., SP - short-period, LP - long-period, BB - broadband)
VX_IN	Velocity amplitude of phase of type X and instrument of type IN (as above)
A	Unspecified displacement amplitude measurement
V	Unspecified velocity amplitude measurement
AML	Displacement amplitude measurement for nonstandard local magnitude
AMs	Displacement amplitude measurement for nonstandard surface-wave magnitude
Amb	Displacement amplitude measurement for nonstandard short-period body-wave magnitude
AmB	Displacement amplitude measurement for nonstandard medium to long-period body-wave magnitude
END	Time of visible end of record for duration magnitude

Unidentified Arrivals

x	unidentified arrival (old: i, e, NULL)
rx	unidentified regional arrival (old: i, e, NULL)
tx	unidentified teleseismic arrival (old: i, e, NULL)
Px	unidentified arrival of P type (old: i, e, NULL, (P), P?)
Sx	unidentified arrival of S type (old: i, e, NULL, (S), S?)

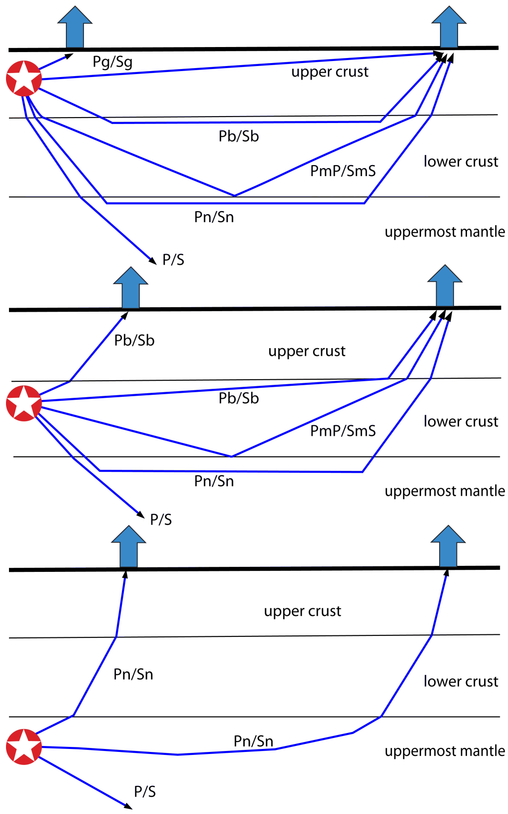

Figure 6.1: *Seismic 'crustal phases' observed in the case of a two-layer crust in local and regional distance ranges (0°<D< about 20°) from the seismic source in the: upper crust (top); lower crust (middle); and uppermost mantle (bottom).*

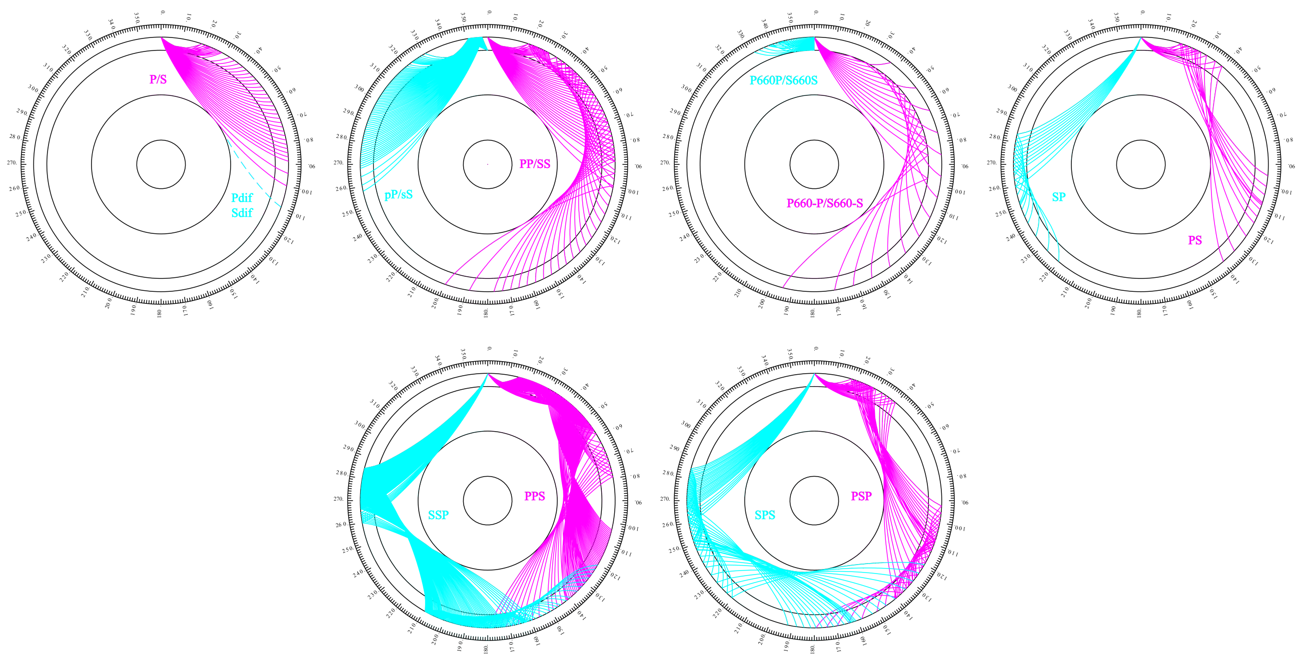

Figure 6.2: *Mantle phases observed at the teleseismic distance range D > about 20°.*

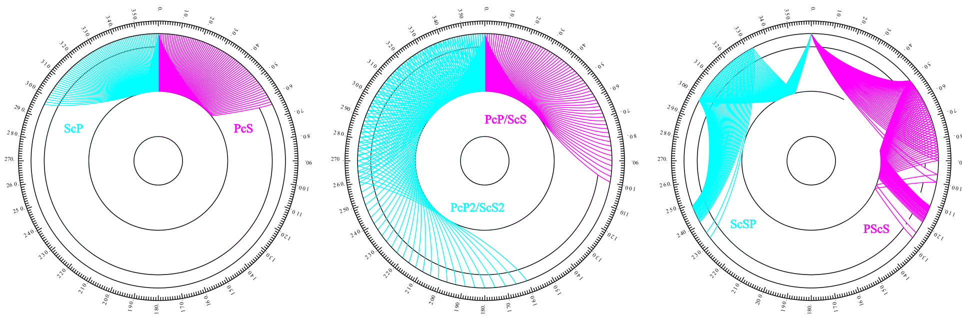

Figure 6.3: *Reflections from the Earth's core.*

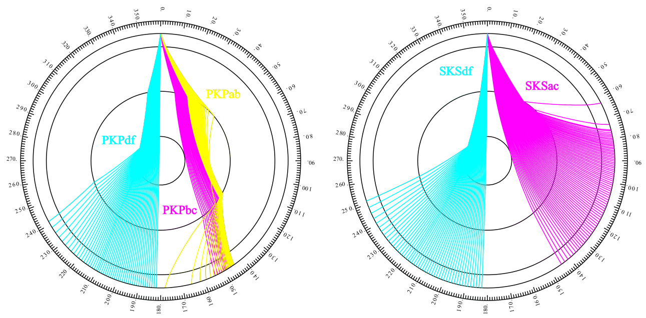

Figure 6.4: *Seismic rays of direct core phases.*

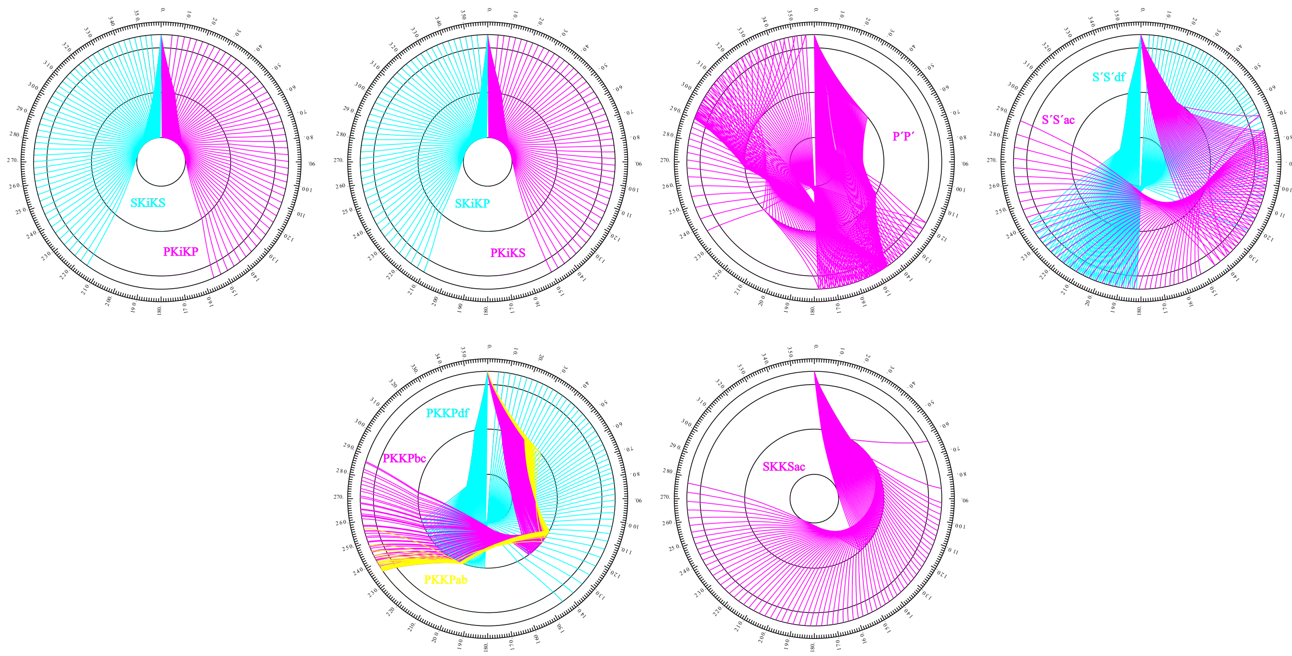

Figure 6.5: *Seismic rays of single-reflected core phases.*

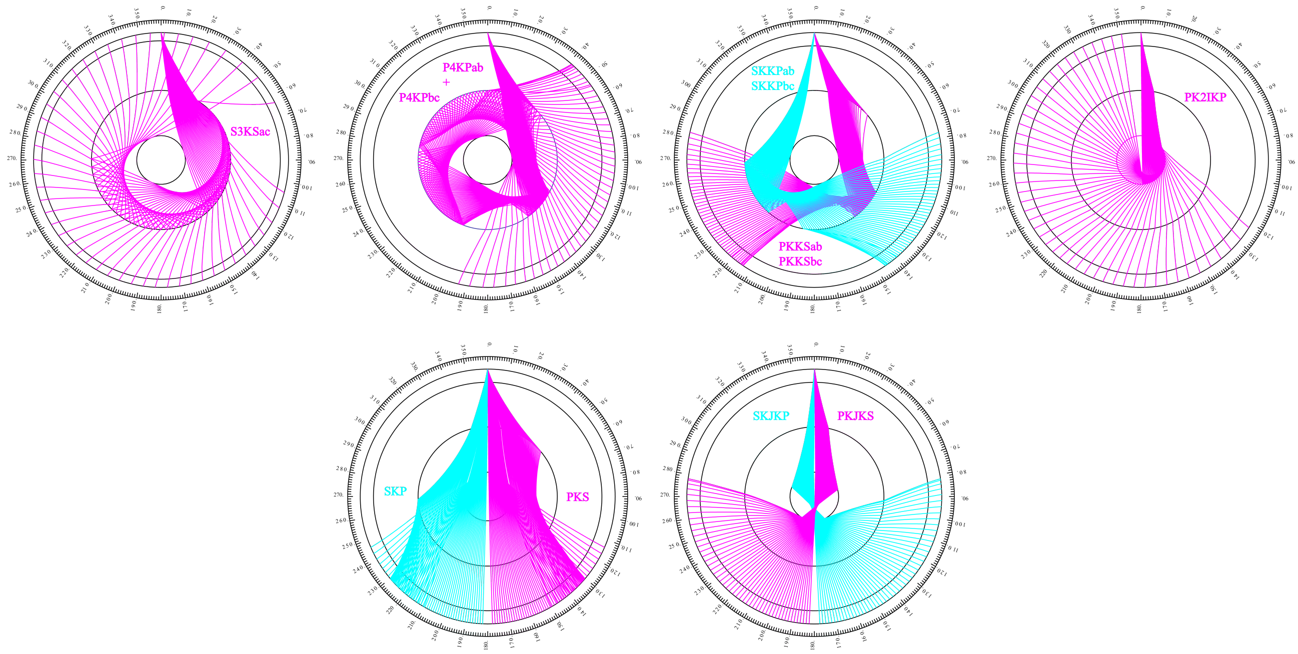

Figure 6.6: *Seismic rays of multiple-reflected and converted core phases.*

6.2 Flinn-Engdahl Regions

The Flinn-Engdahl regions were first proposed by *Flinn and Engdahl* (1965), with the standard defined by *Flinn et al.* (1974). The latest version of the schema, published by *Young et al.* (1996), divides the Earth into 50 seismic regions (Figure 6.7), which are further subdivided producing a total of 754 geographical regions (listed below). The geographic regions are numbered 1 to 757 with regions 172, 299 and 550 no longer in use. The boundaries of these regions are defined at one-degree intervals.

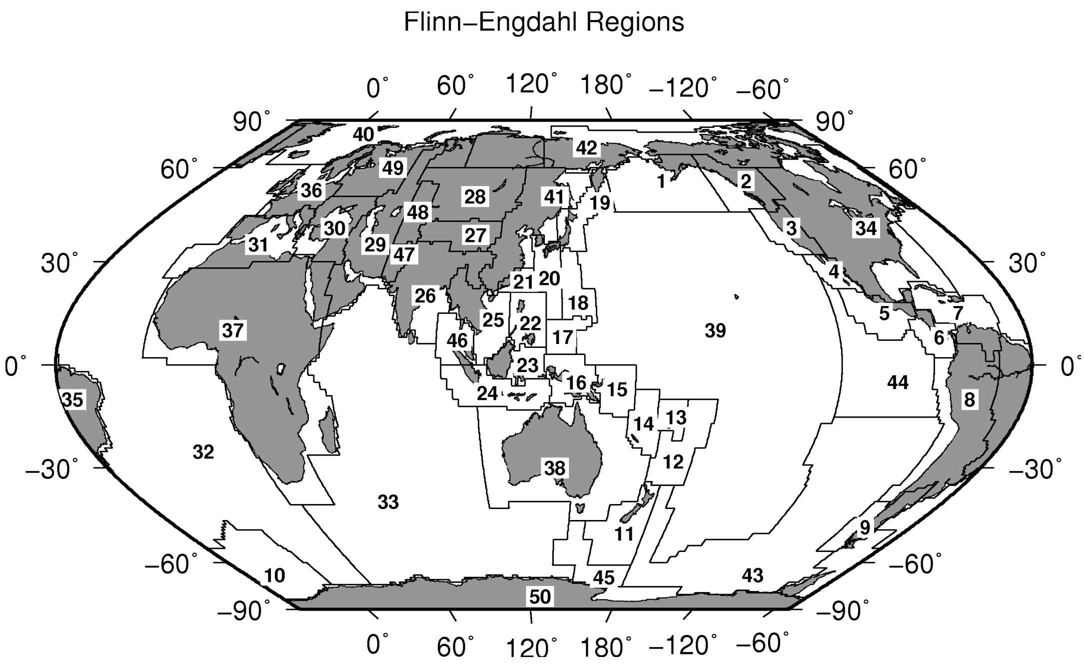

Figure 6.7: *Map of all Flinn-Engdahl seismic regions.*

Seismic Region 1
Alaska-Aleutian Arc
1. Central Alaska
2. Southern Alaska
3. Bering Sea
4. Komandorsky Islands region
5. Near Islands
6. Rat Islands
7. Andreanof Islands
8. Pribilof Islands
9. Fox Islands
10. Unimak Island region
11. Bristol Bay
12. Alaska Peninsula
13. Kodiak Island region
14. Kenai Peninsula
15. Gulf of Alaska
16. South of Aleutian Islands
17. South of Alaska

Seismic Region 2
Eastern Alaska to Vancouver Island
18. Southern Yukon Territory
19. Southeastern Alaska
20. Off coast of southeastern Alaska
21. West of Vancouver Island
22. Queen Charlotte Islands region
23. British Columbia
24. Alberta
25. Vancouver Island region
26. Off coast of Washington
27. Near coast of Washington
28. Washington-Oregon border region
29. Washington

Seismic Region 3
California-Nevada Region
30. Off coast of Oregon
31. Near coast of Oregon
32. Oregon
33. Western Idaho
34. Off coast of northern California
35. Near coast of northern California
36. Northern California
37. Nevada
38. Off coast of California
39. Central California
40. California-Nevada border region
41. Southern Nevada
42. Western Arizona
43. Southern California
44. California-Arizona border region
45. California-Baja California border region
46. Western Arizona-Sonora border region

Seismic Region 4
Lower California and Gulf of California
47. Off west coast of Baja California
48. Baja California
49. Gulf of California
50. Sonora
51. Off coast of central Mexico
52. Near coast of central Mexico

Seismic Region 5
Mexico-Guatemala Area
53. Revilla Gigedo Islands region
54. Off coast of Jalisco
55. Near coast of Jalisco
56. Near coast of Michoacan
57. Michoacan
58. Near coast of Guerrero
59. Guerrero
60. Oaxaca
61. Chiapas
62. Mexico-Guatemala border region
63. Off coast of Mexico
64. Off coast of Michoacan
65. Off coast of Guerrero
66. Near coast of Oaxaca
67. Off coast of Oaxaca
68. Off coast of Chiapas
69. Near coast of Chiapas
70. Guatemala
71. Near coast of Guatemala
730. Northern East Pacific Rise

Seismic Region 6
Central America
72. Honduras
73. El Salvador
74. Near coast of Nicaragua
75. Nicaragua
76. Off coast of central America
77. Off coast of Costa Rica
78. Costa Rica
79. North of Panama
80. Panama-Costa Rica border region
81. Panama
82. Panama-Colombia border region
83. South of Panama

Seismic Region 7
Caribbean Loop
84. Yucatan Peninsula
85. Cuba region
86. Jamaica region
87. Haiti region
88. Dominican Republic region
89. Mona Passage
90. Puerto Rico region
91. Virgin Islands
92. Leeward Islands
93. Belize
94. Caribbean Sea
95. Windward Islands
96. Near north coast of Colombia
97. Near coast of Venezuela
98. Trinidad
99. Northern Colombia
100. Lake Maracaibo
101. Venezuela
731. North of Honduras

Seismic Region 8
Andean South America
102. Near west coast of Colombia
103. Colombia
104. Off coast of Ecuador
105. Near coast of Ecuador
106. Colombia-Ecuador border region
107. Ecuador
108. Off coast of northern Peru
109. Near coast of northern Peru
110. Peru-Ecuador border region
111. Northern Peru
112. Peru-Brazil border region
113. Western Brazil
114. Off coast of Peru
115. Near coast of Peru
116. Central Peru
117. Southern Peru
118. Peru-Bolivia border region
119. Northern Bolivia
120. Central Bolivia
121. Off coast of northern Chile
122. Near coast of northern Chile
123. Northern Chile
124. Chile-Bolivia border region
125. Southern Bolivia
126. Paraguay
127. Chile-Argentina border region
128. Jujuy Province
129. Salta Province
130. Catamarca Province
131. Tucuman Province
132. Santiago del Estero Province
133. Northeastern Argentina
134. Off coast of central Chile
135. Near coast of central Chile
136. Central Chile
137. San Juan Province
138. La Rioja Province
139. Mendoza Province

140. San Luis Province
141. Cordoba Province
142. Uruguay

Seismic Region 9
Extreme South America
143. Off coast of southern Chile
144. Southern Chile
145. Southern Chile-Argentina border region
146. Southern Argentina

Seismic Region 10
Southern Antilles
147. Tierra del Fuego
148. Falkland Islands region
149. Drake Passage
150. Scotia Sea
151. South Georgia Island region
152. South Georgia Rise
153. South Sandwich Islands region
154. South Shetland Islands
155. Antarctic Peninsula
156. Southwestern Atlantic Ocean
157. Weddell Sea
732. East of South Sandwich Islands

Seismic Region 11
New Zealand Region
158. Off west coast of North Island
159. North Island
160. Off east coast of North Island
161. Off west coast of South Island
162. South Island
163. Cook Strait
164. Off east coast of South Island
165. North of Macquarie Island
166. Auckland Islands region
167. Macquarie Island region
168. South of New Zealand

Seismic Region 12
Kermadec-Tonga-Samoa Area
169. Samoa Islands region
170. Samoa Islands
171. South of Fiji Islands
172. West of Tonga Islands (REGION NOT IN USE)
173. Tonga Islands
174. Tonga Islands region
175. South of Tonga Islands
176. North of New Zealand
177. Kermadec Islands region
178. Kermadec Islands
179. South of Kermadec Islands

Seismic Region 13
Fiji Area
180. North of Fiji Islands
181. Fiji Islands region
182. Fiji Islands

Seismic Region 14
Vanuatu (New Hebrides)
183. Santa Cruz Islands region
184. Santa Cruz Islands
185. Vanuatu Islands region
186. Vanuatu Islands
187. New Caledonia
188. Loyalty Islands
189. Southeast of Loyalty Islands

Seismic Region 15
Bismarck and Solomon Islands
190. New Ireland region
191. North of Solomon Islands
192. New Britain region
193. Bougainville-Solomon Islands region
194. D'Entrecasteaux Islands region
195. South of Solomon Islands

Seismic Region 16
New Guinea
196. Irian Jaya region
197. Near north coast of Irian Jaya
198. Ninigo Islands region
199. Admiralty Islands region
200. Near north coast of New Guinea
201. Irian Jaya
202. New Guinea
203. Bismarck Sea
204. Aru Islands region
205. Near south coast of Irian Jaya
206. Near south coast of New Guinea
207. Eastern New Guinea region
208. Arafura Sea

Seismic Region 17
Caroline Islands to Guam
209. Western Caroline Islands
210. South of Mariana Islands

Seismic Region 18
Guam to Japan
211. Southeast of Honshu
212. Bonin Islands region
213. Volcano Islands region
214. West of Mariana Islands
215. Mariana Islands region
216. Mariana Islands

Seismic Region 19
Japan-Kurils-Kamchatka
217. Kamchatka Peninsula
218. Near east coast of Kamchatka Peninsula
219. Off east coast of Kamchatka Peninsula
220. Northwest of Kuril Islands
221. Kuril Islands
222. East of Kuril Islands
223. Eastern Sea of Japan
224. Hokkaido region
225. Off southeast coast of Hokkaido
226. Near west coast of eastern Honshu
227. Eastern Honshu
228. Near east coast of eastern Honshu
229. Off east coast of Honshu
230. Near south coast of eastern Honshu

Seismic Region 20
Southwestern Japan and Ryukyu Islands
231. South Korea
232. Western Honshu
233. Near south coast of western Honshu
234. Northwest of Ryukyu Islands
235. Kyushu
236. Shikoku
237. Southeast of Shikoku
238. Ryukyu Islands
239. Southeast of Ryukyu Islands
240. West of Bonin Islands
241. Philippine Sea

Seismic Region 21
Taiwan
242. Near coast of southeastern China
243. Taiwan region
244. Taiwan
245. Northeast of Taiwan
246. Southwestern Ryukyu Islands
247. Southeast of Taiwan

Seismic Region 22
Philippines
248. Philippine Islands region
249. Luzon
250. Mindoro
251. Samar
252. Palawan
253. Sulu Sea
254. Panay

255. Cebu
256. Leyte
257. Negros
258. Sulu Archipelago
259. Mindanao
260. East of Philippine Islands

Seismic Region 23
Borneo-Sulawesi
261. Borneo
262. Celebes Sea
263. Talaud Islands
264. North of Halmahera
265. Minahassa Peninsula, Sulawesi
266. Northern Molucca Sea
267. Halmahera
268. Sulawesi
269. Southern Molucca Sea
270. Ceram Sea
271. Buru
272. Seram

Seismic Region 24
Sunda Arc
273. Southwest of Sumatera
274. Southern Sumatera
275. Java Sea
276. Sunda Strait
277. Jawa
278. Bali Sea
279. Flores Sea
280. Banda Sea
281. Tanimbar Islands region
282. South of Jawa
283. Bali region
284. South of Bali
285. Sumbawa region
286. Flores region
287. Sumba region
288. Savu Sea
289. Timor region
290. Timor Sea
291. South of Sumbawa
292. South of Sumba
293. South of Timor

Seismic Region 25
Myanmar and Southeast Asia
294. Myanmar-India border region
295. Myanmar-Bangladesh border region
296. Myanmar
297. Myanmar-China border region
298. Near south coast of Myanmar
299. Southeast Asia (REGION NOT IN USE)
300. Hainan Island
301. South China Sea
733. Thailand
734. Laos
735. Kampuchea
736. Vietnam
737. Gulf of Tongking

Seismic Region 26
India-Xizang-Szechwan-Yunnan
302. Eastern Kashmir
303. Kashmir-India border region
304. Kashmir-Xizang border region
305. Western Xizang-India border region
306. Xizang
307. Sichuan
308. Northern India
309. Nepal-India border region
310. Nepal
311. Sikkim
312. Bhutan
313. Eastern Xizang-India border region
314. Southern India
315. India-Bangladesh border region
316. Bangladesh
317. Northeastern India
318. Yunnan
319. Bay of Bengal

Seismic Region 27
Southern Xinjiang to Gansu
320. Kyrgyzstan-Xinjiang border region
321. Southern Xinjiang
322. Gansu
323. Western Nei Mongol
324. Kashmir-Xinjiang border region
325. Qinghai

Seismic Region 28
Alma-Ata to Lake Baikal
326. Southwestern Siberia
327. Lake Baykal region
328. East of Lake Baykal
329. Eastern Kazakhstan
330. Lake Issyk-Kul region
331. Kazakhstan-Xinjiang border region
332. Northern Xinjiang
333. Tuva-Buryatia-Mongolia border region
334. Mongolia

Seismic Region 29
Western Asia
335. Ural Mountains region
336. Western Kazakhstan
337. Eastern Caucasus
338. Caspian Sea
339. Northwestern Uzbekistan
340. Turkmenistan
341. Iran-Turkmenistan border region
342. Turkmenistan-Afghanistan border region
343. Turkey-Iran border region
344. Iran-Armenia-Azerbaijan border region
345. Northwestern Iran
346. Iran-Iraq border region
347. Western Iran
348. Northern and central Iran
349. Northwestern Afghanistan
350. Southwestern Afghanistan
351. Eastern Arabian Peninsula
352. Persian Gulf
353. Southern Iran
354. Southwestern Pakistan
355. Gulf of Oman
356. Off coast of Pakistan

Seismic Region 30
Middle East-Crimea-Eastern Balkans
357. Ukraine-Moldova-Southwestern Russia region
358. Romania
359. Bulgaria
360. Black Sea
361. Crimea region
362. Western Caucasus
363. Greece-Bulgaria border region
364. Greece
365. Aegean Sea
366. Turkey
367. Turkey-Georgia-Armenia border region
368. Southern Greece
369. Dodecanese Islands
370. Crete
371. Eastern Mediterranean Sea
372. Cyprus region
373. Dead Sea region
374. Jordan-Syria region
375. Iraq

Seismic Region 31
Western Mediterranean Area
376. Portugal
377. Spain

378. Pyrenees
379. Near south coast of France
380. Corsica
381. Central Italy
382. Adriatic Sea
383. Northwestern Balkan Peninsula
384. West of Gibraltar
385. Strait of Gibraltar
386. Balearic Islands
387. Western Mediterranean Sea
388. Sardinia
389. Tyrrhenian Sea
390. Southern Italy
391. Albania
392. Greece-Albania border region
393. Madeira Islands region
394. Canary Islands region
395. Morocco
396. Northern Algeria
397. Tunisia
398. Sicily
399. Ionian Sea
400. Central Mediterranean Sea
401. Near coast of Libya

Seismic Region 32
Atlantic Ocean

402. North Atlantic Ocean
403. Northern Mid-Atlantic Ridge
404. Azores Islands region
405. Azores Islands
406. Central Mid-Atlantic Ridge
407. North of Ascension Island
408. Ascension Island region
409. South Atlantic Ocean
410. Southern Mid-Atlantic Ridge
411. Tristan da Cunha region
412. Bouvet Island region
413. Southwest of Africa
414. Southeastern Atlantic Ocean
738. Reykjanes Ridge
739. Azores-Cape St. Vincent Ridge

Seismic Region 33
Indian Ocean

415. Eastern Gulf of Aden
416. Socotra region
417. Arabian Sea
418. Lakshadweep region
419. Northeastern Somalia
420. North Indian Ocean
421. Carlsberg Ridge
422. Maldive Islands region
423. Laccadive Sea
424. Sri Lanka
425. South Indian Ocean
426. Chagos Archipelago region
427. Mauritius-Reunion region
428. Southwest Indian Ridge
429. Mid-Indian Ridge
430. South of Africa
431. Prince Edward Islands region
432. Crozet Islands region
433. Kerguelen Islands region
434. Broken Ridge
435. Southeast Indian Ridge
436. Southern Kerguelen Plateau
437. South of Australia
740. Owen Fracture Zone region
741. Indian Ocean Triple Junction
742. Western Indian-Antarctic Ridge

Seismic Region 34
Eastern North America

438. Saskatchewan
439. Manitoba
440. Hudson Bay
441. Ontario
442. Hudson Strait region
443. Northern Quebec
444. Davis Strait
445. Labrador
446. Labrador Sea
447. Southern Quebec
448. Gaspe Peninsula
449. Eastern Quebec
450. Anticosti Island
451. New Brunswick
452. Nova Scotia
453. Prince Edward Island
454. Gulf of St. Lawrence
455. Newfoundland
456. Montana
457. Eastern Idaho
458. Hebgen Lake region, Montana
459. Yellowstone region
460. Wyoming
461. North Dakota
462. South Dakota
463. Nebraska
464. Minnesota
465. Iowa
466. Wisconsin
467. Illinois
468. Michigan
469. Indiana
470. Southern Ontario
471. Ohio
472. New York
473. Pennsylvania
474. Vermont-New Hampshire region
475. Maine
476. Southern New England
477. Gulf of Maine
478. Utah
479. Colorado
480. Kansas
481. Iowa-Missouri border region
482. Missouri-Kansas border region
483. Missouri
484. Missouri-Arkansas border region
485. Missouri-Illinois border region
486. New Madrid region, Missouri
487. Cape Girardeau region, Missouri
488. Southern Illinois
489. Southern Indiana
490. Kentucky
491. West Virginia
492. Virginia
493. Chesapeake Bay region
494. New Jersey
495. Eastern Arizona
496. New Mexico
497. Northwestern Texas-Oklahoma border region
498. Western Texas
499. Oklahoma
500. Central Texas
501. Arkansas-Oklahoma border region
502. Arkansas
503. Louisiana-Texas border region
504. Louisiana
505. Mississippi
506. Tennessee
507. Alabama
508. Western Florida
509. Georgia
510. Florida-Georgia border region
511. South Carolina
512. North Carolina
513. Off east coast of United States
514. Florida Peninsula
515. Bahama Islands
516. Eastern Arizona-Sonora border region
517. New Mexico-Chihuahua border region
518. Texas-Mexico border region
519. Southern Texas
520. Near coast of Texas
521. Chihuahua
522. Northern Mexico
523. Central Mexico
524. Jalisco
525. Veracruz
526. Gulf of Mexico
527. Bay of Campeche

Seismic Region 35
Eastern South America
528. Brazil
529. Guyana
530. Suriname
531. French Guiana

Seismic Region 36
Northwestern Europe
532. Eire
533. United Kingdom
534. North Sea
535. Southern Norway
536. Sweden
537. Baltic Sea
538. France
539. Bay of Biscay
540. The Netherlands
541. Belgium
542. Denmark
543. Germany
544. Switzerland
545. Northern Italy
546. Austria
547. Czech and Slovak Republics
548. Poland
549. Hungary

Seismic Region 37
Africa
550. Northwest Africa (REGION NOT IN USE)
551. Southern Algeria
552. Libya
553. Egypt
554. Red Sea
555. Western Arabian Peninsula
556. Chad region
557. Sudan
558. Ethiopia
559. Western Gulf of Aden
560. Northwestern Somalia
561. Off south coast of northwest Africa
562. Cameroon
563. Equatorial Guinea
564. Central African Republic
565. Gabon
566. Congo
567. Zaire
568. Uganda
569. Lake Victoria region
570. Kenya
571. Southern Somalia
572. Lake Tanganyika region
573. Tanzania
574. Northwest of Madagascar
575. Angola
576. Zambia
577. Malawi
578. Namibia
579. Botswana
580. Zimbabwe
581. Mozambique
582. Mozambique Channel
583. Madagascar
584. South Africa
585. Lesotho
586. Swaziland
587. Off coast of South Africa
743. Western Sahara
744. Mauritania
745. Mali
746. Senegal-Gambia region
747. Guinea region
748. Sierra Leone
749. Liberia region
750. Cote d'Ivoire
751. Burkina Faso
752. Ghana
753. Benin-Togo region
754. Niger
755. Nigeria

Seismic Region 38
Australia
588. Northwest of Australia
589. West of Australia
590. Western Australia
591. Northern Territory
592. South Australia
593. Gulf of Carpentaria
594. Queensland
595. Coral Sea
596. Northwest of New Caledonia
597. New Caledonia region
598. Southwest of Australia
599. Off south coast of Australia
600. Near coast of South Australia
601. New South Wales
602. Victoria
603. Near southeast coast of Australia
604. Near east coast of Australia
605. East of Australia
606. Norfolk Island region
607. Northwest of New Zealand
608. Bass Strait
609. Tasmania region
610. Southeast of Australia

Seismic Region 39
Pacific Basin
611. North Pacific Ocean
612. Hawaiian Islands region
613. Hawaiian Islands
614. Eastern Caroline Islands region
615. Marshall Islands region
616. Enewetak Atoll region
617. Bikini Atoll region
618. Gilbert Islands region
619. Johnston Island region
620. Line Islands region
621. Palmyra Island region
622. Kiritimati region
623. Tuvalu region
624. Phoenix Islands region
625. Tokelau Islands region
626. Northern Cook Islands
627. Cook Islands region
628. Society Islands region
629. Tubuai Islands region
630. Marquesas Islands region
631. Tuamotu Archipelago region
632. South Pacific Ocean

Seismic Region 40
Arctic Zone
633. Lomonosov Ridge
634. Arctic Ocean
635. Near north coast of Kalaallit Nunaat
636. Eastern Kalaallit Nunaat
637. Iceland region
638. Iceland
639. Jan Mayen Island region
640. Greenland Sea
641. North of Svalbard
642. Norwegian Sea
643. Svalbard region
644. North of Franz Josef Land
645. Franz Josef Land
646. Northern Norway
647. Barents Sea
648. Novaya Zemlya
649. Kara Sea
650. Near coast of northwestern Siberia
651. North of Severnaya Zemlya
652. Severnaya Zemlya
653. Near coast of northern Siberia
654. East of Severnaya Zemlya
655. Laptev Sea

Seismic Region 41
Eastern Asia
656. Southeastern Siberia
657. Priamurye-Northeastern China border region
658. Northeastern China
659. North Korea

660. Sea of Japan
661. Primorye
662. Sakhalin Island
663. Sea of Okhotsk
664. Southeastern China
665. Yellow Sea
666. Off east coast of southeastern China

Seismic Region 42
Northeastern Asia, Northern Alaska to Greenland
667. North of New Siberian Islands
668. New Siberian Islands
669. Eastern Siberian Sea
670. Near north coast of eastern Siberia
671. Eastern Siberia
672. Chukchi Sea
673. Bering Strait
674. St. Lawrence Island region
675. Beaufort Sea
676. Northern Alaska
677. Northern Yukon Territory
678. Queen Elizabeth Islands
679. Northwest Territories
680. Western Kalaallit Nunaat
681. Baffin Bay
682. Baffin Island region

Seismic Region 43
Southeastern and Antarctic Pacific Ocean
683. Southeastcentral Pacific Ocean
684. Southern East Pacific Rise
685. Easter Island region
686. West Chile Rise
687. Juan Fernandez Islands region
688. East of North Island
689. Chatham Islands region
690. South of Chatham Islands
691. Pacific-Antarctic Ridge
692. Southern Pacific Ocean
756. Southeast of Easter Island

Seismic Region 44
Galapagos Area
693. Eastcentral Pacific Ocean
694. Central East Pacific Rise
695. West of Galapagos Islands
696. Galapagos Islands region
697. Galapagos Islands
698. Southwest of Galapagos Islands
699. Southeast of Galapagos Islands
757. Galapagos Triple Junction region

Seismic Region 45
Macquarie Loop
700. South of Tasmania
701. West of Macquarie Island
702. Balleny Islands region

Seismic Region 46
Andaman Islands to Sumatera
703. Andaman Islands region
704. Nicobar Islands region
705. Off west coast of northern Sumatera
706. Northern Sumatera
707. Malay Peninsula
708. Gulf of Thailand

Seismic Region 47
Baluchistan
709. Southeastern Afghanistan
710. Pakistan
711. Southwestern Kashmir
712. India-Pakistan border region

Seismic Region 48
Hindu Kush and Pamir
713. Central Kazakhstan
714. Southeastern Uzbekistan
715. Tajikistan
716. Kyrgyzstan
717. Afghanistan-Tajikistan border region
718. Hindu Kush region
719. Tajikistan-Xinjiang border region
720. Northwestern Kashmir

Seismic Region 49
Northern Eurasia
721. Finland
722. Norway-Murmansk border region
723. Finland-Karelia border region
724. Baltic States-Belarus-Northwestern Russia
725. Northwestern Siberia
726. Northern and central Siberia

Seismic Region 50
Antarctica
727. Victoria Land
728. Ross Sea
729. Antarctica

6.3 IASPEI Magnitudes

The ISC publishes a diversity of magnitude data. Although trying to be as complete and specific as possible, preference is now given to magnitudes determined according to standard procedures recommended by the Working Group on Magnitude Measurements of the IASPEI Commission on Seismological Observation and Interpretation (CoSOI). So far, such standards have been agreed upon for the local magnitude ML, the local-regional mb_Lg, and for two types each of body-wave (mb and mB_BB) and surface-wave magnitudes (Ms_20 and Ms_BB). With the exception of ML, all other standard magnitudes are measured on vertical-component records only. BB stands for direct measurement on unfiltered velocity broadband records in a wide range of periods, provided that their passband covers at least the period range within which mB_BB and Ms_BB are supposed to be measured. Otherwise, a deconvolution has to be applied prior to the amplitude and period measurement so as to assure that this specification is met. In contrast, mb_Lg, mb and Ms_20 are based on narrowband amplitude measurements around periods of 1 s and 20 s, respectively.

ML is consistent with the original definition of the local magnitude by *Richter* (1935) and mB_BB in close agreement with the original definition of medium-period body-wave magnitude mB measured in a wide range of periods between some 2 to 20 s and calibrated with the *Gutenberg and Richter* (1956) Q-function for vertical-component P waves. Similarly, Ms_BB is best tuned to the unbiased use of the IASPEI (1967) recommended standard magnitude formula for surface-wave amplitudes in a wide range of periods and distances, as proposed by its authors *Vaněk et al.* (1962). In contrast, mb and Ms_20 are chiefly based on measurement standards defined by US agencies in the 1960s in conjunction with the global deployment of the World-Wide Standard Seismograph Network (WWSSN), which did not include medium or broadband recordings. Some modifications were made in the 1970s to account for IASPEI recommendations on extended measurement time windows for mb. Although not optimal for calibrating narrow-band spectral amplitudes measured around 1 s and 20 s only, mb and Ms_20 use the same original calibrations functions as mB_BB and Ms_BB. But mb and Ms_20 data constitute by far the largest available magnitude data sets. Therefore they continue to be used, with appreciation for their advantages (e.g., mb is by far the most frequently measured teleseismic magnitude and often the only available and reasonably good magnitude estimator for small earthquakes) and their shortcomings (see section 3.2.5.2 of Chapter 3 in NMSOP-2).

Abbreviated descriptions of the standard procedures for ML, mb_Lg, mb, mB_BB and Ms_BB are summarised below. For more details, including also the transfer functions of the simulation filters to be used, see www.iaspei.org/commissions/CSOI/Summary_WG-Recommendations_20130327.pdf.

All amplitudes used in the magnitude formulas below are in most circumstances to be measured as one-half the maximum deflection of the seismogram trace, peak-to-adjacent-trough or trough-to-adjacent-peak, where the peak and trough are separated by one crossing of the zero-line: this measurement is sometimes described as "one-half peak-to-peak amplitude." The periods are to be measured as twice the time-intervals separating the peak and adjacent-trough from which the amplitudes are measured. The amplitude-phase arrival-times are to be measured and reported too as the time of the zero-crossing between the peak and adjacent-trough from which the amplitudes are measured. The issue of amplitude and period measuring procedures, and circumstances under which alternative procedures are acceptable or preferable, is discussed further in Section 5 of IS 3.3 and in section 3.2.3.3 of Chapter 3 of NMSOP-2.

Amplitudes measured according to recommended IASPEI standard procedures should be reported with the following ISF amplitude "phase names": IAML, IAmb_Lg, IAmb, IAMs_20, IVmB_BB and IVMs_BB. "I" stands for "International" or "IASPEI", "A" for displacement amplitude, measured in nm, and "V" for velocity amplitude, measured in nm/s. Although the ISC will calculate standard surface-wave magnitudes only for earthquakes shallower than 60 km, contributing agencies or stations are encouraged to report standard amplitude measurements of IAMs_20 and IVMs_BB for deeper earthquakes as well.

Note that the commonly known classical calibration relationships have been modified in the following to be consistent with displacements measured in nm, and velocities in nm/s, which is now common with high-resolution digital data and analysis tools. With these general definitions of the measurement parameters, where R is hypocentral distance in km (typically less than 1000 km), Δ is epicentral distance in degrees and h is hypocentre depth in km, the standard formulas and procedures read as follows:

ML:

$$ML = \log_{10}(A) + 1.11\log_{10} R + 0.00189R - 2.09 \tag{6.1}$$

for crustal earthquakes in regions with attenuative properties similar to those of southern California, and with A being the maximum trace amplitude in nm that is measured on output from a horizontal-component instrument that is filtered so that the response of the seismograph/filter system replicates that of a Wood-Anderson standard seismograph (but with a static magnification of 1). For the normalised simulated response curve and related poles and zeros see Figure 1 and Table 1 in IS 3.3 of NMSOP-2.

Equation (6.1) is an expansion of that of *Hutton and Boore* (1987). The constant term in equation (6.1), −2.09, is based on an experimentally determined static magnification of the Wood-Anderson of 2080 (see *Uhrhammer and Collins* (1990)), rather than the theoretical magnification of 2800 that was specified by the seismograph´s manufacturer. The formulation of equation (6.1) assures that reported ML amplitude data are not affected by uncertainty in the static magnification of the Wood-Anderson seismograph.

For seismographic stations containing two horizontal components, amplitudes are measured independently from each horizontal component and each amplitude is treated as a single datum. There is no effort to measure the two observations at the same time, and there is no attempt to compute a vector average. For crustal earthquakes in regions with attenuative properties that are different from those of coastal California and for measuring magnitudes with vertical-component seismographs the constants in the above equation have to be re-determined to adjust for the different regional attenuation and travel paths as well as for systematic differences between amplitudes measured on horizontal and vertical seismographs.

mb_Lg:

$$mb\_Lg = \log_{10}(A) + 0.833\log_{10} R + 0.434\gamma(R - 10) - 0.87 \tag{6.2}$$

where A = "sustained ground-motion amplitude" in nm, defined as the third largest amplitude in the time window corresponding to group velocities of 3.6 to 3.2 km/s, in the period (T) range 0.7 s to 1.3 s; R = epicentral distance in km, γ = coefficient of attenuation in km^{-1}. γ is related to the quality factor Q through the equation $\gamma = \pi/(QUT)$, where U is group velocity and T is the wave period of the L_g wave. γ is a strong function of crustal structure and should be determined specifically for the region in which the mb_Lg is to be used. A and T are measured on output from a vertical-component instrument that is filtered so that the frequency response of the seismograph/filter system replicates that of a WWSSN short-period seismograph (see Figure 1 and Table 1 in IS 3.3 of NMSOP-2). Arrival times with respect to the origin of the seismic disturbance are used, along with epicentral distance, to compute group velocity U.

mb:

$$mb = \log_{10}(A/T) + Q(\Delta, h) - 3.0 \tag{6.3}$$

where A = vertical component P-wave ground amplitude in nm measured at distances $20° \leq \Delta \leq 100°$ and calculated from the maximum trace-amplitude with $T < 3$ s in the entire P-phase train (time spanned by P, pP, sP, and possibly PcP and their codas, and ending preferably before PP). A and T are measured on output from an instrument that is filtered so that the frequency response of the seismograph/filter system replicates that of a WWSSN short-period seismograph (see Figure 1 and Table 1 in IS 3.3 of NMSOP-2). A is determined by dividing the maximum trace amplitude by the magnification of the simulated WWSSN-SP response at period T.

$Q(\Delta, h)$ = attenuation function for PZ (P-waves recorded on vertical component seismographs) established by *Gutenberg and Richter* (1956) in the tabulated or algorithmic form as used by the U.S. Geological Survey/National Earthquake Information Center (USGS/NEIC) (see Table 2 in IS 3.3 and program description PD 3.1 in NMSOP-2);

mB_BB:

$$mB\_BB = \log_{10}(Vmax/2\pi) + Q(\Delta, h) - 3.0 \tag{6.4}$$

where $Vmax$ = vertical component ground velocity in nm/s at periods between 0.2 s $< T <$ 30 s, measured in the range $20° \leq \Delta \leq 100°$. $Vmax$ is calculated from the maximum trace-amplitude in the entire P-phase train (see mb), as recorded on a seismogram that is proportional to velocity at least in the period range of measurements. $Q(\Delta, h)$ = attenuation function for PZ established by *Gutenberg and Richter* (1956) (see 6.3). Equation (6.3) differs from the equation for mB of *Gutenberg and Richter* (1956) by virtue of the $log_{10}(Vmax/2\pi)$ term, which replaces the classical $\log_{10}(A/T)_{max}$ term. Contributors should continue to send observations of A and T to ISC.

Ms_20:

$$Ms\_20 = \log_{10}(A/T) + 1.66\log_{10}\Delta + 0.3 \tag{6.5}$$

where A = vertical-component ground displacement in nm at $20° \leq \Delta \leq 160°$ epicentral distance measured from the maximum trace amplitude of a surface-wave phase having a period T between 18 s and 22 s on a waveform that has been filtered so that the frequency response of the seismograph/filter replicates that of a WWSSN long-period seismograph (see Figure 1 and Table 1 in IS 3.3 of NMSOP-2). A is determined by dividing the maximum trace amplitude by the magnification of the simulated WWSSN-LP response at period T. Equation (6.5) is formally equivalent to the Ms equation proposed by *Vaněk et al.* (1962) but is here applied to vertical motion measurements in a narrow range of periods.

Ms_BB:

$$Ms\_BB = \log_{10}(Vmax/2\pi) + 1.66\log_{10}\Delta + 0.3 \quad (6.6)$$

where $Vmax$ = vertical-component ground velocity in nm/s associated with the maximum trace-amplitude in the surface-wave train at periods between 3 s $< T <$ 60 s as recorded at distances $2° \leq \Delta \leq 160°$ on a seismogram that is proportional to velocity in that range of considered periods. Equation (6.6) is based on the Ms equation proposed by *Vaněk et al.* (1962), but is here applied to vertical motion measurements and is used with the $\log_{10}(Vmax/2\pi)$ term replacing the $\log_{10}(A/T)_{max}$ term of the original. As for mB_BB, observations of A and T should be reported to ISC.

Mw:

$$Mw = (\log_{10} M_0 - 9.1)/1.5 \quad (6.7)$$

Moment magnitude Mw is calculated from data of the scalar seismic moment M_0 (when given in Nm), or

$$Mw = (\log_{10} M_0 - 16.1)/1.5 \quad (6.8)$$

its CGS equivalent when M_0 is in dyne·cm.

Please note that the magnitude nomenclature used in this Section uses the IASPEI standards as the reference. However, the magnitude type is typically written in plain text in most typical data reports and so it is in this document. Moreover, writing magnitude types in plain text allows us to reproduce the magnitude type as stored in the database and provides a more direct identification of the magnitude type reported by different agencies. A short description of the common magnitude types available in this Summary is reported in 9.6.

6.4 The IASPEI Seismic Format (ISF)

The ISF is the IASPEI approved standard format for the exchange of parametric seismological data (hypocentres, magnitudes, phase arrivals, moment tensors etc.) and is one of the formats used by the ISC. It was adopted as standard in August 2001 and is an extension of the International Monitoring System 1.0 (IMS1.0) standard, which was developed for exchanging data used to monitor the Comprehensive Nuclear-Test-Ban Treaty. An example of the ISF is shown in Listing 6.1.

Bulletins which use the ISF are comprised of origin and arrival information, provided in a series of data blocks. These include: a bulletin title block; an event title block; an origin block; a magnitude sub-block; an effect block; a reference block; and a phase block.

Within these blocks an important extension of the IMS1.0 standard is the ability to add additional comments and thus provide further parametric information. The ISF comments are distinguishable within the open parentheses required for IMS1.0 comments by beginning with a hash mark (#) followed by a keyword identifying the type of formatted comment. Each additional line required in the ISF comment begins with the hash (within the comment parentheses) followed by blank spaces at least as long as the keyword. Optional lines within the comment are signified with a plus sign (+) instead of a hash mark. The keywords include `PRIME` (to designate a prime origin of a hypocentre); `CENTROID` (to indicate the centroid origin); `MOMTENS` (moment tensor solution); `FAULT_PLANE` (fault plane solution); `PRINAX` (principal axes); `PARAM` (an origin parameter e.g. hypocentre depth given by a depth phase).

The full documentation for the ISF is maintained at the ISC and can be downloaded from:
www.isc.ac.uk/doc/code/isf/isf.pdf

The documentation for the IMS1.0 standard can be downloaded from:
www.isc.ac.uk/doc/code/isf/ims1_0.pdf

Listing 6.1: *Example of an ISF formatted event*

```
Event 15146084 Near east coast of eastern Honshu
   Date       Time        Err   RMS Latitude Longitude  Smaj  Smin  Az Depth   Err Ndef Nsta Gap  mdist  Mdist Qual   Author      OrigID
2010/09/01 07:32:00                  37.9000  141.9000f                      44.0                                              NIED      17047453
 (#MOMTENS sc    M0 fCLVD    MRR    MTT    MPP    MRT    MTP    MPR NST1 NST2 Author   )
 (#             eM0 eCLVD    eRR    eTT    ePP    eRT    eTP    ePR NCO1 NCO2 Duration )
 (#       16 5.760                                                   NIED     )
 (#                                                                           )
 (#FAULT_PLANE Typ Strike   Dip    Rake  NP  NS Plane Author    )
 (#            BDC 199.00 19.00   86.00                NIED     )
 (+                23.00 71.00   91.00                          )
 (Epicenter information from JMA Focal Mechanism Solution Determined Manually Variance reduction = 96.98%)
2010/09/01 07:32:47.50        1.470  37.8300  142.2400                    37.0          71      281  11.00  51.10     uk BJI       15275482
2010/09/01 07:32:52.20   0.92        38.0320  141.8090   6.7   4.5 110  44.0         114                                   MOS       16741494
2010/09/01 07:32:52.53   0.35 0.889  37.9202  141.8229 4.090 2.740 145  49.7  2.76  490  478 122   0.65  92.01 m i fe ISCJB     01631732
 (#PARAM pP_DEPTH=41.11021)
2010/09/01 07:32:52.60   0.10        37.9100  141.8700   1.1   0.9  -1  43.0   1.0                                    fe JMA       16271222
 (Felt I=III-III J1)
2010/09/01 07:32:53.66   0.42 0.770  37.9250  141.7880   5.1   3.4 140  44.4   3.9  102       127   3.17 127.67     fe NEIC      01134459
 (#MOMTENS sc    M0 fCLVD    MRR    MTT    MPP    MRT    MTP    MPR NST1 NST2 Author   )
 (#             eM0 eCLVD    eRR    eTT    ePP    eRT    eTP    ePR NCO1 NCO2 Duration )
 (#       16 5.800        3.600 -0.550 -3.040  1.850 -1.140  4.150           NIED     )
 (#                                                                           )
 (#FAULT_PLANE Typ Strike   Dip    Rake  NP  NS Plane Author    )
 (#            BDC 199.00 19.00   86.00                NIED     )
 (+                23.00 71.00   91.00                          )
 (Recorded [3 JMA] in Miyagi; [2 JMA] in Fukushima and Iwate; [1 JMA] in Akita, Aomori, Ibaraki, Tochigi and Yamagata.)
2010/09/01 07:32:53.70   0.20        37.9300  142.0600 2.224 1.112  -1  50.3   1.0  262   89                                  GCMT      00124877
 (#CENTROID)
 (#MOMTENS sc    M0 fCLVD    MRR    MTT    MPP    MRT    MTP    MPR NST1 NST2 Author   )
 (#             eM0 eCLVD    eRR    eTT    ePP    eRT    eTP    ePR NCO1 NCO2 Duration )
 (#       16 6.891        5.430 -0.440 -4.990  1.500 -2.070  3.710   64   89 GCMT     )
 (#                       0.173  0.118  0.120  0.100  0.094  0.110  102  160     0.90 )
 (#FAULT_PLANE Typ Strike   Dip    Rake  NP  NS Plane Author    )
 (#            BDC  22.00 63.00   91.00                GCMT     )
 (+               201.00 27.00   89.00                          )
 (#PRINAX sc  T_val T_azim  T_pl  B_val B_azim  B_pl  P_val P_azim  P_pl Author    )
 (#       16  6.711 293.00 72.00  0.360 201.00  0.00 -7.072 111.00 18.00 GCMT      )
 (nsta1 refers to body waves, cutoff=40s. nsta2 refers to surface waves, cutoff=50s.)
2010/09/01 07:32:55.05   1.77 1.070  37.8692  141.9450  12.9  10.4 100  63.6  16.8   36       127   3.24 117.04     uk IDC       16680924
2010/09/01 07:32:52.23   0.30 1.333  37.8836  141.9148 5.558 4.001 142  38.9  2.33  542  478  61   0.72 141.68 m i se ISC       01237353
 (#PRIME)
 (#PARAM pP_DEPTH=39.00000)

Magnitude  Err Nsta Author      OrigID
Mw      5.1         NIED       17047453
Ms      4.8      61 BJI        15275482
Ms7     4.6      58 BJI        15275482
mB      5.1      48 BJI        15275482
mb      5.0      63 BJI        15275482
MS      4.7      19 MOS        16741494
mb      5.2      49 MOS        16741494
MS      4.6      43 ISCJB      01631732
mb      4.9     138 ISCJB      01631732
        5.0         JMA        16271222
mb      5.0      55 NEIC       01134459
MW      5.1         NIED       01134459
MW      5.2      89 GCMT       00124877
MS      4.4 0.1  28 IDC        16680924
Ms1     4.4 0.1  28 IDC        16680924
mb      4.4 0.1  27 IDC        16680924
mb1     4.5 0.0  33 IDC        16680924
mb1mx   4.4 0.0  37 IDC        16680924
mbtmp   4.7 0.1  33 IDC        16680924
ms1mx   4.3 0.1  31 IDC        16680924
MS      4.7 0.2  43 ISC        01237353
mb      4.9 0.2 145 ISC        01237353

Sta     Dist  EvAz Phase        Time      TRes  Azim AzRes   Slow   SRes Def   SNR       Amp   Per Qual Magnitude    ArrID
JIO      0.72 322.1 Pn       07:33:05.9   -0.06                              T__                        d_              49540510
JIO      0.72 322.1 Sn       07:33:15.0   -0.82                              T__                        __              49540511
JMM      0.89 269.2 Pn       07:33:08.4    0.2                               T__                        d_              49540512
JMM      0.89 269.2 Sn       07:33:19.2   -0.68                              T__                        __              49540513
JFK      0.97 238.3 Pn       07:33:09.5    0.1                               T__                        d_              49540514
JFK      0.97 238.3 Sn       07:33:21.5   -0.54                              T__                        __              49540515
JOU      1.10 296.4 Pn       07:33:11.5    0.4                               T__                        d_              49540516
JOU      1.10 296.4 Sn       07:33:25.4    0.3                               T__                        _e              49540517
ONAJ     1.18 229.0 Pn       07:33:12.4    0.1                               T__                        d_              49540530
JMK      1.20 333.1 Pn       07:33:12.5    0.0                               T__                        d_              49540518
JMK      1.20 333.1 Sn       07:33:27.1   -0.39                              T__                        _e              49540519
OFUJ     1.21 350.9 Pn       07:33:12.3   -0.34                              T__                        d_              49540531
.
.
.
532A    91.05  49.8 P        07:45:52.799 -0.00  90.9                        T__                        __              05504129
334A    91.18  47.9 P        07:45:54.012   0.7  91.0                        T__                        __              05504128
H06N1   91.36  64.9 T        09:27:33.559                                    ___   6.0                  __              58438458
MIAR    91.43  42.9 P        07:45:54.85    0.5  91.2                        T__                        __              05504179
Y39A    91.60  43.6 P        07:45:55.543   0.4  91.4                        T__                        __              05504214
534A    91.98  49.0 P        07:45:57.308   0.2  91.8                        T__                        __              05504130
KEST    94.59 323.1 LR       08:33:52.432       320.5          38.70         ___             466.5 18.65 __              58438480
ESDC    96.70 334.2 LR       08:34:40.011       345.0          38.30         ___             375.8 20.18 __              58438449
TORD   117.01 315.6 PKPdf    07:51:32.55  -0.82  17.7           2.30         T__   5.1         0.4  0.70 __              58438504
TORD   117.01 315.6 PP       07:52:39.3   -2.90  31.2           6.30         T__   6.5         1.3  0.68 __              58438505
QSPA   127.62 180.0 PKPdf    07:51:52.02  -0.16                              T__                        _e              23535420
SNAA   141.68 197.1 PKPdf    07:52:13.751 -4.52                              T__                        __              20375340
VNA2   143.24 196.3 PKPbc    07:52:18.562   0.4 122.0           2.31         ___                        __              20375338
VNA1   143.64 196.2 PKPbc    07:52:19.77    0.6                              ___                        __              20375339
```

6.5 Ground Truth (GT) Events

Accurate locations are crucial in testing Earth models derived from body and surface wave tomography as well as in location calibration studies. 'Ground Truth' (GT) events are well-established source locations and origin times. A database of IASPEI reference events (GT earthquakes and explosions) is hosted at the ISC (www.isc.ac.uk). A full description of GT selection criteria can be found in *Bondár and McLaughlin* (2009a).

The events are coded by category GT0, GT1, GT2 or GT5, where the epicentre of a GTX event is known to within X km to a 95% confidence level. A map of all IASPEI reference events is shown in Figure 6.8 and the types of event are categorised in Figure 6.9. GT0 are explosions with announced locations and origin times. GT1 and GT2 are typically explosions, mine blasts or rock bursts either associated to explosion phenomenology located upon overhead imagery with seismically determined origin times, or precisely located by in-mine seismic networks. GT1-2 events are assumed to be shallow, but depth is unknown.

The database consists of nuclear explosions of GT0–5 quality, adopted from the Nuclear Explosion Database (*Bennett et al.*, 2010); GT0–5 chemical explosions, rock bursts, mine-induced events, as well as a few earthquakes, inherited from the reference event set by *Bondár et al.* (2004); GT5 events (typically earthquakes with crustal depths) which have been identified using either the method of *Bondár et al.* (2008) (2,275 events) or *Bondár and McLaughlin* (2009a) (updated regularly from the EHB catalogue (*Engdahl et al.*, 1998)), which uses the following criteria:

- 10 or more stations within 150 km from the epicentre
- one or more stations within 10 km
- $\Delta U \leq 0.35$
- a secondary azimuthal gap $\leq 160°$

where ΔU is the network quality metric defined as the mean absolute deviation between the best-fitting uniformly distributed network of stations and the actual network:

$$\Delta U = \frac{4\sum |esaz_i - (unif_i + b)|}{360N}, 0 \leq \Delta U \leq 1 \qquad (6.9)$$

where N is the number of stations, $esaz_i$ is the ith event-to-station azimuth, $unif_i = 360i/N$ for $i = 0$, ..., $N-1$, and $b = avg\,(esaz_i) - avg\,(unif_i)$. ΔU is normalised so that it is 0 when the stations are uniformly distributed in azimuth and 1 when all the stations are at the same azimuth.

The seismological community is invited to participate in this project by nominating seismic events for the reference event database. Submitters may be contacted for further confirmation and for arrival time data. The IASPEI Reference Event List will be periodically published both in written and electronic form with proper acknowledgement of all submitters.

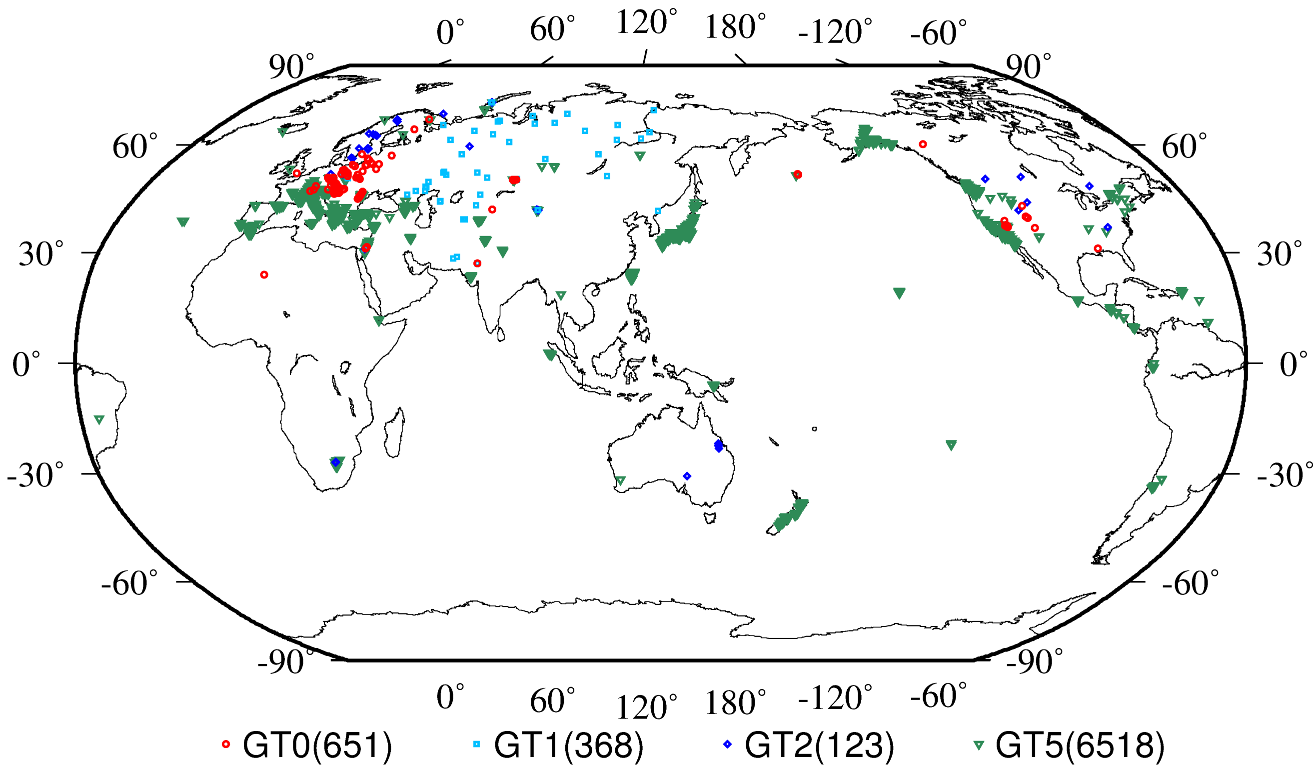

Figure 6.8: *Map of all IASPEI Reference Events as of September 2012.*

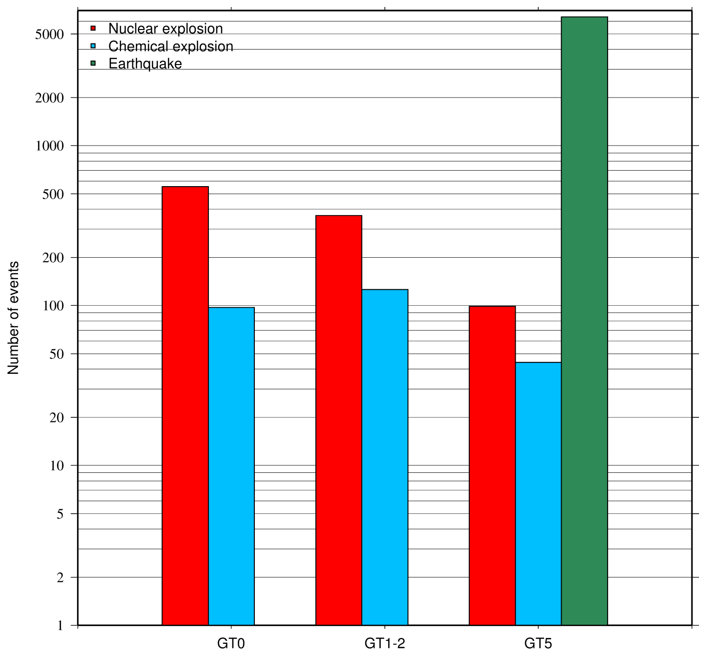

Figure 6.9: *Histogram showing the event types within the IASPEI Reference Event list as of September 2012.*

6.6 Nomenclature of Event Types

The nomenclature of event types currently used in the ISC Bulletin takes its origin from the IASPEI International Seismic Format (ISF).

Event type codes are composed of a leading character that generally indicates the confidence with which the type of the event is asserted and a trailing character that generally gives the type of the event. The leading and trailing characters may be used in any combination.

The **leading** characters are:

- s = suspected
- k = known
- f = felt (implies known)
- d = damaging (implies felt and known)

The **trailing** characters are:

- c = meteoritic event
- e = earthquake
- h = chemical explosion
- i = induced event
- l = landslide
- m = mining explosion
- n = nuclear explosion
- r = rock burst
- x = experimental explosion

A chemical explosion might be for mining or experimental purposes, and it is conceivable that other types of event might be assigned two or more different event type codes. This is deliberate, and matches the ambiguous identification of events in existing databases.

In addition, the code `uk` is used for events of unknown type and `ls` is used for known landslides.

The frequency of the different event types designated in the ISC Bulletin since 1964 is indicated in Figure 6.10.

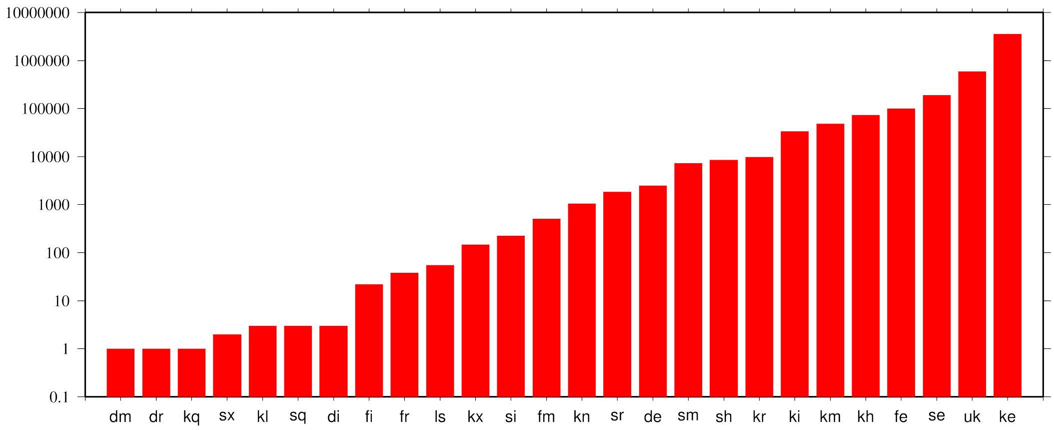

Figure 6.10: *Event types in the ISC Bulletin*

There are currently plans to revise this nomenclature as part of the coordination process between the National Earthquake Information Center (NEIC/USGS), European-Mediterranean Seismological Centre (CSEM) and the ISC.

7

Operational Procedures of Contributing Agencies

7.1 The Brazilian Seismographic Network: Historical Overview and Current Status

Bianchi, M.[1], Assumpção, M.[1], Agurto-Detzel, H.[1], Carvalho, J., Rocha, M.[2], Drouet, S.[3], Fontes, S.[3], Ferreira, J.M.[4], Nascimento, A.[4], and Veloso, J.A.V.[2]

[1] University of São Paulo, [2] University of Brasília, [3] National Observatory, and [4] Rio Grande do Norte Federal University

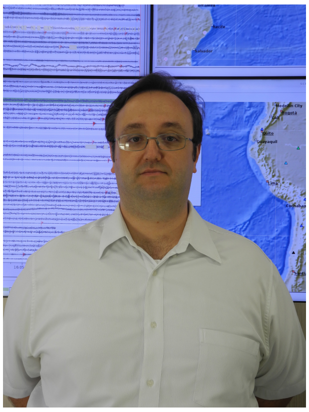

Bianchi, M.

Assumpção, M.

7.1.1 Introduction

Brazil occupies more than 47% of South American territory and is about three times the area of Argentina, which is the second largest country in the continent. Although Brazil has significant area, Brazilian intraplate seismicity is almost negligible compared to that in neighbouring countries. Intraplate seismicity in Brazil results from a complex interaction of more stable and less seismic cratonic areas with relatively more active surrounding Neoproterozoic foldbelts, where stresses from plate-boundary forces are more likely to be in effect (Assumpção *et al.*, 2014; Agurto *et al.*, 2015).

Efforts to study Brazilian seismicity nevertheless date back to the 1860's when Emperor Don Pedro II ordered a survey of felt reports for past Brazilian earthquakes. The first seismograph installation, with a German Rebeur-Ehlert triple pendulum at the National Observatory in Rio de Janeiro, was in 1899. Despite a promising start in the early 20th century, following the establishment of the RDJ station in 1905, further development was discontinued and no instruments were operational in the 1940's. In 1955, when the two largest earthquakes of magnitude mb 6.2 and mb 6.1 occurred in Brazil, no seismic stations were in operation in Brazil. The RDJ station was then reactivated in 1957.

In the latter part of the 20th century, several institutions in Brazil, from north to south, operated seismic stations and studied different aspects of Brazilian seismicity. In the late 1960's and early 1970's interest in Brazilian seismicity was renewed, spurred by studies of seismic hazard at the nuclear power plants and the occurrence of dam-induced seismicity. The Universities of São Paulo (USP), Brasília (UnB) and Rio Grande do Norte (UFRN) and the National Observatory (ON) then started to deploy their own seismic stations. At the start of the 21st century, six institutions (USP, UnB, UFRN and ON, together with the Institute of Technological Research, São Paulo, and the State University of São Paulo, Rio Claro) were involved in seismology, operating permanent and temporary network stations, but without a unifying central organization.

The Brazilian Seismographic Network (RSBR) was created in this context through a coordinated effort of all Brazilian seismology groups. Its main purposes are a) to monitor in real-time the national territory and b) to provide a reference network for research projects on earth structure and national seismicity. The network is made up of four sub-networks (FDSN network codes BL, BR, ON and NB), each with varying sets of instrumentation and technologies. In total there are 80 broad-band stations.

The vast majority of stations transmit real-time data that are relayed to all institutions using SeisComP3 SeedLink protocols. A few stations are still not online but should be incorporated in the near future. Each sub-network covers a specific region of the country, as shown in Figure 7.1. While the main purpose of RSBR is to improve earthquake monitoring in Brazil, it also significantly improves detection and locations of seismic events in this part of South America previously covered by only five permanent stations in global networks: BDFB (network GT), PTGA, RCBR and SAML (IU), and SPB (G).

RSBR is the result of a long process of development of Brazilian seismology, dating back to the regular bulletins for RDJ station published by the National Observatory between 1906 and 1944. Seismology grew mainly in universities deploying several temporary and a few permanent stations and then exchanging picks to publish the joint Brazilian Seismic Bulletin (BSB). With support from Petrobras (a Brazilian oil company), the implementation of RSBR, started in 2009, is the first jointly coordinated major project of all Brazilian universities and research institutions working in seismology.

7.1.2 Historical Overview

We present now a brief historical summary of seismographic stations installed in Brazil, some successfully accomplished and others not so well. In the first half of the 20th century, several attempts were made to install stations soon after the occurrences of large felt events. However, as often happens, practical and financial difficulties usually beset the scientific interests.

1899: Rebeur-Ehlert Triple Pendulum at the National Observatory

This instrument was brought from Germany by Luiz Cruls, an astronomer and one of the early directors of the National Observatory (ON), to be installed in Rio de Janeiro. It was installed by Henrique Moritze, who would later succeed Cruls as ON director. Apparently the seismograph worked for a few months but then operation ceased. Nevertheless, it can be regarded as the first operational seismic station in South America.

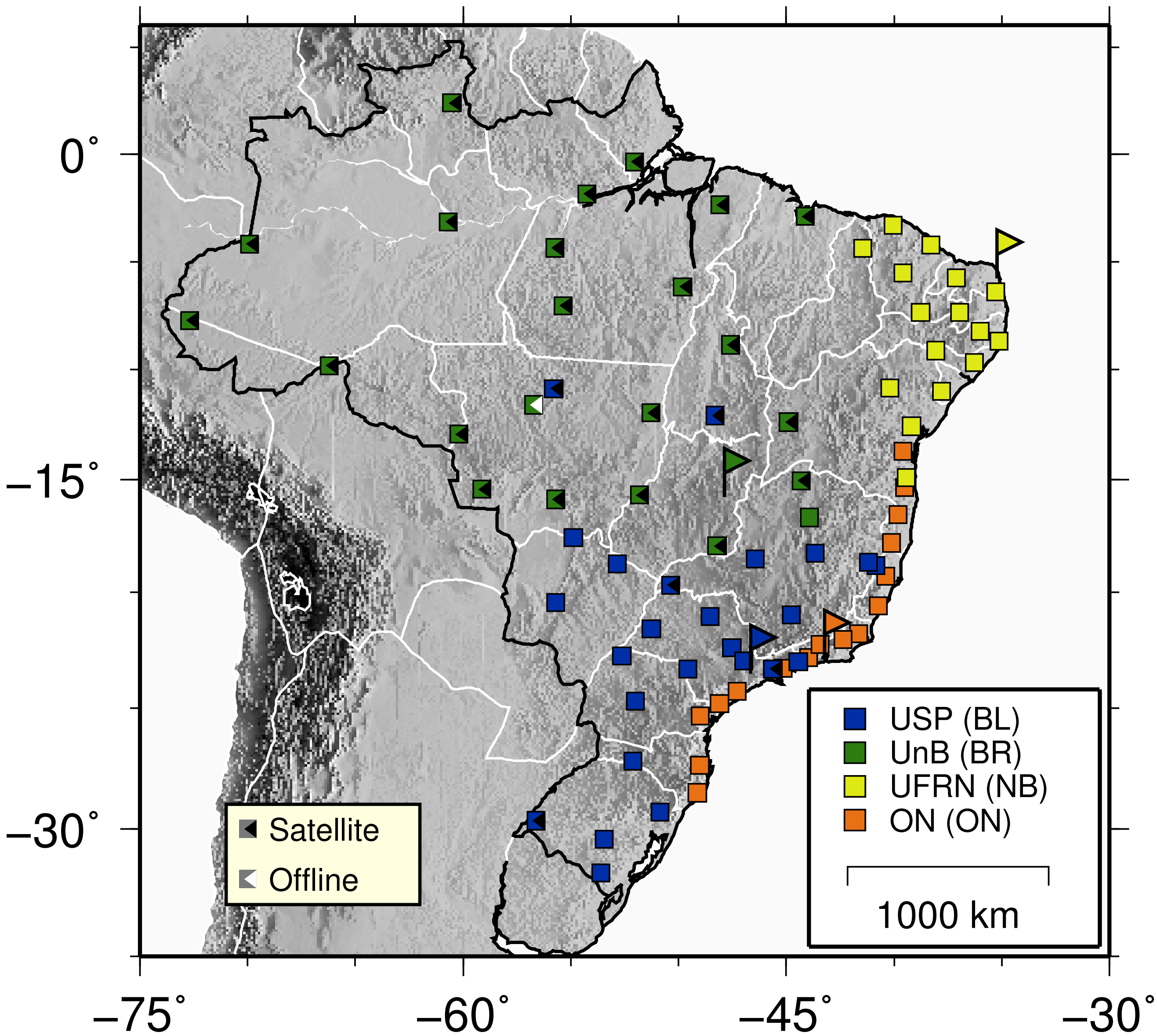

Figure 7.1: *Map of seismic stations (squares) and institutions (flags) participating in the RSBR initiative. Sub-networks and host institutions are coded by color. Further annotations indicate stations that are currently offline or using satellite technology for data links.*

1906-1944: National Observatory, Rio de Janeiro

Following the initial start with the Rebeur-Ehlert triple pendulum, other instruments were used by the National Observatory, sometimes in simultaneous operation. There are early reports of Wiechert (1909-1912), Bosch-Omori (1912-1922), Mainka (1921-1922) and Milne-Shaw (1923-1944) instruments in operation.

A Bosch-Omori seismograph with horizontal components and smoked-paper recording was installed at ON in 1905. It recorded the 1906 San Francisco earthquake and seems to have been in operation until 1922. From 1909 until 1912, a Wiechert seismograph was also in operation at ON (Pérez, 1984).

In June 1921 a Mainka seismograph was started in operation at Rio de Janeiro. On 27 January 1922 it recorded, 400 km away, the mb 5.1 São Paulo earthquake, which was felt across São Paulo and Rio de Janeiro states. Later that year, a more modern Milne-Shaw seismograph was installed and was operated there reliably for two decades, enabling ON to produce regular seismic bulletins until 1944.

1908, 1920: Porto Alegre, Rio Grande do Sul

An attempt was made in 1908 to install a seismograph at the recently created (1907) Astronomical and Meteorological Observatory of Porto Alegre, Rio Grande do Sul state, in southern Brazil, though without much success. A second attempt occurred around 1920 when ON sent a Wiechert seismograph to Porto Alegre. That installation seems to have recorded a few events but was discontinued after 1923.

1910: Fernando de Noronha Island

John Milne included Fernando de Noronha Island, near the equatorial region off northeast Brazil, as a site in the global Milne network (Turner *et al.*, 1911). The instrument was there from March 1910 to 1915 and recorded the $M7$ Avezzano earthquake, which killed 30,000 people in Italy.

1920: Bom Sucesso, Minas Gerais State, SE Brazil

After a series of small earthquakes up to magnitude 4 in 1919-1920 that caused panic and great concern in the local population, a Wiechert seismograph (200kg, two horizontal components) was deployed by ON. It seems to have been in operation there until 1932 but the local seismicity died down and no local events were recorded. Further, it seems to have recorded the São Paulo 1922 earthquake, but the seismograms were lost. In 1935, when local activity occurred in Bom Sucesso, no instruments were in operation.

≈1947: São Paulo

Despite the motivation prompted by the São Paulo earthquake of 1922, and several promises and attempts to get a seismographic station, it was only in the 1940's that the "São Paulo Observatory" (later to become the "Institute of Astronomy and Geophysics" of the University of São Paulo) installed two Wiechert-type seismographs, one vertical and one horizontal pendulum (Santos, 2005). However, it seems they never worked properly and their operation was discontinued. USP resumed its seismological activity in 1975 by deploying a temporary local network in collaboration with the Global Seismology Unit (Edinburgh) of the British Geological Survey.

1957: Lamont-Doherty at the National Observatory

As part of the 1957 International Geophysical Year, the Lamont-Doherty Geological Observatory (now Lamont-Doherty Earth Observatory) installed a complete seismographic station with Press-Ewing horizontal-components and Sprengnether vertical-component. Long-period and short-period seismometers were installed but only the long-period instruments remained operational until the early 1980's.

1965: WWSSN Station in Natal – NAT

As part of the USGS-organized World Wide Standard Seismographic Network, a station was installed near the city of Natal, northeast Brazil, in cooperation with the Brazilian Navy. NAT recorded several important earthquake sequences in northeast Brazil. The operation and maintenance of NAT was transferred from the Navy to the Federal University of Rio Grande do Norte in the late 1970's, when a seismology research group was established in the UFRN Physics Department. This motivated the development of the seismology group at UFRN.

1966-1971: Brasilia Array Station

With the creation of CERESIS (South American Regional Seismological Center) in 1963, a high-sensitivity array station (in T-format with up to 18 short-period seismometers and 2.5 km spacing) was proposed to be installed near the middle of the continent. In 1966, with support from the British Geological Survey, the Brazilian National Research Council and the University of Brasilia (UnB), initial field work and temporary installations were carried out near Brasilia. The SAAS (South American Array System) started operation in 1971 in its finalized form. In addition to the international and national support, the creation of a seismology group at UnB was essential to sustain the development of seismological studies in Brasilia.

1970-2000: Pre-RSBR Aspects

Seismology in Brazil advanced in the 1970's through the formation of the seismology groups in the universities and the National Observatory. Because of a growing importance of seismic hazard studies related to nuclear plants and of monitoring dam-induced seismicity, several permanent stations (with analogue recording) were installed, such as at BDF (the WWSSN station in Brasilia), the VAO network (USP), the CAI station (transferred from NAT by UFRN) and at BEB (Belém, UFPA).

In the 1980's, UnB started operating a network of stations in the Amazon, and IPT (Institute of Technological Research, São Paulo) installed several stations monitoring induced seismicity near dams in southern Brazil. In the 1990's digital stations in the new global networks were installed (BDFB, PTGA, SAML, SPB and RCBR), all of them successfully operating within international programs and backed by local support from the seismology groups at UnB, USP and UFRN.

Despite efforts of astronomers at several observatories early in the 20th century, Brazilian seismology could only be firmly established when full-time seismologists took an academic interest in research. In a country with low seismicity levels, only scientific research was able to sustain the long-time operation of seismic stations when there was normally only ephemeral interest and support after notable regional earthquakes.

During 1990-2010, all seismology groups in Brazil developed several independent research programs using temporary deployments to study earth structure or local seismicity. Cooperation and data exchange enabled the regular preparation of the joint BSB. However, it is only now with the establishment of the RSBR that there is an integrated effort to operate a national seismic network.

7.1.3 Current Status

RSBR network configuration and operational practice has been developed in the last four years and is still evolving. The RSBR is a single network composed of four sub-networks, each operated by a different institution and with various instruments but all following a minimum agreed standard. Because of the vast area, Brazil was geographically divided into four regions and local centers were chosen in each region to operate an independent set of stations. Table 7.1 lists the participant institutions, the areas of operations and the main instrumentations used in each sub-network.

While each institution is responsible for its own sub-network, ON was chosen as the main RSBR aggregator institution in the long term, responsible for archiving and distributing ground-motion and parametric data generated by all sub-networks. Furthermore, ON runs the main website (http://www.rsbr.gov.br) for the project. Please consult the RSBR website for updates.

Table 7.1: *Institutions, regions and technologies used in RSBR network operation*

Acronym	**Institution**	**Net**	**Attributed Region**	**Sensor**	**Datalogger**
ON	National Observatory	ON	South to central coastline	Streckeisen, STS-2	Quanterra, Q330
UFRN	Rio Grande do Norte Federal University	NB	Northeast Brazil	Reftek, RT151 + RT131B	Reftek, RT130
UnB	University of Brasília	BR	Central and north Brazil	Nanometrics, Trillium 120PA	Nanometrics, Trident/Taurus*
USP	University of São Paulo	BL	Central and southeast Brazil	Nanometrics, Trillium 120PA	Nanometrics, Trident/Taurus*

* Trident dataloggers are in many cases used instead of Taurus for stations transmitting over satellite links (Table 7.2).

Station Distribution

As shown in Table 7.1, all stations operate with broad-band sensors (120s to 50Hz). Stations in the UFRN network have additionally an accelerometer installed at each site as northeast Brazil is historically the most seismic area of the country, presenting recurrent intraplate swarms with magnitudes up to *mb* 5.0 at upper-crustal depths. Important historical events there include the 1986 João Câmara earthquake sequence, with the largest earthquake of magnitude *mb* 5.1, and over 50.000 events struck this region between 1986 and 1990.

Each sub-network of the RSBR network has a main target region with the station site locations determined by the responsible institution. Figure 7.1 shows the location map of the 80 stations currently operated in the RSBR network. In general, most of the country has been covered by stations, but with a lower density in the Amazon region mainly due to accessibility and logistic problems. Complementing Figure 7.1, Table 7.2 lists the detailed information of station codes, coordinates, altitude, closest city and transmission technology used for on-line data acquisition.

Table 7.2: *RSBR station parameters by sub-network: Tr, the transmission method, has "S" for Satellite, "W" for Wireless link, "2G" for GSM mobile network and "-" for offline status.*

i	Code	Longitude	Latitude	Alt.(m)	Closest City/State Name	Tr.
			BL network			
1	AQDB	-55.6997	-20.4758	158	Aquidauana, Mato Grosso do Sul	2G
2	BB19B	-48.5279	-21.0662	571	Bebedouro 19, São Paulo	2G
3	BSCB	-44.7635	-20.9984	935	Bom Sucesso, Minas Gerais	2G
4	BSFB	-40.8465	-18.8313	185	Barra do são francisco, Espírito Santo	2G
5	C2SB	-52.8377	-18.7688	757	Chapadão do Sul, Mato Grosso do Sul	W
6	CLDB	-55.7965	-10.8732	298	Colíder, Mato Grosso	S
7	CNLB	-50.8533	-29.3148	712	Canela, Rio Grande do Sul	2G
8	CPSB	-53.4432	-30.4123	290	Caçapava do Sul, Rio Grande do Sul	2G
9	DIAM	-43.6648	-18.2952	1280	Diamantina, Minas Gerais	W
10	ESAR	-44.4403	-23.0207	7	Angra dos Reis, Rio de Janeiro	W
11	FRTB	-49.5640	-23.3439	518	Fartura, São Paulo	2G
12	ITAB	-52.1313	-27.2349	459	Itá, Santa Catarina	W
13	ITQB	-56.6275	-29.6638	95	Itaqui, Rio Grande do Sul	S
14	ITRB	-50.3590	-19.7042	426	Iturama, Minas Gerais	S
15	PARB	-45.6246	-23.3421	777	Paraibuna, São Paulo	S
16	PCMB	-51.2619	-21.6074	346	Pacaembu, São Paulo	2G
17	PEXB	-48.3008	-12.1058	346	Peixes, Tocantins	S
18	PLTB	-53.6044	-31.7637	412	Pelotas/Pedras Altas, Rio Grande do Sul	2G
19	PMNB	-46.4400	-18.5400	950	Patos de Minas, Minas Gerais	2G
20	PP1B	-54.8796	-17.6003	368	Sonora, Mato Grosso do Sul	2G
21	PTGB	-52.0118	-24.7209	981	Pitanga, Paraná	W
22	RCLB	-47.5310	-22.4191	650	Rio Claro, São Paulo	2G
23	SJMB	-41.1847	-18.7029	243	São João de Manteninha, Minas Gerais	W
24	TRCB	-52.6357	-22.7946	490	Terra Rica, Paraná	2G
25	VABB	-46.9657	-23.0021	866	Valinhos, São Paulo	2G
			BR network			

Table 7.2: Continued.

i	Code	Longitude	Latitude	Alt.(m)	Closest City/State Name	Tr.
1	ARAG	-51.8120	-15.7060	237	Araguaiana, Mato Grosso	S
2	BOAV	-60.5225	2.3953	114	Boa Vista, Roraima	S
3	CZSB	-72.7049	-7.7299	196	Cruzeiro do Sul, Acre	S
4	ETMB	-66.2137	-9.8168	196	Extrema, Roraima	S
5	IPMB	-48.2117	-17.9830	706	Ipameri, Goias	S
6	ITTB	-55.7343	-4.3672	118	Itaituba, Pará	S
7	JANB	-44.3112	-15.0581	693	Januária, Minas Gerais	S
8	MACA	-60.6838	-3.1615	75	Manacapuru, Amazonas	S
9	MALB	-54.2649	-1.8529	27	Monte Alegre, Para	S
10	MC01	-43.9417	-16.7074	740	Montes Claros, Minas Gerais	2G
11	MCPB	-52.0567	-0.3602	127	Macapá, Amapá	S
12	NPGB	-55.3579	-7.0454	266	Novo Progresso, Pará	S
13	PDRB	-56.7296	-11.6123	322	Porto dos Gaúchos, Mato Grosso	-
14	PRPB	-49.8150	-6.1724	265	Parauapebas, Pará	S
15	PTLB	-59.1368	-15.4487	72	Pontes e Lacerda, Mato Grosso	S
16	ROSB	-44.1246	-2.8967	60	Rosário, Maranhão	S
17	SALV	-55.6936	-15.9012	213	Santo Antônio do Leverger, Mato Grosso	S
18	SDBA	-44.9030	-12.4085	623	São Desidério, Bahia	S
19	SMTB	-47.5886	-8.8617	292	Santa Maria do Tocantins, Tocantins	S
20	SNDB	-51.2943	-11.9742	252	Serra Nova Dourada, Mato Grosso	S
21	TBTG	-69.9090	-4.1868	91	Tabatinga, Amazonas	S
22	TMAB	-48.0957	-2.3704	26	Tome-Acu,Pará	S
23	VILB	-60.2002	-12.9528	434	Vilhena, Roraima	S
					NB network	
1	NBAN	-36.2746	-9.6686	260	Anadia, Alagoas	2G
2	NBCA	-36.0130	-8.2256	613	Caruaru, Pernambuco	2G
3	NBCL	-38.2910	-4.2243	27	Cascavel, Ceará	2G
4	NBCP	-39.1820	-12.5937	232	Cabeceiras do Paraguaçu, Bahia	2G
5	NBIT	-39.4345	-14.9307	183	Itapé, Bahia	2G
6	NBLA	-37.7890	-10.9925	192	Lagarto, Sergipe	2G
7	NBLI	-36.9498	-7.3645	624	Livramento, Pernambuco	2G
8	NBMA	-38.7641	-7.3654	437	Mauriti, Ceará	2G
9	NBMO	-40.0414	-3.3108	95	Morrinhos, Ceará	2G
10	NBPA	-37.1121	-5.7503	92	Paraú, Rio Grande do Norte	2G
11	NBPB	-39.5837	-5.5432	263	Pedra Branca, Ceará	2G
12	NBPN	-40.1988	-10.8468	386	Ponto Novo, Bahia	2G
13	NBPS	-41.4457	-4.3940	713	Pedro Segundo, Piauí	2G
14	NBPV	-35.2905	-6.4175	91	Pedro Velho, Rio Grande do Norte	2G
15	NBRF	-35.1272	-8.6794	56	Rio Formoso, Pernambuco	2G
16	NBTA	-38.0633	-9.1220	348	Tacaratú, Pernambuco	2G
					ON network	
1	ALF01	-40.7252	-20.6169	22	Guarapari, Espírito Santo	2G
2	CAM01	-41.6574	-21.8257	31	Campos, Rio de Janeiro	2G
3	CMC01	-39.5191	-15.3601	169	Camacan, Bahia	2G
4	DUB01	-42.3742	-22.0810	623	Duas Barras, Rio de Janeiro	2G

Table 7.2: Continued.

i	Code	Longitude	Latitude	Alt.(m)	Closest City/State Name	Tr.
5	GDU01	-39.5753	-13.7200	251	Guandu, Bahia	2G
6	GUA01	-39.8053	-16.5835	198	Guaratinga, Bahia	2G
7	JAC01	-48.1024	-24.8114	297	Jacupiranga, São Paulo	2G
8	MAJ01	-49.0118	-27.3972	344	Major Gercino, Santa Catarina	2G
9	MAN01	-43.9641	-22.8652	617	Mangaratiba, Rio de Janeiro	2G
10	NAN01	-40.1257	-17.8442	206	Guarapari, Espírito Santo	2G
11	PET01	-47.2753	-24.2901	150	Pedro de Toledo, São Paulo	2G
12	RIB01	-40.3944	-19.3142	216	Rio Bananal, Espírito Santo	2G
13	SLP01	-45.1559	-23.3243	1117	São Luis do Paraitinga, São Paulo	2G
14	TER01	-49.1291	-28.5318	315	Treze de Maio, Santa Catarina	2G
15	TIJ01	-49.0046	-25.3235	1049	Tijucas do Sul, Paraná	2G
16	VAS01	-43.4426	-22.2801	402	Vassouras, Rio de Janeiro	2G

Detectability of Regional Events

In this report, we use the Brazilian regional magnitude scale, m_R, determined by the maximum particle velocity in the whole P-wave train using the following equation (Assumpção, 1983):

$$m_R = log(V) + 2.3log(D) - 2.28 \tag{7.1}$$

where V is the ground velocity in μm/s and D is the distance in km in the range 200−1500 km.

This regional magnitude scale is consistent with the teleseismic mb scale in the range $3.5 < m_R < 5.5$ (Assumpção *et al.*, 2014). A preliminary relationship with Mw is given by (Druet, 2014):

$$Mw = 1.12m_R - 0.76 \tag{7.2}$$

In addition to the indicated m_R values, we also use M values, which do not relate to any specific scale but can be taken as an average magnitude as in the case of SeisComP3 practice, which averages all available magnitude types for the event.

An attempt to quantify the current detectability of the RSBR network is presented in Figures 7.2 and 7.3, which indicate the distribution of the "Number of Stations" and "Maximum Azimuth Gap" for given magnitudes. As a rule of thumb we assumed that an earthquake with magnitude m_R 2.5 ($Mw = 2.0$) is recorded to a maximum distance of 150 km, m_R 3.5 ($Mw = 3.0$) to 500 km and finally that an earthquake with magnitude m_R 4.0 ($Mw = 3.5$) can be detected out to a distance of 1200 km.

For an indication of the regional monitoring thresholds, Figure 7.2 was prepared by counting the number of stations within the indicated distance from each grid-position. For earthquakes of m_R 2.5 (Figure 7.2a) only events near the coast and along part of the northeast region would be detected by more than two stations, but earthquakes there of that magnitude would not normally be located automatically

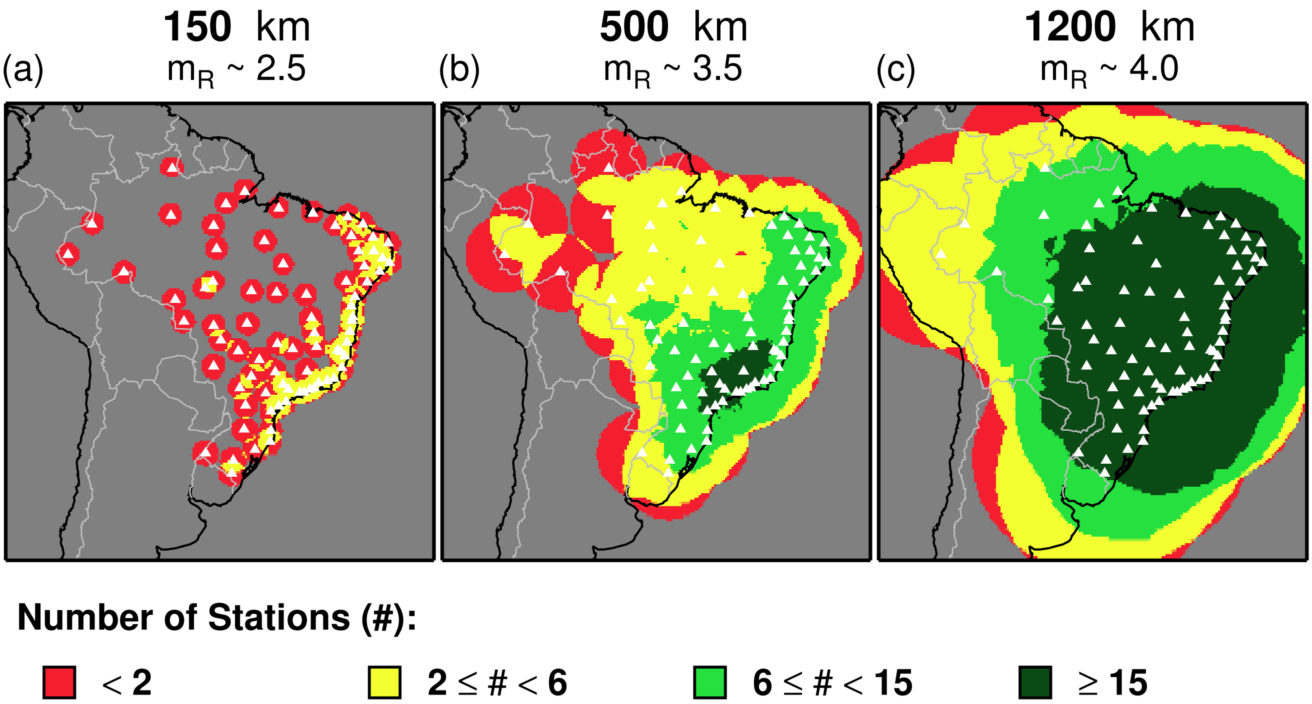

Figure 7.2: *Expected station detections for specified regional magnitudes. The number of detecting stations within the indicated distance for the specified regional magnitude is coded by color.*

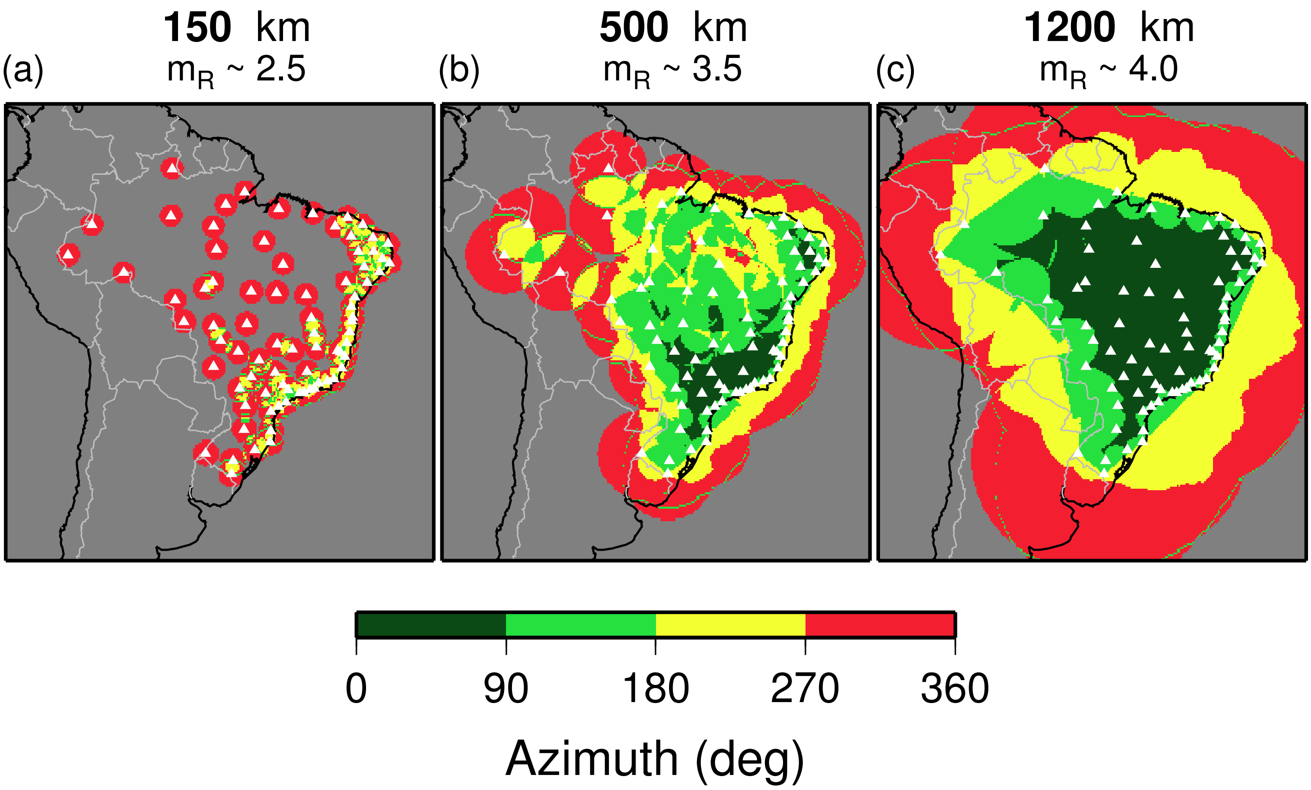

Figure 7.3: *Expected maximum azimuthal gap for the detecting station distribution. The maximum azimuthal gap is coded by color for the cases indicated by the specified regional magnitude and detecting station distance.*

as a minimum of six detections is required by the automatic system. A better result is achieved for earthquakes of m_R 3.5 (Figure 7.2b). In this case sufficient stations for an automatic location (6 - 15) are obtained along the coast in the middle and southeast regions, where sub-networks BL and ON partly overlap. Furthermore, São Paulo and Rio de Janeiro cities (Brazil's most densely populated areas) are monitored with an optimal ($\geq$15) number of stations within a range of 500 km. Finally, for m_R 4.0 (Figure 7.2c), a good coverage is shown for most of the country, with an excellent coverage for the central-south, southeast, northeast and some of the northern areas of the country.

Another way to quantify RSBR coverage is by evaluating the maximum azimuthal gap, as shown in Figure 7.3 where magnitudes and distances previously adopted are again used. Whereas Figure 7.2 relates to the RSBR capacity for detecting and locating an earthquake, Figure 7.3 relates to the RSBR capacity for resolving focal mechanism solutions (and also to the robustness of the location solutions). Earthquakes with magnitude $m_R < 2.5$ (Figure 7.3a) show little or no capacity for resolution of focal mechanism. For earthquakes with magnitudes close to m_R 3.5, some areas near the coast and in southeast and northeast Brazil give maximum azimuthal gaps less than 90°, which may be sufficient to resolve focal mechanisms. For larger earthquakes, of m_R 4.0 or more, a good azimuthal coverage is expected for most of the country, except near the borders: stations outside the RSBR network were not considered in these calculations.

Obviously these analyses should not be considered to represent the actual RSBR resolution but merely a first approximation of the current coverages. Here, stations operated by other networks were not included as RSBR has no control over data latency or influence over neighboring network configuration to optimize any joint operation. When other stations are included, such as in some of the Andean countries, RSBR capacity is greatly improved, resulting in earthquakes with m_R 3.0 being well located automatically along the margins bordering northeast Argentina, Chile and Bolivia.

Station Deployment Quality

As RSBR was a distributed network created by combining sub-networks from different institutions (Table 7.1) an effort was made from the beginning of the project to have some uniformity in the site installations. A major decision was to install stations on surface bedrock (there was no budget allowance for borehole installation) and cover the sensors with sand or soil to guarantee the needed temperature stability and wind protection and to avoid any tilt-induced noise. Another consideration was to bury cables in pipes and install data-loggers inside small masonry constructions to achieve a long-lasting installation. Finally, the stations were mostly sited on private property and normally surrounded by fences for general protection.

Two typical station installations are shown in Figure 7.4, with a tall structure housing the data-loggers, transmission and power equipment next to another over the sensor pit filled with sand or soil for insulation. At some stations the box around the sensor is now being covered by a soil dome that should result in lower noise levels by reducing heat-induced ground tilt.

A power density function (PDF) comparison of site noise for each station (Figure 7.5a-c) and by sub-network medians (Figure 7.5d-f) reveals some interesting aspects for RSBR stations.

At first glance, stations from the NB network (yellow traces on Figure 7.5a-c) show the lowest noise levels,

(a) Station BL/PLTB, South Brazil (b) Station ON/CAM01, Southeast Brazil

Figure 7.4: *Example station sites from the BL and ON networks. Solar panels, batteries, data-loggers, transmission equipment are hosted by the tall masonry constructions separate from lower constructions hosting the sensors and filled with soil/sand materials. Cables ducts are protected by masonry to avoid undesired vibration.*

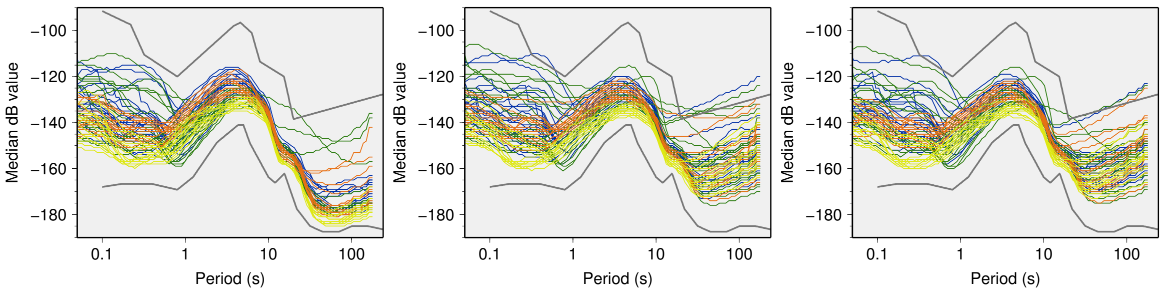

(a) Individual Station, HHZ (b) Individual Station, HHN (c) Individual Station, HHE

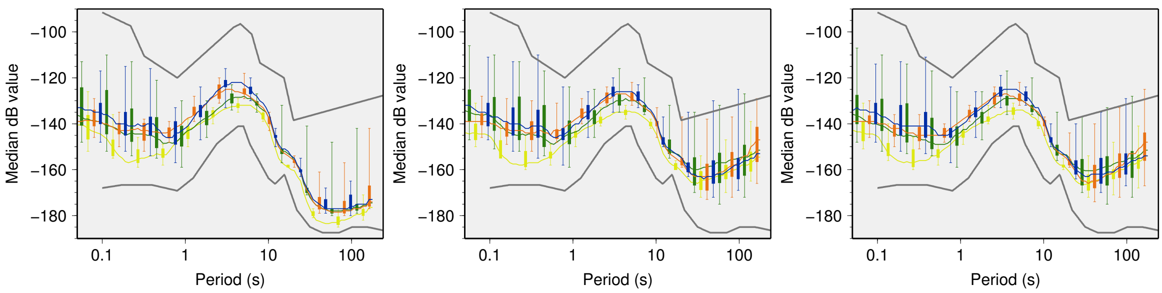

(d) Network Average, HHZ (e) Network Average, HHN (f) Network Average, HHE

Figure 7.5: *PDF plots for RSBR stations, where (a), (b) and (c) are compilations of individual station PDF curves colored according to network code, and (d), (e) and (f) are network-median PDF curves (using 0%, 25%, 75% and 100% percentile box-and-whisker-plots). Green is for the BR (UnB) sub-network, orange for ON (ON), yellow for NB (UFRN) and blue for BL (USP). Stations with problems in metadata or components were manually removed from the comparison.*

especially for the vertical component. On the horizontal components the noise levels are still relatively low at the lower periods but are less so for the higher periods. BL stations (blue traces on Figure 7.5a-c) generally have the highest PDF values on all channels, predominantly at the lower to intermediate periods as they are sited in areas of the country with greater population and industrialization levels, but more average behavior for the longer periods. The other two networks, ON (orange) and BR (green), show intermediate values but with a larger scatter of noise levels for the BR network.

From the comparison of the network-median plots (Figure 7.5d-f) it can be seen that the BL and BR networks show larger boxes for the 25% and 75% quartiles and also larger whiskers. One explanation for this is that the BL and BR networks are the more widespread across the continent, covering the interior, and are thus not similar to the ON and NB networks that cover smaller and more uniform regions. Finally, it is important to observe that RSBR sub-network median PDFs are generally below that for the standard high-noise model, though there is still room for improvement, especially at shorter periods, as the best site was not always chosen because of connectivity constraints.

Data Distribution and Processing

Ground-motion data collected at the stations are transmitted in real-time to their sub-network data-center for processing and re-distribution. Table 7.2 and Figure 7.1 indicate which stations transmit data in real-time and what transmission technology is currently employed. The final link availability is technology dependent.

During the first weeks of March 2015 an average availability of 99.97±0.07% was observed for the satellite stations (BL and BR networks). BL stations had 96±5% for 2G/3G links and 98.6±1.0% for stations connected through local wireless providers. While satellite is the most uniform link with lowest standard deviation, and local wireless provides good link availability with a small standard deviation, mobile 2G/3G links with a standard deviation of 5% are considered to be an acceptable non-uniform technology across the whole country. Final link availability will later be reflected in near real-time data archives as on-site collection is still happening for now after six months on average. Collected field data will continue to be used to fill gaps in local archives, which are finally synchronized using the rsync tool (see http://rsync.samba.org/) at the ON data-center for final archiving and distribution.

Even before the final archiving occurs, data are distributed using SeisComP3 systems installed at each institution. SeisComP3 was the chosen platform for data exchange and earthquake location adopted by RSBR from the beginning. SeedLink and ArcLink servers implemented in the SeisComP3 system are extensively used at RSBR and, for compatibility, all data stored by RSBR are organized into SDS file-structure archives. Using SeisComP3 standard tools, real-time data are shared using the SeedLink protocol, and archived data can be obtained from each institution, using the ArcLink protocol, or from the master ON ArcLink server. SeedLink and ArcLink server addresses for the RSBR sub-networks are shown in Table 7.3 and access is openly available for anyone. The ground-motion data policy for RSBR stations is that **data are open and freely distributed to anyone**.

So far, most of the RSBR effort has been directed to deploying the stations, recording and archiving the ground-motion data. Less time has been devoted to compiling an earthquake bulletin and catalogue. In time, RSBR will produce a composite Bulletin merging all earthquake origins from each node. Each

Table 7.3: *ArcLink (near-realtime, archive data) and SeedLink (realtime) internet server addresses used for network data distribution.*

Node	Network(s)	SeedLink (address:port)	ArcLink (address:port)
ON	ALL	**rsis1.on.br:18000**	**rsis1.on.br:18001**
UFRN	NB	sislink.geofisica.ufrn.br:18000	
USP	BL/BR	seisrequest.iag.usp.br:18000	seisrequest.iag.usp.br:18001
UnB	BR	datasis.unb.br:18000	datasis.unb.br:18001

All servers are open to anyone.

institution should be authoritative for its area while RSBR should be authoritative for Brazil. So far (December, 2015), parametric data (time and amplitude picks, and origins and magnitudes) are exchanged between USP and ON using the scimex tool, which relays the SeisComP3 parametric data messages from one node to another. These messages feed a master SeisComP3 system that drives the main RSBR web-page and an alert service when appropriate.

Earthquake Solutions

At present ON and USP contribute to the RSBR earthquake solutions. USP is responsible for most of the location revision, having allocated two analysts (who were historically responsible for reviewing the BSB) working full-time during weekdays a) to review the automatic solutions coming from the standard SeisComP3 process, and b) to visually inspect day-plots, searching for and locating Brazilian earthquakes with magnitudes close to m_R 3.0 that are for now not processed by the automatic system.

USP and ON seismologists collaborate to improve the automatic system by attempting to tune the RSBR SeisComP3 system working on two fronts: (1) by developing and testing a SeisComP3 plugin for computing the Brazilian regional magnitude (m_R) historically used in Brazil for the BSB, and (2) by tuning trigger and location parameters for the RSBR configuration to minimize false locations normally associated with PKP phases recorded at RSBR stations.

This work forms the first RSBR efforts to maintain a national service of near real-time earthquake locations and alerts in Brazil. Although individual institutions may be currently involved with the location processing, most of the reviewing process is done at USP and injected into the RSBR server located at the ON observatory, where each origin should conform to one RSBR event. Further cooperation between the institutions to improve earthquake locations will depend not only on new technological tools and workflows still to be developed but also on regular training for analysts working on local events at each institution.

RSBR and the Pisagua, Chile 2014, Earthquake Sequence

One way to evaluate RSBR capabilities is to examine results for an earthquake sequence, such as the one that occurred during March/April 2014 near the coast of northern Chile. The Pisagua sequence started on March 16th and culminated with a major Mw 8.1 event on April 1st, followed by the Mw 7.6 event on April 2nd. The sequence was recorded by many RSBR stations (in networks BL and BR

- others networks had transmission problems at the time) together with other South American stations in the G, GT and IU networks. A total of 265 events were automatically located and manually revised by USP seismologists. The results are discussed here.

Figure 7.6 shows all the event locations determined with RSBR stations after phases had been repicked. Hypocenter depths are indicated in the associated profile in Figure 7.6. Depths here were set fixed (to an average value of 40 km) only when the location algorithm did not converge with a reasonable depth (usually from 0 to 100 km).

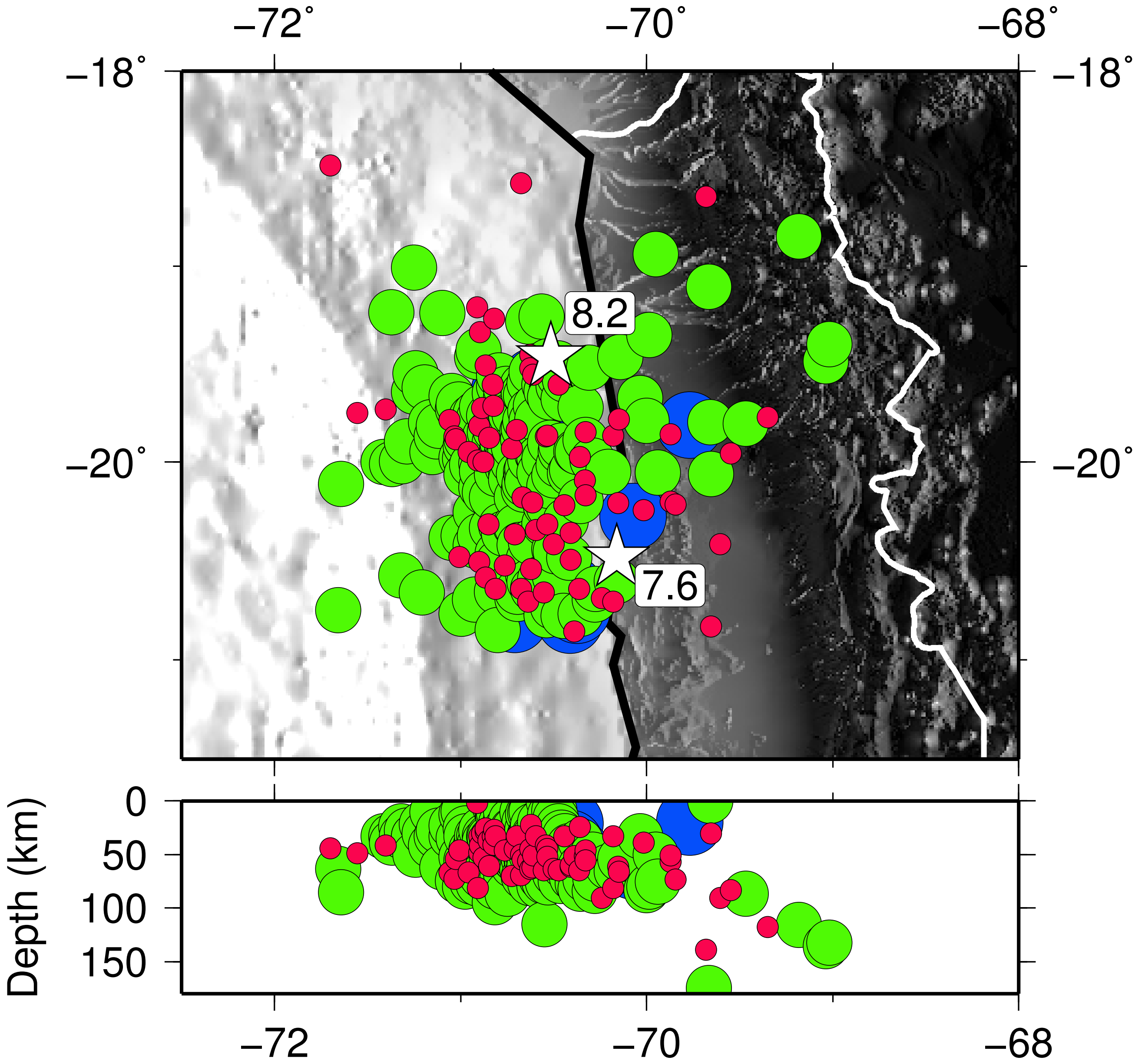

Figure 7.6: *Pisagua earthquake sequence map and depth profile determined using RSBR stations and other South American stations in the global G, GT and IU networks. Events with M < 4.0 are shown green, between M 4.0 and M 5.5 are red and M > 5.5 are blue.*

A first attempt to characterize the RSBR network capability examines the elapsed times taken to automatically locate each earthquake origin in the repeated processing sequence and the observed deviations. Figure 7.7 shows the median delay for the determinations of event origins for events in the sequence. The delay times were calculated using

$$\delta s = O_s - P^t \tag{7.3}$$

where δs is the delay time for the sth solution, s being the solution sequence number starting at 0 for the first solution for an event, 1 for the second and so on. O_s is the origin creation-time for solution s and P^t is the preferred origin-time for the event, simply here the determined origin-time for the event.

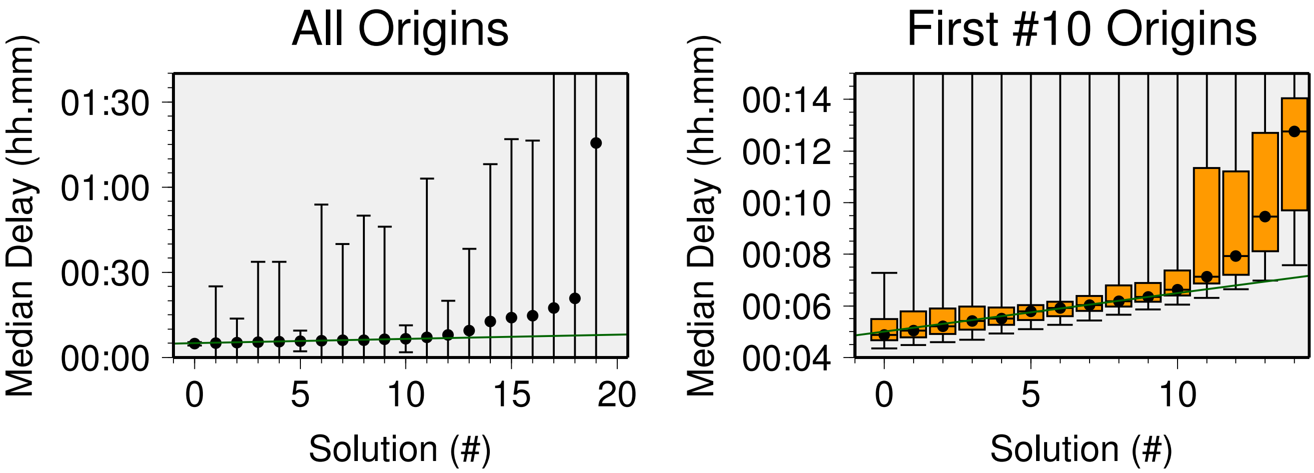

Figure 7.7: *Median delays for automatic origin determinations of RSBR events. A first origin solution was usually determined after about 5±1 minutes. Solution #10 was usually determined after about 6.5±1 minutes. Orange boxes represent 25% and 75% limits for the delay in determining origin-times and the whiskers represent the 0% and 100% limits. The green line represents a linear model where subsequent origin determinations for an event are each delayed an extra nine seconds. Some later origins are still being determined after a delay of more than one hour.*

Figure 7.7 shows that the first solutions were determined within about the first 5±1 minutes after the occurrence time of an event, and subsequent solutions were each delayed by about an extra nine seconds until the tenth solution for an event. The range between 25 and 75 percentiles for the delay times shows some uniformity until the tenth solution, after which this range changes abruptly from ±1 minute to ±4 minutes. The determination of the tenth solution for an event was generated within about 6.5±1 minutes, which corresponds to a travel-time distance of about 32° for the P arrival and marks the approximate limit in range of the RSBR network for the Pisagua sequence. Later solutions for events usually incorporated data from additional stations of the global network sited in other continents, giving a delay greater than the earlier extra nine seconds per solution because of the longer transmission times over the internet in addition to the greater seismic travel-times. Furthermore, the larger whiskers in Figure 7.7 may be due to other link delays that could have affected some events, causing the system to take longer to resolve and generate solutions for the later events.

Next we compared the catalogue of RSBR events with the catalogue of the University of Chile (UCL), which has a total of 1804 events. A similar comparison was made with the 474 events located by the United States Geological Survey (USGS/NEIC/PDE) for the same region (latitude from 21°S to 18°S and longitude from 72°W to 69°W) and period (from 2014-03-16 00:00:00 UTC to 2014-05-02 00:00:00 UTC). We assumed that the UCL catalogue is the most complete and most accurate as it used observations from many local stations near the epicentral region.

The event association process was carried out in two stages. First the source catalogue was self-associated by grouping close individual origins into single events to minimize the effect of the chosen comparison parameters (mainly the distance and time differences) on the association process. In the second stage a cross-association process was done between the auto-associated source catalogue and the target catalogue. Association was based on a maximum epicenter separation of 120 km, maximum origin-time difference of 60 s and a magnitude difference of two that allowed a one-to-one association and minimized the number of orphan events (events in target catalogue that didn't match any event in the source catalogue). Finally, once the origins were associated we estimated the completeness of the RSBR and NEIC catalogues in relation to the UCL catalogue. Using the parameters indicated in the above resulted in 31 origins being isolated in the UCL catalogue auto-association and the final cross-associations resulted in 7 RSBR orphan origins and 66 NEIC orphan origins (i.e., events located by RSBR or NEIC but not included in the UCL catalogue).

The completeness of the RSBR and NEIC catalogues is compared to the UCL catalogue in Figure 7.8. With the auto-association carried out for RSBR and NEIC catalogues the performance for RSBR is slightly poorer than that for NEIC. The RSBR magnitude threshold is M 3.4 *vs* M 3.1 (NEIC), with a minimum complete magnitude of M 5.5 *vs* M 4.8 (NEIC) and an event-loss percentage of 85% *vs* 77% (NEIC). However, it is important to note that NEIC receives a direct contribution of arrival picks and parameter data from UCL stations and other partners in South America not yet used in RSBR operations. When this taken into account, the minimum detected event size for RSBR (M 3.4) is more similar to that for NEIC (M 3.1). Nevertheless, the RSBR completeness magnitude (M 5.5) is much higher than that for NEIC (M 4.8), which indicates a need to improve the SeisComP3 detection parameters presently being used in the absence of manual scans for near-threshold events as done currently by the analysts searching for missed Brazilian regional events.

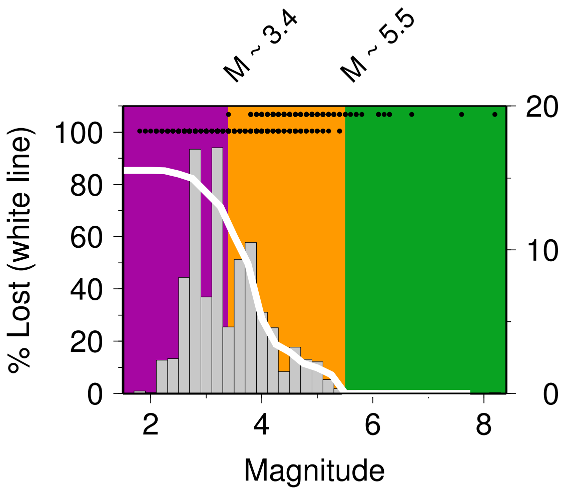

(a) RSBR vs UCL

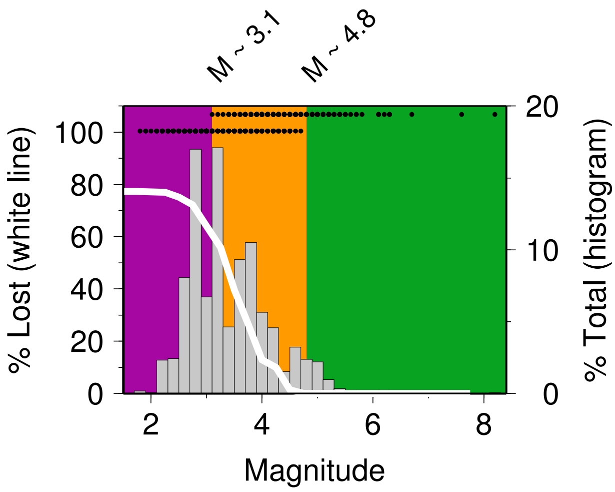

(b) NEIC vs UCL

Figure 7.8: *Comparison histograms for catalogue completeness. The purple, orange and green zones indicate magnitudes ranges where the target catalogue has no events, is partly complete or complete, respectively, according to the UCL reference catalogue. A white line indicates the accumulated-loss percentage, grey bars show the UCL catalogue magnitude histogram, and the black dots indicate the magnitudes of individual events that are only in the UCL catalogue (lower dots) or are also in the target catalogue (upper dots).*

Further, the differences in location (Figure 7.9), depth (Figure 7.10) and magnitude (Figure 7.11) can be compared for the associated events. Figure 7.9 shows the differences in latitude and longitude of the target catalogue origin (RSBR or NEIC) from the reference catalogue (UCL) origin against the latitude or longitude for the UCL origin. RSBR has median differences in location of 21 km whereas NEIC has median differences of only 8 km. The NEIC origins are therefore closer to the corresponding UCL locations. Figure 7.9b suggests a trend of larger differences to the west (towards the trench, see Figure 7.6), which may be related to RSBR solutions not having fixed depths and a trade-off of depth against longitude when most of the stations are sited to the east. The NEIC origins do not show this behavior but, as indicated in Figure 7.10, the NEIC focal depths are usually under-estimated relative to the UCL depths.

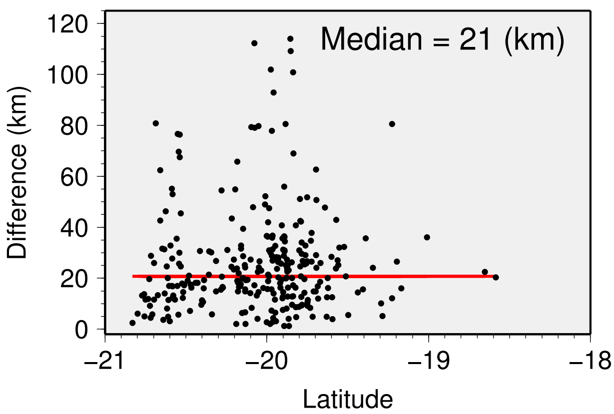

(a) RSBR vs UCL

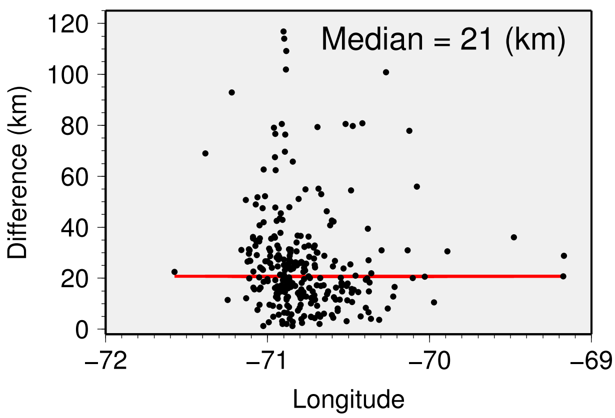

(b) RSBR vs UCL

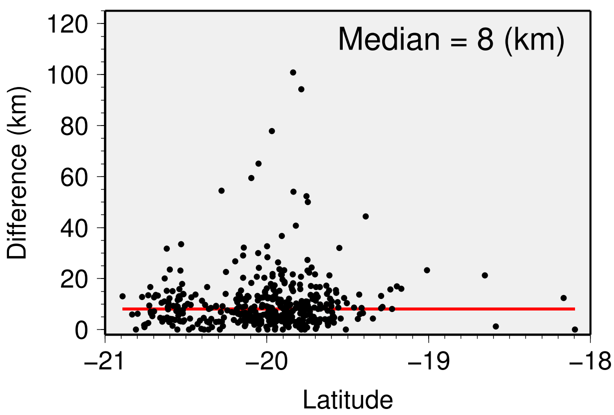

(c) NEIC vs UCL

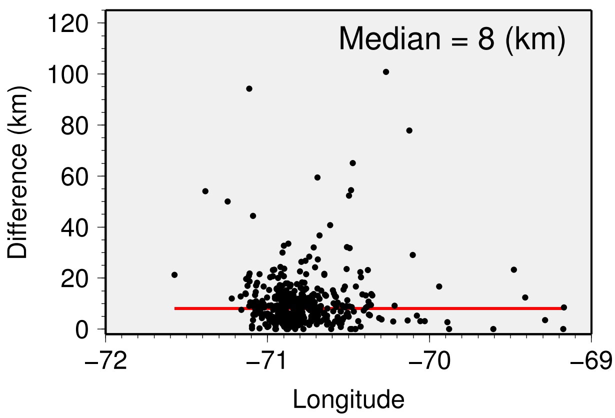

(d) NEIC vs UCL

Figure 7.9: *Location offsets for associated events, showing the differences in latitude and longitude between the target and reference catalogue (UCL) epicenters. The red lines indicate the medians of differences from the UCL latitude or longitude.*

Figure 7.10a compares the depth distribution from the RSBR and NEIC catalogues with that of UCL. Whereas Figure 7.10b shows that the UCL catalogue has depths concentrated at ∼40 km, RSBR does not show any dominant depth range, with values scattered from 0 to 90 km. Deep events (probably not associated with the sequence) are well correlated, however, showing a slightly deeper trend for RSBR that is possibly reflected also in the earthquake location. On the other hand, NEIC solutions are mostly shallower than corresponding UCL solutions, although the deep events are almost perfectly correlated. NEIC depths cloud around 15 km while UCL depths concentrate around 40 km.

Finally, the magnitude comparisons in Figure 7.11 show more uniform characteristics. First, RSBR and

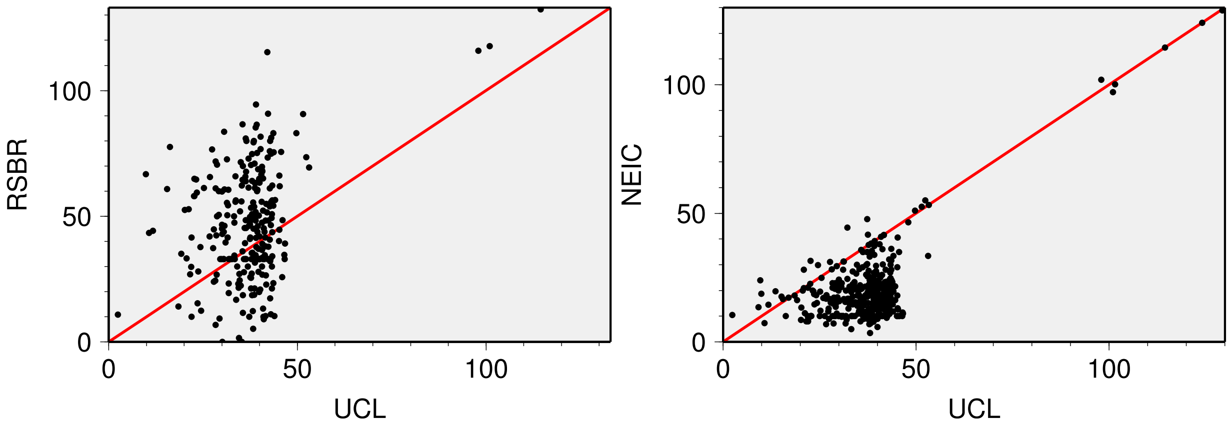

Figure 7.10: Depth comparison plots. Each dot represents an event in the target catalogue, either RSBR or NEIC, associated with an event in the reference UCL catalogue. The red line represents the line of perfect correlation.

NEIC magnitudes are more closely matched to the UCL value for magnitudes larger than M 5.5. For smaller events, the RSBR magnitudes tend to be lower while NEIC magnitudes tend to be higher than the UCL estimates. These features should be investigated further, but ultimately with consideration of the different magnitude scales used.

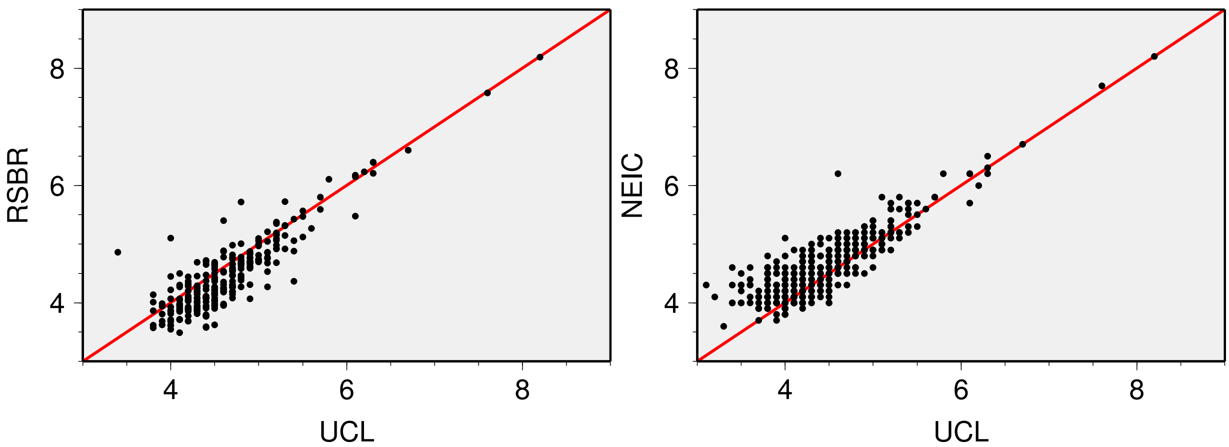

Figure 7.11: Magnitude comparison plots. Each dot represents an event in the target catalogue, either RSBR or NEIC, associated with an event in the reference UCL catalogue. The red line represents the line of perfect correlation.

7.1.4 Future

Given the vast size of Brazil and its low seismicity, the development of a national network was always going to be a challenge. With Petrobras support and joint efforts from four research institutions, the RSBR network has grown in the last few years and has become a reality. The initial installation plan is now almost complete: there are still two more stations planned for the Amazon region. The next challenge facing each of the four institutions is the sustainability of their sub-network, including maintenance costs as well as minimum personnel for field work and routine analyses.

The network design fulfils its initial goals. For example, one of the major products of RSBR today is the improvement of the Brazilian Seismic Bulletin with on-line information. However, further work is still necessary to tune the detection parameters, review workflows and improve inter-institution data exchange for routine analysis, as demonstrated by the results for the Pisagua sequence earthquakes. Some important points that need to be considered are: how to increase the detectability of the network to match NEIC levels in South America; and how to estimate earthquake depths more reliably in the Andean region without origin-depth trade-offs given that we have larger errors for our earthquake locations there. Also, a velocity model more representative of the Brazilian lithosphere should be implemented to improve earthquake locations in Brazil generally.

The choice of SeisComP3 software for the operation of the whole RSBR network has proved to be quite a useful coordinating platform. The implementation of robust protocols and the large user community allows the development of additional specific tools for the network operation and control, such as the implementation of the Brazilian regional magnitude m_R. As all the four nodes use the same tools and similar workflows, solutions and manpower for common problems can be easily shared.

7.1.5 Acknowledgments

Although RSBR resulted from the joint efforts of four institutions (National Observatory, ON, Rio Grande Federal University, UFRN, University of Brasília, UnB and University of São Paulo, USP), directly supported by Petrobras, many other groups also contributed significantly in the installation of several stations. We thank colleagues from IPT (Institute of Technological Research, São Paulo), UFMS (Federal University of Mato Grosso do Sul, Campo Grande and Aquidauana), UNESP (State University of São Paulo, Rio Claro), Unipampa (Univ. dos Pampas, Caçapava do Sul), UFRR (Federal Univ. of Rondonia, Boa Vista) as well as all government organizations and farm owners for allowing installation of seismic stations on their lands.

7.1.6 References

Agurto-Detzel, H., M. Assumpção, M. Bianchi, and M. Pirchiner (2015). Intraplate seismicity in mid-plate south america: correlations with geophysical lithospheric parameters. *Special Publication of the Geological Society of London*, Seismicity, Fault Rupture and Earthquake Hazards in Slowly Deforming Regions. Accepted.

Assumpção, M. (1983). A regional magnitude scale for Brazil. *Bulletin of the Seismological Society of America*, 73(1):237–246, http://www.bssaonline.org/content/73/1/237. abstract.

Assumpção, M., J. Ferreira, L. Barros, H. Bezerra, G. S. França, J. R. Barbora, E. Menezes, L. C. Ribotta, M. Pirchiner, A. Nascimento, and J. C. Dourado (2014). *Intraplate Earthquakes*, Chapter 3, Intraplate seismicity in Brazil, pages 50–71. Cambridge University Press.

Drouet, S.; Almeida, A. A. D. ; Assumpção, M.; Bommer, J. J. ; Prates, C. L. ; Riccomini, C. ; Berrocal, J. ; Riera, J. D. (2014). Preliminary Probabilistic Seismic Hazard Analysis for the Angra dos Reis Nuclear Power Plant Site, State of Rio de Janeiro, Brazil. *Latin American and Caribbean Seismological Commission Conference*, Bogotá, Colombia.

Turner, H. H., J. Milne, C. Boys Vernon, G. Darwin, H. Darwin, L. Darwin, R. T. Glazebrook, M.H.

Gray, R.K. Gray, J.W. Judd, C.G. Knott, R. Meldola, R.D. Oldham, J. Perry, W.E. Plummer, C. Reid, R. A. Sampson, and A. Schuster (1911). Srs - sixteenth report on seismological investigations. In John Murray, editor, *Report of the Eightieth Meeting of the British Association for the Advancement of Science*, volume 80, page 30, Burlington House, London, W., August - September 1911.

Pérez, A. B. (1984). A estação sismológica do Rio de Janeiro. *Revista Geofísica*, 20:73–84.

Santos, P. M. (2005). *Instituto Astronômico e Geofísico da USP - Memória Sobre Sua Formação e Evolução*. Edusp. ISBN 10: 85-314-0878-4.

8

Summary of Seismicity, January - June 2012

During the first six months of 2012, the two largest earthquakes, M_W 8.6 and M_W 8.2, were centred off the west coast of northern Sumatera, occurring just over two hours apart on April 11. The first was felt widely across south and southeast Asia, and there were at least ten associated deaths and some building damage in Aceh. Small tsunamis were recorded for both earthquakes and there was an extensive aftershock sequence. An earlier M_W 7.2 earthquake occurring in the same region in January was similarly felt widely across Asia.

There were at least two deaths reported for the M_W 7.5 earthquake near the coast of Guerrero in March and also there was one death reported for the M_W 7.1 earthquake near the coast of central Chile. The other earthquakes of M_W 7 or more in this summary period, also all of shallow origin, were felt widely across their neighbouring regions but were without any reported deaths.

For earthquakes less than M_W 7, there were at least 75 deaths reported for the M_W 5.8 earthquake in June in the Hindu Kush region and at least 51 deaths reported for the M_W 6.7 earthquake in February in the Negros region of the Philippines, also with many buildings damaged or destroyed. In northern Italy, there were at least 7 deaths reported for the M_W 6.1 earthquake on May 20 and at least 17 deaths reported for the M_W 5.8 earthquake there nine days later. Elsewhere there were four deaths reported for the M_W 5.6 earthquake in June in Yunnan, two deaths reported for the MW 6.7 earthquake in April near the coast of central Chile and at least one death reported for the MW 5.7 earthquake in May in the Afghanistan-Tajikistan border region.

The number of events in this Bulletin Summary categorised by type are given in Table 8.1.

The period between January and June 2012 produced eight earthquakes with $M_W \geq 7$; these are listed in Table 8.2.

Figure 8.1 shows the number of moderate and large earthquakes in the first half of 2012. The distribution of the number of earthquakes should follow the Gutenberg-Richter law.

Figures 8.2 to 8.6 show the geographical distribution of moderate and large earthquakes in various magnitude ranges.

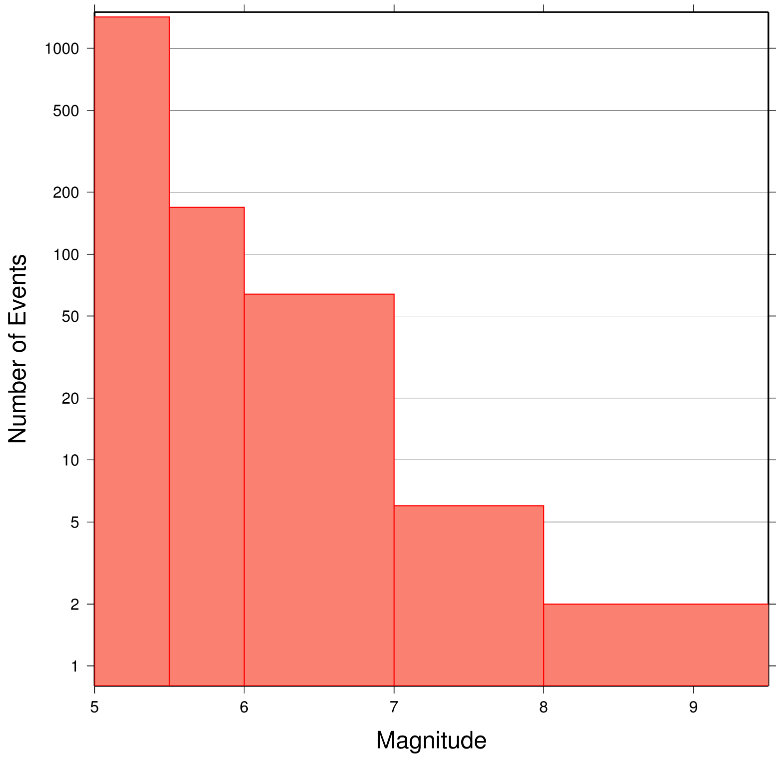

Figure 8.1: *Number of moderate and large earthquakes between January and June 2012. The non-uniform magnitude bias here correspond with the magnitude intervals used in Figures 8.2 to 8.6.*

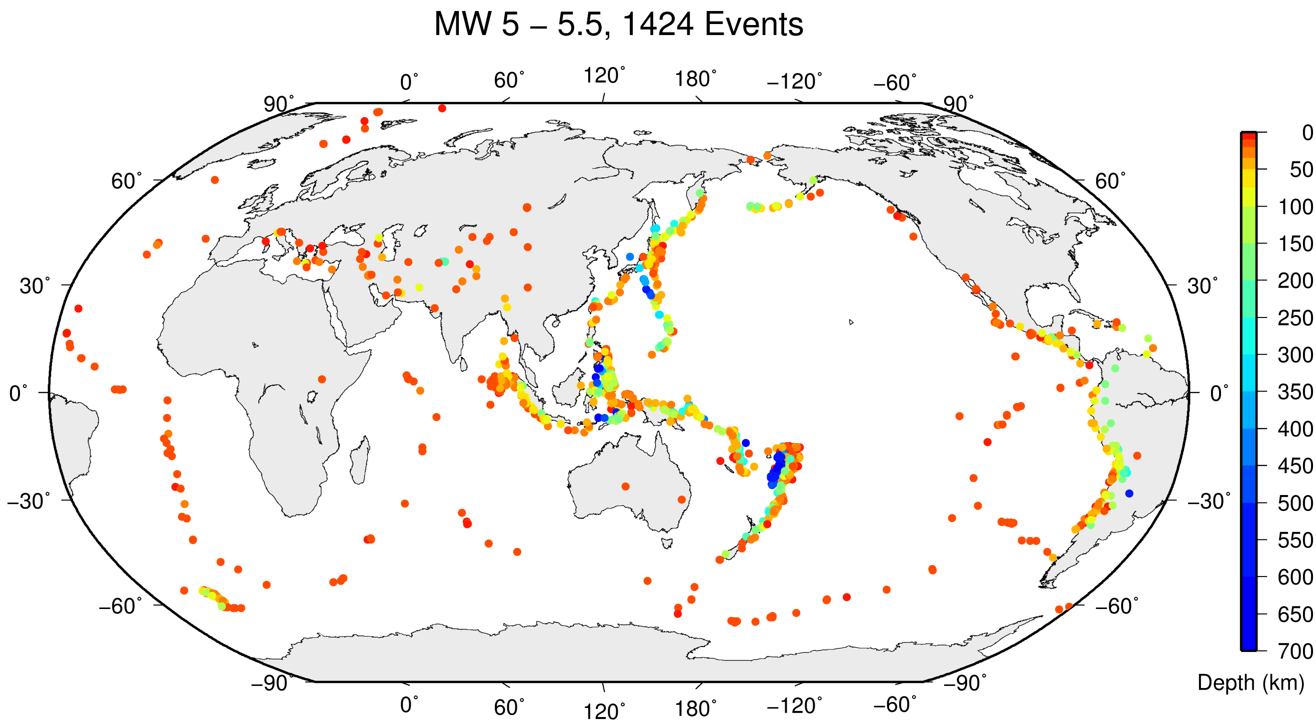

Figure 8.2: *Geographic distribution of magnitude 5-5.5 earthquakes between January and June 2012.*

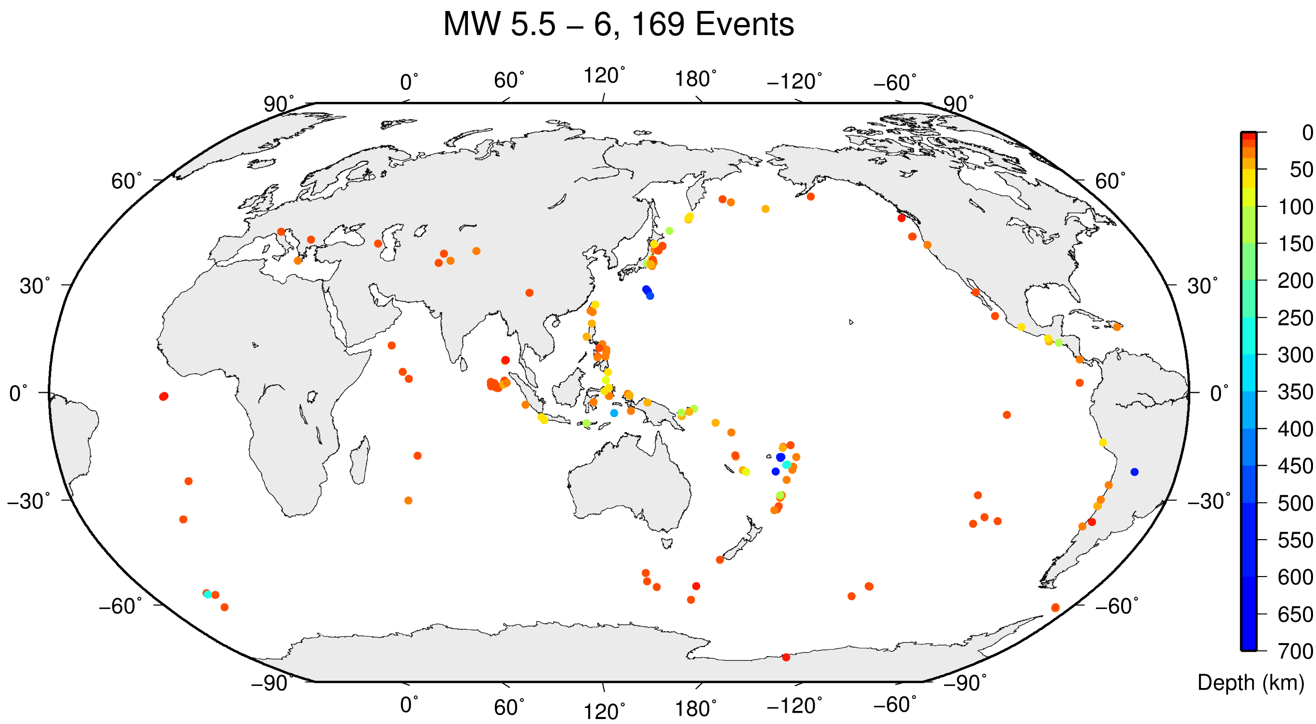

Figure 8.3: *Geographic distribution of magnitude 5.5-6 earthquakes between January and June 2012.*

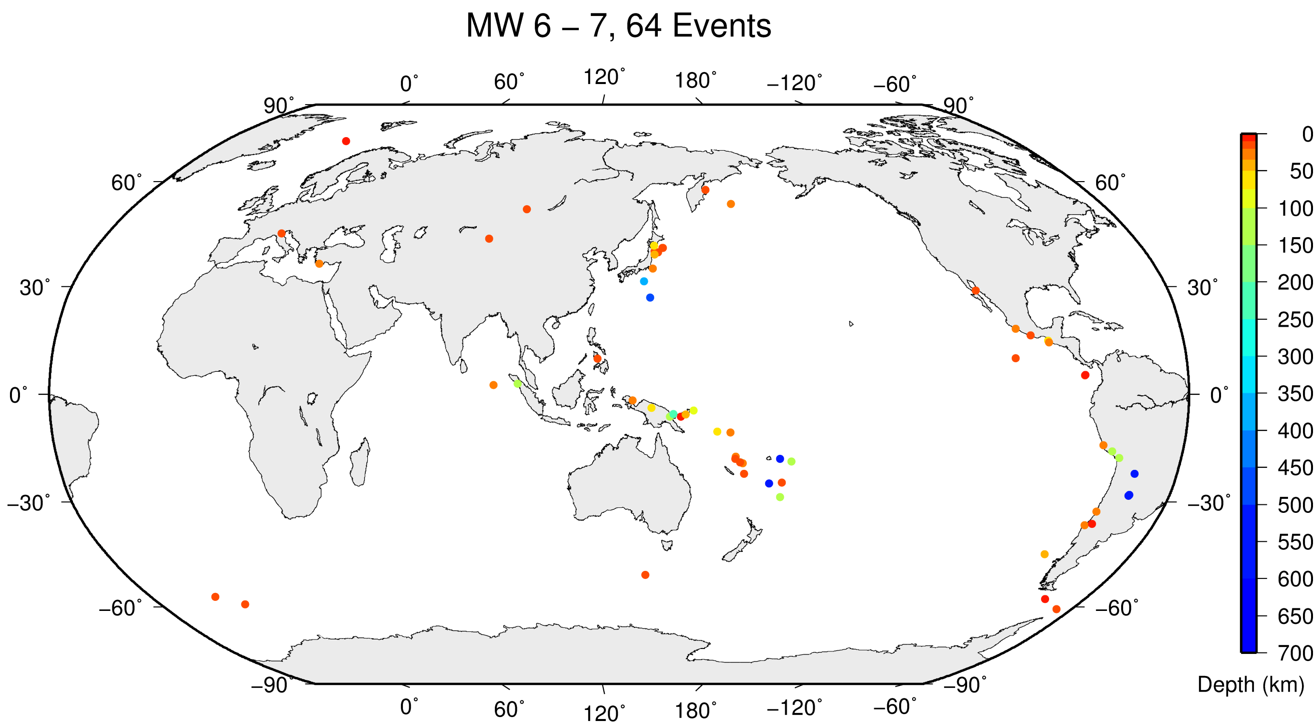

Figure 8.4: *Geographic distribution of magnitude 6-7 earthquakes between January and June 2012.*

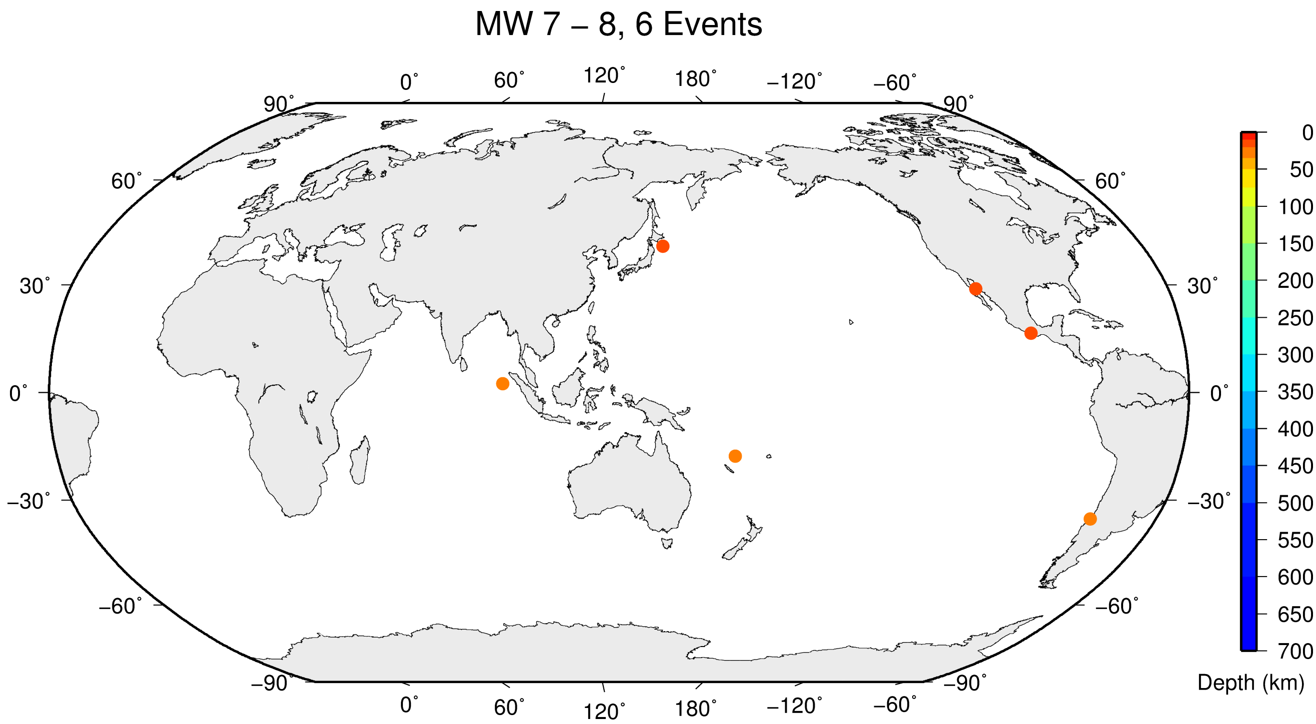

Figure 8.5: *Geographic distribution of magnitude 7-8 earthquakes between January and June 2012.*

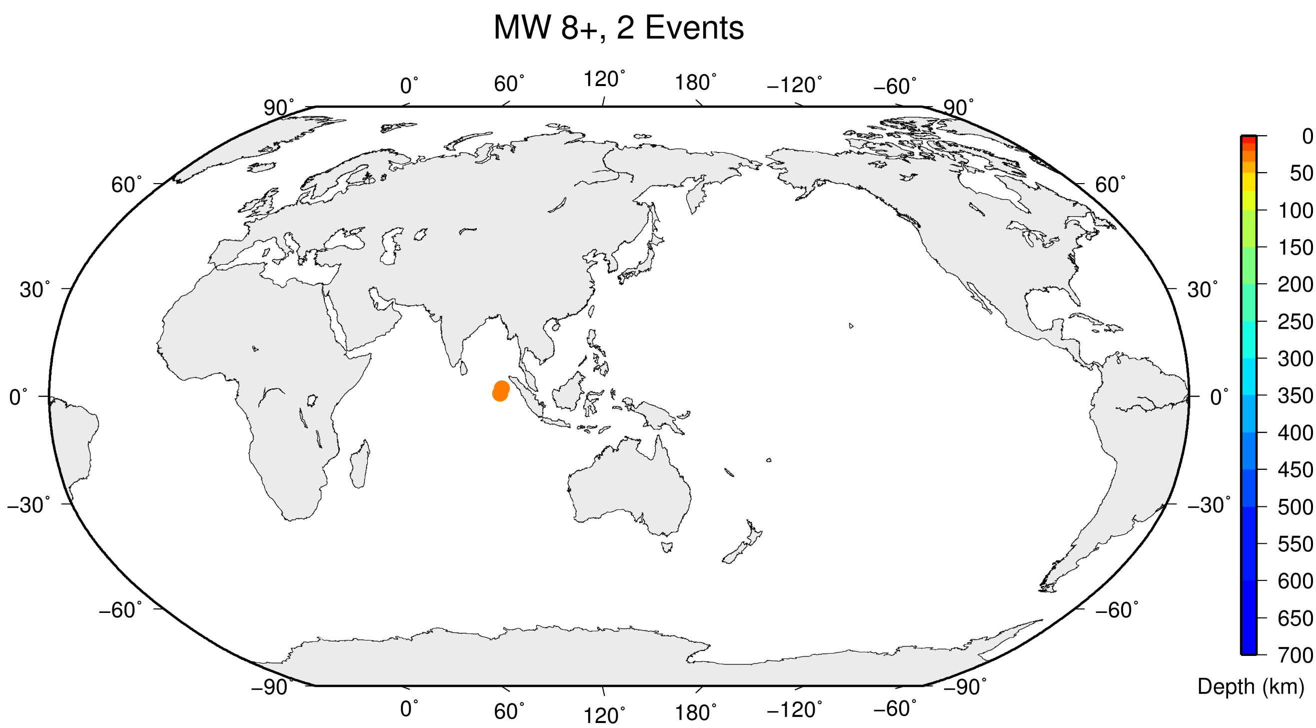

Figure 8.6: *Geographic distribution of magnitude 8+ earthquakes between January and June 2012.*

Table 8.1: Summary of events by type between January and June 2012.

damaging earthquake	24
damaging induced event	1
felt earthquake	1799
felt mine explosion	2
known earthquake	198788
known chemical explosion	2564
known induced event	2688
known mine explosion	8106
known rockburst	21
known experimental explosion	45
suspected earthquake	10366
suspected chemical explosion	80
suspected induced event	7
suspected mine explosion	4554
suspected rockburst	195
unknown	1159
total	230399

Table 8.2: Summary of the earthquakes of magnitude Mw $\geq$ 7 between January and June 2012.

Date	lat	lon	depth	Mw	Flinn-Engdahl Region
2012-04-11 08:38:37	2.24	93.01	26	8.6	Off west coast of northern Sumatera
2012-04-11 10:43:10	0.77	92.43	21	8.2	Off west coast of northern Sumatera
2012-03-20 18:02:47	16.47	-98.37	19	7.5	Near coast of Guerrero
2012-01-10 18:37:00	2.43	93.21	20	7.2	Off west coast of northern Sumatera
2012-03-25 22:37:06	-35.20	-72.13	28	7.1	Near coast of central Chile
2012-02-02 13:34:41	-17.75	167.18	27	7.1	Vanuatu Islands
2012-04-12 07:15:49	28.84	-113.13	10	7.0	Baja California
2012-03-14 09:08:36	40.84	145.02	19	7.0	Off east coast of Honshu

9

Statistics of Collected Data

9.1 Introduction

The ISC Bulletin is based on the parametric data reports received from seismological agencies around the world. With rare exceptions, these reports include the results of waveform review done by analysts at network data centres and observatories. These reports include combinations of various bulletin elements such as event hypocentre estimates, moment tensors, magnitudes, event type and felt and damaging data as well as observations of the various seismic waves recorded at seismic stations.

Data reports are received in different formats that are often agency specific. Once an authorship is recognised, the data are automatically parsed into the ISC database and the original reports filed away to be accessed when necessary. Any reports not recognised or processed automatically are manually checked, corrected and re-processed. This chapter describes the data that are received at the ISC before the production of the reviewed Bulletin.

Notably, the ISC integrates all newly received data reports into the automatic ISC Bulletin (available on-line) soon after these reports are made available to ISC, provided it is done before the submission deadline that currently stands at 12 months following an event occurrence.

With data constantly being reported to the ISC, even after the ISC has published its review, the total data shown as collected, in this chapter, is limited to two years after the time of the associated reading or event, i.e. any hypocentre data collected two years after the event are not reflected in the figures below.

9.2 Summary of Agency Reports to the ISC

A total of 137 agencies have reported data for January 2012 to June 2012. The parsing of these reports into the ISC database is summarised in Table 9.1.

Table 9.1: *Summary of the parsing of reports received by the ISC from a total of 137 agencies, containing data for this summary period.*

	Number of reports
Total collected	2358
Automatically parsed	1644
Manually parsed	714

Data collected by the ISC consists of multiple data types. These are typically one of:

- Bulletin, hypocentres with associated phase arrival observations.

- Catalogue, hypocentres only.
- Unassociated phase arrival observations.

In Table 9.2, the number of different data types reported to the ISC by each agency is listed. The number of each data type reported by each agency is also listed. Agencies reporting indirectly have their data type additionally listed for the agency that reported it. The agencies reporting indirectly may also have 'hypocentres with associated phases' but with no associated phases listed - this is because the association is being made by the agency reporting directly to the ISC. Summary maps of the agencies and the types of data reported are shown in Figure 9.1 and Figure 9.2.

Table 9.2: *Agencies reporting to the ISC for this summary period. Entries in bold are for new or renewed reporting by agencies since the previous six-month period.*

Agency	Country	Directly or indirectly reporting (D/I)	Hypocentres with associated phases	Hypocentres without associated phases	Associated phases	Unassociated phases	Amplitudes
TIR	Albania	D	631	348	3788	793	0
ALG	**Algeria**	**I NEIC**	**0**	**2**	**0**	**0**	**0**
CRAAG	Algeria	D	601	222	2962	406	0
LPA	Argentina	D	0	0	0	373	3
SJA	Argentina	D	3334	18	52712	103	8727
NSSP	Armenia	D	127	127	641	0	0
AUST	Australia	D	834	8	17481	0	0
IDC	Austria	D	20358	0	437941	0	405203
VIE	Austria	D	3878	1222	35296	1712	35844
AZER	Azerbaijan	D	25	318	757	0	0
BELR	Belarus	D	0	0	0	3216	688
UCC	Belgium	D	0	45	0	2954	742
SCB	Bolivia	D	85	0	744	0	140
SAR	Bosnia and Herzegovina	I CSEM	0	572	0	0	0
MASS	**Brazil**	**I IASPEI**	**0**	**0**	**0**	**14**	**0**
VAO	Brazil	D	0	0	0	54	0
SOF	Bulgaria	D	153	48	806	2199	0
OTT	Canada	D	1187	52	31840	0	3372
PGC	Canada	I OTT	789	0	19239	0	0
GUC	Chile	D	2515	38	45944	1017	12322
BJI	China	D	2318	19	136891	31074	82175
ASIES	Chinese Taipei	D	0	71	0	0	0
TAP	Chinese Taipei	D	17394	4	436862	0	0
RSNC	Colombia	D	6740	1	108553	11518	28949
UCR	Costa Rica	D	341	24	10995	0	962
ZAG	Croatia	D	0	1	0	10482	0
NIC	Cyprus	D	241	206	1705	436	0
IPEC	Czech Republic	D	87	406	577	4136	266
PRU	Czech Republic	D	5280	2343	40796	472	10490
WBNET	Czech Republic	D	254	0	5486	0	5435
GOM	**Democratic Republic of the Congo**	**D**	**12**	**0**	**51**	**27**	**0**
DNK	Denmark	D	0	156	0	6590	2582
ARO	Djibouti	D	52	0	477	0	0
IGQ	Ecuador	D	124	1	3688	58	529
HLW	Egypt	D	167	123	1498	0	0
SNET	El Salvador	I NEIC	1	5	0	0	0
SSS	El Salvador	I UCR	0	10	0	0	0
EST	Estonia	I HEL	470	42	0	0	0
AAE	Ethiopia	D	27	2	201	491	0
SKO	FYR Macedonia	D	919	0	7003	3200	2316
FIA0	Finland	I HEL	250	16	0	0	0
HEL	Finland	D	6623	7778	117338	0	17722

Table 9.2: *(continued)*

Agency	Country	Directly or indirectly reporting (D/I)	Hypocentres with associated phases	Hypocentres without associated phases	Associated phases	Unassociated phases	Amplitudes
CSEM	France	D	55167	81392	1154790	0	161216
LDG	France	D	2075	2140	43478	8	18354
STR	France	D	813	592	10538	0	0
PPT	French Polynesia	D	1539	0	12154	483	12597
TIF	Georgia	D	0	1302	0	14141	0
AWI	Germany	D	1232	0	4397	2029	0
BGR	Germany	D	136	368	5469	0	131
BNS	Germany	I BGR	2	33	0	0	0
BRG	Germany	D	0	0	0	6019	4598
BUG	Germany	I BGR	12	0	0	0	0
CLL	Germany	D	1	0	28	8973	3219
GDNRW	Germany	I BGR	0	17	0	0	0
GFZ	Germany	I INMG	24	0	0	0	0
LEDBW	Germany	I BGR	22	7	0	0	0
ATH	Greece	D	13171	12763	409445	0	147437
THE	Greece	D	4819	4858	107561	9359	36225
UPSL	Greece	I CSEM	0	121	0	0	0
HKC	Hong Kong	D	0	0	0	43	0
BUD	Hungary	D	0	31	0	2853	0
REY	Iceland	D	27	12	663	0	0
HYB	India	D	1158	2	6670	19	1699
NDI	India	D	636	442	17781	7490	5552
DJA	Indonesia	D	4436	81	77946	0	46123
TEH	Iran	D	1507	313	28709	0	13157
THR	Iran	D	197	617	1983	0	702
ISN	Iraq	D	593	433	3523	0	155
DIAS	Ireland	D	0	0	0	206	0
GII	Israel	D	347	98	5875	0	0
GEN	Italy	I CSEM	0	895	0	0	0
MED_RCMT	Italy	D	0	118	0	0	0
ROM	Italy	D	8577	7471	312651	0	184072
TRI	Italy	D	0	0	0	19206	0
LIC	Ivory Coast	D	892	0	2679	0	1777
JSN	Jamaica	D	127	0	716	6	0
JMA	Japan	D	92053	3	644904	714	0
MAT	Japan	D	0	0	0	12752	0
NIED	Japan	D	0	1596	0	0	0
SYO	Japan	D	0	0	0	2854	0
JSO	Jordan	D	9	8	95	0	0
NNC	Kazakhstan	D	7495	105	58331	0	53933
SOME	Kazakhstan	D	3762	109	56116	2	50911
KNET	Kyrgyzstan	D	1651	0	14135	0	3066
KRNET	Kyrgyzstan	D	3805	0	60652	0	0
LVSN	Latvia	I CSEM	0	574	0	0	0
GRAL	Lebanon	D	322	262	2404	628	0
LIT	Lithuania	D	294	425	2193	1778	1773
MCO	Macao, China	D	0	0	0	100	0
GSDM	Malawi	D	0	0	0	96	0
KLM	Malaysia	D	163	0	1360	0	0
ECX	Mexico	D	962	5	14975	0	2130
MEX	Mexico	D	2667	136	22516	8	0
MOLD	Moldova	D	0	24	0	2075	705
OBM	Mongolia	D	3	0	92	0	29
PDG	Montenegro	D	461	366	10206	0	5389
CNRM	Morocco	I CSEM	0	124	0	0	0
MOZ	**Mozambique**	**I EAF**	**0**	**1**	**10**	**0**	**0**
NAM	Namibia	D	93	0	780	10	14
DMN	Nepal	D	2187	0	21204	0	15837
DBN	Netherlands	D	0	0	0	1243	371
WEL	New Zealand	D	2850	10	108757	149	22884
INET	**Nicaragua**	**I UCR**	**0**	**6**	**0**	**0**	**0**
BER	Norway	D	1773	1449	23662	2226	5267
NAO	Norway	D	2803	1376	6530	6	2127

Table 9.2: (continued)

Agency	Country	Directly or indirectly reporting (D/I)	Hypocentres with associated phases	Hypocentres without associated phases	Associated phases	Unassociated phases	Amplitudes
OMAN	Oman	D	976	215	11057	0	0
MSSP	Pakistan	D	0	0	0	905	0
ARE	Peru	I NEIC	0	21	0	0	0
LIM	**Peru**	**I IRIS**	**1**	**0**	**0**	**0**	**0**
MAN	Philippines	D	0	2131	0	38123	10893
QCP	Philippines	D	0	0	0	96	0
WAR	Poland	D	0	220	0	13011	480
IGIL	Portugal	D	800	0	4253	0	1407
INMG	Portugal	D	1557	852	47615	2419	15791
PDA	Portugal	I CSEM	541	448	0	0	0
SVSA	Portugal	D	604	0	9152	5571	5117
KMA	Republic of Korea	D	30	0	313	0	0
BUC	Romania	D	787	71	11148	48908	0
ASRS	Russia	D	69	0	1319	0	0
BYKL	Russia	D	130	0	10121	0	3536
CMWS	**Russia**	**I MOS**	**20**	**0**	**0**	**0**	**0**
DRS	**Russia**	**I MOS**	**26**	**55**	**0**	**0**	**0**
IEPN	**Russia**	**D**	**193**	**0**	**1067**	**5195**	**0**
KOLA	Russia	D	153	0	603	0	0
KRSC	Russia	D	575	0	21118	0	0
MIRAS	**Russia**	**D**	**91**	**0**	**1274**	**0**	**0**
MOS	Russia	D	2874	503	495644	0	194067
NERS	Russia	D	22	0	785	0	341
NORS	**Russia**	**I MOS**	**15**	**38**	**0**	**0**	**0**
SKHL	Russia	D	522	523	16698	0	7744
YARS	Russia	D	516	518	10844	0	4899
SGS	Saudi Arabia	D	132	2	625	0	0
BEO	Serbia	D	1616	1294	26472	0	995
BRA	Slovakia	D	0	0	0	19011	0
LJU	Slovenia	D	817	686	11654	6008	4458
HNR	Solomon Islands	D	0	0	0	1351	0
PRE	South Africa	D	802	0	11969	18	4020
MDD	Spain	D	2833	6266	72737	0	57146
MRB	Spain	D	83	28	2022	0	680
SFS	Spain	I CSEM	0	224	0	0	0
UPP	Sweden	D	1779	5191	16645	0	0
ZUR	Switzerland	D	310	342	4332	0	3500
NSSC	Syria	D	199	0	2622	8	1110
BKK	Thailand	D	1400	66	11525	0	15483
TRN	Trinidad and Tobago	D	2	884	0	25168	0
TUN	Tunisia	I CSEM	0	10	0	0	0
ATA	Turkey	D	798	0	11983	0	2990
DDA	Turkey	D	14703	12190	168530	8336	0
ISK	Turkey	D	9452	12444	129796	28010	70713
AEIC	U.S.A.	I NEIC	59	48	0	0	0
ANF	U.S.A.	I IRIS	1134	733	0	0	0
BRK	U.S.A.	I NEIC	0	0	0	0	0
BUT	U.S.A.	I OTT	9	6	108	0	0
CERI	U.S.A.	I IRIS	66	18	0	0	0
GCMT	U.S.A.	D	0	3170	0	0	0
HVO	**U.S.A.**	**I NEIC**	**2**	**2**	**0**	**0**	**0**
IASPEI	U.S.A.	D	0	0	0	128	21
IRIS	U.S.A.	D	2971	3081	272070	0	0
LDO	U.S.A.	I NEIC	0	5	0	0	0
NCEDC	U.S.A.	I NEIC	141	65	0	0	0
NEIC	U.S.A.	D	15242	4895	771429	0	287281
PAL	**U.S.A.**	**I IRIS**	**1**	**0**	**0**	**0**	**0**
PAS	U.S.A.	I NEIC	143	72	0	0	0
PNSN	U.S.A.	D	4	135	0	0	0
REN	U.S.A.	I NEIC	21	22	0	0	0
RSPR	U.S.A.	D	681	4	10903	0	0

Table 9.2: *(continued)*

Agency	Country	Directly or indirectly reporting (D/I)	Hypocentres with associated phases	Hypocentres without associated phases	Associated phases	Unassociated phases	Amplitudes
SCEDC	U.S.A.	I IRIS	161	142	0	0	0
SEA	U.S.A.	I NEIC	18	7	0	0	0
SIO	U.S.A.	I IRIS	18	3	0	0	0
SLC	U.S.A.	I IRIS	13	8	0	0	0
SLM	U.S.A.	I NEIC	0	0	0	0	0
TUL	U.S.A.	I IRIS	37	0	0	0	0
UUSS	U.S.A.	I IRIS	3	13	0	0	0
WES	U.S.A.	I OTT	0	6	0	0	0
SIGU	Ukraine	D	78	78	2228	0	893
DSN	United Arab Emirates	D	608	193	7020	0	0
BGS	United Kingdom	D	282	165	9262	13	3660
EAF	**Unknown**	**D**	**58**	**5**	**341**	**8360**	**0**
MOSS	**Unknown**	**I MOS**	**0**	**0**	**1863**	**0**	**0**
SIK	Unknown	I CSEM	0	72	0	0	0
USP	**Unknown**	**I IASPEI**	**0**	**0**	**0**	**22**	**0**
CAR	Venezuela	I VIE	2	0	0	0	0
FUNV	Venezuela	I IRIS	2	0	0	0	0
PLV	Vietnam	D	4	0	140	0	62
DHMR	Yemen	D	51	27	477	865	274
LSZ	Zambia	D	37	0	113	50	0
BUL	Zimbabwe	D	107	2	613	220	0

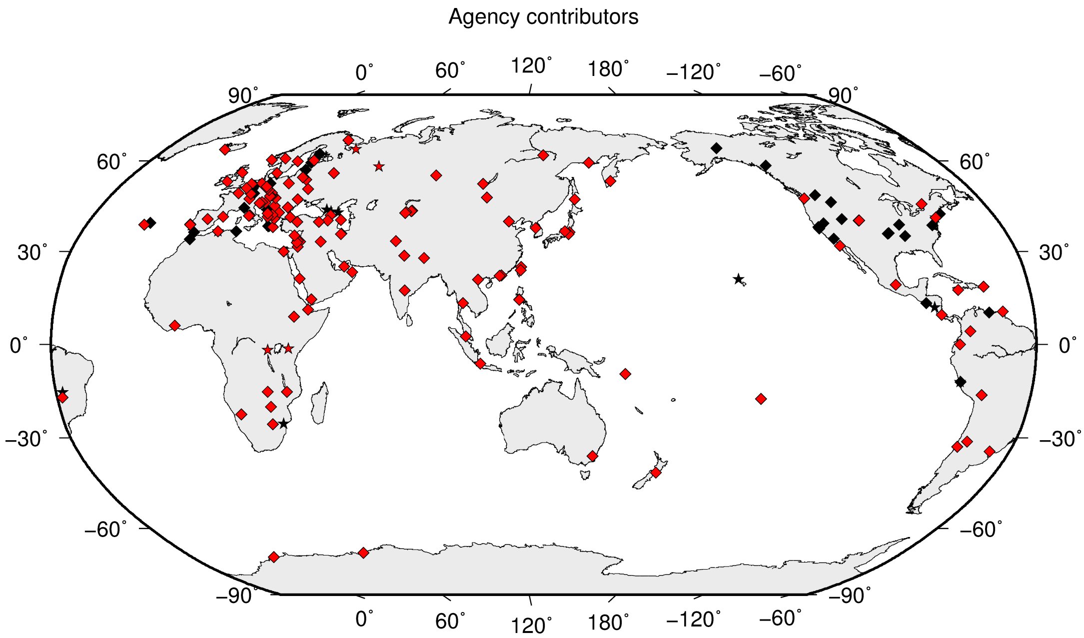

Figure 9.1: *Map of agencies that have contributed data to the ISC for this summary period. Agencies that have reported directly to the ISC are shown in red. Those that have reported indirectly (via another agency) are shown in black. Any new or renewed agencies, since the last six-month period, are shown by a star. Each agency is listed in Table 9.2.*

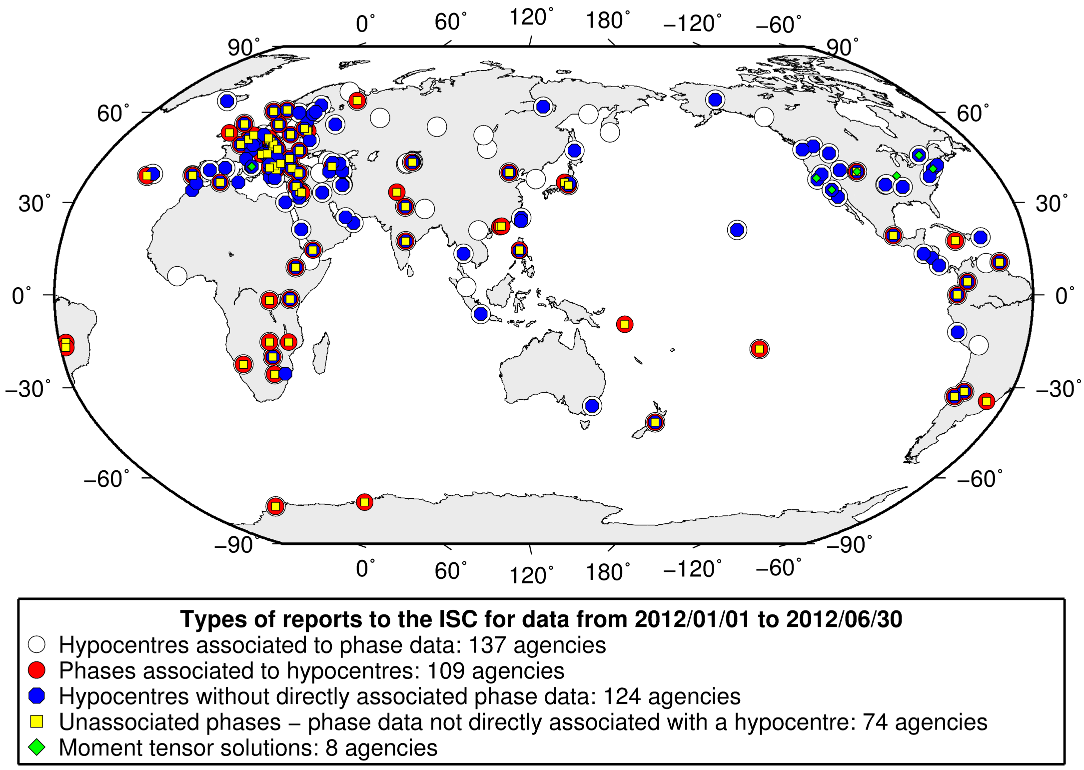

Figure 9.2: *Map of the different data types reported by agencies to the ISC. A full list of the data types reported by each agency is shown in Table 9.2.*

9.3 Arrival Observations

The collection of phase arrival observations at the ISC has increased dramatically with time. The increase in reported phase arrival observations is shown in Figure 9.3.

The reports with phase data are summarised in Table 9.3. This table is split into three sections, providing information on the reports themselves, the phase data, and the stations reporting the phase data. A map of the stations contributing these phase data is shown in Figure 9.4.

The ISC encourages the reporting of phase arrival times together with amplitude and period measurements whenever feasible. Figure 9.5 shows the percentage of events reported by each station was accompanied with amplitude and period measurements.

Figure 9.6 indicates the number of amplitude and period measurement for each station.

Together with the increase in the number of phases (Figure 9.3), there has been an increase in the number of stations reported to the ISC. The increase in the number of stations is shown in Figure 9.7. This increase can also be seen on the maps for stations reported each decade in Figure 9.8.

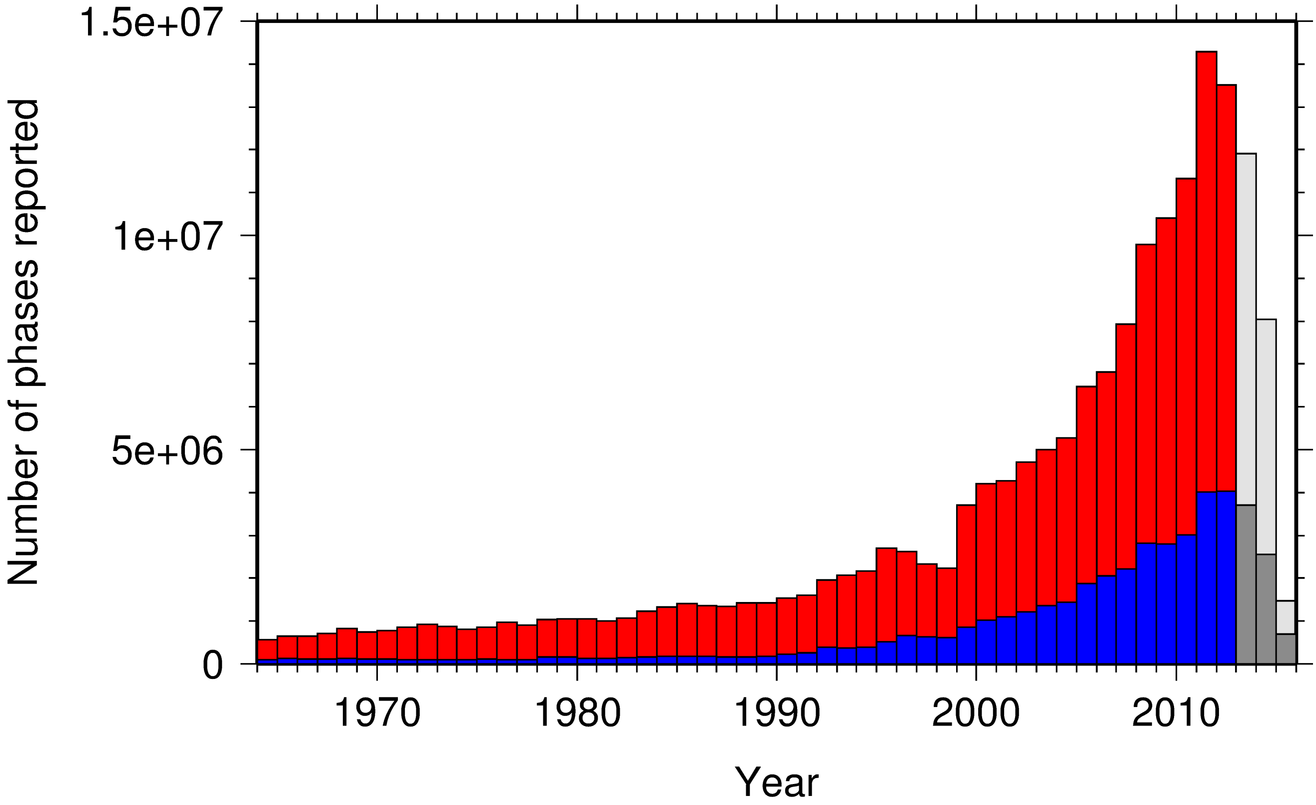

Figure 9.3: *Histogram showing the number of phases (red) and number of amplitudes (blue) collected by the ISC for events each year since 1964. The data in grey covers the current period where data are still being collected before the ISC review takes place and is accurate at the time of publication.*

Table 9.3: *Summary of reports containing phase arrival observations.*

Reports with phase arrivals	1904
Reports with phase arrivals including amplitudes	675
Reports with only phase arrivals (no hypocentres reported)	259
Total phase arrivals received	7335216
Total phase arrival-times received	6843377
Number of duplicate phase arrival-times	1405920 (20.5%)
Number of amplitudes received	2121249
Stations reporting phase arrivals	6980
Stations reporting phase arrivals with amplitude data	3453
Max number of stations per report	2134

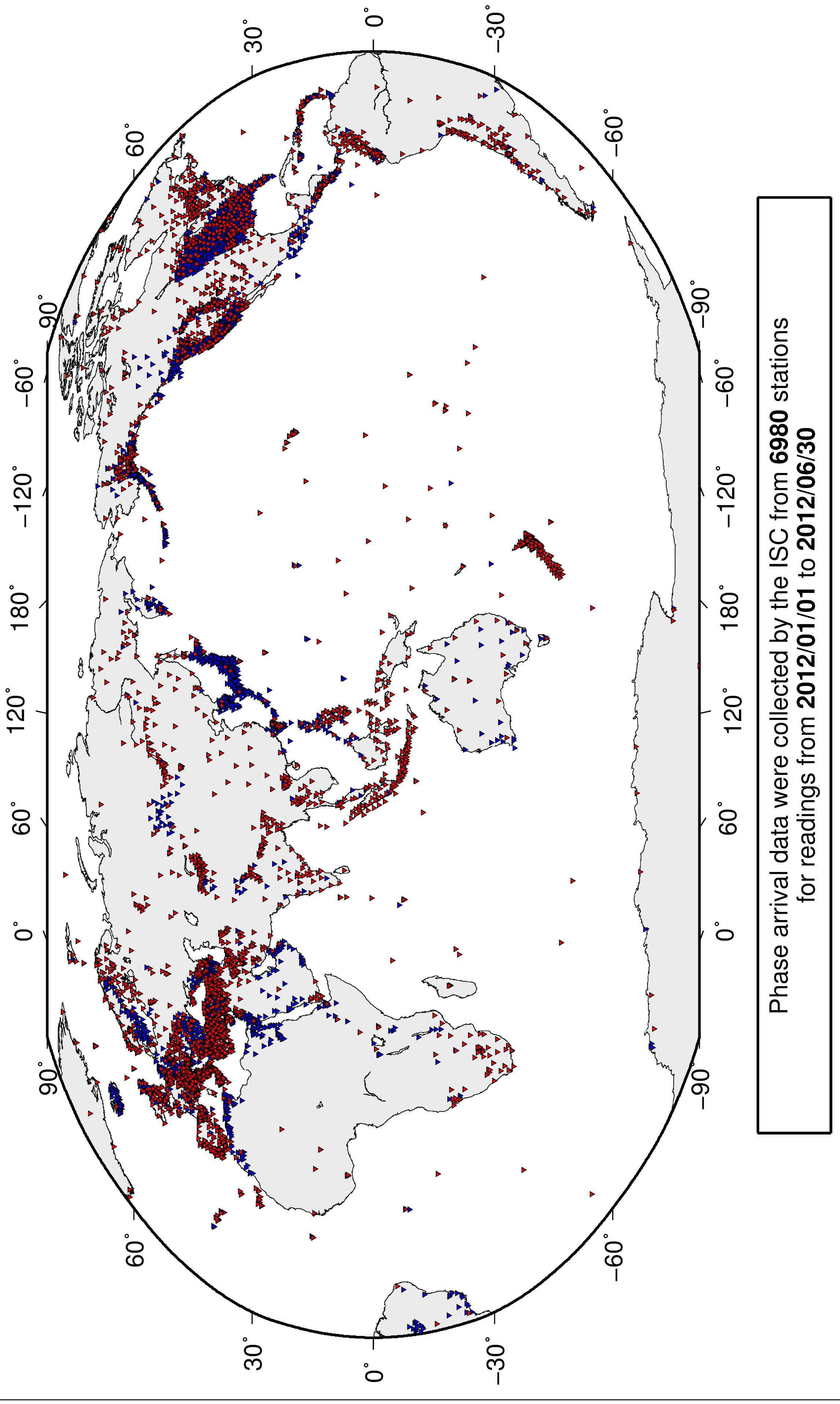

Figure 9.4: *Stations contributing phase data to the ISC for readings from January 2012 to the end of June 2012. Stations in blue provided phase arrival times only; stations in red provided both phase arrival times and amplitude data.*

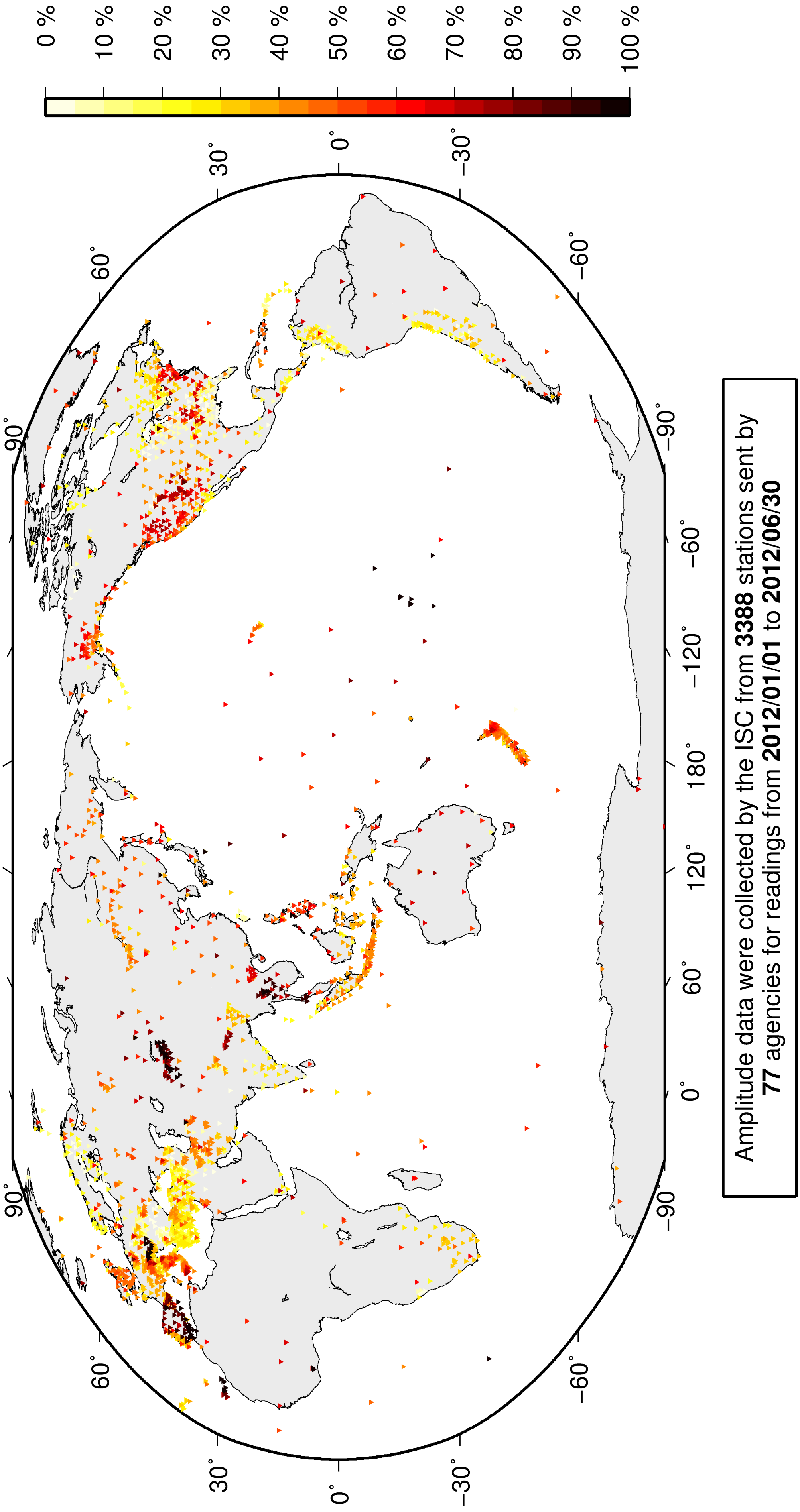

Figure 9.5: *Percentage of events for which phase arrival times from each station are accompanied with amplitude and period measurements.*

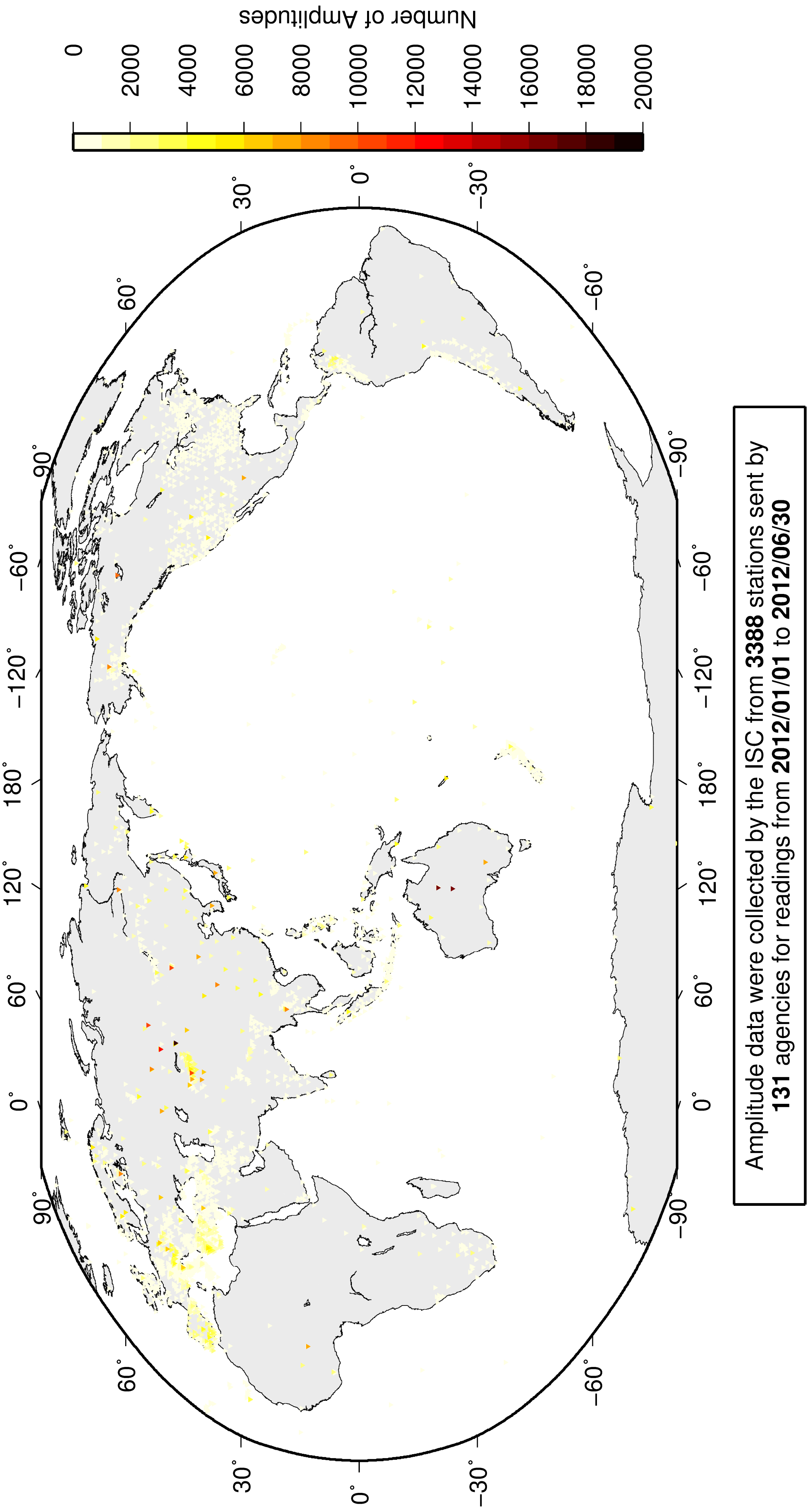

Figure 9.6: *Number of amplitude and period measurements for each station.*

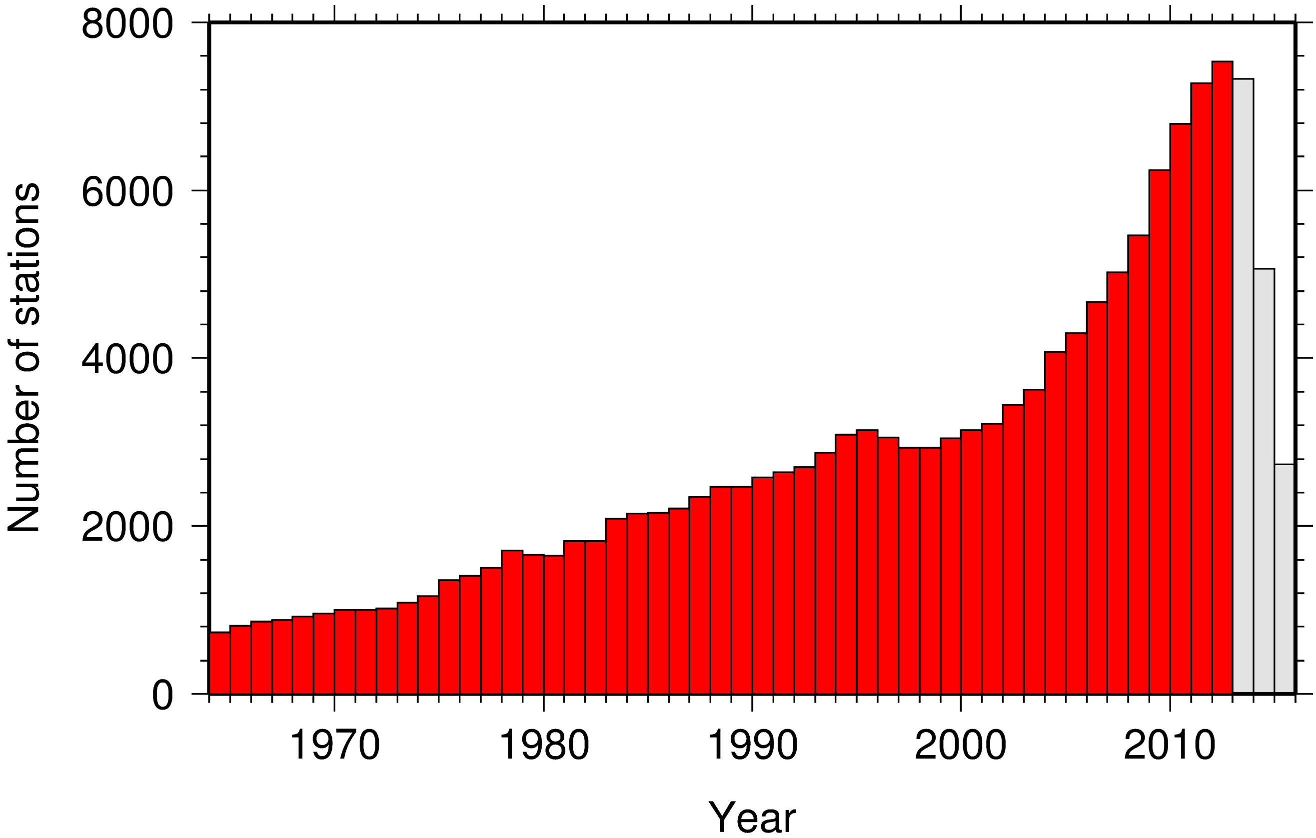

Figure 9.7: *Histogram showing the number of stations reporting to the ISC each year since 1964. The data in grey covers the current period where station information is still being collected before the ISC review of events takes place and is accurate at the time of publication.*

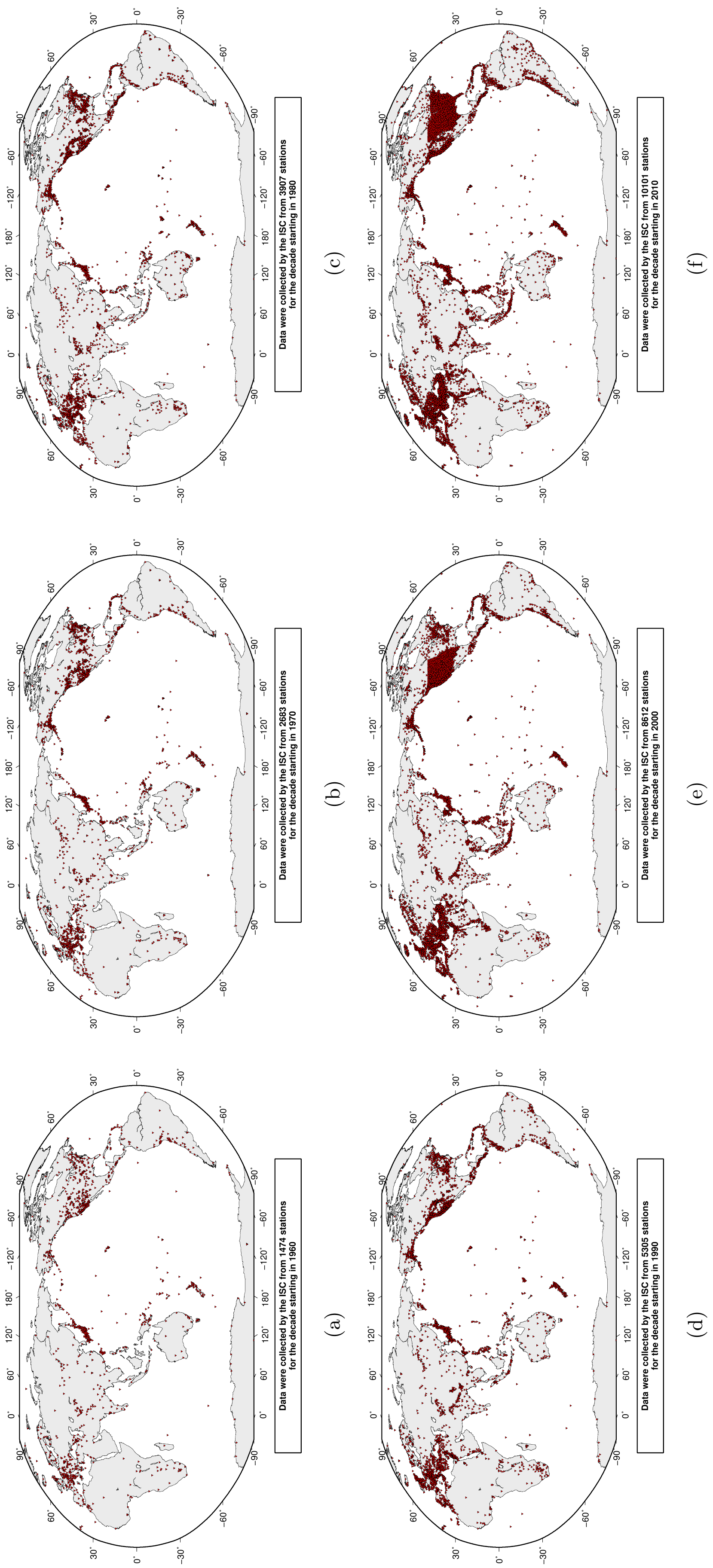

Figure 9.8: *Maps showing the stations reported to the ISC for each decade since 1960. Note that the last map covers a shorter time period.*

9.4 Hypocentres Collected

The ISC Bulletin groups multiple estimates of hypocentres into individual events, with an appropriate prime hypocentre solution selected. The collection of these hypocentre estimates are described in this section.

The reports containing hypocentres are summarised in Table 9.4. The number of hypocentres collected by the ISC has also increased significantly since 1964, as shown in Figure 9.9. A map of all hypocentres reported to the ISC for this summary period is shown in Figure 9.10. Where a network magnitude was reported with the hypocentre, this is also shown on the map, with preference given to reported values, first of M_W followed by M_S, m_b and M_L respectively (where more than one network magnitude was reported).

Table 9.4: *Summary of the reports containing hypocentres.*

Reports with hypocentres	2099
Reports of hypocentres only (no phase readings)	454
Total hypocentres received	454948
Number of duplicate hypocentres	106299 (23.4%)
Agencies determining hypocentres	163

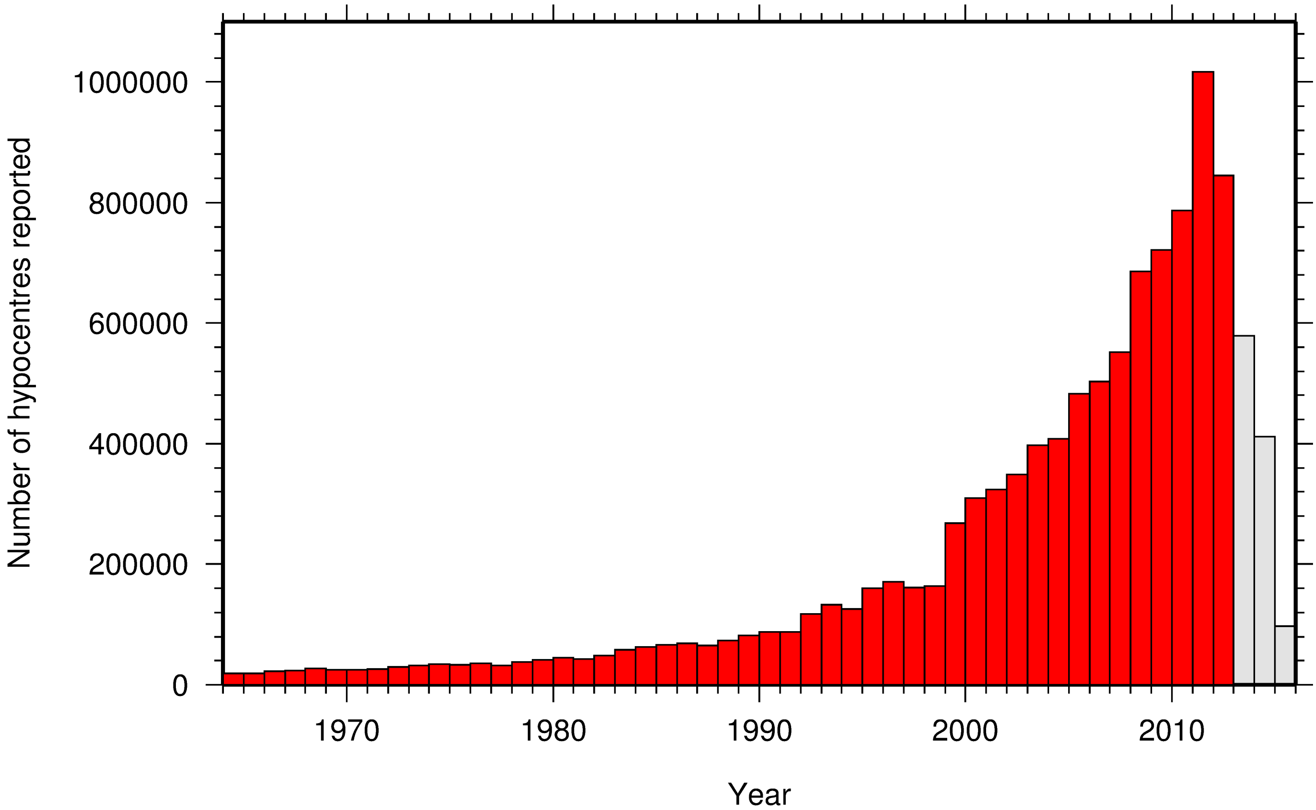

Figure 9.9: *Histogram showing the number of hypocentres collected by the ISC for events each year since 1964. For each event, multiple hypocentres may be reported.*

All the hypocentres that are reported to the ISC are automatically grouped into events, which form the basis of the ISC Bulletin. For this summary period 493951 hypocentres (including ISC) were grouped

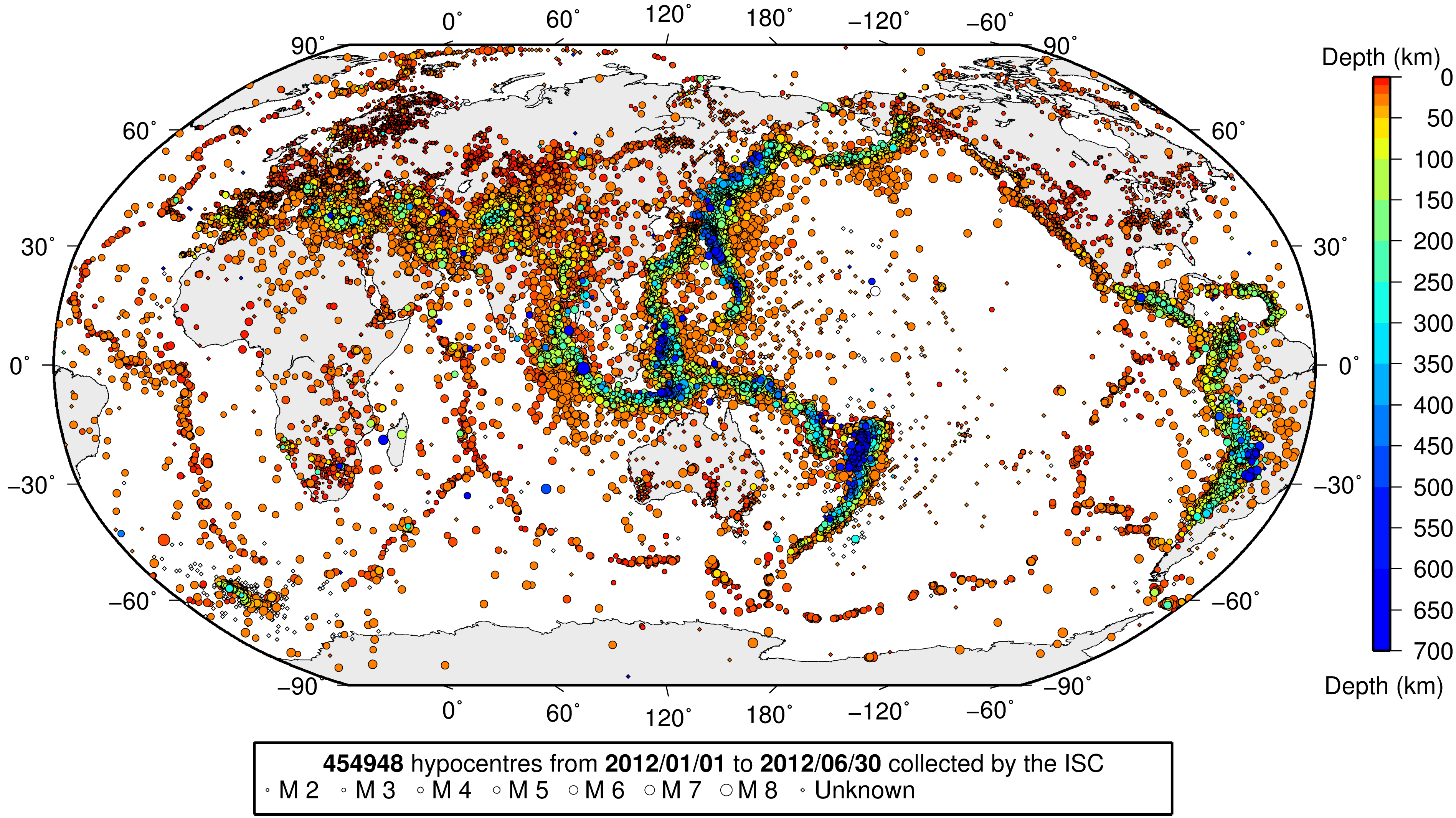

Figure 9.10: *Map of all hypocentres collected by the ISC. The scatter shows the large variation of the multiple hypocentres that are reported for each event. The magnitude corresponds with the reported network magnitude. If more than one network magnitude type was reported, preference was given to values of M_W, M_S, m_b and M_L respectively. Compare with Figure 10.2*

into 237166 events, the largest of these having 77 hypocentres in one event. The total number of events shown here is the result of an automatic grouping algorithm, and will differ from the total events in the published ISC Bulletin, where both the number of events and the number of hypocentre estimates will have changed due to further analysis. The process of grouping is detailed in Section 3.3.1. Figure 10.2 on page 122 shows a map of all prime hypocentres.

9.5 Collection of Network Magnitude Data

Data contributing agencies normally report earthquake hypocentre solutions along with magnitude estimates. For each seismic event, each agency may report one or more magnitudes of the same or different types. This stems from variability in observational practices at regional, national and global level in computing magnitudes based on a multitude of wave types. Differences in the amplitude measurement algorithm, seismogram component(s) used, frequency range, station distance range as well as the instrument type contribute to the diversity of magnitude types. Table 9.5 provides an overview of the complexity of reported network magnitudes reported for seismic events during this summary period.

Table 9.5: *Statistics of magnitude reports to the ISC; M – average magnitude of estimates reported for each event.*

	M<3.0	3.0≤M<5.0	M≥5.0
Number of seismic events	185591	35454	432
Average number of magnitude estimates per event	1.8	5.5	30.8
Average number of magnitudes (by the same agency) per event	1.3	2.8	4.2
Average number of magnitude types per event	1.1	4.3	11.1
Number of magnitude types	19	33	28

Table 9.6 gives the basic description, main features and scientific paper references for the most commonly reported magnitude types.

Table 9.6: *Description of the most common magnitude types reported to the ISC.*

Magnitude type	Description	References	Comments
M	Unspecified		Often used in real or near-real time magnitude estimations
mB	Medium-period and Broad-band body-wave magnitude	*Gutenberg* (1945a); *Gutenberg* (1945b); *IASPEI* (2005); *IASPEI* (2013); *Bormann et al.* (2009); *Bormann and Dewey* (2012)	
mb	Short-period body-wave magnitude	*IASPEI* (2005); *IASPEI* (2013); *Bormann et al.* (2009); *Bormann and Dewey* (2012)	Classical mb based on stations between 21°-100° distance

Table 9.6: *continued*

Magnitude type	Description	References	Comments
mb1	Short-period body-wave magnitude	*IDC* (1999) and references therein	Reported only by the IDC; also includes stations at distances less than 21°
mb1mx	Maximum likelihood short-period body-wave magnitude	*Ringdal* (1976); *IDC* (1999) and references therein	Reported only by the IDC
mbtmp	short-period body-wave magnitude with depth fixed at the surface	*IDC* (1999) and references therein	Reported only by the IDC
mbLg	Lg-wave magnitude	*Nuttli* (1973); *IASPEI* (2005); *IASPEI* (2013); *Bormann and Dewey* (2012)	Also reported as MN
Mc	Coda magnitude		
MD (Md)	Duration magnitude	*Bisztricsany* (1958); *Lee et al.* (1972)	
ME (Me)	Energy magnitude	*Choy and Boatwright* (1995)	Reported only by NEIC
MJMA	JMA magnitude	*Tsuboi* (1954)	Reported only by JMA
ML (Ml)	Local (Richter) magnitude	*Richter* (1935); *Hutton and Boore* (1987); *IASPEI* (2005); *IASPEI* (2013)	
MLSn	Local magnitude calculated for Sn phases	*Balfour et al.* (2008)	Reported by PGC only for earthquakes west of the Cascadia subduction zone
MLv	Local (Richter) magnitude computed from the vertical component		Reported only by DJA and BKK
MN (Mn)	Lg-wave magnitude	*Nuttli* (1973); *IASPEI* (2005)	Also reported as mbLg
MS (Ms)	Surface-wave magnitude	*Gutenberg* (1945c); *Vaněk et al.* (1962); *IASPEI* (2005)	Classical surface-wave magnitude computed from station between 20°-160° distance
Ms1	Surface-wave magnitude	*IDC* (1999) and references therein	Reported only by the IDC; also includes stations at distances less than 20°
ms1mx	Maximum likelihood surface-wave magnitude	*Ringdal* (1976); *IDC* (1999) and references therein	Reported only by the IDC

Table 9.6: *continued*

Magnitude type	Description	References	Comments
Ms7	Surface-wave magnitude	*Bormann et al.* (2007)	Reported only by BJI and computed from records of a Chinese-made long-period seismograph in the distance range 3°-177°
MW (Mw)	Moment magnitude	*Kanamori* (1977); *Dziewonski et al.* (1981)	Computed according to the *IASPEI* (2005) and *IASPEI* (2013) standard formula
Mw(mB)	Proxy Mw based on mB	*Bormann and Saul* (2008)	Reported only by DJA and BKK
Mwp	Moment magnitude from P-waves	*Tsuboi et al.* (1995)	Reported only by DJA and BKK and used in rapid response
mbh	Unknown		
mbv	Unknown		
MG	Unspecified type		Contact contributor
Mm	Unknown		
msh	Unknown		
MSV	Unknown		

Table 9.7 lists all magnitude types reported, the corresponding number of events in the ISC Bulletin and the agency codes along with the number of earthquakes.

Table 9.7: *Summary of magnitude types in the ISC Bulletin for this summary period. The number of events with values for each magnitude type is listed. The agencies reporting these magnitude types are listed, together with the total number of values reported.*

Magnitude type	Events	Agencies reporting magnitude type (number of values)
M	1816	SKO (722), BEO (680), STR (462), PRU (23), IGQ (21), FDF (11)
mB	2391	BJI (1953), DJA (783), STR (43), IGQ (23)
mb	29094	IDC (19070), NEIC (6232), NNC (4472), KRNET (3801), MOS (2583), MAN (2071), BJI (1911), DJA (1158), VIE (1084), CSEM (623), MDD (194), STR (100), IASPEI (65), NIC (60), SIGU (48), DSN (42), GII (34), IGQ (25), WEL (19), PGC (14), IGIL (5), BGS (5), NDI (4), CRAAG (3), PDG (3), UCR (3), PDA (3), OTT (2), ATA (1), PRE (1), THR (1)
mb1	20053	IDC (20053)
mb1mx	20053	IDC (20053)
mbLg	1339	MDD (1339)
mbtmp	20053	IDC (20053)
Mc	36	BER (35), CSEM (1)

Table 9.7: *Continued.*

Magnitude type	Events	Agencies reporting magnitude type (number of values)
MD	15789	CSEM (3753), ROM (3645), MEX (3104), DDA (2191), LDG (1519), RSPR (1179), ECX (917), ISK (822), BUC (789), TRN (754), PDA (399), TIR (391), GRAL (323), GII (175), UCR (165), NCEDC (154), HLW (138), PNSN (112), PDG (79), SOF (74), JSN (68), NAM (64), INMG (61), SJA (55), CNRM (48), HVO (35), SEA (28), LSZ (25), CERI (24), SNET (23), EAF (10), TUN (10), GOM (10), BUL (6), JSO (6), NSSC (4), SIGU (3), WES (2), BUT (2), NEIC (2), SLC (2), SSS (1), DHMR (1)
ME	89	NEIC (89)
MJMA	90367	JMA (90367)
ML	108672	CSEM (47752), TAP (17421), ATH (13050), DDA (12540), IDC (12055), ISK (10401), ROM (8162), RSNC (6724), HEL (5996), UPP (5035), THE (4883), SJA (3088), GUC (2667), WEL (2158), MAN (2067), LDG (2032), VIE (1800), TEH (1473), AEIC (1407), BER (1092), INMG (1039), ECX (978), GEN (890), PRE (802), ATA (775), LJU (772), SKO (756), NAO (718), ISN (585), KRSC (574), PGC (517), IGIL (510), CRAAG (465), PDA (442), IPEC (411), PDG (365), BJI (362), ZUR (320), FIA0 (265), UCR (257), THR (256), KNET (245), PAS (243), NIC (242), SFS (224), TIR (208), DSN (175), HLW (150), BGR (136), NDI (131), NEIC (130), MRB (107), PPT (105), NSSC (103), OTT (97), MIRAS (91), AZER (89), WBNET (87), SCB (82), BGS (78), HVO (57), CNRM (56), ARE (49), DHMR (47), ARO (46), TUL (45), UCC (45), BNS (35), REN (33), NCEDC (30), SEA (23), SLC (22), BUT (17), DMN (13), BUG (12), IGQ (12), SSS (9), TIF (8), LDO (8), AUST (7), ALG (7), SOF (5), INET (5), BUC (5), PLV (4), EAF (4), BEO (4), OBM (3), REY (2), HYB (2), DNK (2), RSPR (2), SZGRF (1), JSO (1), ZAG (1), IASPEI (1), CLL (1), LIT (1), NSSP (1)
MLSn	332	PGC (331), NEIC (1)
MLV	4	NERS (4)
MLv	4549	DJA (3670), STR (844), IGQ (104)
MN	507	OTT (347), TEH (97), NEIC (70), CERI (6), WES (6), TUL (3), MDD (2), OGSO (1), BDF (1)
MPV	4	NERS (4)
mpv	4577	NNC (4577)
MS	10981	IDC (8914), MAN (2068), BJI (1648), MOS (583), NEIC (199), NSSP (126), ASRS (67), CSEM (40), SOME (32), VIE (20), IASPEI (20), LDG (7), ATA (5), BGS (5), DSN (3), AZER (1), BER (1)
Ms1	8914	IDC (8914)
ms1mx	8914	IDC (8914)
Ms7	1613	BJI (1613)
MSH	1	NERS (1)

Table 9.7: *Continued.*

Magnitude type	Events	Agencies reporting magnitude type (number of values)
MW	7188	SJA (3079), NIED (1595), GCMT (1116), ATA (767), NEIC (453), PGC (414), WAR (162), CSEM (117), RSNC (110), OTT (32), BRK (31), WEL (15), GUC (10), CAR (9), CRAAG (7), ROM (6), SLM (4), PAS (4), IGQ (3), SSS (2), SIGU (2), UCR (2), PDA (2), UPA (1), NCEDC (1), MEX (1), MDD (1)
Mw(mB)	62	STR (43), IGQ (23)
MwMwp	5	IGQ (6)
Mwp	51	DJA (40), IGQ (9), STR (8)

The most commonly reported magnitude types are short-period body-wave, surface-wave, local (or Richter), moment, duration and JMA magnitude type. For a given earthquake, the number and type of reported magnitudes greatly vary depending on its size and location. The large earthquake of October 25, 2010 gives an example of the multitude of reported magnitude types for large earthquakes (Listing 9.1). Different magnitude estimates come from global monitoring agencies such as the IDC, NEIC and GCMT, a local agency (GUC) and other agencies, such as MOS and BJI, providing estimates based on the analysis of their networks. The same agency may report different magnitude types as well as several estimates of the same magnitude type, such as NEIC estimates of Mw obtained from W-phase, centroid and body-wave inversions.

Listing 9.1: *Example of reported magnitudes for a large event*

```
Event   15264887 Southern Sumatera
   Date       Time        Err   RMS Latitude Longitude  Smaj  Smin  Az Depth   Err Ndef Nsta Gap  mdist  Mdist Qual   Author      OrigID
2010/10/25 14:42:22.18   0.27 1.813  -3.5248  100.1042 4.045 3.327  54  20.0  1.37 2102 2149  23   0.76 176.43 m i de ISC       01346132
 (#PRIME)

Magnitude  Err Nsta Author      OrigID
mb      6.1       61 BJI       15548963
mB      6.9       68 BJI       15548963
Ms      7.7       85 BJI       15548963
Ms7     7.5       86 BJI       15548963
mb      5.3 0.1   48 IDC       16686694
mb1     5.3 0.1   51 IDC       16686694
mb1mx   5.3 0.0   52 IDC       16686694
mbtmp   5.3 0.1   51 IDC       16686694
ML      5.1 0.2    2 IDC       16686694
MS      7.1 0.0   31 IDC       16686694
Ms1     7.1 0.0   31 IDC       16686694
ms1mx   6.9 0.1   44 IDC       16686694
mb      6.1      243 ISCJB     01677901
MS      7.3      228 ISCJB     01677901
M       7.1      117 DJA       01268475
mb      6.1 0.2  115 DJA       01268475
mB      7.1 0.1  117 DJA       01268475
MLv     7.0 0.2   26 DJA       01268475
        7.1 0.4  117 DJA       01268475
Mwp     6.9 0.2  102 DJA       01268475
mb      6.4       49 MOS       16742129
MS      7.2       70 MOS       16742129
mb      6.5      110 NEIC      01288303
ME      7.3          NEIC      01288303
MS      7.3      143 NEIC      01288303
MW      7.7          NEIC      01288303
MW      7.8      130 GCMT      00125427
mb      5.9          KLM       00255772
ML      6.7          KLM       00255772
MS      7.6          KLM       00255772
mb      6.4       20 BGR       16815854
Ms      7.2        2 BGR       16815854
mb      6.3 0.3  250 ISC       01346132
MS      7.3 0.1  237 ISC       01346132
```

An example of a relatively small earthquake that occurred in northern Italy for which we received magnitude reports of mostly local and duration type from six agencies in Italy, France and Austria is given in Listing 9.2.

Listing 9.2: *Example of reported magnitudes for a small event*

```
Event 15089710 Northern Italy
   Date       Time        Err   RMS Latitude Longitude  Smaj  Smin  Az Depth   Err Ndef Nsta Gap  mdist  Mdist Qual   Author      OrigID
2010/08/08 15:20:46.22   0.94 0.778  45.4846    8.3212 2.900 2.539 110  28.6  9.22  172  110  82   0.41   5.35 m i ke ISC       01249414
 (#PRIME)
```

Magnitude		Err	Nsta	Author	OrigID
ML	2.4		10	ZUR	15925566
Md	2.6	0.2	19	ROM	16861451
Ml	2.2	0.2	9	ROM	16861451
ML	2.5			GEN	00554757
ML	2.6	0.3	28	CSEM	00554756
Md	2.3	0.0	3	LDG	14797570
Ml	2.6	0.3	32	LDG	14797570

Figure 9.11 shows a distribution of the number of agencies reporting magnitude estimates to the ISC according to the magnitude value. The peak of the distribution corresponds to small earthquakes where many local agencies report local and/or duration magnitudes. The number of contributing agencies rapidly decreases for earthquakes of approximately magnitude 5.5 and above, where magnitudes are mostly given by global monitoring agencies.

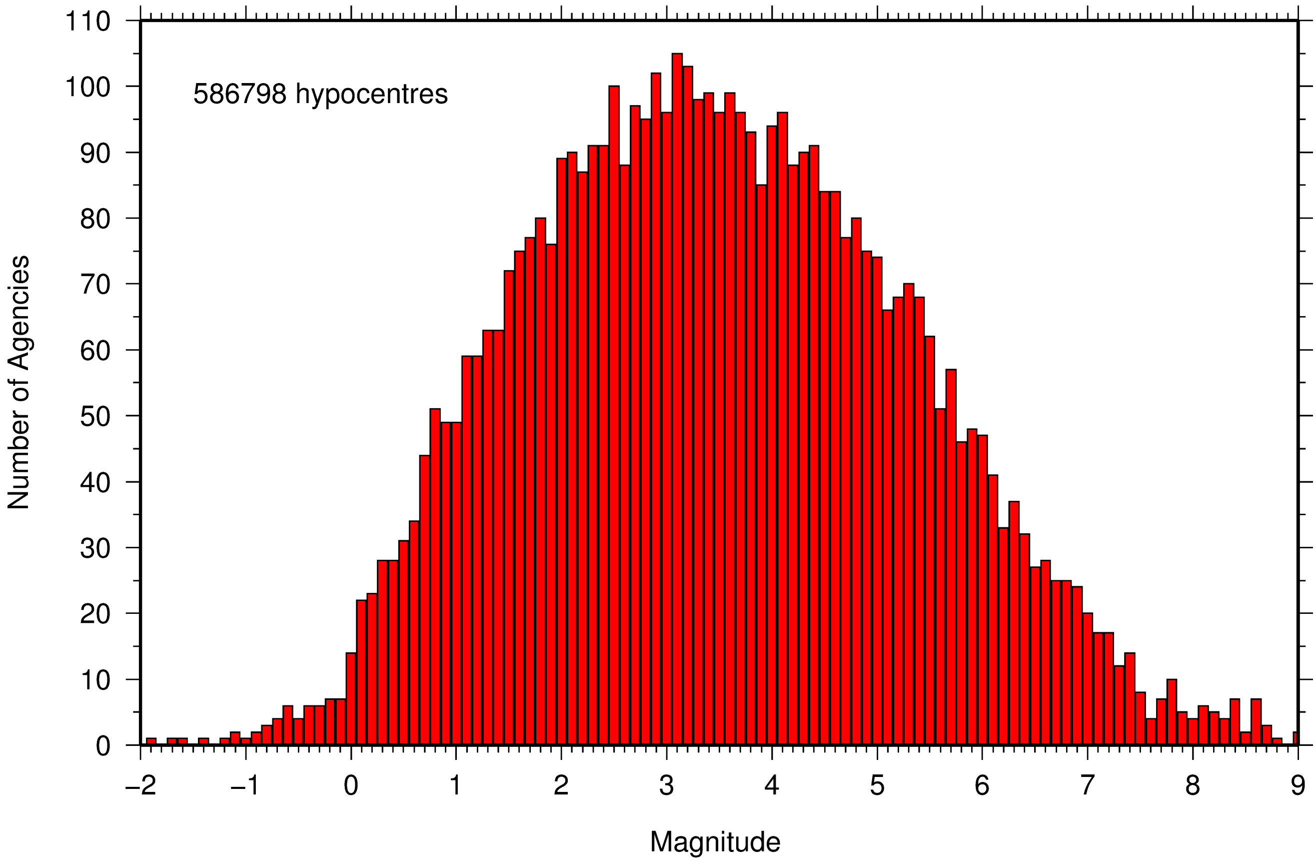

Figure 9.11: *Histogram showing the number of agencies that reported network magnitude values. All magnitude types are included.*

9.6 Moment Tensor Solutions

The ISC Bulletin publishes moment tensor solutions, which are reported to the ISC by other agencies. The collection of moment tensor solutions is summarised in Table 9.8. A histogram showing all moment tensor solutions collected throughout the ISC history is shown in Figure 9.12. Several moment tensor solutions from different authors and different moment tensor solutions calculated by different methods from the same agency may be present for the same event.

The number of moment tensors for this summary period, reported by each agency, is shown in Table 9.9. The moment tensor solutions are plotted in Figure 9.13.

Table 9.8: Summary of reports containing moment tensor solutions.

Reports with Moment Tensors	13
Total moment tensors received	3908
Agencies reporting moment tensors	8

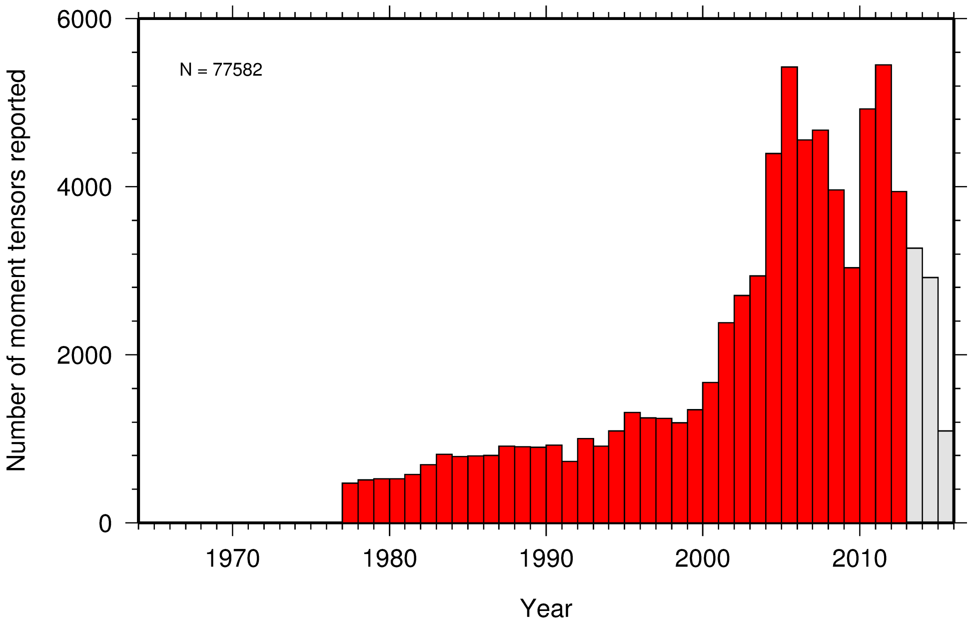

Figure 9.12: *Histogram showing the number of moment tensors reported to the ISC since 1964. The regions in grey represent data that are still being actively collected.*

Table 9.9: *Summary of moment tensor solutions in the ISC Bulletin reported by each agency.*

Agency	Number of moment tensor solutions
GCMT	1116
NEIC	410
BRK	28
OTT	19
SLM	4
PAS	2

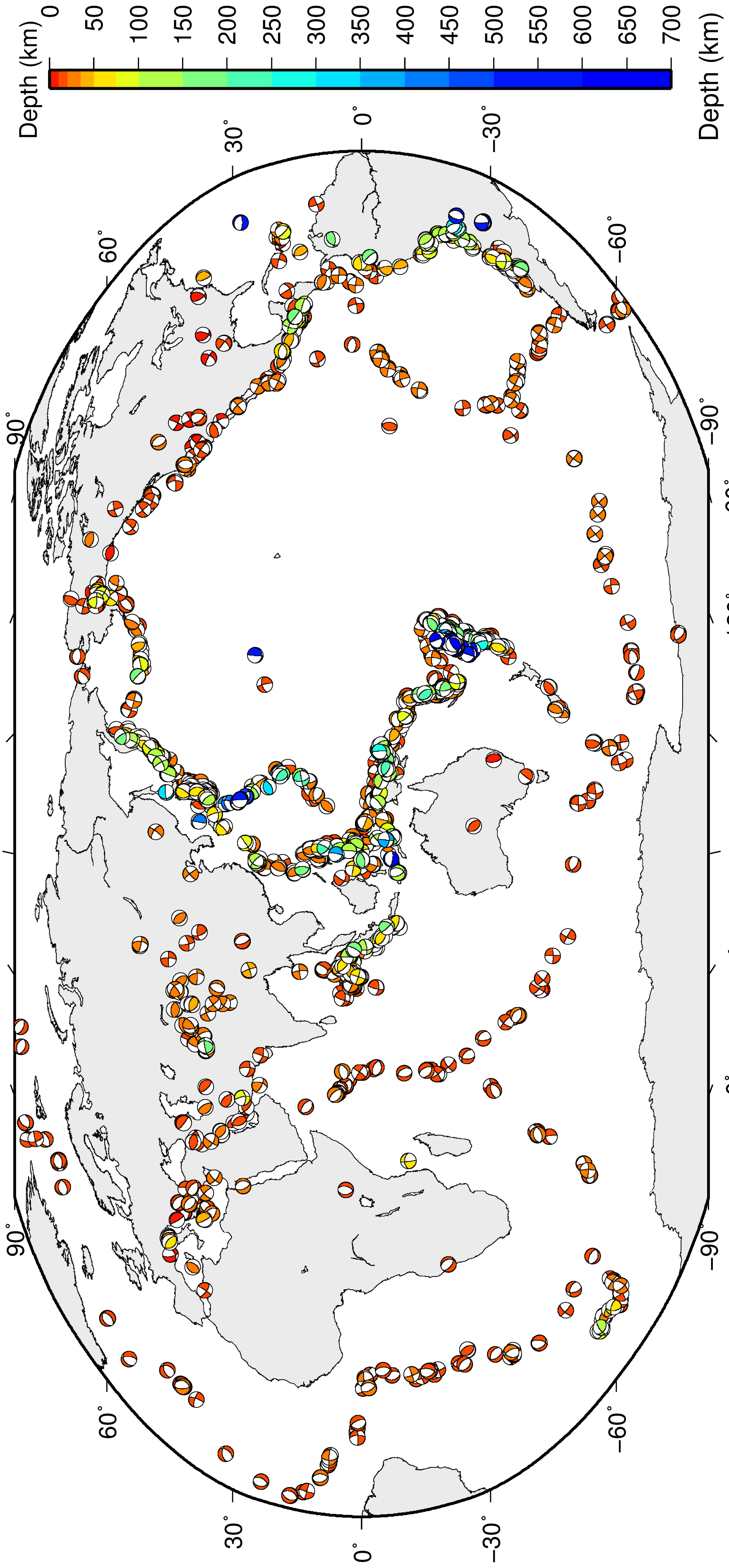

ISC Bulletin: **1579** focal mechanism solutions for **1204** events from **2012/01/01** to **2012/06/30**

Figure 9.13: *Map of all moment tensor solutions in the ISC Bulletin for this summary period.*

9.7 Timing of Data Collection

Here we present the timing of reports to the ISC. Please note, this does not include provisional alerts, which are replaced at a later stage. Instead, it reflects the final data sent to the ISC. The absolute timing of all hypocentre reports, regardless of magnitude, is shown in Figure 9.14. In Figure 9.15 the reports are grouped into one of six categories - from within three days of an event origin time, to over one year. The histogram shows the distribution with magnitude (for hypocentres where a network magnitude was reported) for each category, whilst the map shows the geographic distribution of the reported hypocentres.

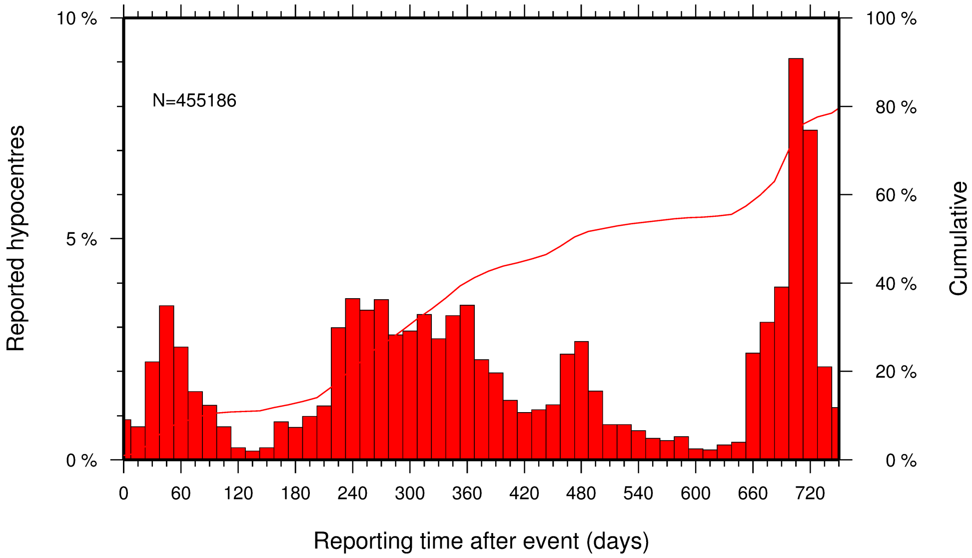

Figure 9.14: Histogram showing the timing of final reports of the hypocentres (total of N) to the ISC. The cumulative frequency is shown by the solid line.

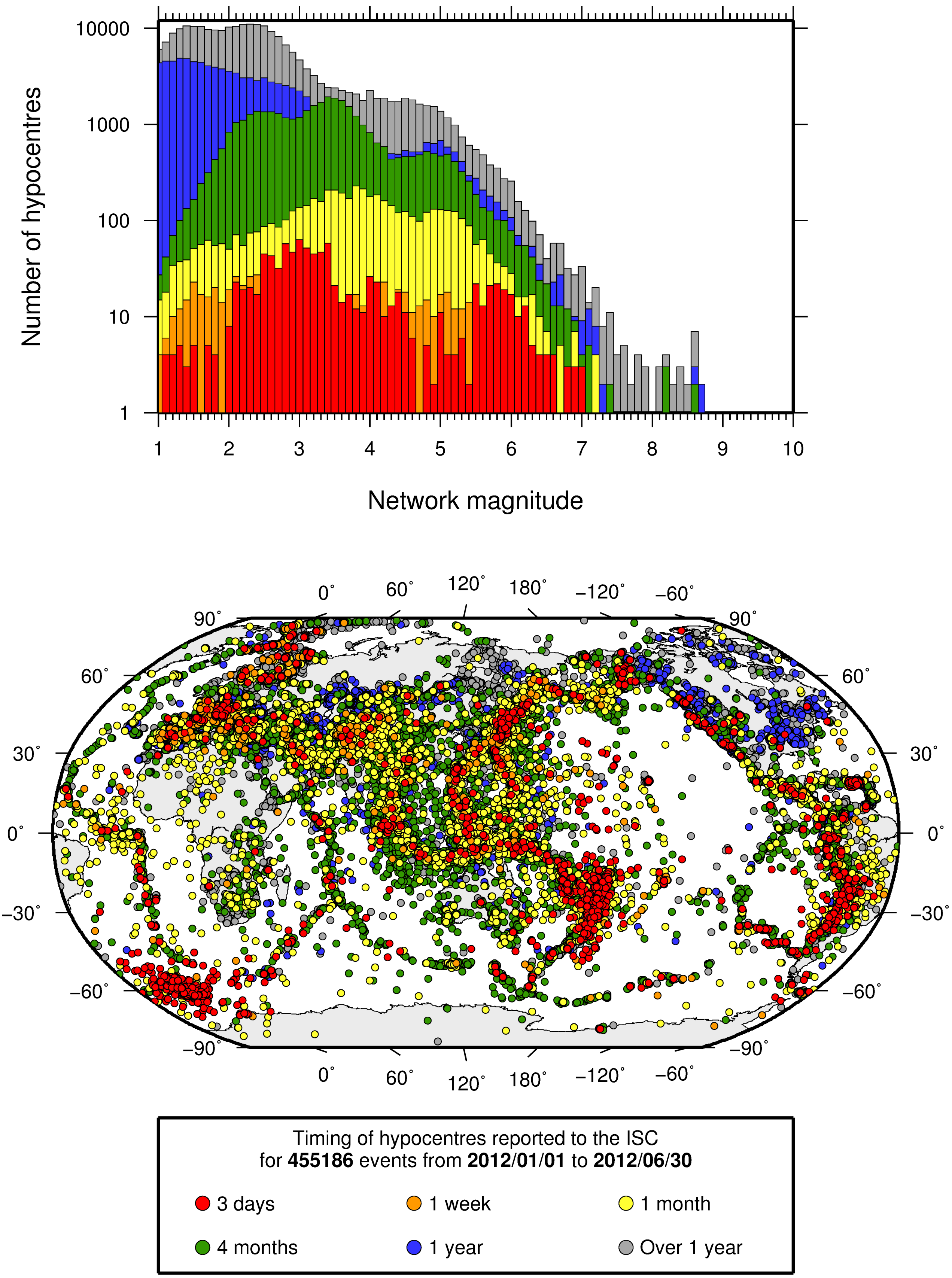

Figure 9.15: *Timing of hypocentres reported to the ISC. The colours show the time after the origin time that the corresponding hypocentre was reported. The histogram shows the distribution with magnitude. If more than one network magnitude was reported, preference was given to a value of M_W followed by M_S, m_b and M_L respectively; all reported hypocentres are included on the map. Note: early reported hypocentres are plotted over later reported hypocentres, on both the map and histogram.*

10

Overview of the ISC Bulletin

This chapter provides an overview of the seismic event data in the ISC Bulletin. We indicate the differences between all ISC events and those ISC events that are reviewed or located. We describe the wealth of phase arrivals and phase amplitudes and periods observed at seismic stations worldwide, reported in the ISC Bulletin and often used in the ISC location and magnitude determination. Finally, we make some comparisons of the ISC magnitudes with those reported by other agencies, and discuss magnitude completeness of the ISC Bulletin.

10.1 Events

The ISC Bulletin had 230458 reported events in the summary period between January and June 2012. Some 91% (210977) of the events were identified as earthquakes, the rest (19481) were of anthropogenic origin (including mining and other chemical explosions, rockbursts and induced events) or of unknown origin. As discussed in Section 3.3.3, typically about 20% of the events are selected for ISC review, and about half of the events selected for review are located by the ISC. In this summary period 15% of the events were reviewed and 9% of the events were located by the ISC. For events that are not located by the ISC, the prime hypocentre is identified according to the rules described in Section 3.3.1.

Of the 7335775 reported phase observations, 44% are associated to ISC-reviewed events, and 41% are associated to events selected for ISC location. Note that all large events are reviewed and located by the ISC. Since large events are globally recorded and thus reported by stations worldwide, they will provide the bulk of observations. This explains why only about one-fifth of the events in any given month is reviewed although the number of phases associated to reviewed events has increased nearly exponentially in the past decades.

Figure 10.1 shows the daily number of events throughout the summary period. The large increase in event numbers in March is associated with the aftershock sequence following the M_W 9.1 event off the Pacific coast of Tohoku, Japan. Figure 10.2 shows the locations of the events in the ISC Bulletin; the locations of ISC-reviewed and ISC-located events are shown in Figures 10.3 and 10.4, respectively.

Figure 10.5 shows the hypocentral depth distributions of events in the ISC Bulletin for the summary period. The vast majority of events occur in the Earth's crust. Note that the peaks at 0, 10, 35 km, and at every 50 km intervals deeper than 100 km are artifacts of analyst practices of fixing the depth to a nominal value when the depth cannot be reliably resolved.

Figure 10.6 shows the depth distribution of free-depth solutions in the ISC Bulletin. The depth of a hypocentre reported to the ISC is assumed to be determined as a free parameter, unless it is explicitly labelled as a fixed-depth solution. On the other hand, as described in Section 3.4.3, the ISC locator

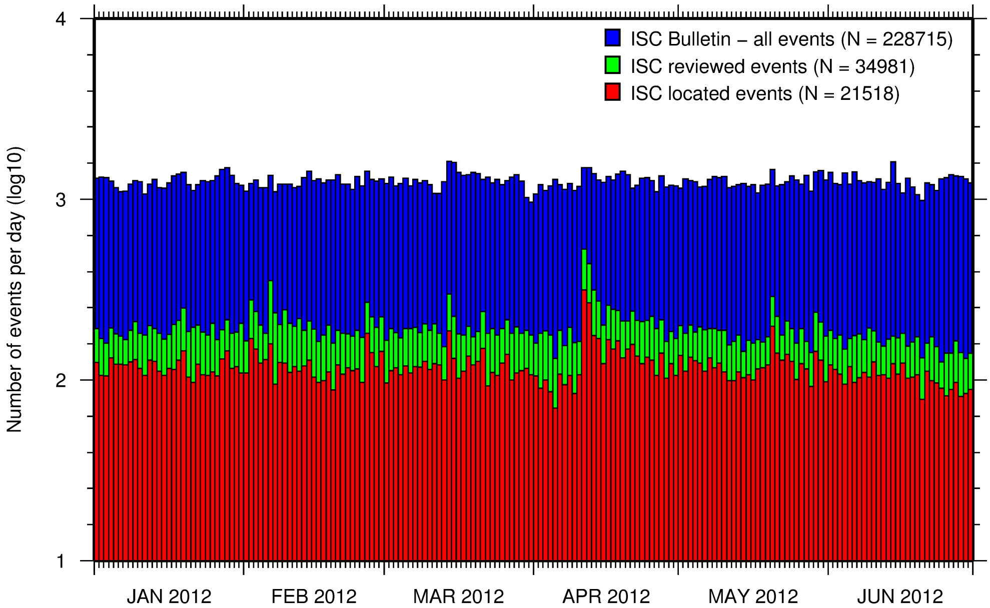

Figure 10.1: *Histogram showing the number of events in the ISC Bulletin for the current summary period. The vertical scale is logarithmic.*

attempts to get a free-depth solution if, and only if, there is resolution for the depth in the data, i.e. if there is a local network and/or sufficient depth-sensitive phases are reported.

Figure 10.7 shows the depth distribution of fixed-depth solutions in the ISC Bulletin. Except for a fraction of events whose depth is fixed to a shallow depth, this set comprises mostly ISC-located events. If there is no resolution for depth in the data, the ISC locator fixes the depth to a value obtained from the ISC default depth grid file, or if no default depth exists for that location, to a nominal default depth assigned to each Flinn-Engdahl region (see details in Section 3.4.3). During the ISC review editors are inclined to accept the depth obtained from the default depth grid, but they typically change the depth of those solutions that have a nominal (10 or 35 km) depth. When doing so, they usually fix the depth to a round number, preferably divisible by 50.

For events selected for ISC location, the number of stations typically increases as arrival data reported by several agencies are grouped together and associated to the prime hypocentre. Consequently, the network geometry, characterised by the secondary azimuthal gap (the largest azimuthal gap a single station closes), is typically improved. Figure 10.8 illustrates that the secondary azimuthal gap is indeed generally smaller for ISC-located events than that for all events in the ISC Bulletin. Figure 10.9 shows the distribution of the number of associated stations. For large events the number of associated stations is usually larger for ISC-located events than for any of the reported event bulletins. On the other hand, events with just a few reporting stations are rarely selected for ISC location. The same is true for the number of defining stations (stations with at least one defining phase that were used in the location). Figure 10.10 indicates that because the reported observations from multiple agencies are associated to the prime, large ISC-located events typically have a larger number of defining stations than any of the reported event bulletins.

The formal uncertainty estimates are also typically smaller for ISC-located events. Figure 10.11 shows the distribution of the area of the 90% confidence error ellipse for ISC-located events during the summary period. The distribution suffers from a long tail indicating a few poorly constrained event locations.

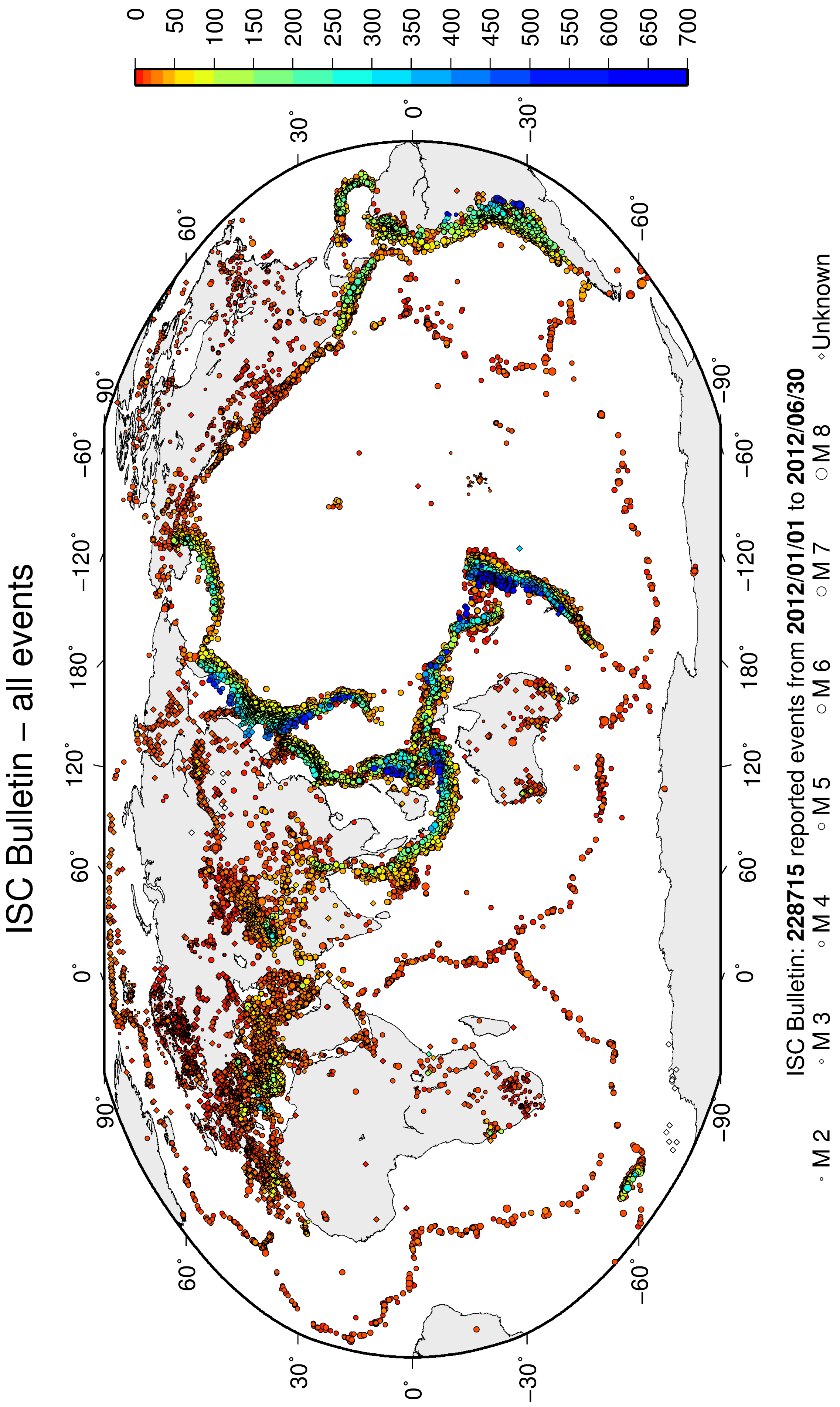

Figure 10.2: *Map of all events in the ISC Bulletin. Prime hypocentre locations are shown. Compare with Figure 9.10.*

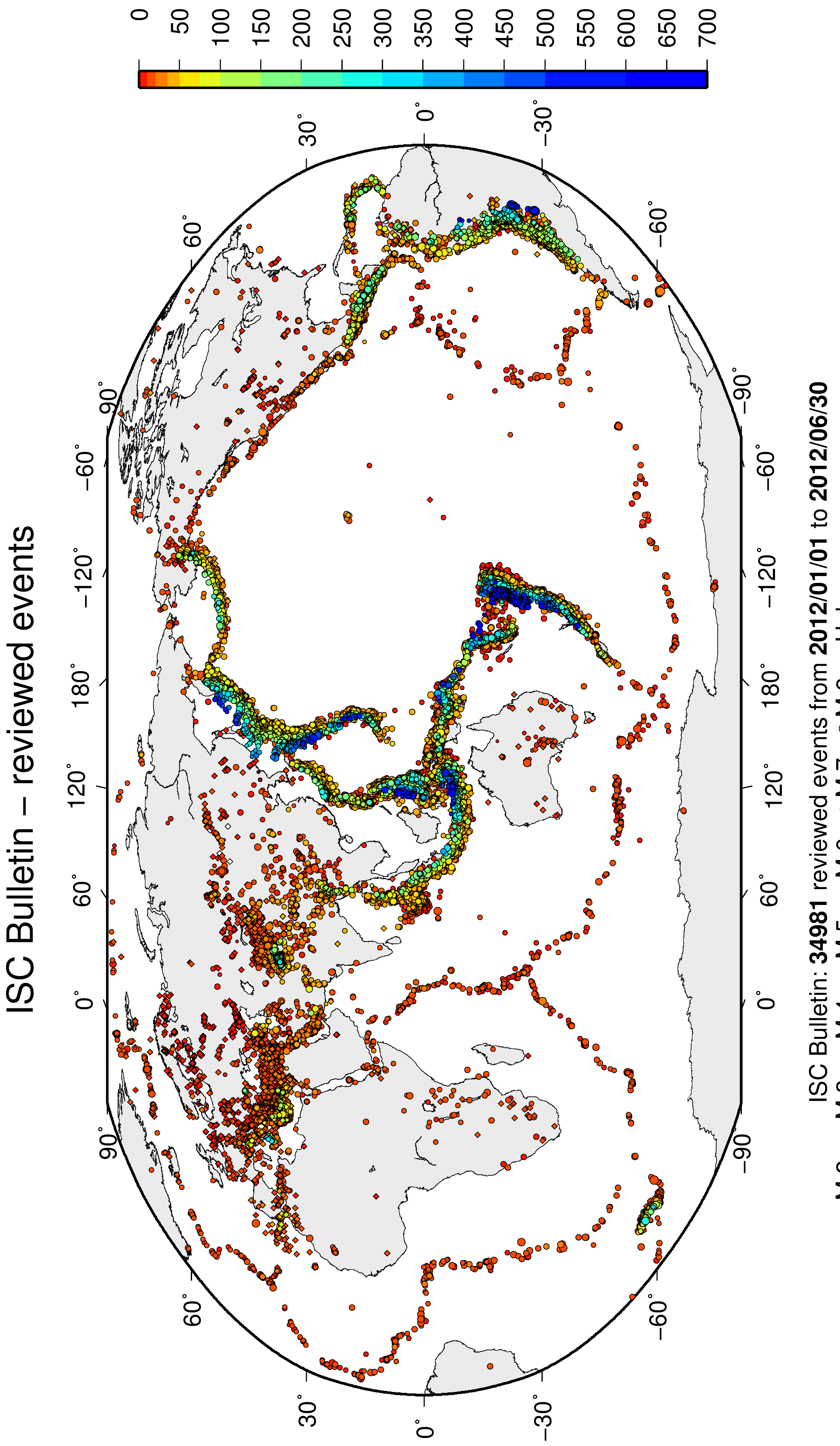

Figure 10.3: *Map of all events reviewed by the ISC for this time period. Prime hypocentre locations are shown.*

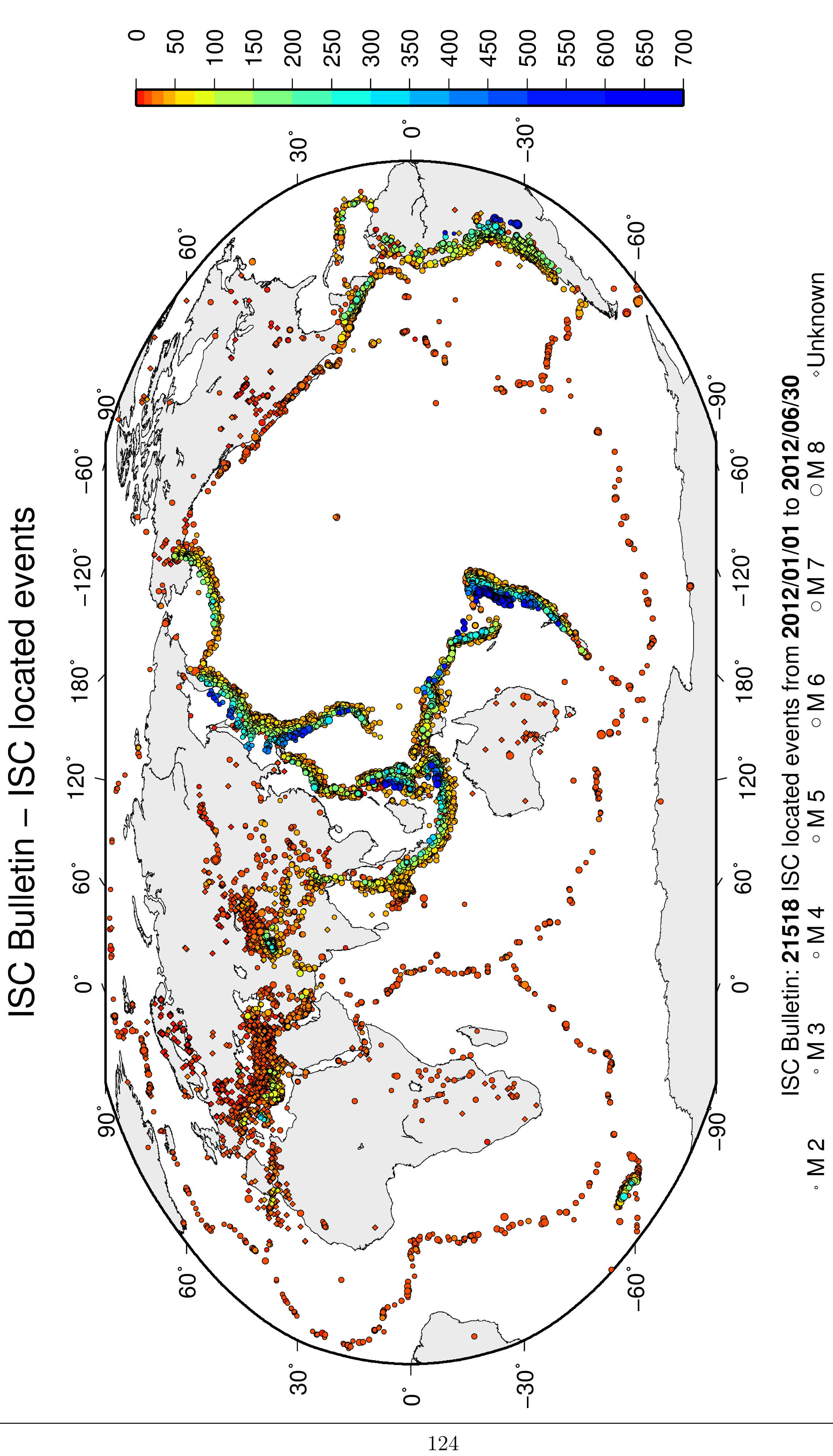

Figure 10.4: *Map of all events located by the ISC for this time period. ISC determined hypocentre locations are shown.*

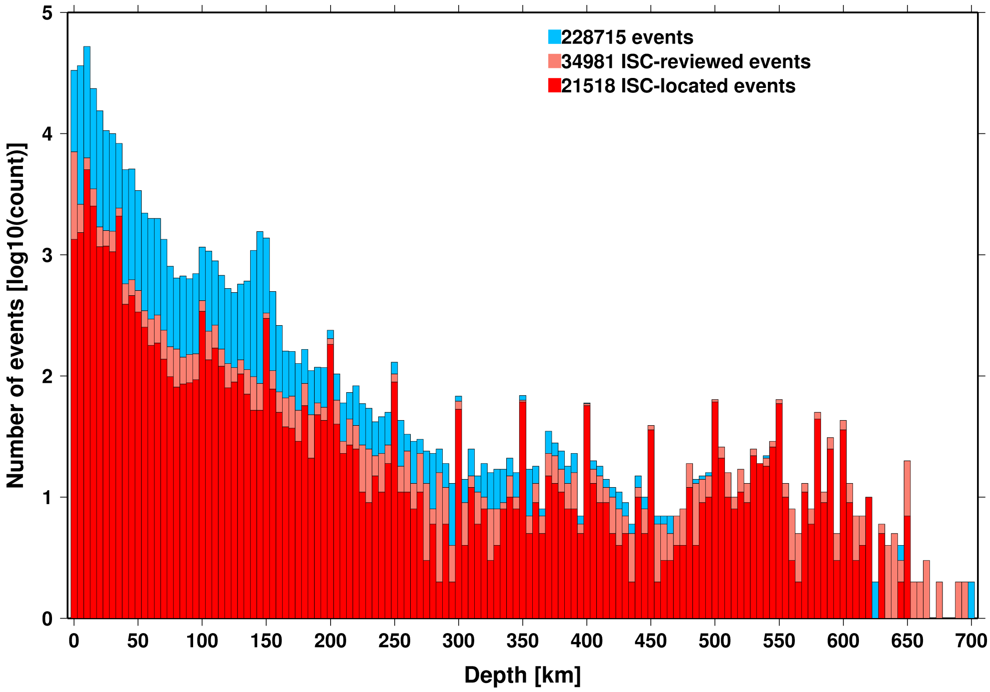

Figure 10.5: *Distribution of event depths in the ISC Bulletin (blue) and for the ISC-reviewed (pink) and the ISC-located (red) events during the summary period. All ISC-located events are reviewed, but not all reviewed events are located by the ISC. The vertical scale is logarithmic.*

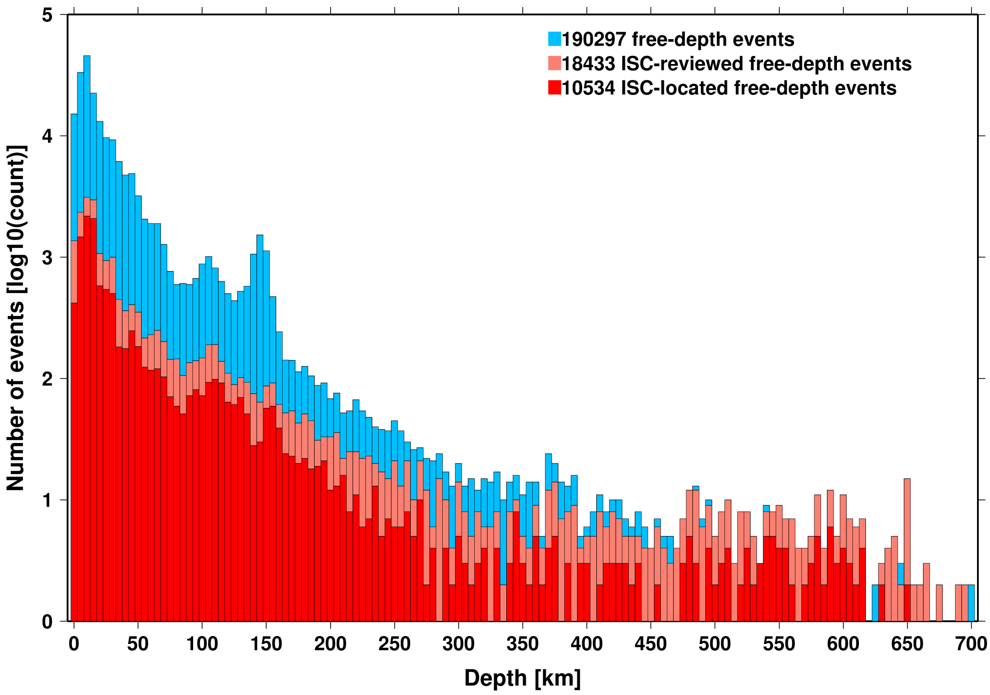

Figure 10.6: *Hypocentral depth distribution of events where the prime hypocentres are reported/located with a free-depth solution in the ISC Bulletin. The vertical scale is logarithmic.*

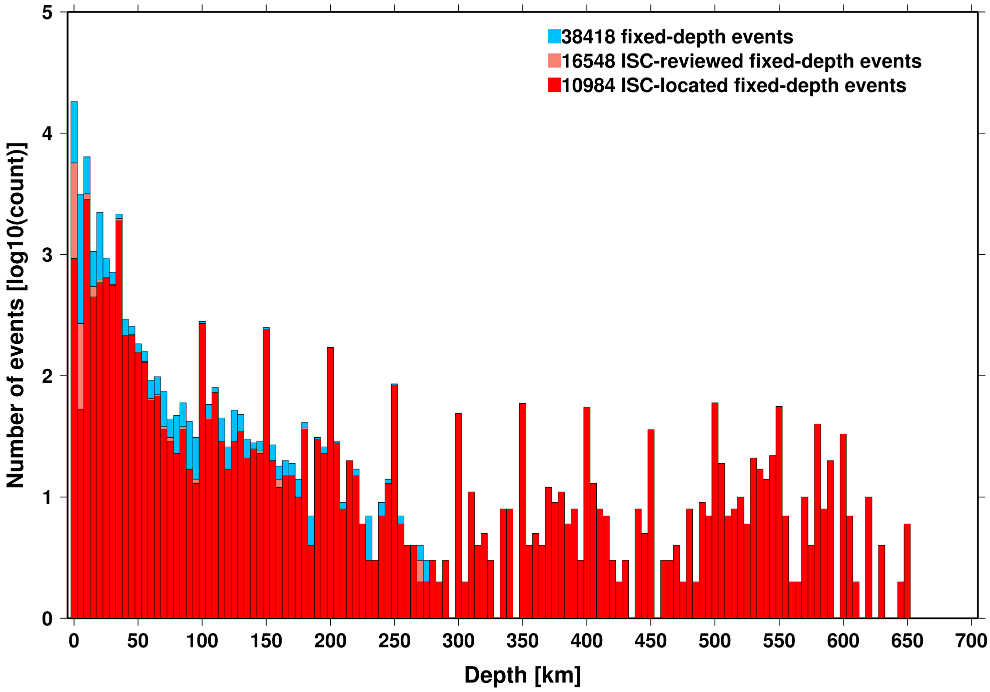

Figure 10.7: *Hypocentral depth distribution of events where the prime hypocentres are reported/located with a fixed-depth solution in the ISC Bulletin. The vertical scale is logarithmic.*

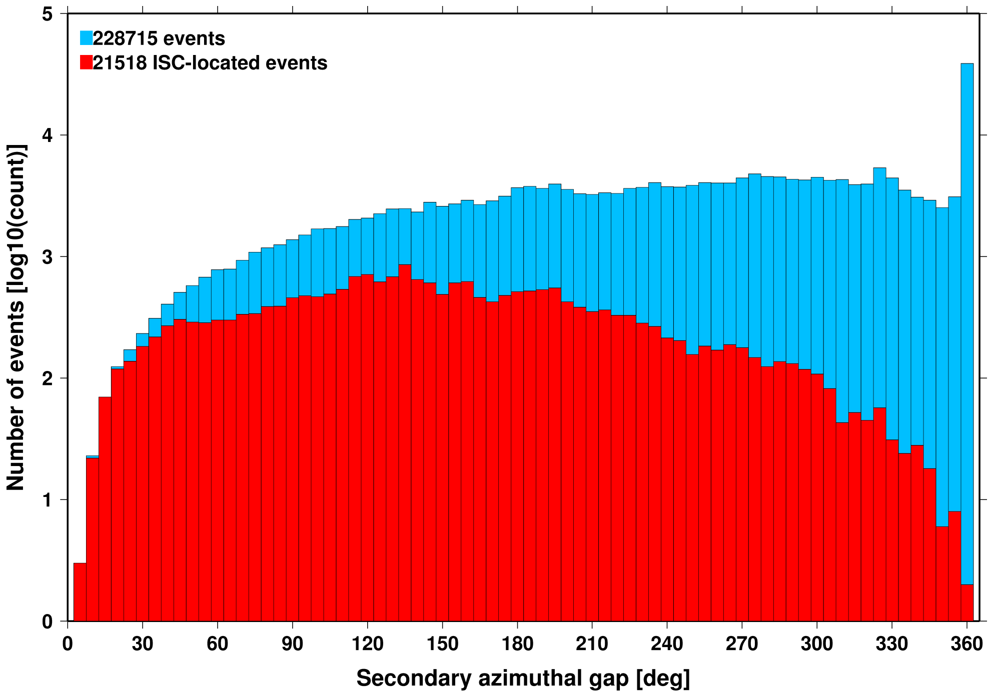

Figure 10.8: *Distribution of secondary azimuthal gap for events in the ISC Bulletin (blue) and those selected for ISC location (red). The vertical scale is logarithmic.*

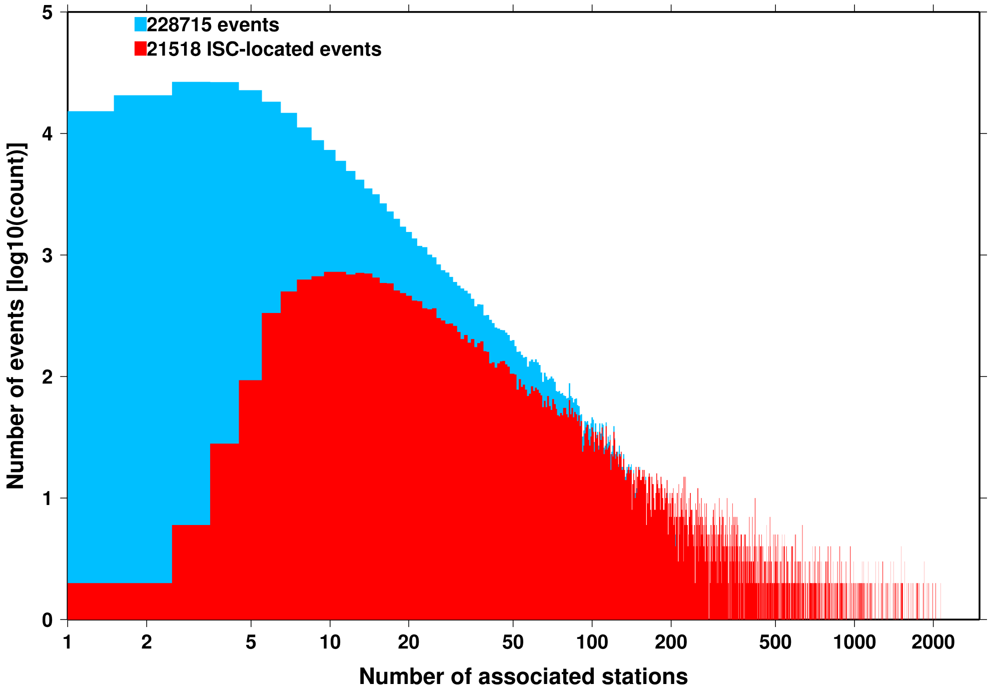

Figure 10.9: *Distribution of the number of associated stations for events in the ISC Bulletin (blue) and those selected for ISC location (red). The vertical scale is logarithmic.*

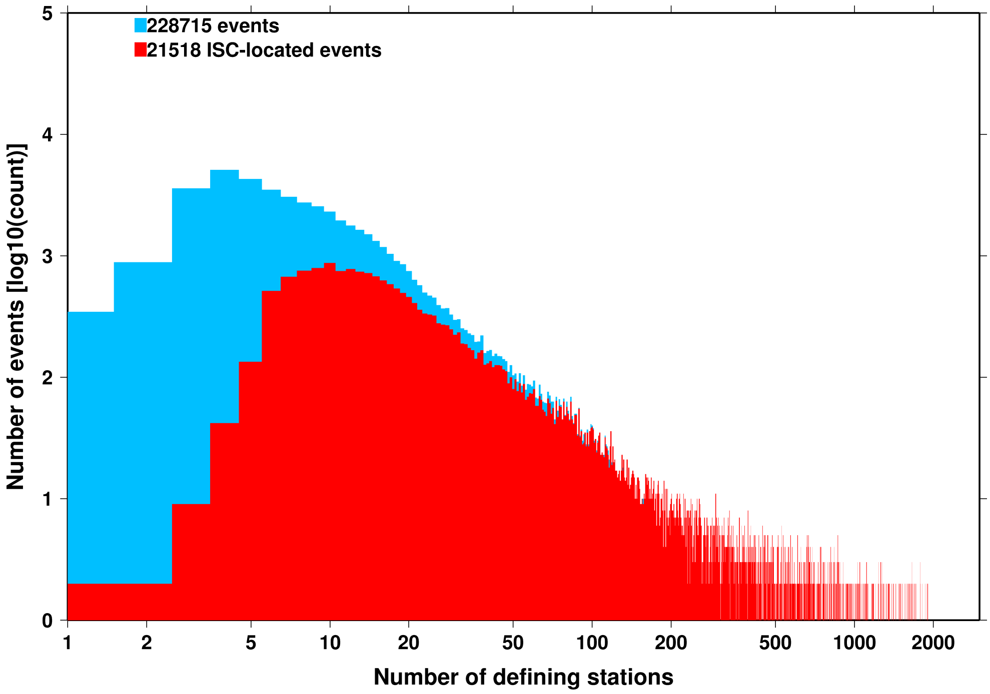

Figure 10.10: *Distribution of the number of defining stations for events in the ISC Bulletin (blue) and those selected for ISC location (red). The vertical scale is logarithmic.*

Nevertheless, half of the events are characterised by an error ellipse with an area less than 181 km^2, 90% of the events have an error ellipse area less than 1241 km^2, and 95% of the events have an error ellipse area less than 2009 km^2.

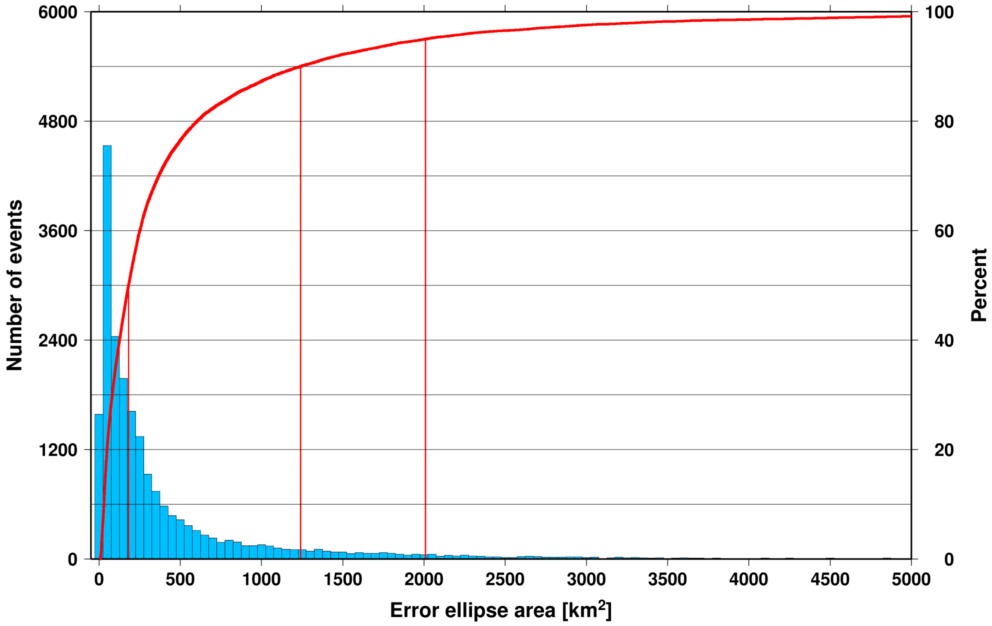

Figure 10.11: *Distribution of the area of the 90% confidence error ellipse of the ISC-located events. Vertical red lines indicate the 50th, 90th and 95th percentile values.*

Figure 10.12 shows one of the major characteristic features of the ISC location algorithm (Bondár and Storchak, 2011). Because the ISC locator accounts for correlated travel-time prediction errors due to unmodelled velocity heterogeneities along similar ray paths, the area of the 90% confidence error ellipse does not decrease indefinitely with increasing number of stations, but levels off once the information carried by the network geometry is exhausted, thus providing more realistic uncertainty estimates.

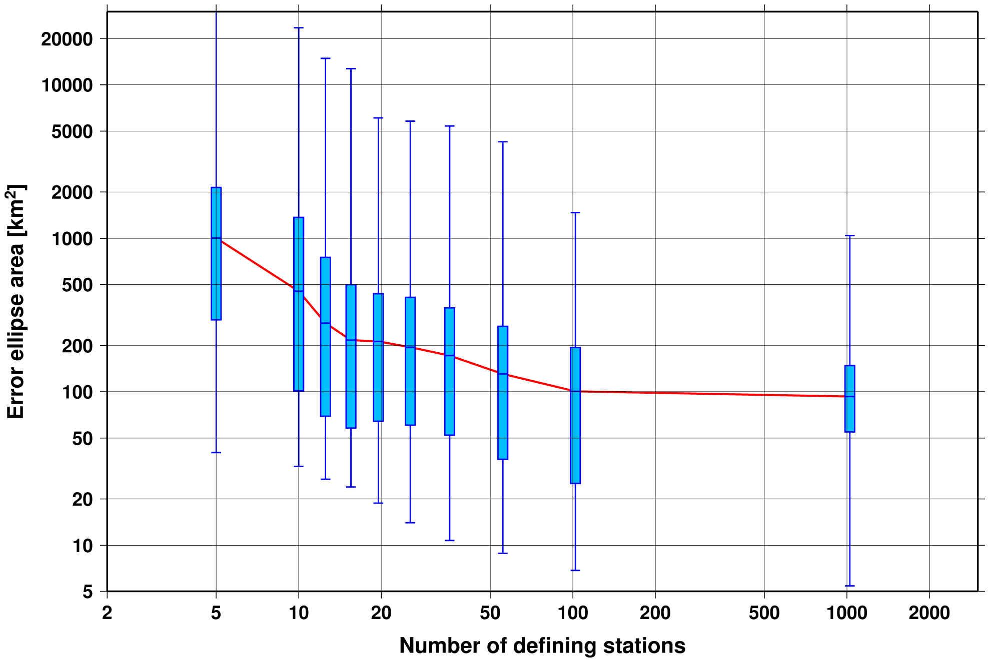

Figure 10.12: *Box-and-whisker plot of the area of the 90% confidence error ellipse of the ISC-located events as a function of the number of defining stations. Each box represents one-tenth-worth of the total number of data. The red line indicates the median 90% confidence error ellipse area.*

10.2 Seismic Phases and Travel-Time Residuals

The number of phases that are associated to events over the summary period in the ISC Bulletin is shown in Figure 10.13. Phase types and their total number in the ISC Bulletin is shown in the Appendix, Table 12.2. A summary of phase types is indicated in Figure 10.14.

In computing ISC locations, the current (for events since 2009) ISC location algorithm (*Bondár and Storchak*, 2011) uses all *ak135* phases where possible. Within the Bulletin, the phases that contribute to an ISC location are labelled as *time defining*. In this section, we summarise these time defining phases.

In Figure 10.15, the number of defining phases is shown in a histogram over the summary period. Each defining phase is listed in Table 10.1, which also provides a summary of the number of defining phases per event. A pie chart showing the proportion of defining phases is shown in Figure 10.16. Figure 10.17 shows travel times of seismic waves. The distribution of residuals for these defining phases is shown for the top five phases in Figures 10.18 through 10.22.

Table 10.1: *Numbers of 'time defining' phases (N) within the ISC Bulletin for 21518 ISC located events.*

Phase	Number of 'defining' phases	Number of events	Max per event	Median per event
P	988277	14623	2152	10
Pn	546594	19866	1440	11
Sn	179624	17157	331	5
Pg	117297	8105	121	11
Pb	111011	10068	135	6
PKPdf	88375	5217	1064	3
Sg	78733	7868	133	6
Sb	71337	9737	88	5
S	38950	3907	287	3
PKPbc	38132	4303	338	2
PKPab	19561	3219	254	2
PcP	17067	3750	132	2

Table 10.1: *(continued)*

Phase	Number of 'defining' phases	Number of events	Max per event	Median per event
pP	14252	1748	342	3
Pdif	11439	1236	501	2
PP	11187	2072	302	2
PKiKP	8614	1188	244	2
SS	5239	1503	71	2
ScP	4569	1295	48	2
sP	3599	1181	60	2
PKKPbc	2589	495	101	2
SKSac	2268	546	50	1
PnPn	2005	969	15	1
SnSn	1963	894	14	1
ScS	1358	720	24	1
pPKPdf	1325	460	55	2
SKPbc	1007	290	51	2
PKKPab	687	267	42	1
PKKPdf	663	266	21	2
P'P'df	607	168	32	2
SKiKP	595	302	34	1
pPKPbc	587	272	21	1
SKSdf	515	328	16	1
PS	515	114	40	2
SKKSac	492	322	12	1
PcS	486	380	8	1
sS	484	324	13	1
PKSdf	443	320	11	1
pPKPab	404	171	34	1
sPKPdf	346	189	23	1
SKPab	332	145	42	1
PnS	295	151	9	1
sPKPbc	218	118	15	1
SP	174	61	17	1
Sdif	157	102	16	1
SKPdf	119	47	32	1
pS	86	79	3	1
SKKPbc	81	32	13	1
sPKPab	74	44	10	1
pPdif	50	19	11	1
SPn	48	39	5	1
pPKiKP	45	21	8	1
sPdif	24	9	9	2
SKKPab	23	10	4	2
P'P'ab	22	17	2	1
SKKSdf	18	15	3	1
SKKPdf	8	5	4	1
sPKiKP	7	6	2	1
P'P'bc	6	4	3	1
S'S'ac	6	6	1	1
pPn	4	1	4	4
PKSbc	4	4	1	1
SbSb	3	3	1	1
sPn	2	1	2	2
PgS	2	2	1	1
sSKSac	2	2	1	1
PbPb	2	2	1	1
PKSab	2	2	1	1
sSdif	2	2	1	1
PKKSdf	1	1	1	1
PKKSbc	1	1	1	1
sPb	1	1	1	1
SgSg	1	1	1	1

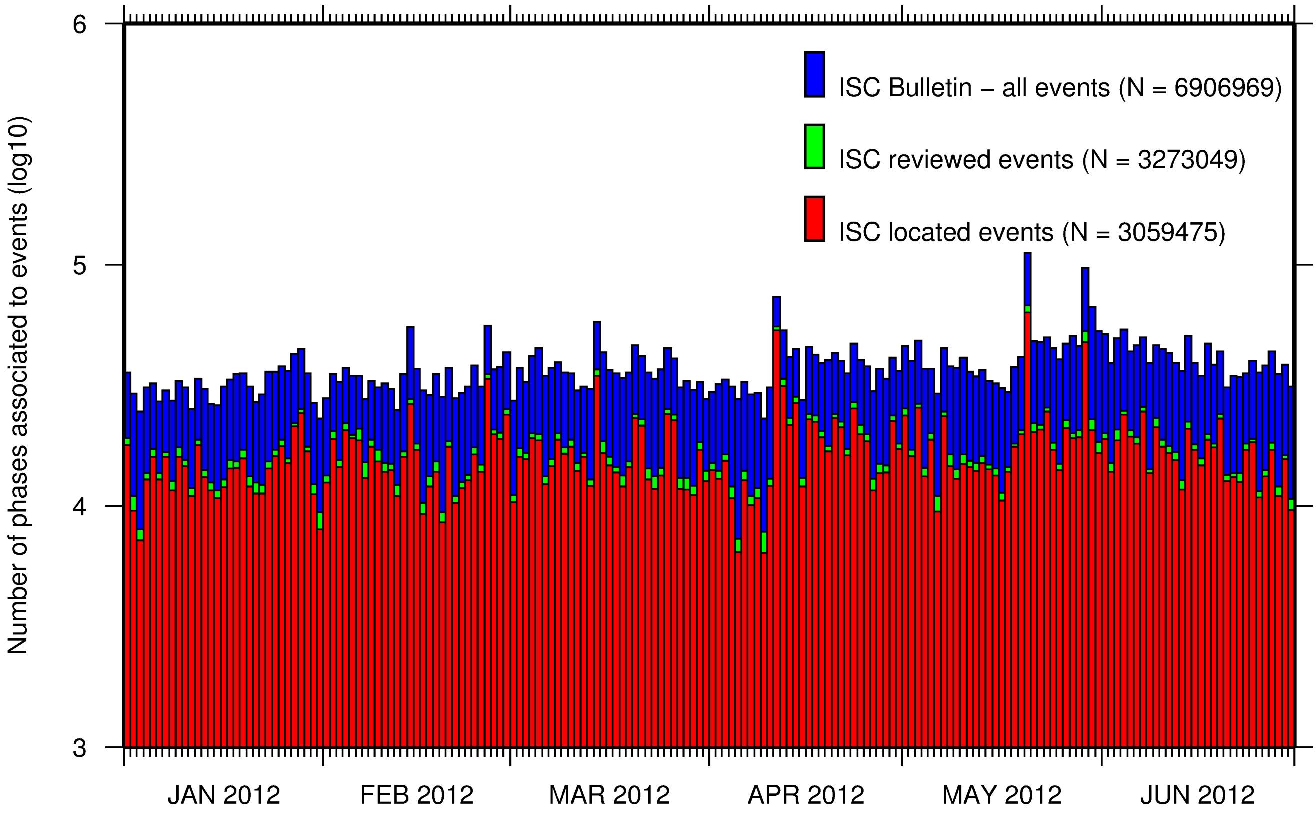

Figure 10.13: *Histogram showing the number of phases (N) that the ISC has associated to events within the ISC Bulletin for the current summary period.*

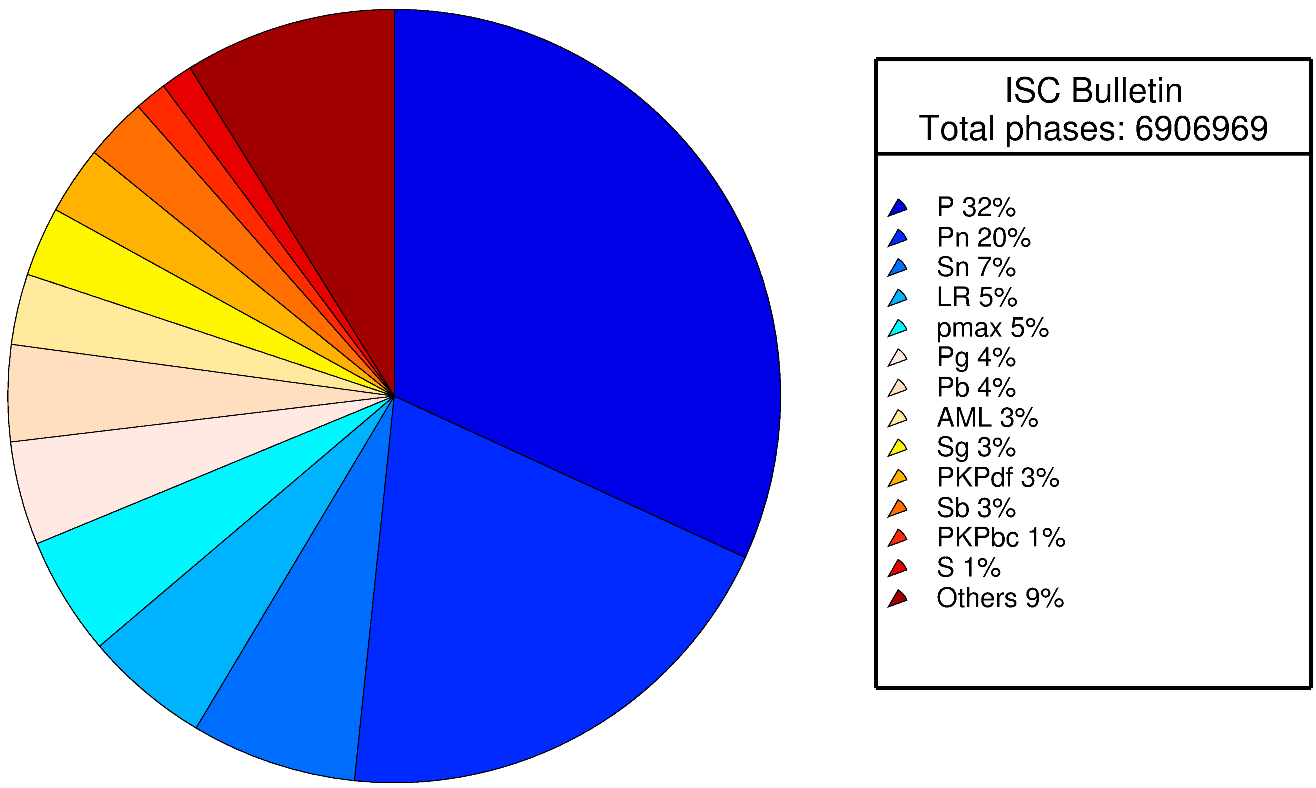

Figure 10.14: *Pie chart showing the fraction of various phase types in the ISC Bulletin for this summary period.*

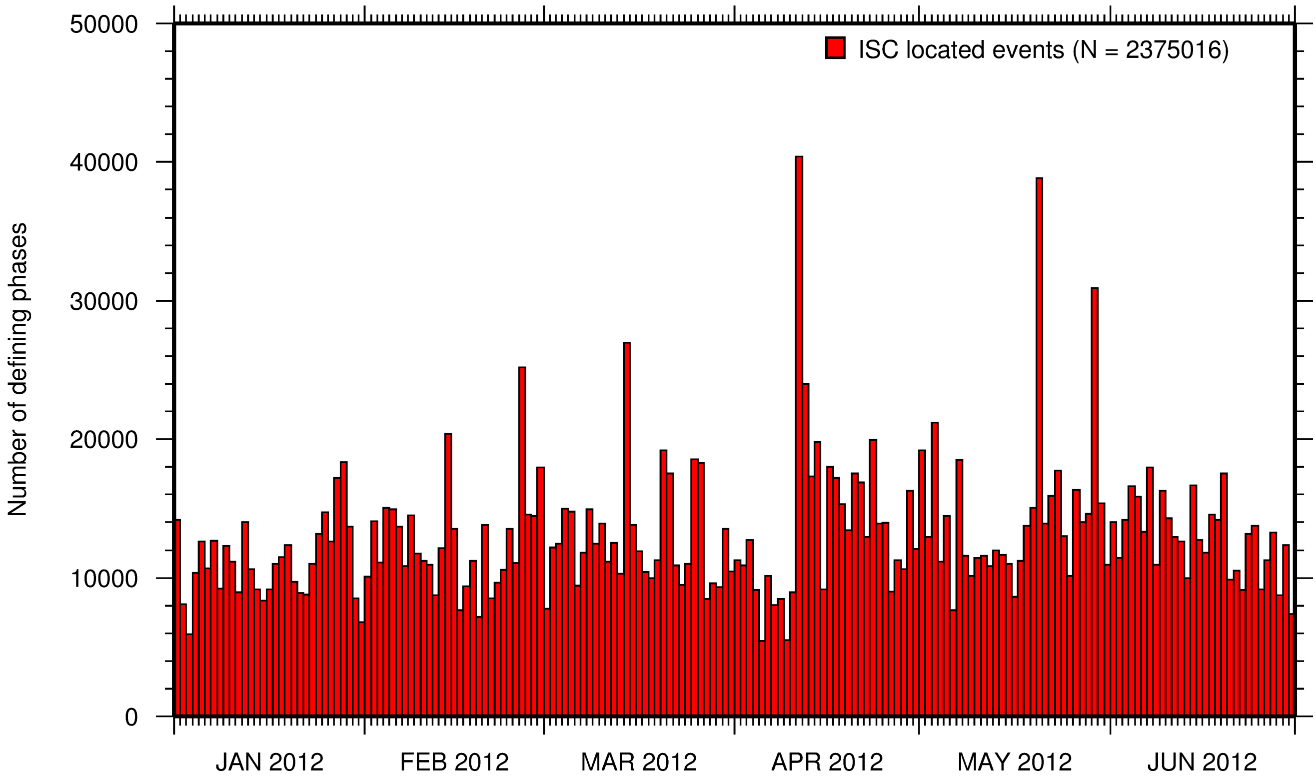

Figure 10.15: *Histogram showing the number of defining phases in the ISC Bulletin, for events located by the ISC.*

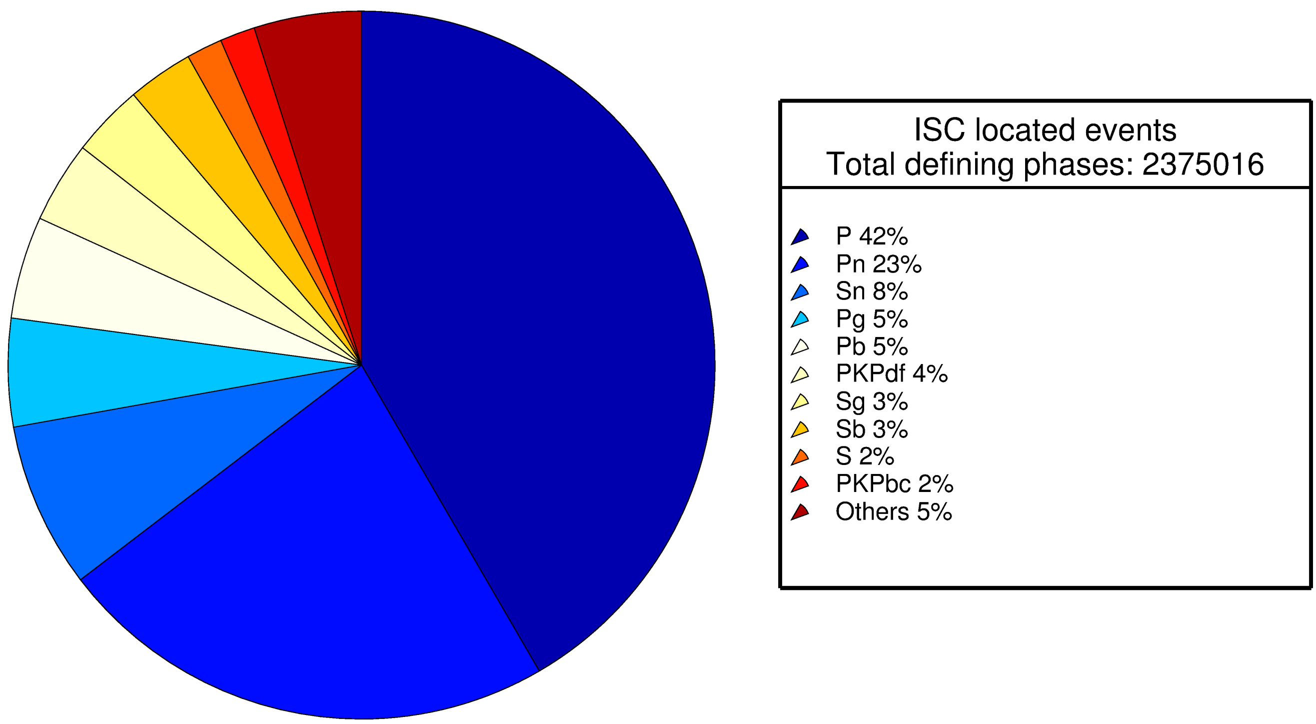

Figure 10.16: *Pie chart showing the defining phases in the ISC Bulletin, for events located by the ISC. A complete list of defining phases is shown in Table 10.1.*

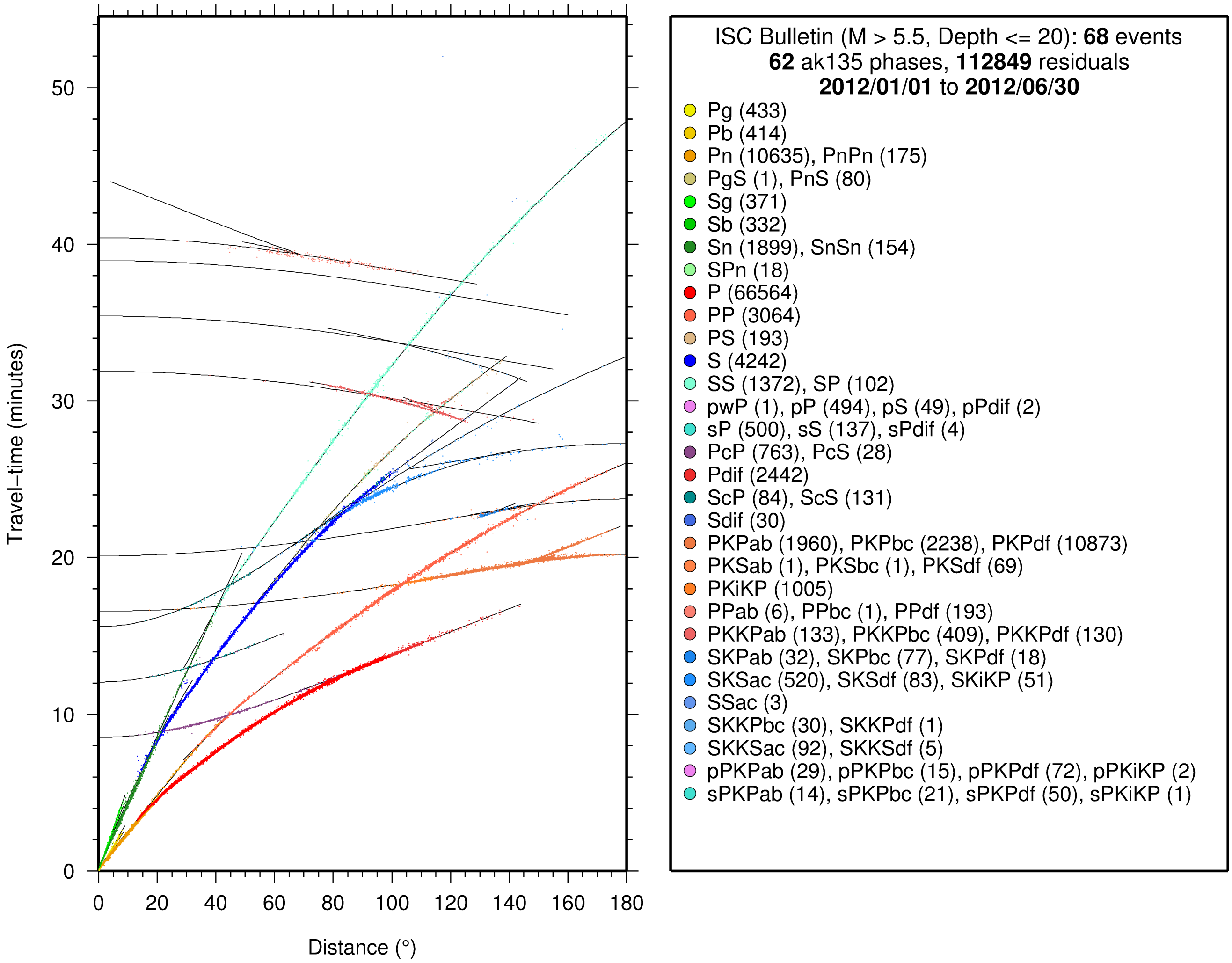

Figure 10.17: *Distribution of travel-time observations in the ISC Bulletin for events with M > 5.5 and depth less than 20 km. The travel-time observations are shown relative to a 0 km source and compared with the theoretical ak135 travel-time curves (solid lines). The legend lists the number of each phase plotted.*

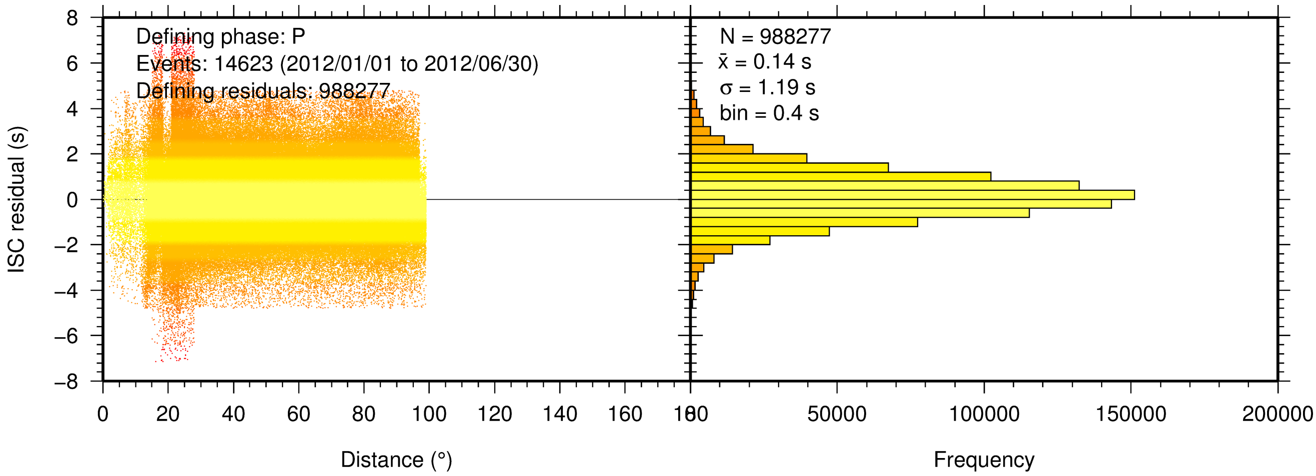

Figure 10.18: *Distribution of travel-time residuals for the defining P phases used in the computation of ISC located events in the Bulletin.*

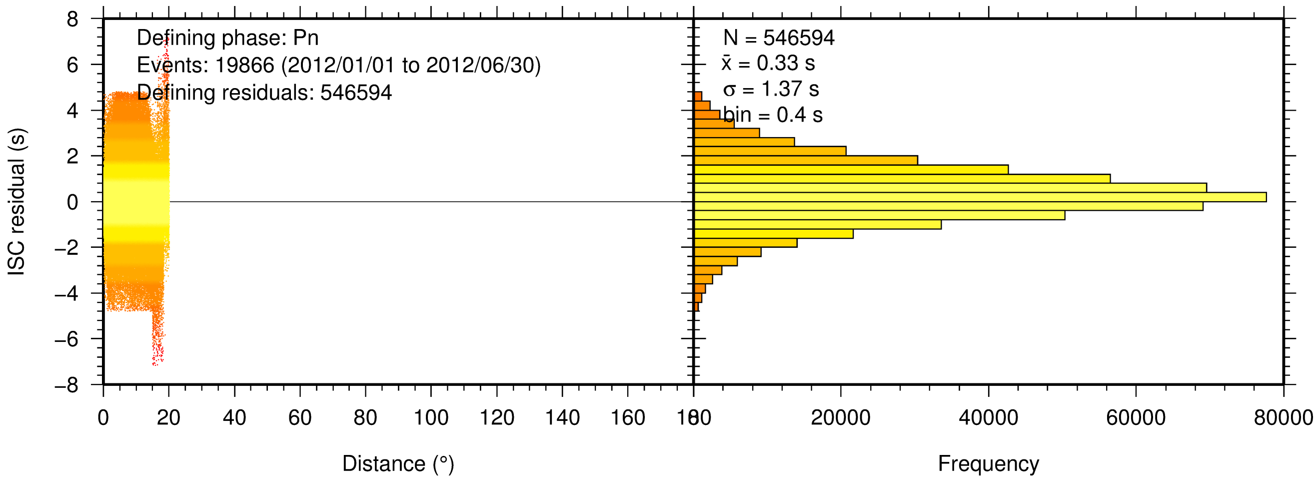

Figure 10.19: *Distribution of travel-time residuals for the defining Pn phases used in the computation of ISC located events in the Bulletin.*

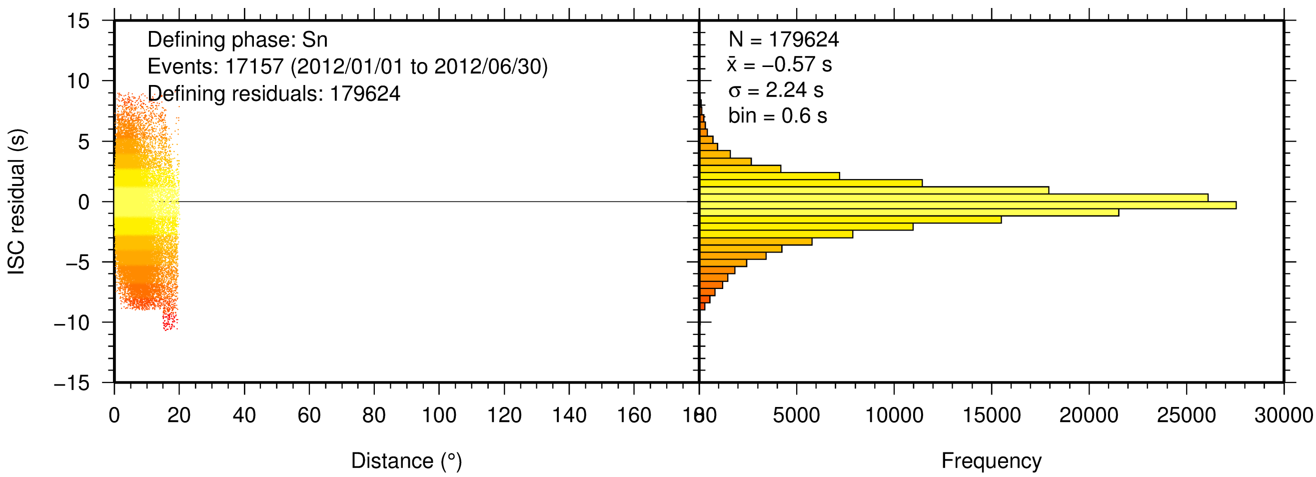

Figure 10.20: *Distribution of travel-time residuals for the defining Sn phases used in the computation of ISC located events in the Bulletin.*

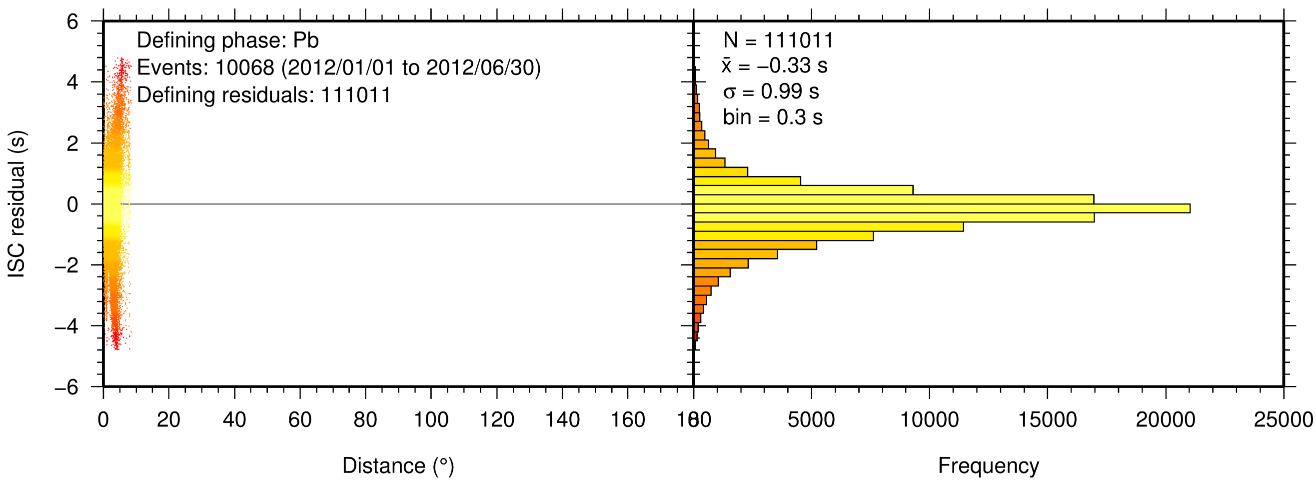

Figure 10.21: *Distribution of travel-time residuals for the defining Pb phases used in the computation of ISC located events in the Bulletin.*

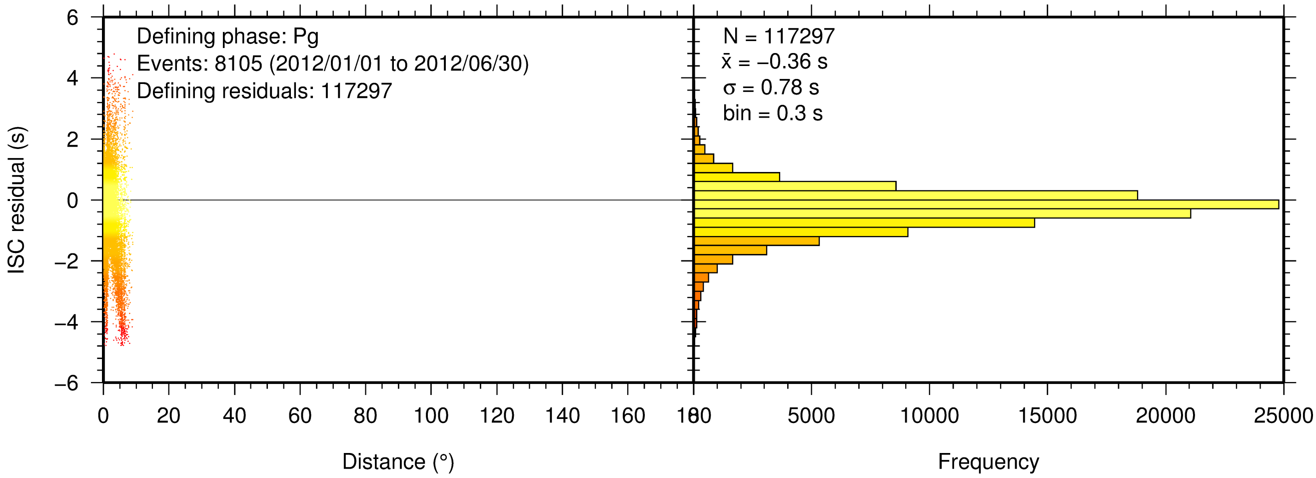

Figure 10.22: *Distribution of travel-time residuals for the defining Pg phases used in the computation of ISC located events in the Bulletin.*

10.3 Seismic Wave Amplitudes and Periods

The ISC Bulletin contains a variety of seismic wave amplitudes and periods measured by reporting agencies. For this Bulletin Summary, the total of collected amplitudes and periods is 668555 (see Section 9.3). For the determination of the ISC magnitudes MS and mb, only a fraction of such data can be used. Indeed, the ISC network magnitudes are computed only for ISC located events. Here we recall the main features of the ISC procedure for MS and mb computation (see detailed description in Section 3.4). For each amplitude-period pair in a reading the ISC algorithm computes the magnitude (a reading can include several amplitude-period measurements) and the reading magnitude is assigned to the maximum A/T in the reading. If more than one reading magnitude is available for a station, the station magnitude is the median of the reading magnitudes. The network magnitude is computed then as the 20% alpha-trimmed median of the station magnitudes (at least three required). MS is computed for shallow earthquakes (depth $\leq$ 60 km) only and using amplitudes and periods on all three components (when available) if the period is within 10-60 s and the epicentral distance is between 20° and 160°. mb is computed also for deep earthquakes (depth down to 700 km) but only with amplitudes on the vertical component measured at periods $\leq$ 3 s in the distance range 21°-100°.

Table 10.2 is a summary of the amplitude and period data that contributed to the computation of station and ISC MS and mb network magnitudes for this Bulletin Summary.

Table 10.2: *Summary of the amplitude-period data used by the ISC Locator to compute MS and mb.*

	MS	mb
Number of amplitude-period data	141322	527233
Number of readings	123895	521484
Percentage of readings in the ISC located events with qualifying data for magnitude computation	13.8	51.5
Number of station magnitudes	114961	448977
Number of network magnitudes	3370	13176

A small percentage of the readings with qualifying data for MS and mb calculation have more than one amplitude-period pair. Notably, only 14% of the readings for the ISC located (shallow) events included qualifying data for MS computation, whereas for mb the percentage is much higher at 51%. This is due to the seismological practice of reporting agencies. Agencies contributing systematic reports of amplitude and period data are listed in Appendix Table 12.3. Obviously the ISC Bulletin would benefit if more agencies included surface wave amplitude-period data in their reports.

Figure 10.23 shows the distribution of the number of station magnitudes versus distance. For mb there is a significant increase in the distance range 70°-90°, whereas for MS most of the contributing stations are below 100°. The increase in number of station magnitude between 70°-90° for mb is partly due to the very dense distribution of seismic stations in North America and Europe with respect to earthquake occurring in various subduction zones around the Pacific Ocean.

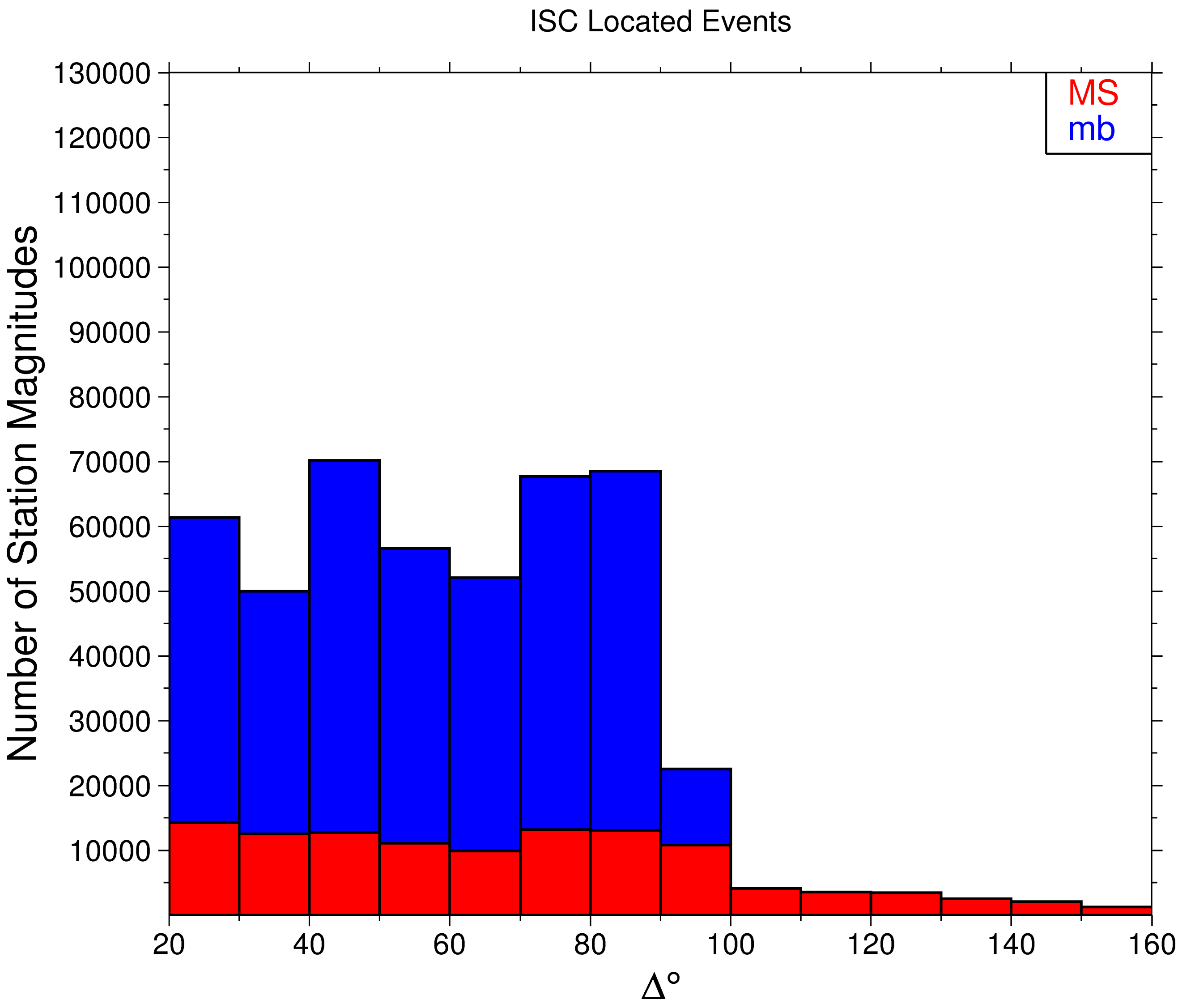

Figure 10.23: *Distribution of the number of station magnitudes computed by the ISC Locator for mb (blue) and MS (red) versus distance.*

Finally, Figure 10.24 shows the distribution of network MS and mb as well as the median number of stations for magnitude bins of 0.2. Clearly with increasing magnitude the number of events is smaller but with a general tendency of having more stations contributing to the network magnitude.

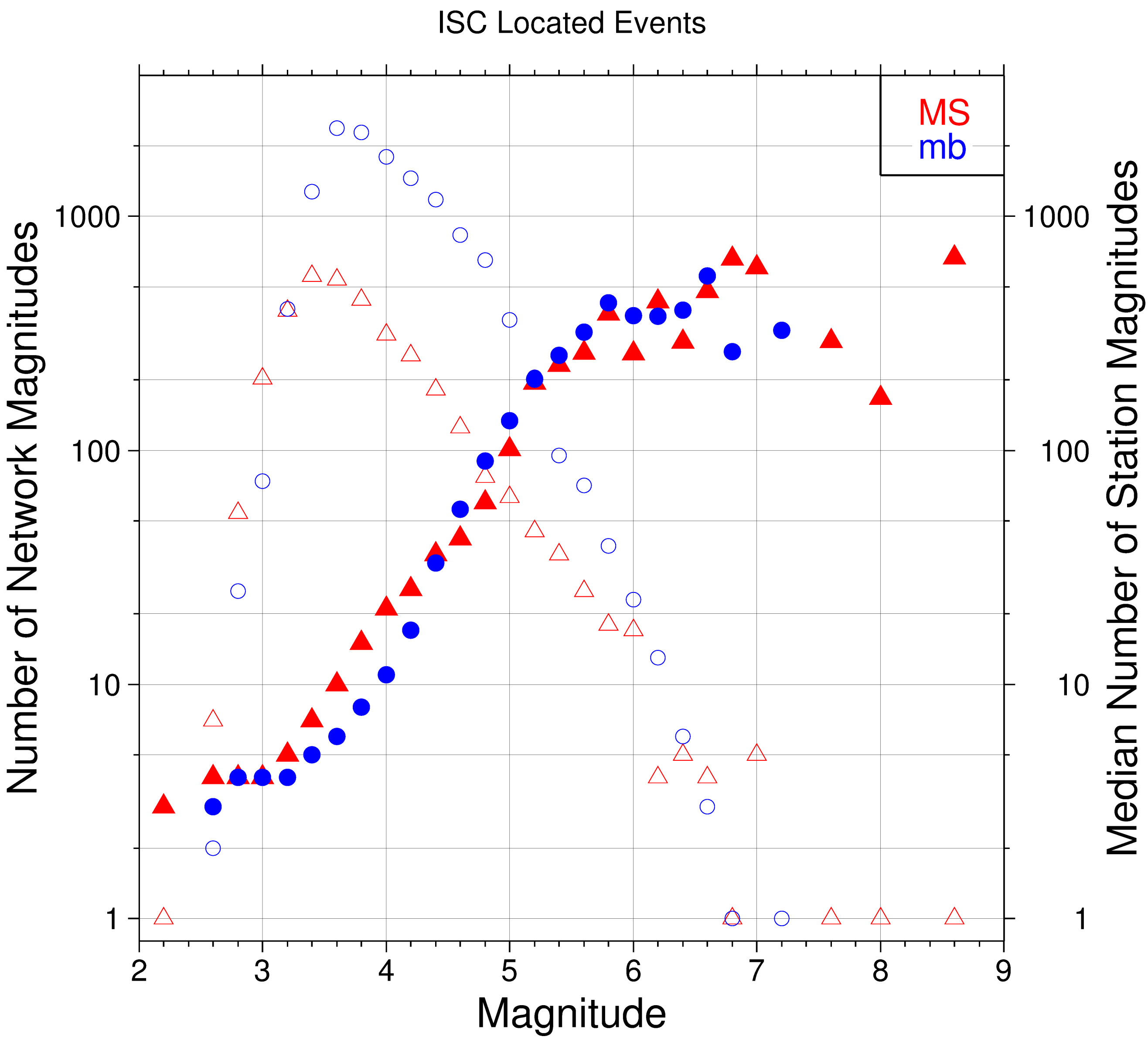

Figure 10.24: *Number of network magnitudes (open symbols) and median number of stations magnitudes (filled symbols). Blue circles refer to mb and red triangles to MS. The width of the magnitude interval δM is 0.2, and each symbol includes data with magnitude in $M \pm \delta M/2$.*

10.4 Completeness of the ISC Bulletin

The completeness of the ISC Bulletin can be expressed as a magnitude value, above which we expect the Bulletin to contain 100% of events. This magnitude of completeness, M_C can be measured as the point where the seismicity no longer follows the Gutenberg-Richter relationship. We compute an estimate of M_C using the maximum curvature technique of *Woessner and Wiemer* (2005).

The completeness of the ISC Bulletin for this summary period is shown in Figure 10.25. A history of completeness for the ISC Bulletin is shown in Figure 10.26. The step change in 1996 corresponds with the inclusion of the Prototype IDC (EIDC) Bulletin, followed by the Reviewed Event Bulletin (REB) of the IDC.

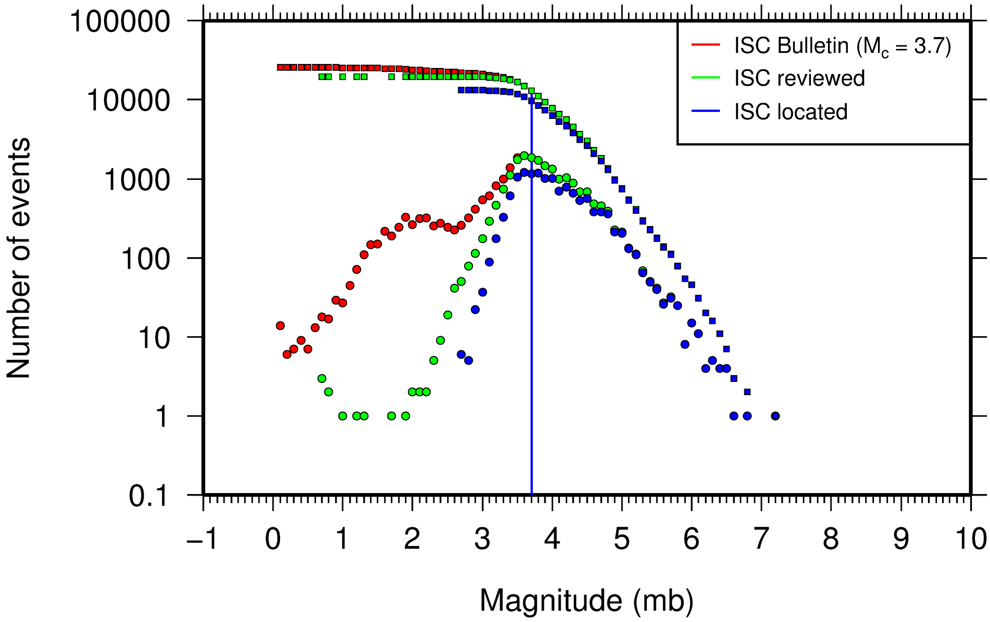

Figure 10.25: *Frequency and cumulative frequency magnitude distribution for all events in the ISC Bulletin, ISC reviewed events and events located by the ISC. The magnitude of completeness (M_C) is shown for the ISC Bulletin. Note: only events with values of mb are represented in the figure.*

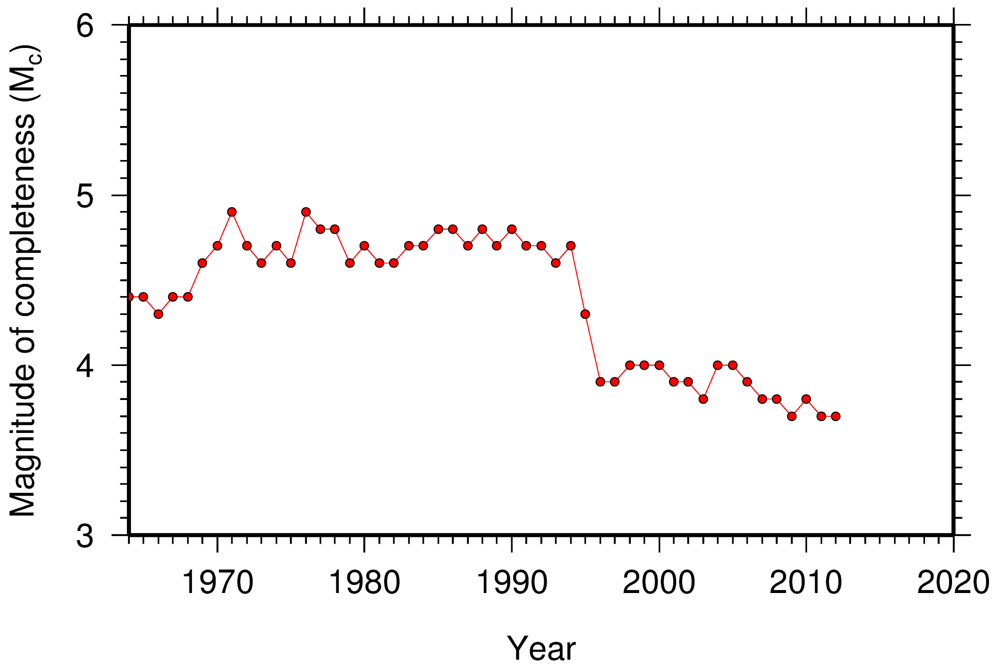

Figure 10.26: *Variation of magnitude of completeness (M_C) for each year in the ISC Bulletin. Note: M_C is calculated only using those events with values of mb.*

10.5 Magnitude Comparisons

The ISC Bulletin publishes network magnitudes reported by multiple agencies to the ISC. For events that have been located by the ISC, where enough amplitude data has been collected, the MS and mb magnitudes are calculated by the ISC (MS is computed only for depths $\leq$ 60 km). In this section, ISC magnitudes and some other reported magnitudes in the ISC Bulletin are compared.

The comparison between MS and mb computed by the ISC locator for events in this summary period is shown in Figure 10.27, where the large number of data pairs allows a colour coding of the data density. The scatter in the data reflects the fundamental differences between these magnitude scales.

Similar plots are shown in Figure 10.28 and 10.29, respectively, for comparisons of ISC mb and ISC MS with M_W from the GCMT catalogue. Since M_W is not often available below magnitude 5, these distributions are mostly for larger, global events. Not surprisingly, the scatter between mb and M_W is larger than the scatter between MS and M_W. Also, the saturation effect of mb is clearly visible for earthquakes with $M_W > 6.5$. In contrast, MS scales well with $M_W > 6$, whereas for smaller magnitudes MS appears to be systematically smaller than M_W.

In Figure 10.30 ISC values of mb are compared with all reported values of mb, values of mb reported by NEIC and values of mb reported by IDC. Similarly in Figure 10.31, ISC values of MS are compared with all reported values of MS, values of MS reported by NEIC and values of MS reported by IDC. There is a large scatter between the ISC magnitudes and the mb and MS reported by all other agencies.

The scatter decreases both for mb and MS when ISC magnitudes are compared just with NEIC and IDC magnitudes. This is not surprising as the latter two agencies provide most of the amplitudes and periods used by the ISC locator to compute MS and mb. However, ISC mb appears to be smaller than NEIC mb for $mb < 4$ and larger than IDC mb for $mb > 4$. Since NEIC does not include IDC amplitudes, it seems these features originate from observations at the high-gain, low-noise sites reported by the IDC. For the MS comparisons between ISC and NEIC a similar but smaller effect is observed for $MS < 4.5$, whereas a good scaling is generally observed for the MS comparisons between ISC and IDC.

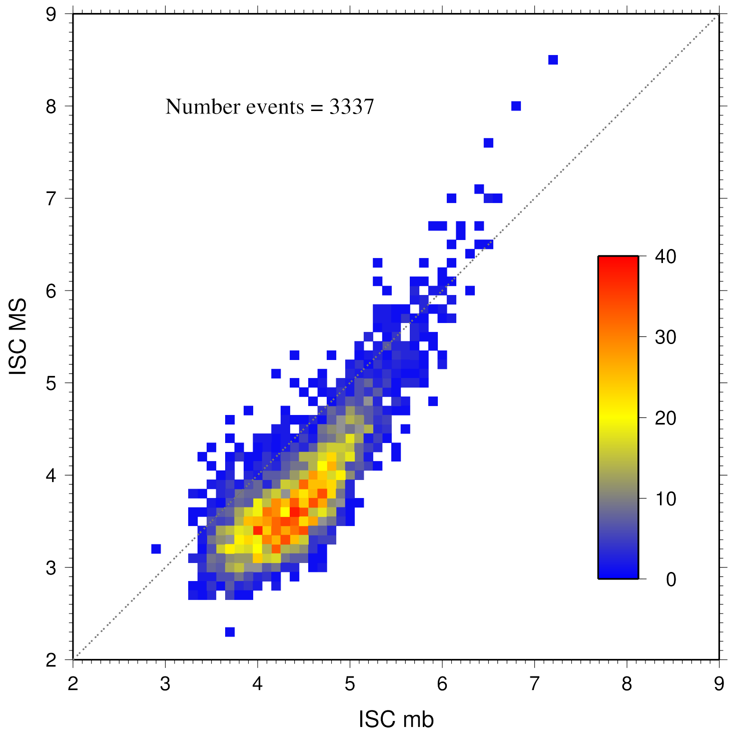

Figure 10.27: *Comparison of ISC values of MS with mb for common event pairs.*

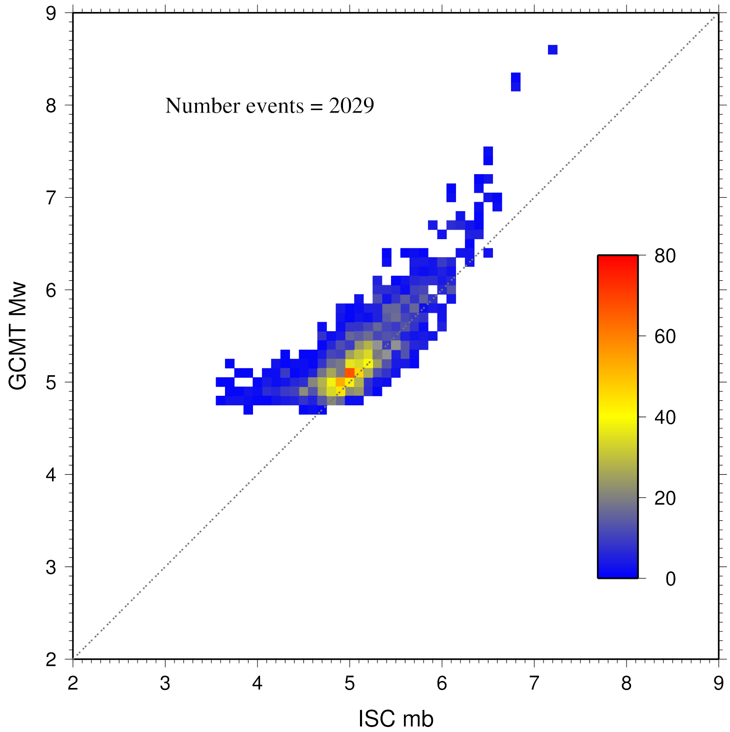

Figure 10.28: *Comparison of ISC values of mb with GCMT M_W for common event pairs.*

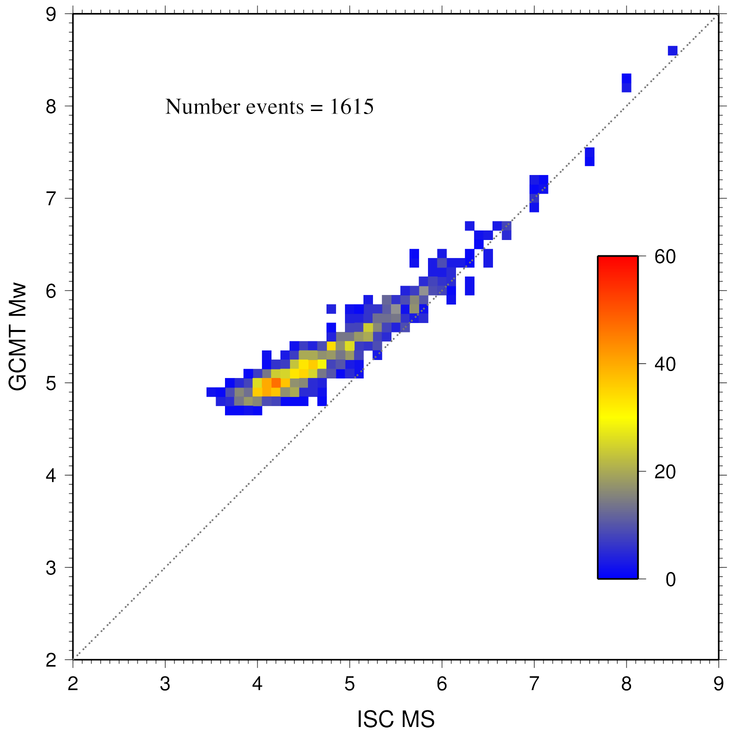

Figure 10.29: *Comparison of ISC values of MS with GCMT M_W for common event pairs.*

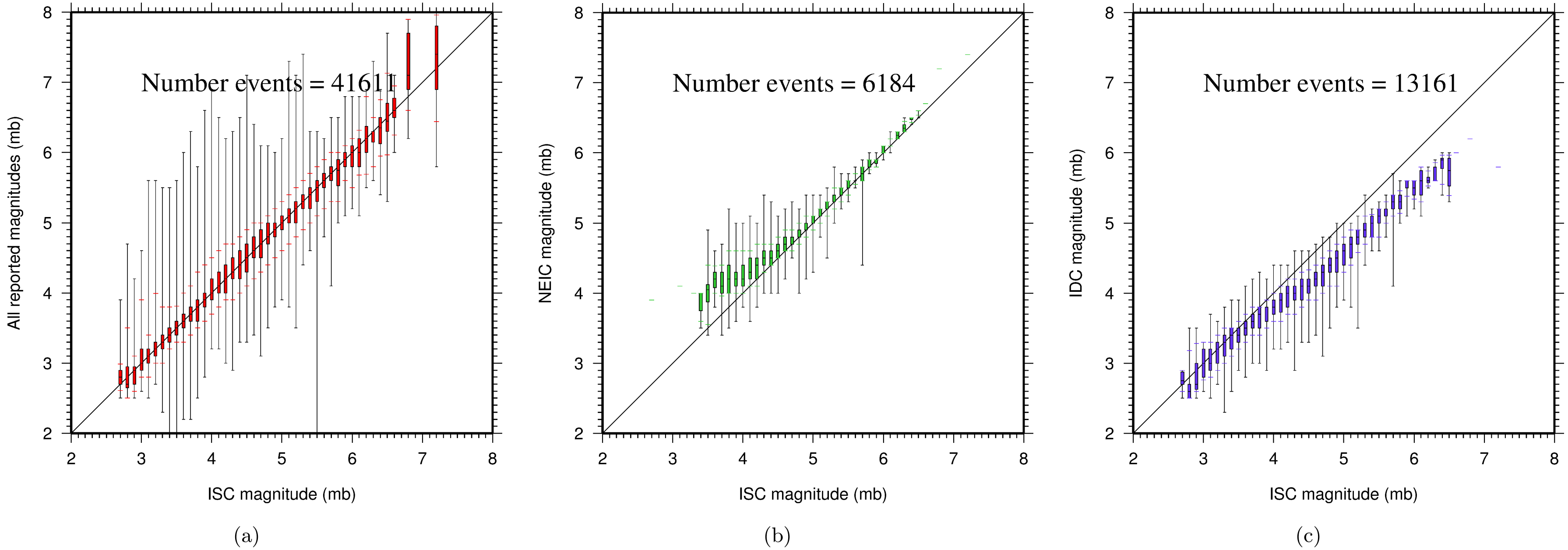

Figure 10.30: *Comparison of ISC magnitude data (mb) with additional agency magnitudes (mb). The statistical summary is shown in box-and-whisker plots where the 10th and 90th percentiles are shown in addition to the max and min values. (a): All magnitudes reported; (b): NEIC magnitudes; (c): IDC magnitudes.*

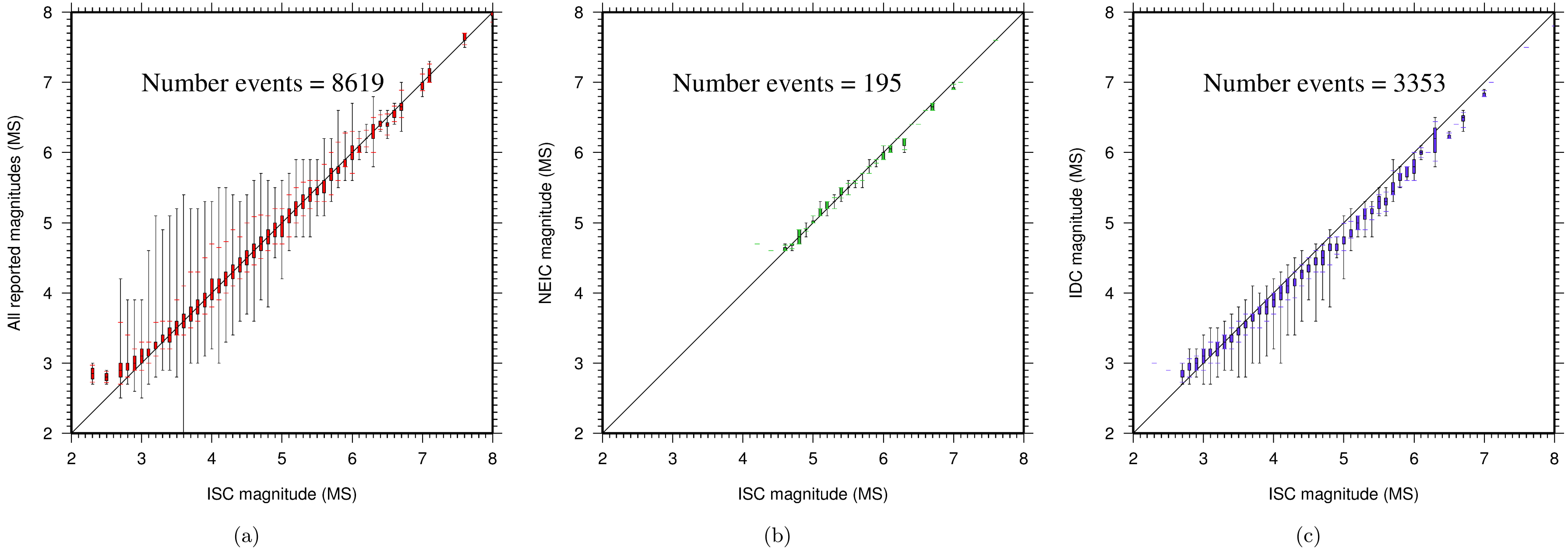

Figure 10.31: *Comparison of ISC magnitude data (MS) with additional agency magnitudes (MS). The statistical summary is shown in the box-and-whisker plots where the 10th and 90th percentiles are shown in addition to the max and min values. (a): All magnitudes reported; (b): NEIC magnitudes; (c): IDC magnitudes.*

11

The Leading Data Contributors

For the current six-month period, 137 agencies reported related bulletin data. Although we are grateful for every report, we nevertheless would like to acknowledge those agencies that made the most useful or distinct contributions to the contents of the ISC Bulletin. Here we note those agencies that:

- provided a comparatively large volume of parametric data (see Section 11.1),
- reported data that helped quite considerably to improve the quality of the ISC locations or magnitude determinations (see Section 11.2),
- helped the ISC by consistently reporting data in one of the standard recognised formats and in-line with the ISC data collection schedule (see Section 11.3).

We do not aim to discourage those numerous small networks who provide comparatively smaller yet still most essential volumes of regional data regularly, consistently and accurately. Without these reports the ISC Bulletin would not be as comprehensive and complete as it is today.

11.1 The Largest Data Contributors

We acknowledge the contribution of NEIC, IDC, MOS, BJI, PRU, USArray, IEPN, CLL, GCMT and a few others (Figure 11.1) that reported the majority of moderate to large events recorded at teleseismic distances. The contributions of IDC, JMA, CSEM, NEIC, DJA, MEX and NNC and several others are also acknowledged with respect to smaller seismic events. The contributions of JMA, CSEM, TAP, DDA, ATH, ISK and ROM and a number of others are also acknowledged with respect to small seismic events. Note that the NEIC bulletin accumulates a contribution of all regional networks in the USA. Similarly, the CSEM communicates contributions of many tens of European and Mediterranean networks a few of which the ISC does not always receive directly. Several agencies monitoring highly seismic regions routinely report large volumes of small to moderate magnitude events, such as those in Japan, Chinese Taipei, Turkey, Chile, Italy, Greece, New Zealand, Norway, Mexico and Columbia. Contributions of small magnitude events by agencies in regions of low seismicity, such as Finland and Saudia Arabia are also gratefully received.

We also would like to acknowledge contributions of those agencies that report a large portion of arrival time and amplitude data (Figure 11.2). For small magnitude events, these are local agencies in charge of monitoring local and regional seismicity. For moderate to large events, contributions of IDC, USArray, NEIC, MOS are especially acknowledged. Notably, three agencies (IDC, NEIC and MOS) together reported approximately 80% of all amplitude measurements made for teleseismically recorded events.

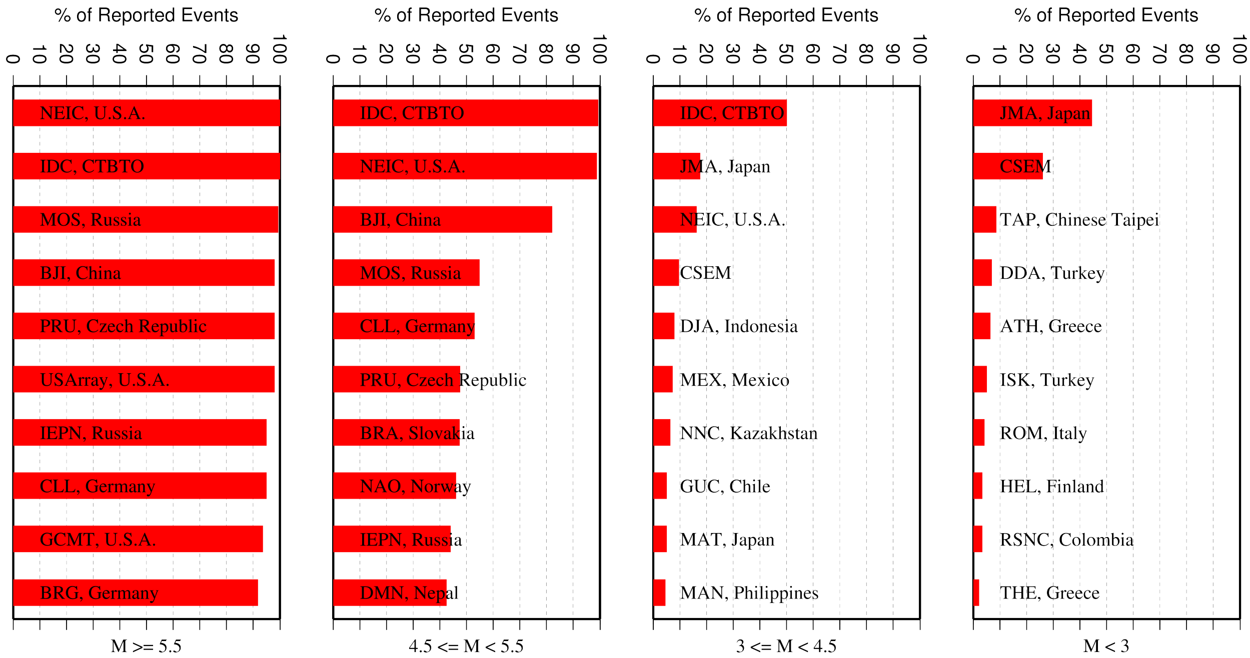

Figure 11.1: *Frequency of events in the ISC Bulletin for which an agency reported at least one item of data: a moment tensor, a hypocentre, a station arrival time or an amplitude. The top ten agencies are shown for four magnitude intervals.*

We hope that other agencies would also be able to update their monitoring routines in the future to include the amplitude reports for teleseismic events compliant with the IASPEI standards.

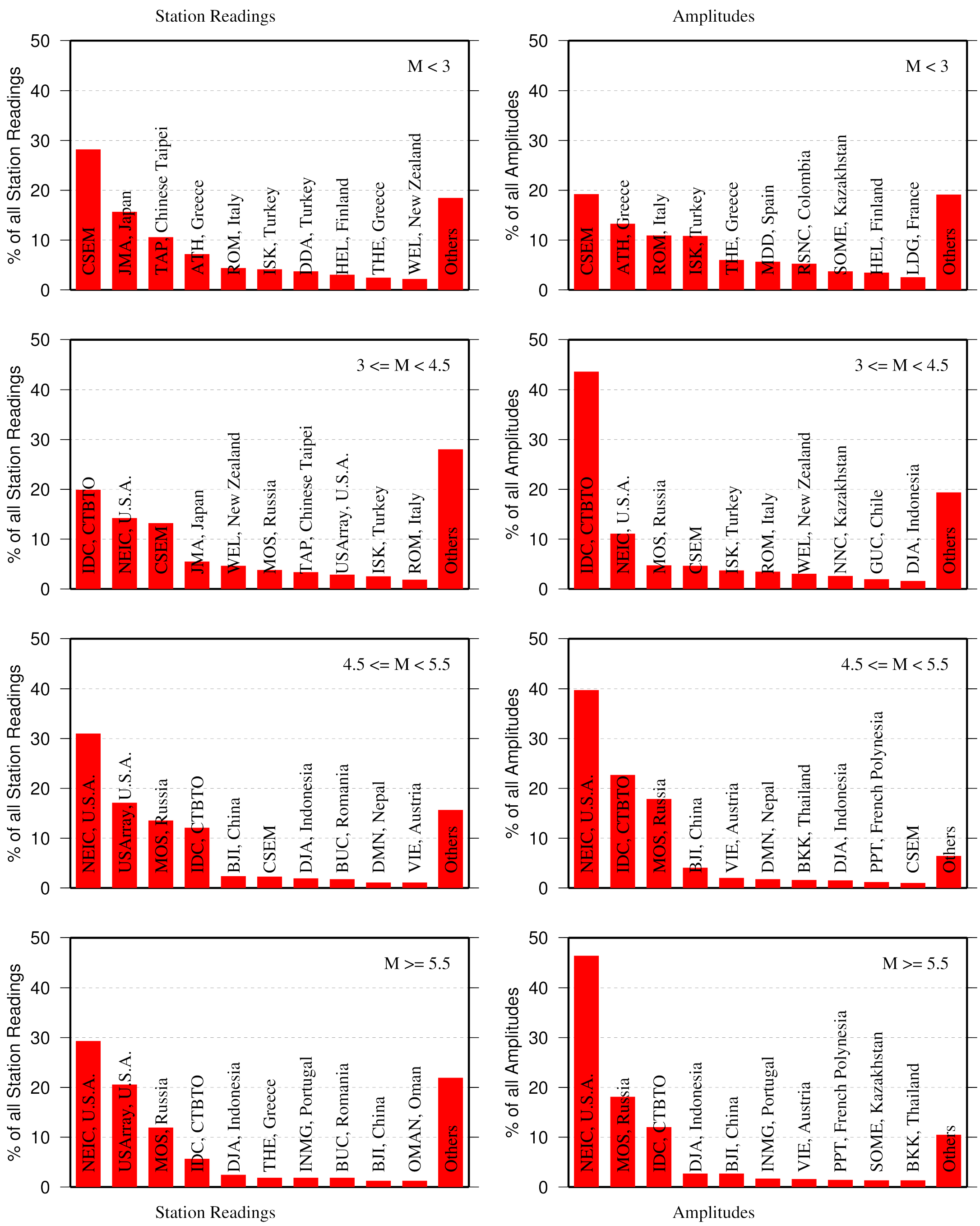

Figure 11.2: *Contributions of station arrival time readings (left) and amplitudes (right) of agencies to the ISC Bulletin. Top ten agencies are shown for four magnitude intervals.*

11.2 Contributors Reporting the Most Valuable Parameters

One of the main ISC duties is to re-calculate hypocentre estimates for those seismic events where a collective wealth of all station reports received from all agencies is likely to improve either the event location or depth compared to the hypocentre solution from each single agency. For areas with a sparse local seismic network or an unfavourable station configuration, readings made by other networks at teleseismic distances are very important. All events near mid-oceanic ridges as well as those in the majority of subduction zones around the world fall into this category. Hence we greatly appreciate the effort made by many agencies that report data for remote earthquakes (Figure 11.3). For some agencies, such as the IDC and the NEIC, it is part of their mission. For instance, the IDC reports almost every seismic event that is large enough to be recorded at teleseismic distance (20 degrees and beyond). This is largely because the International Monitoring System of primary arrays and broadband instruments is distributed at quiet sites around the world in order to be able to detect possible violations of the Comprehensive Nuclear-Test-Ban Treaty. The NEIC reported over 30% of those events as their mission requires them to report events above magnitude 4.5 outside the United States of America. For other agencies reporting distant events it is an extra effort that they undertake to notify their governments and relief agencies as well as to help the ISC and academic research in general. Hence these agencies usually report on the larger magnitude events. BJI, MOS, NAO, CLL, DMN, PRU, BRA and IEPN each reported individual station arrivals for several percent of all relevant events. We encourage other agencies to report distant events to us.

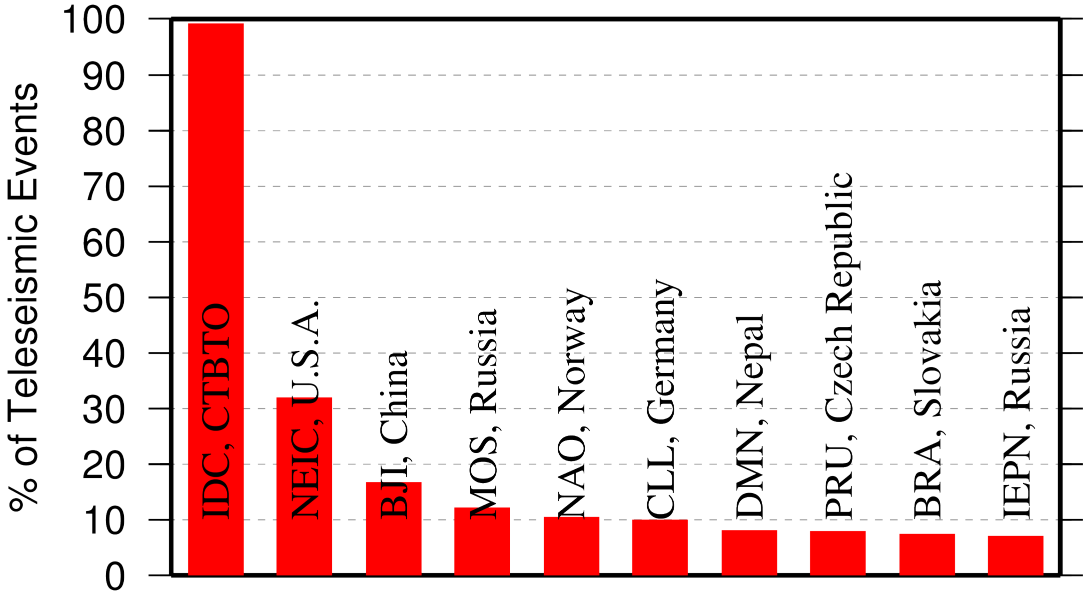

Figure 11.3: *Top ten agencies that reported teleseismic phase arrivals for a large portion of ISC events.*

In addition to the first arriving phase we encourage reporters to contribute observations of secondary seismic phases that help constrain the event location and depth: S, Sn, Sg and pP, sP, PcP (Figure 11.4). We expect though that these observations are actually made from waveforms, rather than just predicted by standard velocity models and modern software programs. It is especially important that these arrivals are manually reviewed by an operator (as we know takes place at the IDC and NEIC), as opposed to some lesser attempts to provide automatic phase readings that are later rejected by the ISC due to a generally poor quality of unreviewed picking.

Another important long-term task that the ISC performs is to compute the most definitive values of MS and mb network magnitudes that are considered reliable due to removal of outliers and consequent averaging (using alpha-trimmed median) across the largest network of stations, generally not feasible for a single agency. Despite concern over the bias at the lower end of mb introduced by the body wave amplitude data from the IDC, other agencies are also known to bias the results. This topic is further discussed in Section 10.5.

Notably, the IDC reports almost 100% of all events for which MS and mb are estimated. This is due to the standard routine that requires determination of body and surface wave magnitudes useful for

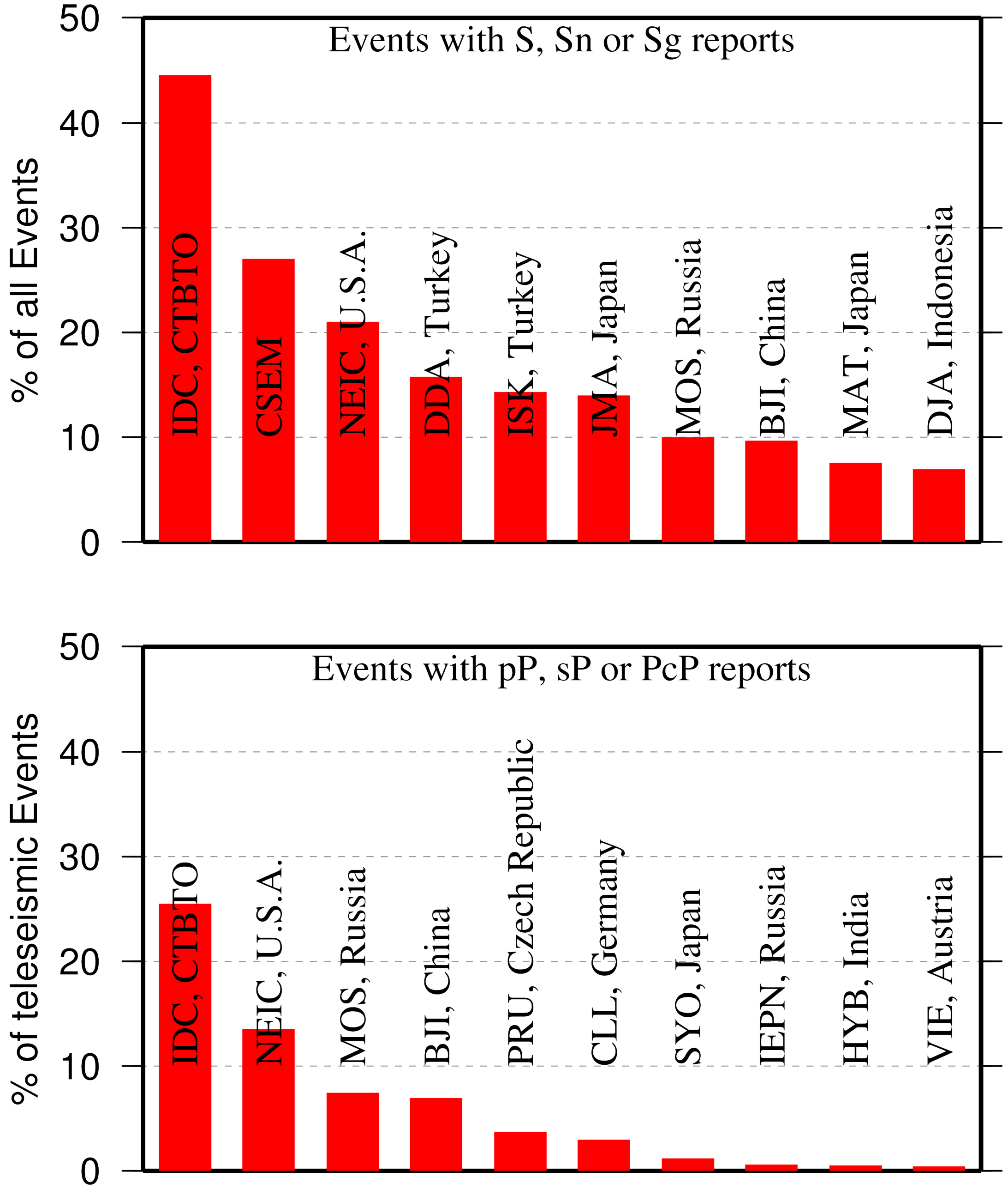

Figure 11.4: *Top ten agencies that reported secondary phases important for an accurate epicentre location (top) and focal depth determination (bottom).*

discrimination purposes. NEIC, MOS, BJI, NAO, PRU and a few other agencies (Figure 11.5) are also responsible for the majority of the amplitude and period reports that contribute towards the ISC magnitudes.

Since the ISC does not routinely process waveforms, we rely on other agencies to report moment magnitudes as well as moment tensor determinations (Figure 11.6).

Among other event parameters the ISC Bulletin also contains information on event type. We cannot independently verify the type of each event in the Bulletin and thus rely on other agencies to report the event type to us. Practices of reporting non-tectonic events vary greatly from country to country. Many agencies do not include anthropogenic events in their reports. Suppression of such events from

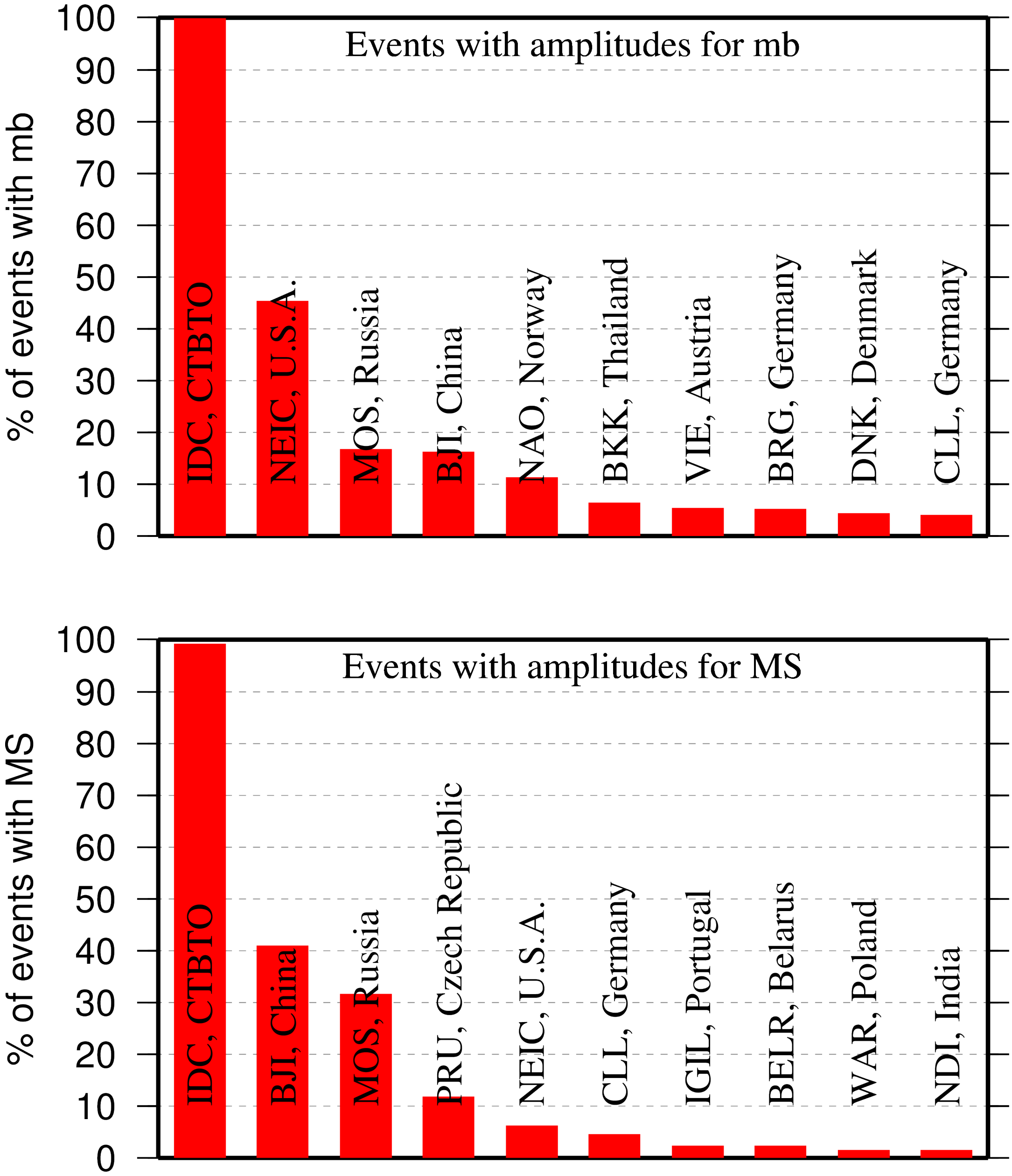

Figure 11.5: *Agencies that report defining body (top) and surface (bottom) wave amplitudes and periods for the largest fraction of those ISC Bulletin events with MS/mb determinations.*

reports to the ISC may lead to a situation where a neighbouring agency reports the anthropogenic event as an earthquake for which expected data are missing. This in turn is detrimental to ISC Bulletin users studying natural seismic hazard. Hence we encourage all agencies to join the agencies listed on Figure 11.7 and several others in reporting both natural and anthropogenic events to the ISC.

The ISC Bulletin also contains felt and damaging information when local agencies have reported it to us. Agencies listed on Figure 11.8 provide such information for the majority of all felt or damaging events in the ISC Bulletin.

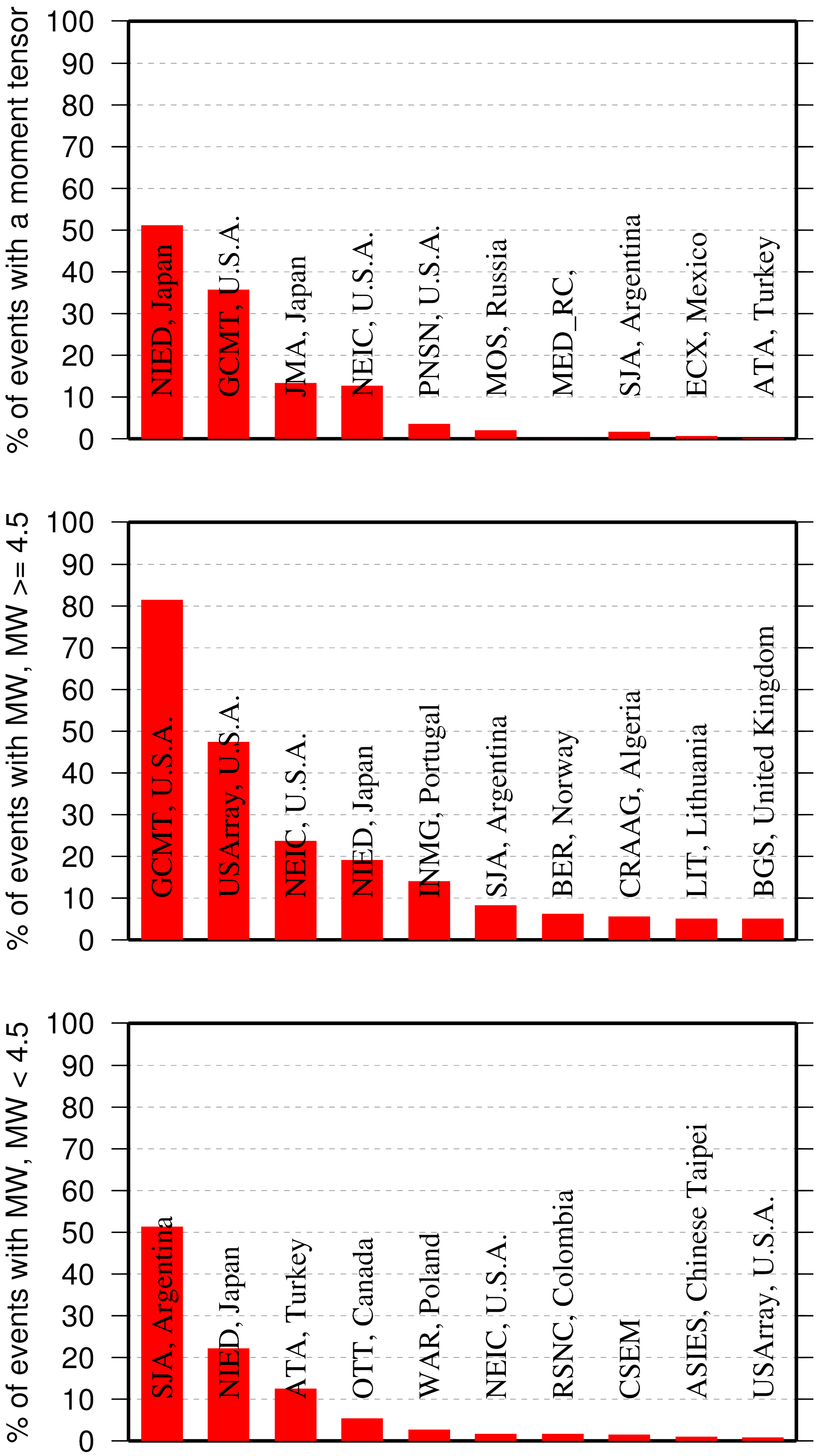

Figure 11.6: *Top ten agencies that most frequently report determinations of seismic moment tensor (top) and moment magnitude (middle/bottom for M greater/smaller than 4.5).*

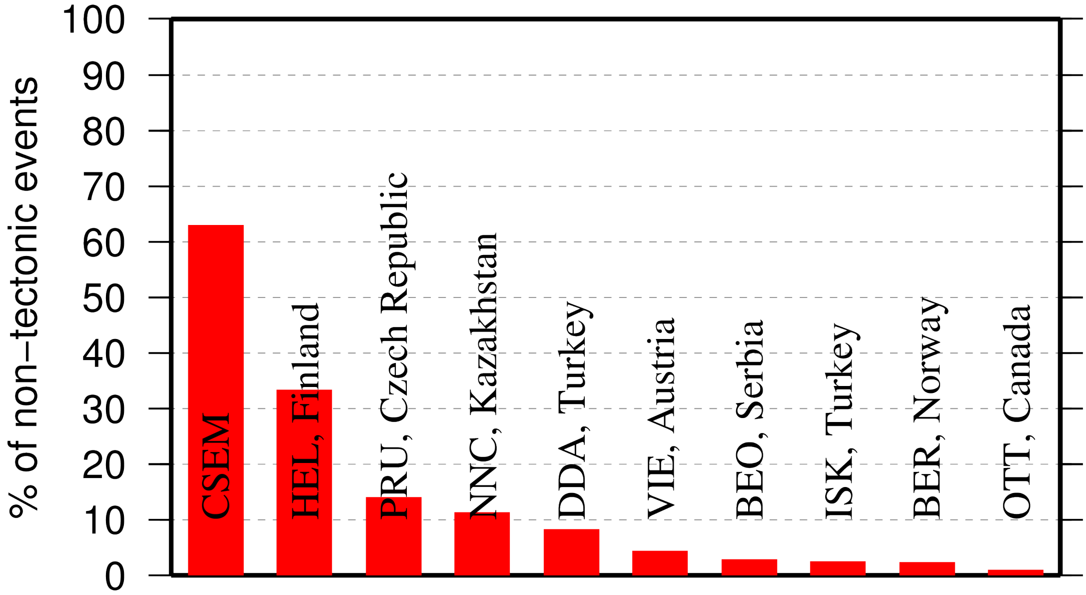

Figure 11.7: *Top ten agencies that most frequently report non-tectonic seismic events to the ISC.*

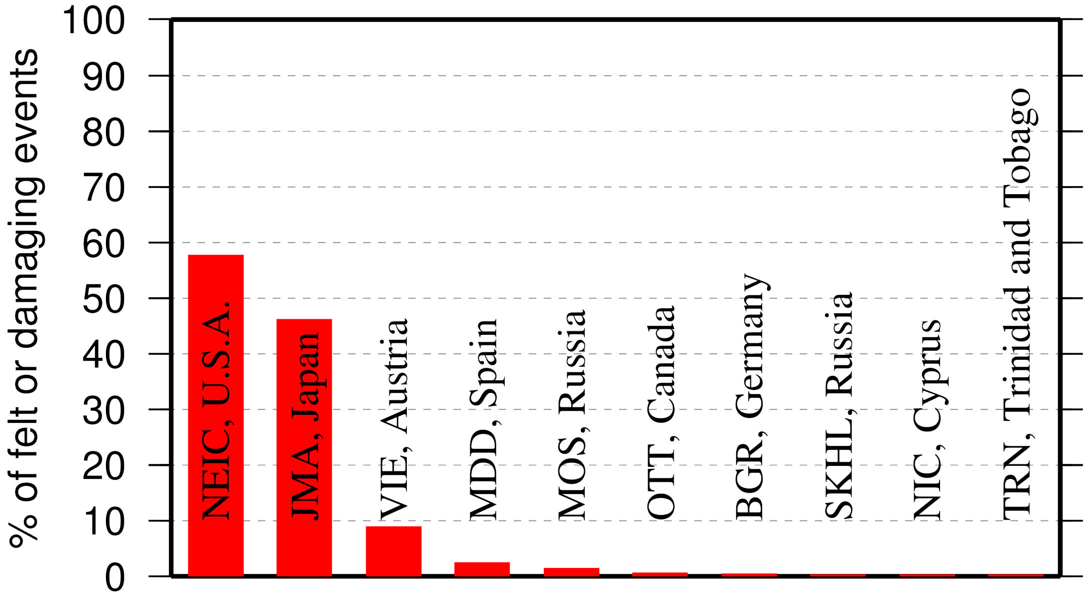

Figure 11.8: *Top ten agencies that most frequently report macroseismic information to the ISC.*

11.3 The Most Consistent and Punctual Contributors

During this six-month period, 36 agencies reported their bulletin data in one of the standard seismic formats (ISF, IMS, GSE, Nordic or QuakeML) and within the current 12-month deadline. Here we must reiterate that the ISC accepts reviewed bulletin data after a final analysis as soon as they are ready. These data, even if they arrive before the deadline, are immediately parsed into the ISC database, grouped with other data and become available to the ISC users on-line as part of the preliminary ISC Bulletin. There is no reason to wait until the deadline to send the data to the ISC. Table 11.1 lists all agencies that have been helpful to the ISC in this respect during the six-month period.

Table 11.1: *Agencies that contributed reviewed bulletin data to the ISC in one of the standard international formats before the submission deadline.*

Agency Code	Country	Average Delay from real time (days)
WEL	New Zealand	1
PPT	French Polynesia	22
NAO	Norway	26
LDG	France	26
LIC	Ivory Coast	32
PDG	Montenegro	33
IGIL	Portugal	34
TIR	Albania	40
KRSC	Russia	46
UCC	Belgium	53
SVSA	Portugal	55
IDC	Austria	55
BUL	Zimbabwe	62
AUST	Australia	82
BJI	China	88
DMN	Nepal	89
BGR	Germany	91
ISK	Turkey	99
BEO	Serbia	120
THE	Greece	147
INMG	Portugal	154
ZUR	Switzerland	167
TEH	Iran	170
BGS	United Kingdom	183
NSSC	Syria	201
ATA	Turkey	235
ISN	Iraq	255
BYKL	Russia	272
IRIS	U.S.A.	276
LIT	Lithuania	292
ASRS	Russia	320
NERS	Russia	328
MOS	Russia	329
ATH	Greece	339
QCP	Philippines	363
BUC	Romania	364

12

Appendix

Table 12.1: *Listing of all 324 agencies that have directly reported to the ISC. The 137 agencies highlighted in bold have reported data to the ISC Bulletin for the period of this Bulletin Summary.*

Agency Code	Agency Name
AAA	Alma-ata, Kazakhstan
AAE	**University of Addis Ababa, Ethiopia**
AAM	University of Michigan, USA
ADE	Primary Industries and Resources SA, Australia
ADH	Observatorio Afonso Chaves, Portugal
AEIC	Alaska Earthquake Information Center, USA
AFAR	The Afar Depression: Interpretation of the 1960-2000 Earthquakes, Israel
ALG	Algiers University, Algeria
ANF	USArray Array Network Facility, USA
ANT	Antofagasta, Chile
ARE	Instituto Geofisico del Peru, Peru
ARO	**Observatoire Géophysique d'Arta, Djibouti**
ASIES	**Institute of Earth Sciences, Academia Sinica, Chinese Taipei**
ASL	Albuquerque Seismological Laboratory, USA
ASM	University of Asmara, Eritrea
ASRS	**Altai-Sayan Seismological Centre, GS SB RAS, Russia**
ATA	**The Earthquake Research Center Ataturk University, Turkey**
ATH	**National Observatory of Athens, Greece**
AUST	**Geoscience Australia, Australia**
AWI	**Alfred Wegener Institute for Polar and Marine Research, Germany**
AZER	**Republic Center of Seismic Survey, Azerbaijan**
BCIS	Bureau Central International de Sismologie, France
BDF	Observatório Sismológico da Universidade de Brasília, Brazil
BELR	**Centre of Geophysical Monitoring, Belarus**
BEO	**Seismological Survey of Serbia, Serbia**
BER	**University of Bergen, Norway**
BERK	Berkheimer H, Germany
BGR	**Bundesanstalt für Geowissenschaften und Rohstoffe, Germany**
BGS	**British Geological Survey, United Kingdom**
BHUJ2	Study of Aftershocks of the Bhuj Earthquake by Japanese Research Team, Japan
BIAK	Biak earthquake aftershocks (17-Feb-1996), USA
BJI	**China Earthquake Networks Center, China**
BKK	**Thai Meteorological Department, Thailand**
BNS	Erdbebenstation, Geologisches Institut der Universität, Köl, Germany
BOG	Universidad Javeriana, Colombia
BRA	**Geophysical Institute, Slovak Academy of Sciences, Slovakia**

Table 12.1: Continued.

Agency Code	Agency Name
BRG	**Seismological Observatory Berggießhübel, TU Bergakademie Freiberg**, **Germany**
BRK	Berkeley Seismological Laboratory, USA
BRS	Brisbane Seismograph Station, Australia
BUC	**National Institute for Earth Physics**, **Romania**
BUD	**Geodetic and Geophysical Research Institute**, **Hungary**
BUG	Institute of Geology, Mineralogy & Geophysics, Germany
BUL	**Goetz Observatory**, **Zimbabwe**
BUT	Montana Bureau of Mines and Geology, USA
BYKL	**Baykal Regional Seismological Centre, GS SB RAS**, **Russia**
CADCG	Central America Data Centre, Costa Rica
CAN	Australian National University, Australia
CANSK	Canadian and Scandinavian Networks, Sweden
CAR	Instituto Sismologico de Caracas, Venezuela
CASC	Central American Seismic Center, Costa Rica
CERI	Center for Earthquake Research and Information, USA
CLL	**Geophysikalisches Observatorium Collm**, **Germany**
CMWS	Laboratory of Seismic Monitoring of Caucasus Mineral Water Region, GSRAS, Russia
CNG	Seismographic Station Changalane, Mozambique
CNRM	Centre National de Recherche, Morocco
COSMOS	Consortium of Organizations for Strong Motion Observations, USA
CRAAG	**Centre de Recherche en Astronomie, Astrophysique et Géophysique**, **Algeria**
CSC	University of South Carolina, USA
CSEM	**Centre Sismologique Euro-Méditerranéen (CSEM/EMSC)**, **France**
DASA	Defense Atomic Support Agency, USA
DBN	**Koninklijk Nederlands Meteorologisch Instituut**, **Netherlands**
DDA	**Disaster and Emergency Management Presidency**, **Turkey**
DHMR	**Yemen National Seismological Center**, **Yemen**
DIAS	**Dublin Institute for Advanced Studies**, **Ireland**
DJA	**Badan Meteorologi, Klimatologi dan Geofisika**, **Indonesia**
DMN	**Department of Mines and Geology, Ministry of Industry of Nepal**, **Nepal**
DNK	**Geological Survey of Denmark and Greenland**, **Denmark**
DRS	Dagestan Branch, Geophysical Survey, Russian Academy of Sciences, Russia
DSN	**Dubai Seismic Network**, **United Arab Emirates**
DUSS	Damascus University, Syria, Syria
EAF	**East African Network**, **Unknown**
EAGLE	Ethiopia-Afar Geoscientific Lithospheric Experiment, Unknown
EBR	Observatori de l'Ebre, Spain
EBSE	Ethiopian Broadband Seismic Experiment, Unknown
ECX	**Red Sismica del Noroeste de Mexico (RESOM)**, **Mexico**
EFATE	OBS Experiment near Efate, Vanuatu, USA
EHB	Engdahl, van der Hilst and Buland, USA

Table 12.1: *Continued.*

Agency Code	Agency Name
EIDC	Experimental (GSETT3) International Data Center, USA
EKA	Eskdalemuir Array Station, United Kingdom
ENT	Geological Survey and Mines Department, Uganda
EPSI	Reference events computed by the ISC for EPSI project, United Kingdom
ERDA	Energy Research and Development Administration, USA
EST	Geological Survey of Estonia, Estonia
FBR	Fabra Observatory, Spain
FDF	Fort de France, Martinique
FIA0	Finessa Array, Finland
FOR	Unknown Historical Agency, Unknown - historical agency
FUNV	Fundación Venezolana de Investigaciones Sismológicas, Venezuela
FUR	Geophysikalisches Observatorium der Universität München, Germany
GBZT	Marmara Research Center, Turkey
GCG	INSIVUMEH, Guatemala
GCMT	**The Global CMT Project**, **USA**
GDNRW	Geologischer Dienst Nordrhein-Westfalen, Germany
GEN	Dipartimento per lo Studio del Territorio e delle sue Risorse (RSNI), Italy
GFZ	Helmholtz Centre Potsdam GFZ German Research Centre For Geosciences, Germany
GII	**The Geophysical Institute of Israel**, **Israel**
GOM	**Observatoire Volcanologique de Goma**, **Democratic Republic of the Congo**
GRAL	**National Council for Scientific Research**, **Lebanon**
GSDM	**Geological Survey Department Malawi**, **Malawi**
GTFE	German Task Force for Earthquakes, Germany
GUC	**Departamento de Geofísica, Universidad de Chile**, **Chile**
HAN	Hannover, Germany
HDC	Observatorio Vulcanológico y Sismológico de Costa Rica, Costa Rica
HEL	**Institute of Seismology, University of Helsinki**, **Finland**
HFS	Hagfors Observatory, Sweden
HFS1	Hagfors Observatory, Sweden
HFS2	Hagfors Observatory, Sweden
HKC	**Hong Kong Observatory**, **Hong Kong**
HLUG	Hessisches Landesamt für Umwelt und Geologie, Germany
HLW	**National Research Institute of Astronomy and Geophysics**, **Egypt**
HNR	**Ministry of Mines, Energy and Rural Electrification**, **Solomon Islands**
HON	Pacific Tsunami Warning Center - NOAA, USA
HRVD	Harvard University, USA
HRVD_LR	Department of Geological Sciences, Harvard University, USA
HVO	Hawaiian Volcano Observatory, USA
HYB	**National Geophysical Research Institute**, **India**
HYD	National Geophysical Research Institute, India
IAG	Instituto Andaluz de Geofisica, Spain
IASPEI	**IASPEI Working Group on Reference Events**, **USA**

Table 12.1: *Continued.*

Agency Code	Agency Name
ICE	Instituto Costarricense de Electricidad, Costa Rica
IDC	**International Data Centre, CTBTO**, **Austria**
IDG	Institute of Dynamics of Geosphere, Russian Academy of Sciences, Russia
IEPN	**Institute of Environmental Problems of the North, Russian Academy of Sciences**, **Russia**
IGIL	**Instituto Geofisico do Infante Dom Luiz**, **Portugal**
IGQ	**Servicio Nacional de Sismología y Vulcanología**, **Ecuador**
IGS	Institute of Geological Sciences, United Kingdom
INDEPTH3	International Deep Profiling of Tibet and the Himalayas, USA
INET	Instituto Nicaragüense de Estudios Territoriales, Nicaragua
INMG	**Instituto Português do Mar e da Atmosfera, I.P.**, **Portugal**
IPEC	**The Institute of Physics of the Earth (IPEC)**, **Czech Republic**
IPER	Institute of Physics of the Earth, Academy of Sciences, Moscow, Russia
IPGP	Institut de Physique du Globe de Paris, France
IPRG	Institute for Petroleum Research and Geophysics, Israel
IRIS	**IRIS Data Management Center**, **USA**
IRSM	Institute of Rock Structure and Mechanics, Czech Republic
ISK	**Kandilli Observatory and Research Institute**, **Turkey**
ISN	**Iraqi Meteorological and Seismology Organisation**, **Iraq**
ISS	International Seismological Summary, United Kingdom
IST	Institute of Physics of the Earth, Technical University of Istanbul, Turkey
JEN	Geodynamisches Observatorium Moxa, Germany
JMA	**Japan Meteorological Agency**, **Japan**
JOH	Bernard Price Institute of Geophysics, South Africa
JSN	**Jamaica Seismic Network**, **Jamaica**
JSO	**Jordan Seismological Observatory**, **Jordan**
KBC	Institut de Recherches Géologiques et Minières, Cameroon
KEW	Kew Observatory, United Kingdom
KHC	Geofysikalni Ustav, Ceske Akademie Ved, Czech Republic
KISR	Kuwait Institute for Scientific Research, Kuwait
KLM	**Malaysian Meteorological Service**, **Malaysia**
KMA	**Korea Meteorological Administration**, **Republic of Korea**
KNET	**Kyrgyz Seismic Network**, **Kyrgyzstan**
KOLA	**Kola Regional Seismic Centre, GS RAS**, **Russia**
KRAR	Krasnoyarsk Scientific Research Inst. of Geology and Mineral Resources, Russia, Russia
KRL	Geodätisches Institut der Universität Karlsruhe, Germany
KRNET	**Institute of Seismology, Academy of Sciences of Kyrgyz Republic**, **Kyrgyzstan**
KRSC	**Kamchatkan Experimental and Methodical Seismological Department, GS RAS**, **Russia**
KSA	Observatoire de Ksara, Lebanon
KUK	Geological Survey Department of Ghana, Ghana
LAO	Large Aperture Seismic Array, USA
LDG	**Laboratoire de Détection et de Géophysique/CEA**, **France**
LDN	University of Western Ontario, Canada

Table 12.1: Continued.

Agency Code	Agency Name
LDO	Lamont-Doherty Earth Observatory, USA
LED	Landeserdbebendienst Baden-Württemberg, Germany
LEDBW	Landeserdbebendienst Baden-Württemberg, Germany
LER	Besucherbergwerk Binweide Station, Germany
LIB	Tripoli, Libya
LIC	**Station Géophysique de Lamto**, **Ivory Coast**
LIM	Lima, Peru
LIS	Instituto de Meteorologia, Portugal
LIT	**Geological Survey of Lithuania**, **Lithuania**
LJU	**Environmental Agency of the Republic of Slovenia**, **Slovenia**
LPA	**Universidad Nacional de La Plata**, **Argentina**
LSZ	**Geological Survey Department of Zambia**, **Zambia**
LVSN	Latvian Seismic Network, Latvia
MAN	**Philippine Institute of Volcanology and Seismology**, **Philippines**
MAT	**The Matsushiro Seismological Observatory**, **Japan**
MCO	**Macao Meteorological and Geophysical Bureau, Macao, China**
MDD	**Instituto Geográfico Nacional**, **Spain**
MED_RCMT	**MedNet Regional Centroid - Moment Tensors**, **Italy**
MES	Messina Seismological Observatory, Italy
MEX	**Instituto de Geofísica de la UNAM**, **Mexico**
MIRAS	**Mining Institute of the Ural Branch of the Russian Academy of Sciences**, **Russia**
MOLD	**Institute of Geophysics and Geology**, **Moldova**
MOS	**Geophysical Survey of Russian Academy of Sciences**, **Russia**
MOZ	Direccao Nacional de Geologia, Mozambique
MRB	**Institut Cartogràfic de Catalunya**, **Spain**
MSI	Messina Seismological Observatory, Italy
MSSP	**Micro Seismic Studies Programme, PINSTECH**, **Pakistan**
MUN	Mundaring Observatory, Australia
NAI	University of Nairobi, Kenya
NAM	**The Geological Survey of Namibia**, **Namibia**
NAO	**Stiftelsen NORSAR**, **Norway**
NCEDC	Northern California Earthquake Data Center, USA
NDI	**India Meteorological Department**, **India**
NEIC	**National Earthquake Information Center**, **USA**
NEIS	National Earthquake Information Service, USA
NERS	**North Eastern Regional Seismological Centre, GS RAS**, **Russia**
NIC	**Cyprus Geological Survey Department**, **Cyprus**
NIED	**National Research Institute for Earth Science and Disaster Prevention**, **Japan**
NNC	**National Nuclear Center**, **Kazakhstan**
NORS	North Ossetia (Alania) Branch, Geophysical Survey, Russian Academy of Sciences, Russia
NOU	IRD Centre de Nouméa, New Caledonia
NSSC	**National Syrian Seismological Center**, **Syria**
NSSP	**National Survey of Seismic Protection**, **Armenia**
OBM	**Research Centre of Astronomy and Geophysics**, **Mongolia**

Table 12.1: Continued.

Agency Code	Agency Name
OGSO	Ohio Geological Survey, USA
OMAN	**Sultan Qaboos University**, **Oman**
ORF	Orfeus Data Center, Netherlands
OSUB	Osservatorio Sismologico Universita di Bari, Italy
OTT	**Canadian Hazards Information Service, Natural Resources Canada**, **Canada**
PAL	Palisades, USA
PAS	California Institute of Technology, USA
PDA	Universidade dos Açores, Portugal
PDG	**Seismological Institute of Montenegro**, **Montenegro**
PEK	Peking, China
PGC	Pacific Geoscience Centre, Canada
PLV	**National Center for Scientific Research**, **Vietnam**
PMEL	Pacific seismicity from hydrophones, USA
PMR	Alaska Tsunami Warning Center,, USA
PNSN	**Pacific Northwest Seismic Network**, **USA**
PPT	**Laboratoire de Géophysique/CEA**, **French Polynesia**
PRE	**Council for Geoscience**, **South Africa**
PRU	**Geophysical Institute, Academy of Sciences of the Czech Republic**, **Czech Republic**
PTO	Instituto Geofísico da Universidade do Porto, Portugal
PTWC	Pacific Tsunami Warning Center, USA
QCP	**Manila Observatory**, **Philippines**
QUE	Pakistan Meteorological Department, Pakistan
QUI	Escuela Politécnica Nacional, Ecuador
RAB	Rabaul Volcanological Observatory, Papua New Guinea
RBA	Université Mohammed V, Morocco
REN	MacKay School of Mines, USA
REY	**Icelandic Meteorological Office**, **Iceland**
RISSC	Laboratory of Research on Experimental and Computational Seimology, Italy
RMIT	Royal Melbourne Institute of Technology, Australia
ROC	Odenbach Seismic Observatory, USA
ROM	**Istituto Nazionale di Geofisica e Vulcanologia**, **Italy**
RRLJ	Regional Research Laboratory Jorhat, India
RSMAC	Red Sísmica Mexicana de Apertura Continental, Mexico
RSNC	**Red Sismológica Nacional de Colombia**, **Colombia**
RSPR	**Red Sísmica de Puerto Rico**, **USA**
RYD	King Saud University, Saudi Arabia
SAPSE	Southern Alps Passive Seismic Experiment, New Zealand
SAR	Sarajevo Seismological Station, Bosnia and Herzegovina
SCB	**Observatorio San Calixto**, **Bolivia**
SCEDC	Southern California Earthquake Data Center, USA
SDD	Universidad Autonoma de Santo Domingo, Dominican Republic
SEA	Geophysics Program AK-50, USA
SEPA	Seismic Experiment in Patagonia and Antarctica, USA
SET	Setif Observatory, Algeria

Table 12.1: *Continued.*

Agency Code	Agency Name
SFS	Real Instituto y Observatorio de la Armada, Spain
SGS	**Saudi Geological Survey**, **Saudi Arabia**
SHL	Central Seismological Observatory, India
SIGU	**Subbotin Institute of Geophysics, National Academy of Sciences**, **Ukraine**
SIK	Seismic Institute of Kosovo, Unknown
SIO	Scripps Institution of Oceanography, USA
SJA	**Instituto Nacional de Prevención Sísmica**, **Argentina**
SJS	Instituto Costarricense de Electricidad, Costa Rica
SKHL	**Sakhalin Experimental and Methodological Seismological Expedition, GS RAS**, **Russia**
SKL	Sakhalin Complex Scientific Research Institute, Russia
SKO	**Seismological Observatory Skopje**, **FYR Macedonia**
SLC	Salt Lake City, USA
SLM	Saint Louis University, USA
SNET	Servicio Nacional de Estudios Territoriales, El Salvador
SNM	New Mexico Institute of Mining and Technology, USA
SNSN	Saudi National Seismic Network, Saudi Arabia
SOF	**Geophysical Institute, Bulgarian Academy of Sciences**, **Bulgaria**
SOME	**Seismological Experimental Methodological Expedition**, **Kazakhstan**
SPA	USGS - South Pole, Antarctica
SPGM	Service de Physique du Globe, Morocco
SRI	Stanford Research Institute, USA
SSN	Sudan Seismic Network, Sudan
SSNC	Servicio Sismológico Nacional Cubano, Cuba
SSS	Centro de Estudios y Investigaciones Geotecnicas del San Salvador, El Salvador
STK	Stockholm Seismological Station, Sweden
STR	**Institut de Physique du Globe**, **France**
STU	Stuttgart Seismological Station, Germany
SVSA	**Sistema de Vigilância Sismológica dos Açores**, **Portugal**
SYO	**National Institute of Polar Research**, **Japan**
SZGRF	Seismologisches Zentralobservatorium Gräfenberg, Germany
TAC	Estación Central de Tacubaya, Mexico
TAN	Antananarivo, Madagascar
TANZANIA	Tanzania Broadband Seismic Experiment, USA
TAP	**CWB**, **Chinese Taipei**
TAU	University of Tasmania, Australia
TEH	**Tehran University**, **Iran**
TEIC	Center for Earthquake Research and Information, USA
THE	**Department of Geophysics, Aristotle University of Thessaloniki**, **Greece**
THR	**International Institute of Earthquake Engineering and Seismology (IIEES)**, **Iran**
TIF	**Seismic Monitoring Centre of Georgia**, **Georgia**

Table 12.1: *Continued.*

Agency Code	Agency Name
TIR	**The Institute of Seismology, Academy of Sciences of Albania, Albania**
TRI	**Istituto Nazionale di Oceanografia e di Geofisica Sperimentale (OGS), Italy**
TRN	**University of the West Indies, Trinidad and Tobago**
TTG	Titograd Seismological Station, Montenegro
TUL	Oklahoma Geological Survey, USA
TUN	Institut National de la Météorologie, Tunisia
TVA	Tennessee Valley Authority, USA
TZN	University of Dar Es Salaam, Tanzania
UAV	Red Sismológica de Los Andes Venezolanos, Venezuela
UCC	**Royal Observatory of Belgium, Belgium**
UCR	**Sección de Sismología, Vulcanología y Exploración Geofísica, Costa Rica**
UGN	Institute of Geonics AS CR, Czech Republic
ULE	University of Leeds, United Kingdom
UNAH	Universidad Nacional Autonoma de Honduras, Honduras
UPA	Universidad de Panama, Panama
UPP	**University of Uppsala, Sweden**
UPSL	University of Patras, Department of Geology, Greece
USAEC	United States Atomic Energy Commission, USA
USCGS	United States Coast and Geodetic Survey, USA
USGS	**United States Geological Survey, USA**
UUSS	The University of Utah Seismograph Stations, USA
UVC	Universidad del Valle, Colombia
VAO	**Instituto Astronomico e Geofísico, Brazil**
VIE	**Österreichischer Geophysikalischer Dienst, Austria**
VKMS	Lab. of Seismic Monitoring, Voronezh region, GSRAS & Voronezh State University, Russia
VLA	Vladivostok Seismological Station, Russia
VSI	University of Athens, Greece
WAR	**Institute of Geophysics, Polish Academy of Sciences, Poland**
WBNET	**West Bohemia Seismic Network, Czech Republic**
WEL	**Institute of Geological and Nuclear Sciences, New Zealand**
WES	Weston Observatory, USA
YARS	**Yakutiya Regional Seismological Center, GS SB RAS, Russia**
ZAG	**Seismological Survey of the Republic of Croatia, Croatia**
ZUR	**Swiss Seismological Sevice (SED), Switzerland**
ZUR_RMT	Zurich Moment Tensors, Switzerland

Table 12.2: *Phases reported to the ISC. These include phases that could not be matched to an appropriate* ak135 *phases. Those agencies that reported at least 10% of a particular phase are also shown.*

Reported Phase	Total	Agencies reporting
P	3243026	NEIC (14%), CSEM (13%)
S	1435615	JMA (22%), CSEM (18%), TAP (14%)
Pn	340829	CSEM (36%), NEIC (29%)
AML	313357	ROM (50%), ATH (47%)
Pg	311448	CSEM (54%)
Sg	206745	CSEM (53%)
pmax	189337	MOS (81%), BJI (19%)
LR	172255	IDC (44%), NEIC (26%), BJI (25%)
Sn	122632	CSEM (28%), NEIC (18%), IDC (11%)
PN	91641	ISK (70%), MOS (15%)
PG	91456	ISK (61%), HEL (18%)
NULL	84351	MOS (39%), RSNC (34%)
Lg	81534	CSEM (41%), MDD (26%), NNC (17%)
SG	69150	ISK (41%), HEL (29%), PRU (18%)
PKP	40757	IDC (45%), NEIC (28%)
IAML	34574	GUC (36%), SJA (25%), BER (11%)
PKPdf	31028	NEIC (84%)
PKPbc	30219	NEIC (50%), IDC (40%)
MLR	30078	MOS (100%)
T	28600	IDC (91%)
pP	28436	BJI (35%), NEIC (32%), IDC (15%)
PcP	22262	NEIC (45%), IDC (39%)
PFAKE	21183	NEIC (100%)
PKIKP	20593	MOS (98%)
A	19491	INMG (55%), SVSA (25%), SKHL (21%)
PP	18063	BJI (36%), NEIC (23%), IDC (17%)
SN	17905	HEL (45%), ISK (19%), OTT (16%)
MSG	17041	HEL (100%)
AMB	15762	TEH (68%), SKHL (21%)
smax	12805	MOS (88%), BJI (12%)
PKPab	11600	NEIC (47%), IDC (31%)
Sb	10797	IRIS (56%), CSEM (41%)
SS	10324	BJI (45%), MOS (34%)
sP	9871	BJI (87%)
Pb	9357	IRIS (50%), CSEM (48%)
PKiKP	8716	IRIS (43%), NEIC (20%), IDC (20%), VIE (12%)
x	7572	NDI (65%), PRU (30%)
IAmb	7422	NDI (32%), LIT (23%), BGS (18%), HYB (13%), BER (13%)
PB	7310	HEL (100%)
SB	7170	HEL (100%)
ScP	5998	IDC (46%), NEIC (38%), BJI (14%)
END	5055	ROM (100%)
Smax	4640	YARS (64%), BYKL (36%)
AMS	4516	PRU (81%)
*PP	4373	MOS (100%)
PKKPbc	4334	IDC (52%), NEIC (46%)
PKP2	4227	MOS (96%)
sS	3857	BJI (98%)
Trac	3332	OTT (100%)
Pdiff	3298	IRIS (72%), IDC (18%)
LG	3256	BRA (59%), OTT (35%)
PKPpre	3239	NEIC (98%)
Pmax	3091	YARS (55%), BYKL (42%)
Pdif	2665	NEIC (83%)
LQ	2241	PPT (40%), IEPN (29%), INMG (16%)
PKhKP	2085	IDC (100%)
pPKP	2059	IDC (31%), BJI (27%), NEIC (20%), PRU (18%)
SKPbc	1989	IDC (54%), NEIC (45%)
PKHKP	1924	MOS (100%)
AMP	1788	IEPN (85%)
PPP	1754	MOS (79%)
SKS	1751	BJI (69%), PRU (12%)
X	1681	JMA (80%), SYO (19%)
ScS	1365	BJI (85%)
IAMs_20	1324	BGS (82%), NDI (14%)

Table 12.2: *(continued)*

Reported Phase	Total	Agencies reporting
SSS	1140	MOS (60%), CLL (18%), BELR (11%)
PS	1117	MOS (48%), CLL (11%)
PKKP	1005	IDC (51%), NEIC (38%)
pPKPbc	922	IDC (48%), NEIC (28%), VIE (12%)
LRM	893	MOLD (46%), BELR (39%), SOME (15%)
sPKP	866	BJI (94%)
P*	862	NEIC (61%), BGR (35%)
PKKPab	772	IDC (49%), NEIC (44%)
PKPPKP	769	IDC (96%)
SKKS	763	BJI (80%)
pPKPdf	711	NEIC (54%), VIE (28%)
IVMs_BB	671	HYB (77%), BER (21%)
SKP	657	IDC (39%), NEIC (25%), IRIS (14%), PRU (11%)
PKPAB	642	PRU (100%)
*SP	627	MOS (100%)
P'P'	554	NEIC (100%)
PKS	539	BJI (86%)
PcS	532	BJI (98%)
max	494	BYKL (100%)
SKSac	479	INMG (24%), HYB (23%)
PCP	478	PRU (73%), BRA (13%)
SP	470	MOS (38%), PRU (33%)
*SS	442	MOS (100%)
LMZ	426	WAR (100%)
PKP1	415	LIC (97%)
L	402	BRA (36%), MOLD (24%), DBN (18%), RSNC (12%)
pPKPab	358	NEIC (36%), IDC (25%), CLL (17%), VIE (16%)
SKKPbc	356	IDC (58%), NEIC (37%)
Lm	335	CLL (100%)
S*	309	BGR (68%), NEIC (32%)
LmV	299	CLL (100%)
PDIFF	291	BRA (47%), PRU (40%)
PKP2bc	286	IDC (100%)
Sm	277	SIGU (100%)
Pm	264	SIGU (100%)
AMb	253	IGIL (77%), NDI (13%)
PM	252	BELR (100%)
PPS	229	CLL (55%), MOS (29%)
Rg	224	IDC (30%), NNC (17%), NAO (17%), BER (17%), DBN (16%)
LmH	210	CLL (100%)
PKKPdf	189	NEIC (56%), VIE (18%), BUD (12%)
Sgmax	186	NERS (100%)
(P)	180	BRG (73%), CLL (27%)
IVmB_BB	164	BER (93%)
pPcP	161	IDC (57%), NEIC (41%)
PKPDF	138	PRU (100%)
SKPab	134	IDC (57%), NEIC (39%)
Sgm	133	SIGU (100%)
sPKPdf	130	VIE (87%)
pPKiKP	130	VIE (60%), OMAN (13%)
SKPdf	125	NEIC (52%), VIE (20%)
P3KPbc	122	IDC (100%)
SmS	118	BGR (100%)
RG	116	HEL (100%)
PmP	111	BGR (100%)
m	108	SIGU (100%)
SSSS	102	CLL (98%)
AP	96	UCC (65%), MOS (35%)
pPn	94	OMAN (70%), BUD (22%)
P4KPbc	91	IDC (100%)
Pgmax	85	NERS (100%)
Snm	84	SIGU (100%)
Lmax	81	CLL (100%)
Sdif	79	CLL (41%), NEIC (24%), INMG (22%), PPT (14%)
SN4	79	ISN (100%)
SKKSac	79	CLL (52%), WAR (22%), HYB (14%)
(sP)	75	CLL (100%)

Table 12.2: (continued)

Reported Phase	Total	Agencies reporting
PKP2ab	71	IDC (100%)
P'P'ab	68	NEIC (100%)
SKKP	67	IDC (46%), NEIC (31%), PRU (12%)
IVMsBB	67	HYB (60%), BER (39%)
Pu	61	NEIC (100%)
Pgm	56	SIGU (100%)
P'P'df	55	NEIC (56%), VIE (25%), PPT (18%)
LQM	52	BELR (96%)
PKPdif	52	NEIC (100%)
PN4	51	ISN (100%)
sPKPab	49	VIE (80%)
SH	47	SYO (98%)
sPKiKP	47	VIE (62%), CLL (23%), BUD (15%)
APKP	45	UCC (100%)
pPP	41	LPA (49%), CLL (46%)
R	40	LDG (100%)
mb	40	OTT (100%)
sPKPbc	39	VIE (74%), CLL (13%)
PsP	39	MOLD (67%), BELR (33%)
XP	39	UCC (72%), MOS (28%)
E	37	ZAG (70%), UCC (14%)
sPP	36	CLL (94%)
IVmBBB	36	BER (97%)
(pP)	33	CLL (100%)
MSN	31	HEL (100%)
Sdiff	30	IDC (67%), LJU (33%)
PSKS	30	CLL (100%)
i	30	INMG (100%)
pPdif	30	HYB (70%), CLL (23%)
pPdiff	30	VIE (50%), SYO (47%)
Pnm	29	SIGU (100%)
SN5	29	ISN (100%)
PN5	29	ISN (97%)
PA	26	ATA (54%), JSN (42%)
P3KP	26	IDC (100%)
(PP)	25	CLL (100%)
PN12	25	ATA (100%)
PnPn	24	OMAN (100%)
(SS)	24	CLL (100%)
SKKPdf	23	BUD (83%)
SKiKP	22	IDC (77%), SOME (18%)
PPPP	22	CLL (86%)
SDIFF	22	BRG (73%), LPA (27%)
PKPPKPdf	22	BUD (55%), CLL (45%)
SM	22	BELR (100%)
PKKKP	21	NEIC (100%)
pScP	20	IDC (55%), NEIC (45%)
XS	20	PRU (100%)
(SSS)	20	CLL (100%)
SKSP	20	MOLD (35%), CLL (35%), BELR (15%)
SKSdf	19	WAR (68%), BUD (21%), CLL (11%)
PgPg	19	BYKL (95%)
sSS	18	CLL (100%)
M	18	MOLD (94%)
SCS	18	LPA (39%), NDI (39%), IPEC (17%)
rx	17	SKHL (100%)
P(2)	17	CLL (100%)
sPdif	17	HYB (53%), CLL (41%)
Li	16	MOLD (100%)
PCS	15	NDI (100%)
n	15	LIT (100%)
AMSG	15	SJA (67%), NAM (33%)
LRmax	14	NERS (100%)
AMPG	14	SJA (57%), NAM (43%)
SDIF	14	PRU (93%)
PKKSdf	14	NEIC (86%), CLL (14%)
(SSSS)	13	CLL (100%)

Table 12.2: (continued)

Reported Phase	Total	Agencies reporting
TT	13	NEIC (100%)
PKSdf	13	CLL (92%)
Plp	12	CLL (100%)
PPM	12	BELR (92%)
XSKS	11	PRU (100%)
PKPc	11	WAR (100%)
SKKKS	11	BELR (100%)
PKPM	11	BELR (100%)
SKIKS	11	LPA (100%)
PSS	11	CLL (91%)
SKSp	11	BRA (100%)
SKIKP	11	LPA (100%)
XM	11	MOLD (100%)
P9	11	EAF (100%)
(PKiKP)	11	CLL (100%)
PKPdiff	11	CLL (100%)
PSP	10	LPA (100%)
(Pg)	9	CLL (89%), BJI (11%)
SKKSdf	9	CLL (78%), WAR (22%)
PKIKS	9	LPA (100%)
sPn	9	SKHL (56%), BUD (33%), OMAN (11%)
PKPBC	9	PRU (100%)
SgSg	9	BYKL (100%)
pPg	8	SKHL (88%), BUD (12%)
LV	8	CLL (100%)
SCP	8	BRG (88%), PRU (12%)
sPdiff	8	VIE (50%), SYO (25%), OMAN (12%), IDC (12%)
pwP	8	NEIC (100%)
(pPKPbc)	7	CLL (100%)
PPlp	7	CLL (100%)
APKPbc	7	UCC (100%)
(PcP)	7	CLL (100%)
PPPrev	7	CLL (100%)
del	7	KNET (86%), PGC (14%)
SPP	7	CLL (57%), MOS (43%)
LME	7	WAR (100%)
(Sg)	6	CLL (100%)
APKPab	6	UCC (100%)
H	6	IDC (100%)
PKKS	6	BRG (83%), WAR (17%)
(PKP)	6	CLL (100%)
(PKPdf)	6	CLL (100%)
Sglp	6	CLL (100%)
PGN	6	HEL (100%)
sSSS	5	CLL (100%)
Pdi	5	SKO (100%)
pS	5	BRA (40%), WAR (40%), NEIC (20%)
PKPab(2)	5	CLL (100%)
I	5	SOME (80%), BER (20%)
P4KP	5	IDC (60%), NEIC (40%)
(sPP)	5	CLL (100%)
LMN	5	WAR (100%)
sPg	5	SKHL (80%), OMAN (20%)
sPb	5	BUD (100%)
(PPP)	4	CLL (100%)
S9	4	EAF (100%)
pPDIFF	4	BRG (100%)
Lg1	4	MOLD (100%)
LH	4	CLL (100%)
Lg2	4	MOLD (100%)
sPPP	4	CLL (100%)
(PPS)	4	CLL (100%)
PSPS	4	CLL (100%)
sPS	4	CLL (100%)
SKSSKSac	4	CLL (100%)
PN6	4	ISN (100%)
(PKPab)	4	CLL (100%)

Table 12.2: *(continued)*

Reported Phase	Total	Agencies reporting
PKSbc	4	CLL (100%)
(pPKPab)	4	CLL (100%)
(pPKPdf)	4	CLL (100%)
sPDIFF	4	BRG (100%)
SKKSp	4	BRA (100%)
(S)	4	CLL (100%)
SN6	4	ISN (100%)
sPKKPbc	3	CLL (100%)
sg	3	BUD (100%)
SKKPab	3	IDC (67%), NEIC (33%)
(PSS)	3	CLL (100%)
PGCN	3	NDI (100%)
(pPKiKP)	3	CLL (100%)
(Pdif)	3	CLL (100%)
sSKSac	3	CLL (100%)
sSSSS	3	CLL (100%)
SN12	3	ATA (100%)
pPKP1	3	BELR (100%)
s	3	MAN (67%), GOM (33%)
(PKPbc)	3	CLL (100%)
SMZ	3	BJI (100%)
sSdiff	3	CLL (100%)
SPS	3	CLL (100%)
PDN	2	NDI (100%)
pg	2	BUD (100%)
sPKKPdf	2	CLL (100%)
PKPmax	2	CLL (100%)
PKPPKPbc	2	BUD (100%)
(PS)	2	CLL (100%)
PcPPKPre	2	CLL (100%)
PCN	2	NDI (100%)
PM2	2	MOLD (100%)
PN11	2	ATA (100%)
PN7	2	ATA (100%)
SKS2	2	IDC (100%)
(PPPP)	2	CLL (100%)
sSKKSac	2	CLL (100%)
pPKP2	2	BELR (50%), BJI (50%)
PKPlp	2	CLL (100%)
PGDN	2	NDI (100%)
(PSKS)	2	CLL (100%)
pPmax	2	CLL (100%)
sPcP	2	CLL (100%)
pPS	2	CLL (100%)
p	2	NDI (100%)
PKiKPmax	2	CLL (100%)
pPb	2	VIE (50%), OMAN (50%)
PKPPKPab	2	BUD (100%)
PKPd	2	NAO (100%)
N	2	EAF (50%), AAE (50%)
PKPdf(2)	2	CLL (100%)
sn	2	ISN (100%)
PbPb	2	OMAN (100%)
S(2)	2	CLL (100%)
pPSKS	2	CLL (100%)
(pPP)	2	CLL (100%)
PSSrev	2	CLL (100%)
(SKPdf)	2	CLL (100%)
PPmax	2	CLL (100%)
(Sn)	2	CLL (100%)
LgX	2	CSEM (100%)
sSKSdf	2	NEIC (100%)
PS(2)	2	CLL (100%)
PKHKPM	2	BELR (100%)
PgS	2	NEIC (100%)
KP	2	BRG (100%)
(SP)	2	CLL (100%)

Table 12.2: *(continued)*

Reported Phase	Total	Agencies reporting
(SPP)	1	CLL (100%)
sPKKPab	1	CLL (100%)
sPKKSdf	1	CLL (100%)
PDSE	1	NDI (100%)
PKpdf	1	INMG (100%)
pPKPab2	1	CLL (100%)
-	1	SVSA (100%)
-Pn	1	BUD (100%)
(sPKiKP)	1	CLL (100%)
pPKPPKPd	1	CLL (100%)
(PN)	1	BRG (100%)
PSn	1	BUD (100%)
ScSp	1	DBN (100%)
PP(2)	1	CLL (100%)
SSlp	1	CLL (100%)
PPPPrev	1	CLL (100%)
(sSdiff)	1	CLL (100%)
(Sdif)	1	CLL (100%)
SSPrev	1	CLL (100%)
(sPKPdf)	1	CLL (100%)
–c	1	BUD (100%)
SKPPKPab	1	CLL (100%)
Pg2	1	SJA (100%)
SKSSKS	1	CLL (100%)
Sk	1	CLL (100%)
sPKKSbc	1	CLL (100%)
sPKP2	1	BELR (100%)
sPKSbc	1	CLL (100%)
PNDN	1	NDI (100%)
LRM1	1	BELR (100%)
pSP	1	CLL (100%)
(SKKPdf)	1	CLL (100%)
AnL	1	INMG (100%)
PM1	1	MOLD (100%)
Pgf	1	BUD (100%)
PKPa	1	NAO (100%)
pPKKPbc	1	CLL (100%)
(SKSac)	1	CLL (100%)
LmV(360	1	CLL (100%)
-Pg	1	BUD (100%)
G	1	MOS (100%)
Sn5	1	ISN (100%)
sPSKS	1	CLL (100%)
(sSP)	1	CLL (100%)
TP	1	BRG (100%)
3PKPdf	1	CLL (100%)
sPmax	1	CLL (100%)
psP	1	SYO (100%)
PDS	1	NDI (100%)
g	1	LIT (100%)
(sPS)	1	CLL (100%)
pPKKPab	1	CLL (100%)
sPPS	1	CLL (100%)
sPKPPKPd	1	CLL (100%)
WS	1	MOS (100%)
SSSrev	1	CLL (100%)
PKPdfd	1	WAR (100%)
sPKP1	1	BELR (100%)
pPPS	1	CLL (100%)
PL	1	NDI (100%)
LM	1	MOLD (100%)
S'S'df	1	NEIC (100%)
PKiKPf	1	CLL (100%)
AMPN	1	RSNC (100%)
PN8	1	ATA (100%)
(PKKPbc)	1	CLL (100%)
(PKSdf)	1	CLL (100%)

Table 12.2: (continued)

Reported Phase	Total	Agencies reporting
(sPdif)	1	CLL (100%)
PGDS	1	NDI (100%)
SPSrev	1	CLL (100%)
pPk	1	CLL (100%)
On	1	BUD (100%)
PKPbc(2)	1	CLL (100%)
PKKSbc	1	CLL (100%)
(sPKPbc)	1	CLL (100%)
sPN	1	BRA (100%)
PSKSrev	1	CLL (100%)
(ScS)	1	CLL (100%)
PPk	1	CLL (100%)
En	1	ISN (100%)
Pp	1	MOLD (100%)
LRg	1	MOLD (100%)
(SKKSac)	1	CLL (100%)
(Pn)	1	CLL (100%)
pPKKPdf	1	CLL (100%)
-ML	1	INMG (100%)
SKSc	1	BUD (100%)
pPKS	1	LPA (100%)
PDIF	1	BRG (100%)
PKPP	1	MOLD (100%)
PKPdiff2	1	CLL (100%)

Table 12.3: Reporters of amplitude data

Agency	Number of reported amplitudes	Number of amplitudes in ISC located events	Number used for ISC mb	Number used for ISC MS
IDC	405203	373079	163219	49755
NEIC	287281	286675	215316	43226
MOS	194067	159972	76902	16626
ROM	184072	34113	0	0
CSEM	161216	33036	2344	0
ATH	147437	16388	0	0
BJI	82175	71632	16853	22764
ISK	70713	23377	0	0
MDD	57146	9830	0	0
NNC	53933	15779	79	0
SOME	50911	16080	2474	0
DJA	46123	26475	4996	0
THE	36225	6547	0	0
VIE	35844	21127	7263	0
RSNC	28949	1434	0	0
WEL	22884	4373	53	0
LDG	18354	6081	12	0
HEL	17722	802	0	0
DMN	15837	15077	0	0
INMG	15791	7773	3255	0
BKK	15483	14703	6430	0
TEH	13154	5013	0	0
PPT	12597	10605	1262	0
GUC	12322	4924	0	0
MAN	10893	3004	0	0
PRU	10490	5959	0	2639
SJA	8727	2752	25	1
SKHL	7744	6054	0	0
NDI	5552	4635	1607	170
WBNET	5435	24	0	0
PDG	5389	4138	0	0
BER	5267	1919	830	39
SVSA	5117	486	244	0
YARS	4899	73	0	0
BRG	4598	2775	723	0
LJU	4458	276	0	0
PRE	4020	221	1	0
BGS	3660	2677	1285	863
BYKL	3536	1413	0	0
ZUR	3500	676	0	0
OTT	3372	480	0	0
CLL	3219	2990	577	276
KNET	3066	783	11	0
ATA	2990	1828	0	0

Table 12.3: *Continued.*

Agency	Number of reported amplitudes	Number of amplitudes in ISC located events	Number used for ISC mb	Number used for ISC MS
DNK	2582	2222	1560	0
SKO	2316	616	0	0
ECX	2130	367	0	0
NAO	2127	2107	1499	0
LIC	1777	1487	911	0
LIT	1773	1616	1161	0
IEPN	1769	1529	0	0
HYB	1699	1677	849	0
IGIL	1407	739	165	249
EAF	1400	15	0	0
NSSC	1110	641	2	0
BEO	995	220	0	0
UCR	962	605	8	0
SIGU	893	523	0	0
UCC	742	693	452	0
MOLD	705	465	77	0
THR	702	702	0	0
BELR	688	660	0	233
MRB	680	0	0	0
MIRAS	602	11	0	0
IGQ	529	529	12	0
WAR	480	480	2	322
DBN	371	272	154	0
NERS	341	139	0	0
DHMR	274	53	2	0
IPEC	266	81	0	0
ISN	155	0	0	0
SCB	140	125	0	0
BGR	131	89	0	0
PLV	62	52	0	0
OBM	29	11	0	0
IASPEI	21	21	0	0
NAM	14	14	0	0
LPA	3	0	0	0

13

Glossary of ISC Terminology

- Agency/ISC data contributor

  An academic or government institute, seismological organisation or company, geological/meteorological survey, station operator or author that reports or contributed data in the past to the ISC or one of its predecessors. Agencies may contribute data to the ISC directly, or indirectly through other ISC data contributors.

- Agency code

  A unique, maximum eight-character code for a data reporting agency (e.g. NEIC, GFZ, BUD) or author (e.g. ISC, EHB, IASPEI). Often the agency code is the commonly used acronym of the reporting institute.

- Arrival

  A phase pick at a station is characterised by a phase name and an arrival time.

- Associated phase

  Associated phase arrival or amplitude measurements represent a collection of observations belonging to (i.e. generated by) an event. The complete set of observations are associated to the prime hypocentre.

- Azimuthal gap/Secondary azimuthal gap

  The azimuthal gap for an event is defined as the largest angle between two stations with defining phases when the stations are ordered by their event-to-station azimuths. The secondary azimuthal gap is the largest azimuthal gap a single station closes.

- BAAS

  Seismological bulletins published by the British Association for the Advancement of Science (1913-1917) under the leadership of H.H. Turner. These bulletins are the predecessors of the ISS Bulletins and include reports from stations distributed worldwide.

- Bulletin

  An ordered list of event hypocentres, uncertainties, focal mechanisms, network magnitudes, as well as phase arrival and amplitude observations associated to each event. An event bulletin may list all the reported hypocentres for an event. The convention in the ISC Bulletin is that the preferred (prime) hypocentre appears last in the list of reported hypocentres for an event.

- Catalogue

  An ordered list of event hypocentres, uncertainties and magnitudes. An event catalogue typically lists only the preferred (prime) hypocentres and network magnitudes.

- CoSOI/IASPEI

  Commission on Seismological Observation and Interpretation, a commission of IASPEI that prepares and discusses international standards and procedures in seismological observation and interpretation.

- Defining/Non-defining phase

  A defining phase is used in the location of the event (time-defining) or in the calculation of the network magnitude (magnitude-defining). Non-defining phases are not used in the calculations because they suffer from large residuals or could not be identified.

- Direct/Indirect report

  A data report sent (e-mailed) directly to the ISC, or indirectly through another ISC data contributor.

- Duplicates

  Nearly identical phase arrival time data reported by one or more agencies for the same station. Duplicates may be created by agencies reporting observations from other agencies, or several agencies independently analysing the waveforms from the same station.

- Event

  A natural (e.g. earthquake, landslide, asteroid impact) or anthropogenic (e.g. explosion) phenomenon that generates seismic waves and its source can be identified by an event location algorithm.

- Grouping

  The ISC algorithm that organises reported hypocentres into groups of events. Phases associated to any of the reported hypocentres will also be associated to the preferred (prime) hypocentre. The grouping algorithm also attempts to associate phases that were reported without an accompanying hypocentre to events.

- Ground Truth

  An event with a hypocentre known to certain accuracy at a high confidence level. For instance, GT0 stands for events with exactly known location, depth and origin time (typically explosions); GT5 stands for events with their epicentre known to 5 km accuracy at the 95% confidence level, while their depth and origin time may be known with less accuracy.

- Ground Truth database

  On behalf of IASPEI, the ISC hosts and maintains the IASPEI Reference Event List, a bulletin of ground truth events.

- IASPEI

  International Association of Seismology and Physics of the Earth Interior, www.iaspei.org.

- International Registry of Seismograph Stations (IR)

  Registry of seismographic stations, jointly run by the ISC and the World Data Center for Seismology, Denver (NEIC). The registry provides and maintains unique five-letter codes for stations participating in the international parametric and waveform data exchange.

- ISC Bulletin

  The comprehensive bulletin of the seismicity of the Earth stored in the ISC database and accessible through the ISC website. The bulletin contains both natural and anthropogenic events. Currently the ISC Bulletin spans more than 50 years (1960-to date) and it is constantly extended by adding both recent and past data. Eventually the ISC Bulletin will contain all instrumentally recorded events since 1900.

- ISC Governing Council

  According to the ISC Working Statutes the Governing Council is the governing body of the ISC, comprising one representative for each ISC Member.

- ISC-located events

  A subset of the events selected for ISC review are located by the ISC. The rules for selecting an event for location are described in Section 3.3.4; ISC-located events are denoted by the author ISC.

- ISC Member

  An academic or government institute, seismological organisation or company, geological/meteorological survey, station operator, national/international scientific organisation that contribute to the ISC budget by paying membership fees. ISC members have voting rights in the ISC Governing Council.

- ISC-reviewed events

  A subset of the events reported to the ISC are selected for ISC analyst review. These events may or may not be located by the ISC. The rules for selecting an event for review are described in Section 3.3.3. Non-reviewed events are explicitly marked in the ISC Bulletin by the comment following the prime hypocentre "Event not reviewed by the ISC".

- ISF

  International Seismic Format (www.isc.ac.uk/standards/isf). A standard bulletin format approved by IASPEI. The ISC Bulletin is presented in this format at the ISC website.

- ISS

  International Seismological Summary (1918-1963). These bulletins are the predecessors of the ISC Bulletin and represent the major source of instrumental seismological data before the digital era. The ISS contains regionally and teleseismically recorded events from several hundreds of globally distributed stations.

- Network magnitude

The event magnitude reported by an agency or computed by the ISC locator. An agency can report several network magnitudes for the same event and also several values for the same magnitude type. The network magnitude obtained with the ISC locator is defined as the median of station magnitudes of the same magnitude type.

- Phase

  A maximum eight-character code for a seismic, infrasonic, or hydroacoustic phase. During the ISC processing, reported phases are mapped to standard IASPEI phase names. Amplitude measurements are identified by specific phase names to facilitate the computation of body-wave and surface-wave magnitudes.

- Prime hypocentre

  The preferred hypocentre solution for an event from a list of hypocentres reported by various agencies or calculated by the ISC.

- Reading

  Parametric data that are associated to a single event and reported by a single agency from a single station. A reading typically includes one or more phase names, arrival time and/or amplitude/period measurements.

- Report/Data report

  All data that are reported to the ISC are parsed and stored in the ISC database. These may include event bulletins, focal mechanisms, moment tensor solutions, macroseismic descriptions and other event comments, as well as phase arrival data that are not associated to events. Every single report sent to the ISC can be traced back in the ISC database via its unique report identifier.

- Shide Circulars

  Collections of station reports for large earthquakes occurring in the period 1899-1912. These reports were compiled through the efforts of J. Milne. The reports are mainly for stations of the British Empire equipped with Milne seismographs. After Milne's death, the Shide Circulars were replaced by the Seismological Bulletins of the BAAS.

- Station code

  A unique, maximum six-character code for a station. The ISC Bulletin contains data exclusively from stations registered in the International Registry of Seismograph Stations.

14

Acknowledgements

We thank Marcelo Bianchi and Marcelo Assumpção of the University of São Paulo as well as they colleagues in the University of Brasília, National Observatory and Rio Grande do Norte Federal University for kindly accepting our invitation and submitting the article on the Brazilian Seismographic Network for this issue of the Summary.

We are also grateful to all the developers of the Generic Mapping Tools (GMT) suite of software (Wessel and Smith, 1998), used extensively here in producing the graphical figures.

Finally, we thank the ISC Member Institutions, Data Contributors, Funding Agencies (including NSF Award EAR-1417970 and USGS Award G14AC00149) and Sponsors for supporting the long-term operation of the ISC.

References

Adams, R. D., A. A. Hughes, and D. M. McGregor (1982), Analysis procedures at the International Seismological Centre, *Physics of the Earth and Planetary Interiors*, *30*, 85–93.

Amante, C., and B. W. Eakins (2009), ETOPO1 1 arc-minute global relief model: procedures, data sources and analysis, *NOAA Technical Memorandum NESDIS NGDC-24*, NOAA.

Balfour, N., R. Baldwin, and A. Bird (2008), Magnitude calculations in Antelope 4.10, *Analysis Group Note of Geological Survey of Canada*, pp. 1–13.

Bennett, T. J., V. Oancea, B. W. Barker, Y.-L. Kung, M. Bahavar, B. C. Kohl, J. . Murphy, and I. K. Bondár (2010), The nuclear explosion database NEDB: a new database and web site for accessing nuclear explosion source information and waveforms, *Seismological Research Letters*, *81*, doi:10.1785/gssrl.81.1.12.

Bisztricsany, E. A. (1958), A new method for the determination of the magnitude of earthquakes, *Geofiz. Kozl*, pp. 69–76.

Bolt, B. A. (1960), The revision of earthquake epicentres, focal depths and origin time using a high-speed computer, *Geophysical Journal of the Royal Astronomical Society*, *3*, 434–440.

Bondár, I., and K. McLaughlin (2009a), A new ground truth data set for seismic studies, *Seismological Research Letters*, *80*, 465–472.

Bondár, I., and K. McLaughlin (2009b), Seismic location bias and uncertainty in the presence of correlated and non-Gaussian travel-time errors, *Bulletin of the Seismological Society of America*, *99*, 172–193.

Bondár, I., and D. Storchak (2011), Improved location procedures at the International Seismological Centre, *Geophysical Journal International*, *186*, 1220–1244.

Bondár, I., E. R. Engdahl, X. Yang, H. A. A. Ghalib, A. Hofstetter, V. Kirchenko, R. Wagner, I. Gupta, G. Ekström, E. Bergman, H. Israelsson, and K. McLaughlin (2004), Collection of a reference event set for regional and teleseismic location calibration, *Bulletin of the Seismological Society of America*, *94*, 1528–1545.

Bondár, I., E. Bergman, E. R. Engdahl, B. Kohl, Y.-L. Kung, and K. McLaughlin (2008), A hybrid multiple event location technique to obtain ground truth event locations, *Geophysical Journal International*, *175*, doi:10.1111/j.1365,246X.2008.03,867x.

Bormann, P., and J. W. Dewey (2012), The new iaspei standards for determining magnitudes from digital data and their relation to classical magnitudes, is 3.3, *New Manual of Seismological Observatory Practice 2 (NMSOP-2), P. Bormann (Ed.)*, pp. 1–44, doi:10.2312/GFZ.NMSOP-2_IS_3.3,10.2312/GFZ.NMSOP-2, `http://nmsop.gfz-postsdam.de`.

Bormann, P., and J. Saul (2008), The new IASPEI standard broadband magnitude mB, *Seism. Res. Lett*, *79*(5), 698–705.

Bormann, P., R. Liu, X. Ren, R. Gutdeutsch, D. Kaiser, and S. Castellaro (2007), Chinese national network magnitudes, their relation to NEIC magnitudes and recommendations for new IASPEI magnitude standards, *Bulletin of the Seismological Society of America*, *97*(1B), 114–127, doi:10.1785/012006007835.

Bormann, P., R. Liu, Z. Xu, R. Ren, and S. Wendt (2009), First application of the new IASPEI teleseismic magnitude standards to data of the China National Seismographic Network, *Bulletin of the Seismological Society of America*, *99*, 1868–1891, doi:10.1785/0120080010.

Chang, A. C., R. H. Shumway, R. R. Blandford, and B. W. Barker (1983), Two methods to improve location estimates - preliminary results, *Bulletin of the Seismological Society of America*, *73*, 281–295.

Choy, G. L., and J. L. Boatwright (1995), Global patterns of readiated seismic energy and apparent stress, *J. Geophys. Res.*, *100*(B9), 18,205–18,228.

Dziewonski, A. M., and F. Gilbert (1976), The effect of small, aspherical perturbations on travel times and a re-examination of the correction for ellipticity, *Geophysical Journal of the Royal Astronomical Society*, *44*, 7–17.

Dziewonski, A. M., T.-A. Chou, and J. H. Woodhouse (1981), Determination of earthquake source parameters from waveform data for studies of global and regional seismicity, *J. Geophys. Res.*, *86*, 2825–2852.

Engdahl, E. R., and R. H. Gunst (1966), Use of a high speed computer for the preliminary determination of earthquake hypocentres, *Bulletin of the Seismological Society of America*, *56*, 325–336.

Engdahl, E. R., and A. Villaseñor (2002), Global seismicity: 1900-1999, *International Handbook of Earthquake Engineering and Seismology, International Geophysics series*, *81A*, 665–690.

Engdahl, E. R., R. van der Hilst, and R. Buland (1998), Global teleseismic earthquake relocation with improved travel times and procedures for depth determination, *Bulletin of the Seismological Society of America*, *88*, 722–743.

Flinn, E. A., and E. R. Engdahl (1965), Proposed basis for geographical and seismic regionalization, *Reviews of Geophysics*, *3*(1), 123–149.

Flinn, E. A., E. R. Engdahl, and A. R. Hill (1974), Seismic and geographical regionalization, *Bulletin of the Seismological Society of America*, *64*, 771–993.

Gutenberg, B. (1945a), Amplitudes of P, PP and S and magnitude of shallow earthquakes, *Bulletin of the Seismological Society of America*, *35*, 57–69.

Gutenberg, B. (1945b), Magnitude determination of deep-focus earthquakes, *Bulletin of the Seismological Society of America*, *35*, 117–130.

Gutenberg, B. (1945c), Amplitudes of surface waves and magnitudes of shallow earthquakes, *Bulletin of the Seismological Society of America*, *35*, 3–12.

Gutenberg, B., and C. F. Richter (1956), Magnitude and Energy of earthquakes, *Ann. Geof.*, *9*, 1–5.

Hutton, L. K., and D. M. Boore (1987), The ML scale in southern California, *Bulletin of the Seismological Society of America*, *77*, 2074–2094.

IASPEI (2005), Summary of magnitude working group recommendations on standard procedures for determining earthquake magnitudes from digital data, `http://www.iaspei.org/commissions/CSOI.html#wgmm,http://www.iaspei.org/commissions/CSOI/summary_of_WG_recommendations_2005.pdf`.

IASPEI (2013), Summary of magnitude working group recommendations on standard procedures for determining earthquake magnitudes from digital data, `http://www.iaspei.org/commissions/CSOI/Summary_of_WG_recommendations_20130327.pdf`.

IDC (1999), IDC processing of seismic, hydroacoustic and infrasonic data, *IDC Documentation*.

Jeffreys, H., and K. E. Bullen (1940), *Seismological Tables*, British Association for the Advancement of Science.

Kanamori, H. (1977), The energy release in great earthquakes, *J. Geophys. Res.*, *82*, 2981–2987.

Kennett, B. L. N. (2006), Non-linear methods for event location in a global context, *Physics of the Earth and Planetary Interiors*, *158*, 45–64.

Kennett, B. L. N., E. R. Engdahl, and R. Buland (1995), Constraints on seismic velocities in the Earth from traveltimes, *Geophysical Journal International*, *122*, 108–124.

Kennett, B. L. N., E. R. Engdahl, and R. Buland (1996), Ellipticity corrections for seismic phases, *Geophysical Journal International*, *127*, 40–48.

Lee, W. H. K., R. Bennet, and K. Meagher (1972), A method of estimating magnitude of local earthquakes from signal duration, *U.S. Geol. Surv.*, Open-File Rep.

Murphy, J. R., and B. W. Barker (2006), Improved focal-depth determination through automated identication of the seismic depth phases pP and sP, *Bulletin of the Seismological Society of America*, *96*, 1213–1229.

NMSOP-2 (2012), *New Manual of Seismological Observatory Practice (NMSOP-2)*, IASPEI, GFZ, German Research Centre for Geosciences, Potsdam, doi:10.2312/GFZ.NMSOP-2, `http://nmsop.gfz-potsdam.de`, urn:nbn:de:kobv:b103-NMSOP-2.

Nuttli, O. W. (1973), Seismic wave attenuation and magnitude relations for eastern North America, *J. Geophys. Res.*, *78*, 876–885.

Richter, C. F. (1935), An instrumental earthquake magnitude scale, *Bulletin of the Seismological Society of America*, *25*, 1–32.

Ringdal, F. (1976), Maximum-likelihood estimation of seismic magnitude, *Bulletin of the Seismological Society of America*, *66*(3), 789–802.

Sambridge, M. (1999), Geophysical inversion with a neighbourhood algorithm, *Geophysical Journal International*, *138*, 479–494.

Sambridge, M., and B. L. N. Kennett (2001), Seismic event location: non-linear inversion using a neighbourhood algorithm, *Pure and Applied Geophysics*, *158*, 241–257.

Storchak, D. A., J. Schweitzer, and P. Bormann (2003), The IASPEI standard seismic phases list, *Seismological Research Letters*, *74*(6), 761–772.

Storchak, D. A., J. Schweitzer, and P. Bormann (2011), Seismic phase names: IASPEI standard, in *Encyclopedia of Solid Earth Geophysics*, edited by H. Gupta, pp. 1162–1173, Springer.

Tsuboi, C. (1954), Determination of the Gutenberg-Richter's magnitude of earthquakes occurring in and near Japan, *Zisin (J. Seism. Soc. Japan), Ser. II*(7), 185–193.

Tsuboi, S., K. Abe, K. Takano, and Y. Yamanaka (1995), Rapid determination of Mw from broadband P waveforms, *Bulletin of the Seismological Society of America*, *85*(2), 606–613.

Uhrhammer, R. A., and E. R. Collins (1990), Synthesis of Wood-Anderson Seismograms from Broadband Digital Records, *Bulletin of the Seismological Society of America*, *80*(3), 702–716.

Vaněk, J., A. Zapotek, V. Karnik, N. V. Kondorskaya, Y. V. Riznichenko, E. F. Savarensky, S. L. Solov'yov, and N. V. Shebalin (1962), Standardization of magnitude scales, *Izvestiya Akad. SSSR., Ser. Geofiz.*(2), 153–158, pages 108–111 in the English translation.

Villaseñor, A., and E. R. Engdahl (2005), A digital hypocenter catalog for the International Seismological Summary, *Seismological Research Letters*, *76*, 554–559.

Villaseñor, A., and E. R. Engdahl (2007), Systematic relocation of early instrumental seismicity: Earthquakes in the International Seismological Summary for 1960–1963, *Bulletin of the Seismological Society of America*, *97*, 1820–1832.

Woessner, J., and S. Wiemer (2005), Assessing the quality of earthquake catalogues: estimating the magnitude of completeness and its uncertainty, *Bulletin of the Seismological Society of America*, *95*(2), doi:10/1785/012040,007.

Young, J. B., B. W. Presgrave, H. Aichele, D. A. Wiens, and E. A. Flinn (1996), The Flinn-Engdahl regionalisation scheme: the 1995 revision, *Physics of the Earth and Planetary Interiors*, *96*, 223–297.

WHITE PAPER

COMPLETE INTEGRATED AFTERSHOCK SYSTEM PROVIDES QUICK AND EASY SOLUTION FOR RAPID AFTERSHOCK DEPLOYMENT

LEONID ZIMAKOV

TRIMBLE INFRASTRUCTURE, PLANO, TEXAS, USA

INTRODUCTION

Rapid aftershock mobilization plays an essential role in the understanding of both focal mechanism and rupture propagation caused by strong earthquakes. A quick assessment of the data provides a unique opportunity to study the dynamics of the entire earthquake process in-situ. Aftershock study also provides practical information for local authorities regarding post-earthquake activity, which is very important in order to conduct the necessary actions for public safety in the area affected by a strong earthquake.

Due to a relatively short aftershock activity period (several weeks to several months), it is critical to rapidly deploy emergency personnel to the affected area in order to minimize the time required to estimate the extent and amplitude of strong shaking from aftershock events.

A dense array of seismic stations consisting of high resolution seismic recorders with short period seismometers and accelerometers is required in order to reduce the time needed to detect an event and provide high resolution maps of ground accelerations across the affected earthquake region. Therefore, the rapid aftershock mobilization of seismic equipment should comply with the following critical requirements:

- Lightweight and small in size
- Integrated design with minimal or no external peripheral equipment
- Very low power consumption
- Minimal or no field programming
- Easy and quick data download in the field
- Low maintenance

WHAT DOES THE 160-03 OFFER?

The REF TEK High Resolution Aftershock System, Model 160-03, is a self-contained, fully integrated Aftershock System providing the customer with simple and quick deployment during aftershock emergency mobilization. The 160-03, six channel recorder, contains three major components integrated in one case:

- 24-bit resolution low power ADC with CPU and lid interconnect boards;
- power source; and
- three component 2 Hz sensors (two horizontals and one vertical and a triaxial +/-4g MEMS accelerometer.

Figure 1: REF TEK 160-03 High Resolution Aftershock System

Figure 2: Inside the case of the REF TEK 160-03 High Resolution Aftershock System

The self-contained rechargeable battery pack provides power autonomy for up to 7 days during continuous data acquisition at 200 sps on three weak motion and three triggered strong motion recording channels. For longer power autonomy, the 160-03 Aftershock System battery pack can be charged from an external source (solar power system). To download recorded data the customer has two options:

- Connect a laptop to the 160-03 and the data is then automatically uploaded; or
- Connect the REF TEK Wi-Fi Serial Adaptor to upload data to the REF TEK iFSC Controller.

The 160-03 configuration is fixed based on a configuration file stored in the system, so no external command/control interface is required for parameter setup in the field. For visual control of the system performance in the field, the 160-03 has a built-in LED display which indicates the system's recording status, as well as a hot swappable USB drive and battery status. As an added customer convenience, four 160-03 systems can be housed in a small, lightweight, watertight rolling case that will keep the recorders safe during transport. The ease of having an all-in-one aftershock system also provides the customer flexibility in sending the equipment to the affected region via a more cost effective way as the equipment/carrying case can easily be checked on both domestic and international commercial flights.

160-03 SPECIFICATIONS

Model	160-03 (Part No. 97124-00)
Mechanical	
Size: Weight: Watertight Integrity:	6” (15.2cm) high x 8.63” (21.9cm) diameter 11.7 lbs. (5.3 kg) IP67
Environmental	
Operating Temp.:	-30°C to +60°C
Storage Temp.:	-40°C to +70°C
Power	
Average Power:	<400 mW
A/D Convertor	
Type:	Delta-Sigma Modulation, 24-bit output resolution
Dynamic Range:	>138 dB@100 sps
Channels:	6
Input Impedance:	Matched to sensors
Sample Rates:	200 sps default; 100, 250, 500 sps optional
Seismometer	
Type:	Moving coil / mass
Natural Frequency:	2 Hz
Accelerometer	
Type:	± 4g
Frequency Response:	DC – 45 Hz
Damping:	0.7 to critical
Data Storage	
Type:	USB Flash
User Interface	
Type:	LED array consisting of 16 LED display recording status, USB drive status, battery voltage, etc.
Power Control:	Magnetic switch to turn on both power and acquisition

Table 1: 160-03 Specifications

CONTACT US

Phone: +1 (214) 440 1265

Email: sales@reftek.com